Université de Bourgogne
Institut Carnot de Bourgogne

Habilitation à diriger des recherches

Par

Dominique SUGNY

Structure et Contrôle des systèmes dynamiques

soutenue le 29 septembre 2009 devant la

Commission d'examen :

M. Osman Atabek	*Rapporteur*
M. Boris Zhilinskií	*Rapporteur*
M. Ugo Boscain	*Rapporteur*
Mme Michèle Desouter-Lecomte	*Examinateur*
M. Steffen Glaser	*Examinateur*
M. Hans-Rudolf Jauslin	*Examinateur*
M. Olivier Faucher	*Examinateur*

Remerciements

Ce manuscript est tout d'abord l'occasion de saluer et de remercier plusieurs chercheurs qui m'ont au cours de ma carrière scientifique donné une chance de poursuivre et d'approfondir mes travaux. Par ordre chronologique, j'adresse mes sincères remerciements à Marc Joyeux qui m'a permis de découvrir la mécanique Hamiltonienne et la dynamique moléculaire au cours de ma thèse. Sur un plan plus personnel, je le remercie de m'avoir poussé sur la voie de la recherche et d'être toujours aussi disponible malgré les années pour les conseils et les idées scientifiques. Je voudrais ensuite saluer Osman Atabek et Arne Keller qui m'ont proposé un post-doc au laboratoire de Photophysique Moléculaire à Orsay et qui m'ont fait découvrir les subtilités du contrôle quantique. Un grand merci également à Hans Jauslin pour m'avoir accueilli en tant que Maître de Conférences à Dijon. Je voudrais également le remercier pour sa gentillesse et sa disponibilité. Mes remerciements vont ensuite à mes chers collègues de l'Institut de Mathématiques de Bourgogne, P. Mardesic, M. Pelletier et B. Bonnard qui ont accepté en 2006 de travailler avec un *simple* physicien. Un merci tout particulier à Bernard à qui je dois toutes mes connaissances en contrôle optimal géométrique et qui me transmet un peu de sa formidable énergie.

Je voudrais également remercier différents collègues avec qui j'ai pu interagir au cours des années : Stéphane Guérin, Antonio Picozzi, Olivier Faucher, Edouard Hertz, Bruno Lavorel, Frédéric Chaussard de l'Institut Carnot de Bourgogne, Jean-Baptiste Caillau de l'Institut de Mathématique de Bourgogne, Michèle Desouter-Lecomte et son équipe du laboratoire de Chimie-Physique d'Orsay, Ugo Boscain du Laboratoire de Mathématique de l'école Polytechnique de Paris et les membres de son groupe, les anciens collègues du laboratoire de Spectrométrie Physique de Grenoble (M. Lombardi, R. Jost...), Boris Zhilinskiı́ et Dmitrii Sadovskiı́ de l'Université du Littoral de Dunkerque, Konstantinos Efstathiou de Gröningen, Steffen

Glaser et son équipe de Munich, Gabriel Turinici et Julien Salomon de l'Université Paris-Dauphine...

Sur un plan plus personnel, je voudrais remercier Sophie et mes deux petits monstres pour leur soutien.

Table des matières

Chapitre 1

Introduction

Ce document présente une synthèse des activités de recherche que j'ai menées depuis la soutenance de ma thèse en octobre 2002. Il couvre mon année de post-doctorat au laboratoire de Photophysique Moléculaire de l'Université d'Orsay dans l'équipe d'Osman Atabek et mon travail en tant que Maître de Conférences depuis ma nomination en septembre 2003 à l'Université de Bourgogne.

La deuxième partie de ce document est dédiée à mon Curriculum Vitae dans lequel je détaille notamment mes études, mes principaux thèmes de recherche et les projets correspondants, mes autres travaux de recherche comme l'organisation de congrès ou mes activités d'expertise, les différents encadrements de doctorants et d'étudiants dont j'ai eu la charge ainsi que mes autres activités liées à l'enseignement, à la vulgarisation scientifique ou aux tâches administratives.

La troisième partie de ce manuscrit replace mon activité de recherche dans un cadre scientifique plus large et résume mes différentes perspectives de recherche.

Les quatrième et cinquième parties sont réservées au développement de mes différents sujets de recherche ainsi qu'aux résultats que j'ai pu obtenir. Mon activité de recherche se décompose en deux parties distinctes : l'étude de la structure des systèmes dynamiques et le contrôle des systèmes quantiques. Mes travaux sont présentés sous la forme de courtes introductions détaillant les résultats obtenus et d'articles reproduits dans le présent rapport. Ces articles sont les plus significatifs parmi l'ensemble de mes publications.

La conclusion de ce manuscrit présente mes différents projets à court et moyen termes qui sont la suite logique de mes différent travaux de recherche.

Les annexes rappellent l'ensemble de ma production scientifique où sont distingués les articles publiés ou soumis dans des revues à comité de lecture, les ouvrages, les actes de colloques sans comité de lecture, les articles de vulgarisation, les conférences invitées, les communications orales, les présentations de poster et enfin les séminaires.

Mon activité de recherche est un travail de physicien théoricien qui se situe à l'interface entre physique et mathématique. J'étudie principalement des systèmes dynamiques à petit nombre de degrès de liberté ou à petites dimensions dont la dynamique est gouvernée par un système d'équations différentielles ordinaires. Ces systèmes peuvent être libres ou contrôlés par un paramètre ou un champ extérieur. La faible dimension de ces systèmes permet d'utiliser des outils topologiques et géométriques pour analyser la structure de la dynamique et en déduire ses propriétés qualitatives. Par qualitative, on entend généralement des propriétés valables pour une classe de systèmes ou des propriétés robustes vis-à-vis de la variation de paramètres dont dépend le système étudié. Je m'intéresse à des systèmes classiques ou quantiques les plus proches possible de systèmes réalistes. Pour déterminer les propriétés géométriques de ces systèmes, il est souvent plus simple d'étudier une approximation (ou forme normale) du système initial qui en préserve cependant toutes les propriétés géométriques. Cette approximation peut être généralement obtenue par des méthodes type théorie des perturbations que j'ai aussi développé pour les systèmes moléculaires. Des méthodes numériques puissantes ont aussi été appliquées et développées pour l'étude de systèmes physiques réalistes d'intérêt chimique. Signalons enfin que ces outils géométriques ont été dernièrement appliqués à des systèmes à nombre infini de degrés de liberté décrit par des équations aux dérivées partielles en physique classique et quantique. Ces activités m'ont amené à développer un grand nombre de collaborations avec des physiciens expérimentateurs (O. Faucher, B. Lavorel, R. Jost, S. Glaser...), des physiciens et chimistes théoriciens (M. Joyeux, O. Atabek, A. Keller, S. Guérin, H. R. Jauslin, A. Picozzi, M. Desouter-Lecomte...) et des mathématiciens (B. Bonnard, J.-B. Caillau, G. Turinici, J. Salomon, U. Boscain, P. Mardesic, M. Pelletier...). Les thèmes développés en physique appartiennent aux domaines de la physique moléculaire, la spectroscopie, la dynamique de systèmes classiques, le contrôle quantique allant des réactions chimiques à l'information

quantique en passant par le contrôle de la rotation moléculaire, l'optique non-linéaire et plus généralement la propagation des ondes dans les milieux non-linéaires... En mathématique, les outils utilisés et développés vont de la géométrie différentielle, la géométrie symplectique, la géometrie complexe, le contrôle optimal géométrique aux méthodes numériques de contrôle.

Mon activité de recherche est subdivisée en deux grandes parties : l'étude de la structure des systèmes dynamiques et le contrôle des systèmes quantiques.

La première partie se compose des sections suivantes :

- Application de la théorie des perturbations canoniques à la dynamique moléculaire
- Monodromie Hamiltonienne et connexion de Gauss-Manin
- Dynamique d'ondes contra-propagatives en milieu non-linéaire

Ces sections sont respectivement illustrées par les articles [29], [17] et [9].

Dans la seconde partie, les thèmes suivants sont développés :

- Contrôle de l'orientation et de l'alignement moléculaire
- Contrôle de systèmes chimiques
- Contrôle optimal de systèmes quantiques par algorithmes monotones
- Contrôle optimal géométrique de systèmes quantiques dissipatifs

Ces sections sont illustrées par les articles [25], [22], [11] et [13].
Tous mes articles publiés sont disponibles sur ma page web :
http ://icb.u-bourgogne.fr/OMR/DQNL/Sugny/professionel.html

Chapitre 2

CURRICULUM VITAE

Date de naissance : 09/07/1974
Nationalité : Francaise
Situation familiale : Marié, 2 enfants
Adresse Professionnelle : Institut Carnot de Bourgogne, Université de Bourgogne
Tél : (33)+380395972
Fax : (33)+380395971
Email : dominique.sugny@u-bourgogne.fr
Web page : http ://icb.u-bourgogne.fr/OMR/DQNL/Sugny/professionel.html
Situation actuelle : Maître de Conférences à l'Institut Carnot de Bourgogne
CNU section 30
CNRS section 04

2.1 Etudes et diplômes

2002-2003 :
A.T.E.R. dans l'équipe d'O. Atabek au Laboratoire de Photophysique Moléculaire de l'Université Paris-Sud, Orsay (91, France).
1999-2002 :
Thèse à l'Université Joseph Fourier de Grenoble, Directeur de thèse : M. Joyeux
Théorie des Perturbations Canoniques et Dynamique Moléculaire Non Linéaire
Laboratoire de Spectrométrie Physique
Moniteur de Physique

1996-1998 :
DEA de physique théorique (ENS Lyon)
Capes de physique-chimie 1997
Agrégation de physique 1997 (ENS Lyon)
Magistère de physique Rhône-Alpin (Université Joseph Fourier, ENS Lyon)

2.2 Activités de recherche

Géométrie et topologie en mécanique classique et quantique :

- Monodromie Hamiltonienne et ses généralisations
- Théorie du contrôle géométrique, principe du maximum de Pontryagin

Contrôle par champ laser de processus moléculaires

- Contrôle de l'orientation et de l'alignement moléculaire par champ laser
- Théorie du contrôle optimal et des techniques de passage adiabatique pour les processus moléculaires
- Contrôle de la dynamique moléculaire, rôle de la dissipation, algorithmes monotones
- Information quantique et processus moléculaires

Structure de la dynamique moléculaire

- Théorie des Perturbations Canoniques, spectroscopie des molécules triatomiques
- Monodromie des systèmes moléculaires

2.3 Projets de recherche

- Membre du projet ANR Comoc (coordinateur S. Guérin, 2007-2010)
- Membre du projet européen FASTQUAST (coordinateur S. Guérin et H. R. Jauslin, 2008-2011)
- Coordinateur avec B. Bonnard (IMB) du projet BQR (2008) et fédération de recherche de l'Université de Bourgogne (2007-2011) : *Contrôle Optimal de la dynamique quantique*
- Coordinateur avec P. Mardesic (IMB) du projet BQR (2008) et fédération de recherche de l'Université de Bourgogne (2007-2011) : *Géométrie et*

topologie des systèmes dynamiques
- Coordinateur avec B. Bonnard (IMB) depuis 2007 du groupe de travail *Théorie et analyse des systèmes*

2.4 Organisation de Congrès et workshops

- Co-organisateur avec B. Bonnard et J-B. Caillau du workshop *Optimal Control in space and quantum dynamics* (Dijon, juin 2008)
- Organisateur du colloquium *Laser Control of photoinduced dynamics* (Dijon, juin 2005)
- Organisateur du colloquium *Structure globale des systèmes dynamiques intégrables* (Dijon, octobre 2008)
- Membre du comité d'organisation du congrès HRMS 2007 (spectroscopie haute-résolution)

2.5 Encadrement de doctorants et d'étudiants de master

Doctorants

- Cyrill Kontz (2005-2008), co-directeur H. R. Jauslin
  Contrôle de la dynamique des systèmes dissipatifs par champ laser, Thèse soutenue le 15/09/08
- Ronald Tehini (2006-2009), co-directeur O. Faucher
  Contrôle de l'orientation moléculaire par impulsions laser
- Marc Lapert (2008-2011), co-directeur H. R. Jauslin
  Contrôle optimal de la dynamique quantique
- Elie Assémat (2009-2012)
  Contrôle optimal géométrique et Résonance Magnétique Nucléaire

Master Seconde année

- Elie Assémat (Janvier à mars 2009, Magistère de Physique Théorique d'Orsay)
  Contrôle optimal d'un spin 1/2 par champs magnétiques
- Marc Lapert (Avril à juin 2008, Master de Physique de Dijon)
  Contrôle optimal de la dynamique quantique

- Cyrill Kontz (Avril à juin 2005, Master de Physique de Dijon)
  Structure et contrôle de la dynamique de molécules triatomiques

Master Première année

- Mamadou Dia Sene (Avril à juin 2009, Master de Physique de Dijon)
  Contrôle de l'orientation moléculaire par algorithme monotone
- Wilfried Oyoumba (Avril à juin 2009, Master de Physique de Dijon)
  Contrôle de l'alignement moléculaire par algorithme monotone
- Marc Lapert (Avril à juin 2007, Master de Physique de Dijon)
  Monodromie et structure des spectres moléculaires
- Thomas Viellard (Avril à juin 2006, Master de Physique de Dijon)
  Orientation de molécules linéaires par impulsions laser
- Co-encadrement avec M. Joyeux de stages de recherche pour des étudiants de première année de l'Ecole Nationale Supérieure de Physique de Grenoble, Avril à juin 2002
  Dynamique moléculaire des molécules triatomiques

2.6 Activité d'expertise

- Referee de *Journal of Chemical Physics*, *Physical Review A* et *Computer Physics Communications.*
- Examinateur de la thèse de M. Ndong (Orsay, 2007, directeur de thèse : M. Desouter-Lecomte)

2.7 Vulgarisation scientifique

- Co-organisateur avec H. R. Jauslin de conférences de physique pour des lycéens dans le cadre de l'année mondiale de la physique 2005.
- Co-organisateur avec H. R. Jauslin et M. Boivineau de la conférence sur Einstein pour l'année mondiale de la physique (Dijon, 4/01/05).
- Co-organisateur de visites de l'Université de Grenoble pour des lycéens (2002).

2.8 Activités et positions administratives

- Membre du bureau du comité de sélection de l'Institut Carnot de Bourgogne (2008-2011).
- Membre suppléant de la commission de spécialiste de l'Institut Carnot de Bourgogne (2005-2008).
- Membre extérieur du comité de sélection de l'Université Paris Sud (collège B) depuis 2008.
- Membre du comité de pilotage de la documentation recherche de l'Université de Bourgogne depuis 2008.
- Membre du groupe d'animation scientifique du département Optique Matière et Rayonnement depuis 2009.

- Responsable des travaux pratiques de physique de la préparation PLP depuis 2008.

- Webmaster du site de l'équipe Dynamique Quantique et Non-Linéaire de l'Institut Carnot de Bourgogne.
- Webmaster du site du groupe de travail *Théorie et analyse des systèmes*

- Titulaire de la Prime d'Encadrement Doctorale et de Recherche (PEDR) depuis le 1er octobre 2007.
- CRCT de 6 mois (01/09/08 au 28/02/09) de la section CNU 30.
- Délégation CNRS de 6 mois (01/09/09 au 28/02/10) de la section CNRS 04.

Chapitre 3

Scientific context

The theoretical analysis of complex dynamical systems can be approached from two complementary points of view. The first one is based on numerical computations, the goal being to simulate systems of growing complexity close to experimental conditions. The second option consists in understanding the qualitative structures of the dynamics via a geometrical analysis of the system. This second approach which is at the heart of my research activity requires the application of advanced tools of differential geometry and topology to physical model systems. The qualitative geometric phenomena are generally characteristic of a family of dynamical systems. Geometrical structures appear on the simplest element of this family, often called *a normal form*. The determination of this normal form requires a precise knowledge of the physical system and of the approximations which can be used. Its construction is based on the elimination of degrees of freedom, preserving only the relevant part of the dynamics. The mathematical expression for the idea of elimination of degrees of freedom depends on the context but it is generally associated to perturbation theory. In classical mechanics, such normal forms correspond to integrable models possessing nontrivial qualitative features and constructed from canonical perturbation theory. The study of the geometry of physical dynamical systems is an old but still little developed field. One reason is due to the use of quite sophisticated mathematical tools which are not widely known in the physics community. A close interaction with mathematicians is therefore needed to achieve this second approach. These two approaches are of course not disconnected and a precise understanding of the geometrical properties of the system can explain quantitative results of numerical simulations and can be an explanation of

their robustness with respect to variations of external parameters.

This problem was raised by B. I. Zhilinskiı́ in the introduction of one of his review papers [124] :

"*During the several last decades the formal abstract theory was enormously developed. In particular, many mathematical results concerning influence of topology and symmetry on general dynamical systems and on Hamiltonian systems were formulated. Apart from some purely abstract models the most important applications of these developed mathematical techniques concern field theory, particle physics, nuclear physics and even other branches of science which are apparently rather far from physics (biology...). At the same time applications to quantum molecular physics problems are still relatively rare except, perhaps, for tentative studies of quantum chaos*".

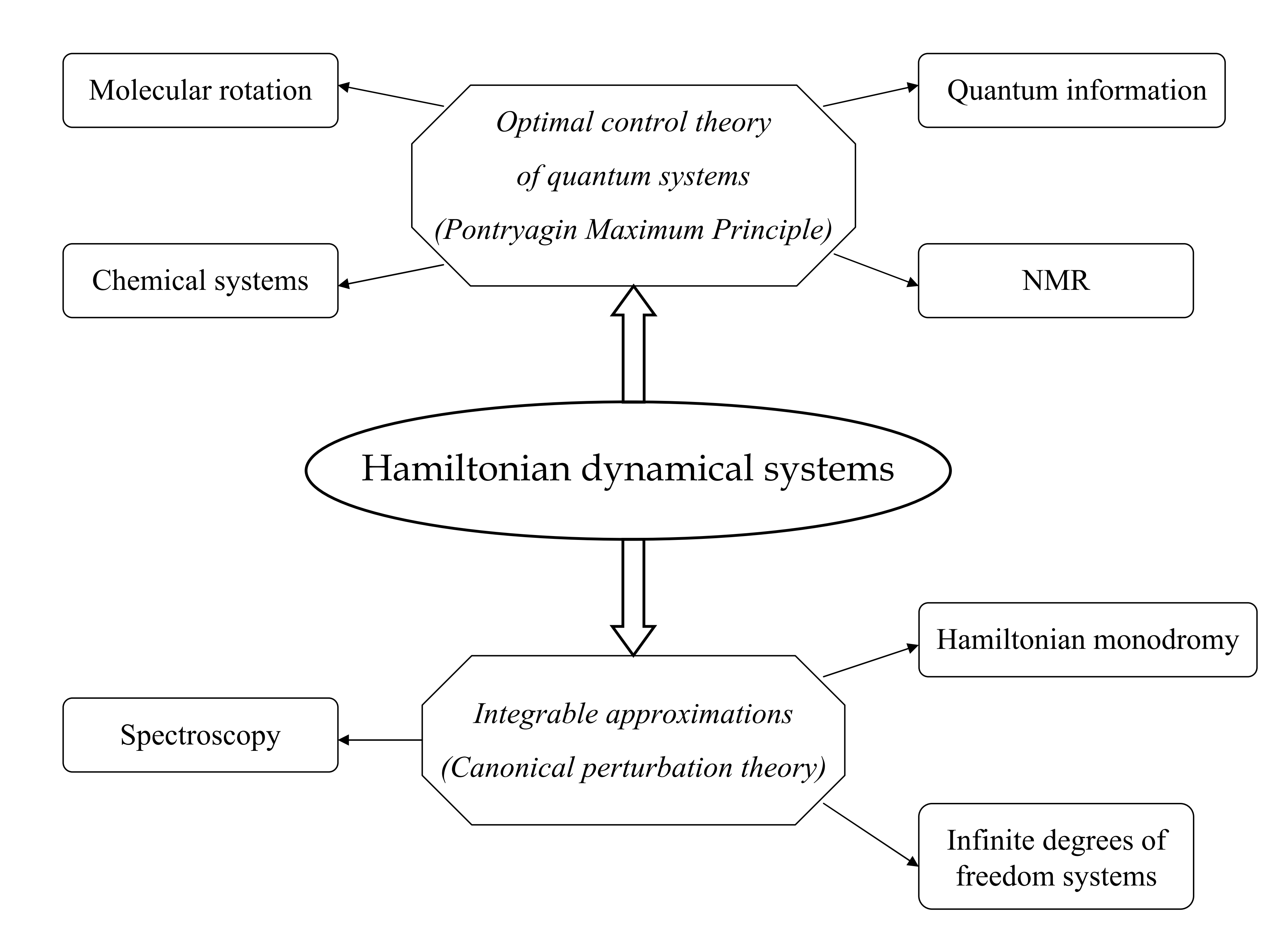
Following the program traced by B. I. Zhilinskiı́ and others, I have oriented my research project towards the analysis of the geometrical structures of physical dynamical systems extending from classical and quantum physics to spectroscopy, chemistry, molecular physics, optics and Nuclear Magnetic Resonance (NMR). In all these domains, the geometrical approach explained above is rare and has to be developed. This work at the interface between mathematics and different branches of physics is, in my opinion, a difficult and long time task, requiring competences in multiple disciplines. This explains why I have developed during the past few years several collaborations with mathematicians and physicists working in these different domains. I intend to pursue in this direction in the next future. Another particularity of my project is to focus on both time-independent and controlled dynamical systems which allows to encompass a large number of physical systems. I detail hereafter some of my projects that I consider most promising.

The first example of geometric properties of dynamical systems is the phenomenon of Hamiltonian monodromy. This concept first introduces by mathematicians in the eighties [55] to describe the obstruction to the existence of global action-angle coordinates in Hamiltonian integrable systems was the starting point of numerous applications in molecular and atomic physics (e.g. the CO_2 molecule [50] or the molecular spectroscopy of the Hydrogen atom under electric and magnetic fields [51]). Nontrivial monodromy is due to the presence of particular singular tori in the phase space

of the Hamiltonian system. A profound analogy can also been established between Hamiltonian monodromy and defects in cristal lattices [125]. Recently, the unbounded analog of monodromy was also defined and could have many implications in scattering problems [56]. The generalizations of Hamiltonian monodromy as fractional monodromy [87, 88] and bidromy [104] and the questions raised by these works were the starting point of my interest for this domain. These generalizations had been introduced in the real domain. The originality of our point of view was to consider a particular complexification of the Hamiltonian system which allows to bypass some singularities encountered in this problem. In [17], we have shown how this complex approach and tools of complex geometry can be used to define fractional monodromy and to compute the corresponding monodromy matrix. Another ambitious objective is to determine a physical dynamical process which allows to *observe* a nontrivial monodromy [53]. Systems with controllable external parameters seem to be good candidates to reach this goal. The development of the concept of Hamiltonian monodromy illustrates in some sense the way I would like to develop my research activity. The benefit of this work at the interface between mathematics and physics is two-fold. Mathematical techniques prove to be useful in the study of physical models but such models also provide new interesting problems as illustrated by the question of fractional monodromy in the mathematical context of Abelian integrals. Another motivating field of research is the study of the dynamics of nonlinear wave systems which are examples of infinite degrees of freedom systems. As a first step, we have studied the interaction of counterpropagating beams for which boundary conditions are imposed at both ends of the nonlinear medium. Under rather general conditions, we have shown that the spatio-temporal dynamics relaxes to a stationary Hamiltonian trajectory lying on a singular torus of the associated Hamiltonian integrable system. In other words, one can say that the singular torus plays the role of an *attractor* for the wave system. The integrable Hamiltonian used here is very close to the ones having a nontrivial monodromy, which makes the link with the first part of my activity. The solution of this problem can be viewed as a promising advance in which tools constructed for finite degrees of freedom systems can be used for infinite ones. We plan to extend this idea to other nonlinear wave systems by considering, for instance, the relation between soliton solutions and singular tori.

The optimal control of quantum dynamics is also one of my main objectives for which many experimental applications are possible (Control of molecular rotation and control of spin dynamics in NMR). Optimal control theory is a well-known and a widely used tool in quantum control (see for instance [123] and references therein) but surprisingly, the geometric aspects are not well developed (see [46, 76] to cite a few) whereas the corresponding mathematical theory [36] and the numerical algorithms in this domain are very mature and advanced [45]. I plan to revisit some control problems studied in the chemical physics literature in the last decades by using these geometric tools. As a first example, we have completely solved the question of the optimal control of two-level dissipative quantum systems whose dynamics is governed by the Lindblad equation. This shows the efficiency of geometric techniques which combined with numerical simulations allow to handle such control problems [45]. We have used the Pontryagin Maximum Principle to select extremal curves that are solutions of a Hamiltonian system and candidates as minimizers. The optimal solutions are extracted from the analysis of the Hamiltonian dynamics combined with second-order necessary and sufficient conditions. The next step consists now in applying such techniques to more complicated systems having for instance three or four levels or corresponding to the coupling of two spin systems. Applications in quantum information or in NMR are also planed.

The following diagram presents a complete overview of my research activity. The mathematical study of the dynamics of Hamiltonian systems is at the heart of my project. Such an analysis can be applied both to control systems via the Pontryagin Maximum Principle or to study integrable approximations constructed from canonical perturbation theory. As a physicist, my main interest resides in the use of these advanced and modern mathematical techniques to analyze a large variety of physical systems. In this approach, powerful numerical algorithms are also used, in order to be as close as possible to potential experimental applications.



Molecular rotation
Optimal control theory
of quantum systems
(Pontryagin Maximum Principle)
Quantum information
Chemical systems
NMR
Hamiltonian dynamical systems
Hamiltonian monodromy
Spectroscopy
Integrable approximations
(Canonical perturbation theory)
Infinite degrees of
freedom systems

Chapitre 4

Structure of dynamical systems

4.1 Canonical perturbation theory and spectroscopy of molecular systems

Corresponding articles : [26, 27, 29, 30, 31, 32, 33, 34, 35]
This work was done during my PhD thesis with M. Joyeux of the *Laboratoire de Spectrométrie Physique* in Grenoble and with some collaborators such as E. Sibert, R. Shinke, M. Lombardi and R. Jost.

Canonical perturbation theory is a powerful tool in the field of molecular physics. It consists in a series of canonical transformations (or unitary ones in quantum mechanics), which are aimed at rewriting the Hamiltonian of the system in a simpler form (that is, in terms of as many classical constants of the motion or good quantum numbers as possible) without modifying the dynamics of the molecule. Until our work with M. Joyeux, explicit high order calculation schemes had been performed only for motions around a single minimum, so that only rigid molecules moving on an uncoupled Born-Oppenheimer electronic surface could be investigated. In order to overcome the restrictive hypotheses of this formalism, we derived two modified versions of canonical perturbation theory. The first one applies to floppy systems with several equilibrium positions (the HCN/CNH molecule is considered as an example) [29, 33, 35] and the second one to nonadiabatic dynamics (i.e. non Born-Oppenheimer dynamics) [29, 30, 31]. This later procedure

has been applied to a simple model which mimics the NO_2 molecule. This work has been pursued by M. Joyeux to study more complex systems such as the hydrogen peroxide H_2O_2 [72] and to construct an accurate effective Hamiltonian of the NO_2 molecule [73].

We have also shown that the use of effective Hamiltonians, obtained from canonical perturbation theory, simplifies drastically the discussion of the highly excited vibrational dynamics in terms of classical bifurcations and periodic orbits. The HCN, HCP and $HOCl$ molecules are discussed in detail [32, 33, 34]. The fact that the quantum dynamics looks much more regular than the classical one is also illustrated for the $HOCl$ molecule [32].

More recently, I have published two works in this field. In [26], we use the canonical perturbation theory to determine a series of zero-point energies of all stable isotopologues of the NO_2, O_3, SO_2 and CO_2 molecules. In each case, we derive an effective Hamiltonian from a kinetic energy depending upon the mass of the atoms (and therefore upon the isotopologues) and from known ab initio potential energy surfaces. We then determine the zero point energies from the different effective Hamiltonians. We finally analyze the agreement between experimental results and the ones given by canonical perturbation theory. The accuracy of the theoretical values obtained show that this method can be used in spectroscopy. In [27], we show how to generalize the canonical perturbation theory to time-dependent Hamiltonians controlled by laser fields of short durations with respect to the period of the field-free dynamics. This perturbation theory which is analogous in its spirit to the interaction picture, consists of a series of unitary transformations aiming at rewriting the evolution operator as a product of other propagators. This theory is applied to the control of molecular orientation by zero area laser pulses (see the corresponding section).

We reproduce here the article [29] which is a review article of the different works on Canonical Perturbation Theory. This paper presents new formulations of Canonical Perturbation Theory proposed to treat either semi-rigid molecules, floppy molecules or non Born-Oppenheimer dynamics.

CANONICAL PERTURBATION THEORY FOR HIGHLY EXCITED DYNAMICS

Marc JOYEUX and Dominique SUGNY,

Laboratoire de Spectrométrie Physique (CNRS UMR 5588), Université Joseph Fourier – Grenoble I,

BP 87, 38402 St Martin d'Hères, FRANCE

ABSTRACT : This article proposes an unified presentation of recent results dealing with canonical perturbation theory (also called contact transformation method in the quantum mechanical context), which show how the theory is best handled for investigating the highly excited dynamics of small molecules. The following systems are successively addressed : (i) semi-rigid molecules (one electronic surface, one minimum), (ii) floppy molecules (one electronic surface, several minima) and (iii) non-Born Oppenheimer dynamics (several interacting electronic surfaces). The perturbative Hamiltonians obtained from the proposed procedures are checked against exact calculations performed on *ab initio* surfaces (HCP and HCN) and model Hamiltonians.

RESUME : Cet article propose une présentation unifiée de résultats récents portant sur la théorie des perturbations canoniques (aussi appelée la méthode des transformations de contact en mécanique quantique), qui ont montré comment utiliser au mieux les divers degrés de liberté de la théorie pour étudier la dynamique de molécules très excitées. On s'intéresse successivement aux systèmes suivants : (i) les molécules semi-rigides (une seule surface électronique, un seul minimum), (ii) les molécules souples (une seule surface électronique, plusieurs minima) et (iii) la dynamique non-Born Oppenheimer (plusieurs surfaces électroniques couplées). Les Hamiltoniens perturbatifs que l'on obtient par les procédures décrites dans cet article sont comparés à des calculs quantiques exacts portant sur des surfaces d'énergie potentielle *ab initio* (pour HCP et HCN) et des Hamiltoniens modèles.

1 - INTRODUCTION

Exact quantum energy levels and wave functions being obtained from the diagonalization of (usually) large Hamiltonian matrices, physicists have been unable to compute the exact spectrum of all but the most simple systems until rather recently. Fortunately, theoretical tools have been developed very early, which allow a precise determination of the quantum spectrum at low energies without having recourse to direct diagonalization. These tools are known as perturbation methods. Their role in the development of quantum mechanics was emphasized by Kemble : “In quantum mechanics… perturbation methods are of fundamental importance due to the fact that so few problems can be rigorously solved by direct attack” [1]. The oldest perturbation theory is known as Rayleigh-Schrödinger's method [2]. It was, however, quickly recognized that this method requires “tedious summations over a large number of intermediate states and that there is a large degree of cancellation in the final algebraic reductions” [3]. Beyond first order of the theory, an other method, known as canonical perturbation theory (CPT) (or the contact transformation method), is better suited for the purpose of practical calculations. CPT was first introduced in physics by Van Vleck to investigate spin multiplets and σ-type doubling in the spectra of diatomic molecules [4] and was applied ten years later by Nielsen, Shaffer and Thomas to the vibration-rotation problem in polyatomic molecules [5-7]. The 1951 review paper by Nielsen [8] can be considered as a pillar of high-resolution spectroscopy.

Modern computers and algorithms make it possible to calculate variationally the whole rovibrational spectrum of triatomic molecules from the ground state up to the dissociation threshold and more (several hundreds of converged states) while, roughly, the first hundred states of tetratomic molecules and the first ten states of pentatomic molecules are becoming gradually amenable to calculations. This, however, does not diminish the practical importance of CPT, for two principal reasons. First, variational calculations are still not routine and remain reserved to specialists. In contrast, the perturbative computation of the spectrum of molecules with up to five atoms requires little programming effort and CPU time. This point of view was recently investigated in detail by Sibert and co-workers [9-12]. Moreover, the perturbative Hamiltonian obtained from CPT is expressed in terms of an as complete as possible set of good quantum numbers, so that this Hamiltonian is a very convenient starting point for understanding the dynamics of a molecule, especially when subjected to a semiclassical analysis (see for example Refs. [13,14]; for recent reviews see Refs. [15,16]). The main bridle to a still more widespread use of CPT in the domain of molecular physics is probably the long-standing idea that CPT is only suitable for studying the low-lying states of an uncoupled electronic surface of a semi-rigid molecule. The aim of this article is to report on some recent advances, which show that this is certainly not the case. More precisely, it will be shown how CPT must be handled to adapt to (i) highly excited vibrational states of molecules with a single equilibrium position (semi-rigid molecules), (ii) highly excited vibrational states of molecules with several equilibrium positions (floppy molecules) and (iii) highly excited vibrational states of molecules with several coupled electronic surfaces.

Part of the results presented below have already been published elsewhere [13,14,17-20]. However, a classical Birkhoff-Gustavson's perturbation method [21-24] was used in Refs. [13,17] and [14,18] to study the highly excited states of semi-rigid and floppy molecules, respectively, while the study of coupled electronic surfaces in Refs. [19,20] is necessarily based on the quantum mechanical Van Vleck's perturbation method [1,4,9,25-29]. Birkhoff-Gustavson's and Van Vleck's methods being conceptually rather different (although they lead to comparable results), all calculations have been performed again according to Van Vleck's formalism, for the sake of a clearer presentation and to emphasize more firmly the important points of the procedure. Moreover, we have just derived a more elegant and powerful method for studying floppy molecules than the one presented in Refs. [14,18], while the method for studying coupled electronic surfaces presented in Refs. [19,20] could be simplified without loss of precision. These new procedures are thus presented in Sects. 4 and 5, instead of those of Refs. [13,14,17,18].

The remainder of this article is organized as follows. The principles of Van Vleck's CPT are recalled in Sect. 2. How this theory are best handled for studying the highly excited vibrational dynamics of various systems is the subject of the next three sections : semi-rigid molecules are discussed in Sect. 3, floppy molecules in Sect. 4 and molecules with interacting electronic surfaces in Sect. 5. Some points which deserve further attention are finally briefly mentioned in Sect. 6.

2 – THE PRINCIPLES OF VAN VLECK'S PERTURBATION THEORY

Canonical perturbation methods rely on the fact that, given a unitary transformation U, a Hamiltonian H and its transform K

$$K = U\,H\,U^{-1} \tag{2.1}$$

have the same spectrum. Note, however, that the wave functions ψ of H and ϕ of K are obviously not identical, but are instead related through

$$\phi = U\,\psi\ . \tag{2.2}$$

CPT just consists of a series of unitary transformations like Eq. (2.1), which are aimed at finding the best set of conjugate coordinates (*i.e.* position coordinates and conjugate momenta) to express the Hamiltonian. Note that these transformations usually involve mixing of coordinates and momenta. What the "best" set of conjugate coordinates is largely depends on the context. For people like us, who are interested in dynamical studies and particularly in semiclassical analyses [13-16],

the best set of conjugate coordinates is the one for which the non-integrable part of the final Hamiltonian is as small as possible, this part being usually discarded for the purpose of semiclassical studies. Roughly speaking, the best set of conjugate coordinates are approximate actions and angles of the initial Hamiltonian. People like Sibert and co-workers, who are more concerned with the calculation of spectra and eigenvector related properties [9-12,28], are usually less demanding. Their goal is to find a set of conjugate coordinates for which the Hamiltonian matrix factorizes into blocks of easily diagonalizable size, while the terms coupling the blocks should become as small as possible before they are neglected. As will be described in some detail in the next sections, the power of CPT lies in the existence of simple algorithms for transforming gradually from the initial set of conjugate coordinates to the final one.

Lengyel suggested to Kemble [1] that the transformation U should be given the form

$$U = \exp(\mathrm{i}S) \ , \tag{2.3}$$

where S is hermitian, and this form has been widely adopted since then. We instead prefer to use a slightly different form for U, namely

$$U = \exp(S) \ , \tag{2.4}$$

where S is anti-hermitian, because Eq. (2.4) leads to real coefficients for all the computed series (see below), while Eq. (2.3) leads to purely imaginary ones. Let us recall that the exponential of an operator is defined as

$$\exp(S) = \sum_{k=0}^{\infty} \frac{1}{k!} S^k = 1 + S + \frac{S^2}{2} + \frac{S^3}{6} + \ldots \ . \tag{2.5}$$

The reason for writing U in the form of Eq. (2.4) is twofold. First, the inverse transformation is just $U^{-1} = \exp(\text{-}S)$. Moreover, if S is small enough, as must be the case for every perturbation procedure, then, according to Eq. (2.5), the transformation consists of the identity plus corrections, the importance of which decreases with power. The perturbation procedure therefore consists in finding a series of anti-hermitian operators $S^{(k)}$, such that

$$\begin{aligned} H^{(1)} &= \exp(S^{(1)})\, H^{(0)} \exp(\text{-}S^{(1)}) \\ H^{(2)} &= \exp(S^{(2)})\, H^{(1)} \exp(\text{-}S^{(2)}) \\ &\vdots \\ H^{(s)} &= \exp(S^{(s)})\, H^{(s-1)} \exp(\text{-}S^{(s)}) \quad , \\ &\vdots \end{aligned} \tag{2.6}$$

where $H^{(0)} = H$ is the initial Hamiltonian and s=1,2,... is the perturbation order. Simple algebra shows that the transformation at any order s can be rewritten in the most useful form

$$\begin{aligned} H^{(s)} &= H^{(s-1)} + [S^{(s)}, H^{(s-1)}] \\ &\quad + \frac{1}{2!}[S^{(s)},[S^{(s)}, H^{(s-1)}]] \\ &\quad + \frac{1}{3!}[S^{(s)},[S^{(s)},[S^{(s)}, H^{(s-1)}]]] + \ldots \quad , \end{aligned} \tag{2.7}$$

where square brackets denote the commutator of two operators, *i.e.* $[A,B] = AB - BA$. Eq. (2.7) is known as Campbell-Hausdorf's formula. At this point, it should be clear that high-order perturbative calculations can only be performed for relatively simple expressions of the initial Hamiltonian, because the evaluation of the nested commutators in Eq. (2.7) rapidly becomes cumbersome for too complex expressions. This is the reason, why the first step of most of the perturbative calculations dealing with semi-rigid molecules usually consists of a Taylor expansion of the exact Hamiltonian in the neighbourhood of the equilibrium position. Nonetheless, there is some freedom in the form of the expansion that is chosen as input Hamiltonian in perturbative calculations. Trigonometric expansions are for example also amenable to perturbative calculations [14,18,30-35]. It will be shown in Sect. 4, that mixed polynomial/trigonometric expansions are best suited for studying the vibrational dynamics of floppy molecules. A further remark concerns kinetic energy. Indeed, it is well-known that the exact quantum expression for kinetic energy contains extra-potential terms compared to the symmetrized classical expression [36]. These terms might be rather lengthy to calculate, while their influence on eigenvalues and eigenvectors is expected to remain small, usually less than 1 cm^{-1} [37]. In order not to let perturbative calculations become unnecessarily complex, we chose to systematically neglect these extra-potential terms, that is

to simply expand and symmetrize the classical expression for kinetic energy.

The principal flexibility of CPT's consists obviously of the choice of the operator $S^{(s)}$ at each order s of the perturbation procedure. Although not mandatory [20], this choice is usually guided by the introduction of an artificial book-keeping parameter λ, the "meaning of which is to show the order of magnitude of the product of two or more operators having various orders of magnitudes and group the products accordingly" [29] (λ is set to 1 at the end of the calculations). More precisely, each interpolation Hamiltonian $H^{(s)}$ is expanded in the form

$$H^{(s)} = \sum_k \lambda^k H^{(s,k)} \ , \tag{2.8}$$

while the transformation at order s writes

$$H^{(s)} = \exp(\lambda^s S^{(s)})\, H^{(s-1)}\, \exp(-\lambda^s S^{(s)}) \ . \tag{2.9}$$

After expansion according to Campbell-Hausdorf's formula, one gets, by equating the powers of λ

$$\begin{aligned}
&\text{if } k < s, \quad H^{(s,k)} = H^{(s-1,k)} \\
&\text{if } k = s, \quad H^{(s,s)} = H^{(s-1,s)} + [S^{(s)}, H^{(0,0)}] \\
&\text{if } k > s, \quad H^{(s,k)} = H^{(s-1,k)} \\
&\qquad + \sum_m \frac{1}{n!} [\underbrace{S^{(s)}, \ldots [S^{(s)}}_{n \text{ times}}, H^{(s-1,m)}] \ldots]
\end{aligned} \tag{2.10}$$

(in the last equation, the summation runs over all the integers m, for which there exists another integer n larger than or equal to 1, such that $m + n\,s = k$). The first equation in Eq. (2.10) shows that the transformation at order s does not affect the terms of order smaller than s. The second equation in Eq. (2.10) is used to determine the operator $S^{(s)}$, by requiring that $H^{(s,s)}$ contains only the physically important terms of $H^{(s-1,s)}$ or, equivalently, that the second term in the right-hand side of this equation cancels the Hermitian subset $R^{(s-1)}$ of $H^{(s-1,s)}$, which contains the physically unimportant terms. Consequently, the operator $S^{(s)}$ is obtained as the solution of

$$[S^{(s)}, H^{(0,0)}] = -R^{(s-1)} \ , \tag{2.11}$$

while the sum of the physically important terms up to order s, *i.e.*

$$K^{(s)} = \sum_{k=0}^{s} H^{(s,k)} = \sum_{k=0}^{s} H^{(k,k)} \tag{2.12}$$

is called the perturbative Hamiltonian of order s.

It is important to realize that the choice of $H^{(0,0)}$ is of crucial importance, because the possibility to solve Eq. (2.11) with reasonable effort is governed by this choice. The remaining adjustment possibilities of the procedure in Eqs. (2.8)-(2.11) are (i) the partition of the initial Hamiltonian $H^{(0)} = H$ into each of the $H^{(0,k)}$'s, and (ii) the choice of the terms of $H^{(s-1,s)}$ which should be put into $R^{(s-1)}$ to be cancelled by the transformation at order s. How these adjustments are best performed for studying the highly excited vibrational dynamics of molecules with a single or several equilibrium positions, as well as the dynamics on coupled electronic surfaces, will be the subject of the next three sections.

3 – APPLICATION TO SEMI-RIGID MOLECULES

This section is devoted to the application of CPT to the study of the highly excited vibrational dynamics of molecules with a single equilibrium position. Use of CPT for analyzing the low-energy portion of the spectrum has already attracted much attention (see for example Refs. [3,5-8,27]), while its application to the intermediate-energy spectrum has principally been investigated by Sibert and co-workers [9-12,28,38-43] and Jaffé, Reinhardt and co-workers [44-49]. We shall therefore lay emphasis on the specificity of high-energy perturbative calculations, *i.e.* the need for a careful choice of the terms to be put in the successive $R^{(s-1)}$'s to insure convergence up to high orders of the theory. As in Refs. [13,17], the *ab initio* surface for HCP and the associated rotationless bound states calculated by Schinke and co-workers [50,51] will be used for the purpose of illustration.

As explained in Sect. 2, the classical *ab initio* Hamiltonian (expressed in terms of curvilinear internal coordinates [17]) is first expanded in Taylor series in the neighbourhood of the equilibrium position and symmetrized. The obtained polynomial is then rewritten in terms of conjugate sets of dimensionless normal coordinates (p_j, q_j) by using Wilson's GF method [52]

(q_j is the position coordinate and $p_j = -\mathrm{i}\,\partial/\partial q_j$ its conjugate momentum). The goal of this linear canonical transformation is to rewrite the quadratic part of the expansion as a sum of uncoupled harmonic oscillators (see Eq. (3.4) below). One next converts the Hamiltonian to creation and annihilation operators, according to

$$\begin{aligned} q_j &= \frac{1}{\sqrt{2}}(a_j^+ + a_j) \\ p_j &= \frac{\mathrm{i}}{\sqrt{2}}(a_j^+ - a_j)\,, \end{aligned} \tag{3.1}$$

for non-degenerate coordinates, like the CH stretch (mode j=1) and the CP stretch (mode j=3) of HCP, and

$$\begin{aligned} q_j^2 &= a_{jg}^+ a_{jg} + a_{jd}^+ a_{jd} + a_{jg}^+ a_{jd}^+ + a_{jg} a_{jd} + 1 \\ p_j^2 &= a_{jg}^+ a_{jg} + a_{jd}^+ a_{jd} - a_{jg}^+ a_{jd}^+ - a_{jg} a_{jd} + 1 \\ q_j p_j &= \mathrm{i}\,(a_{jg}^+ a_{jd}^+ - a_{jg} a_{jd})\,, \end{aligned} \tag{3.2}$$

for doubly degenerate coordinates, like the bend (mode j=2) of HCP. In Eq. (3.2), the subscripts g and d stand for "gauche" (left) and "droit" (right), respectively. It is recalled that the commutation relations involving these operators write

$$\begin{aligned} [a_i, a_j] &= 0 \\ [a_i, a_j^+] &= \delta_{ij} \,, \end{aligned} \tag{3.3}$$

where δ_{ij} is Kronecker's symbol and i and j take the values 1, 2g, 2d and 3 for HCP. One then proceeds to the partition of the initial Hamiltonian by putting each term with total degree k+2 in $H^{(0,k)}$, so that

$$\begin{aligned} H^{(0,0)} &= \sum_j \omega_j (a_j^+ a_j) \\ H^{(0,k)} &= \sum_{\|\mathbf{m}+\mathbf{n}\|=k+2} h_{\mathbf{mn}}^{(0)} \prod_j (a_j^+)^{m_j} (a_j)^{n_j} \end{aligned} \tag{3.4}$$

(k≥1), where the ω_j's are the fundamental frequencies, $\mathbf{m} = (m_1, m_2, ...)$ and $\mathbf{n} = (n_1, n_2, ...)$ are two vectors of positive integers, $\mathbf{m}+\mathbf{n}$ is the sum $m_1 + n_1 + m_2 + n_2 + \ldots$, and the $h_{\mathbf{mn}}^{(0)}$'s are real coefficients, which satisfy $h_{\mathbf{mn}}^{(0)} = h_{\mathbf{nm}}^{(0)}$. With this definition of $H^{(0,0)}$, the resolution of Eq. (2.11) turns out to be very simple. Indeed, if the hermitian subset $R^{(s-1)}$ of $H^{(s-1,s)}$ to be cancelled at order s of the perturbation procedure is of the form

$$R^{(s-1)} = \sum_{\|\mathbf{m}+\mathbf{n}\|=s+2} c_{\mathbf{mn}}^{(s-1)} \prod_j (a_j^+)^{m_j} (a_j)^{n_j} \,, \tag{3.5}$$

then the solution of Eq. (2.11) is just

$$S^{(s)} = \sum_{\|\mathbf{m}+\mathbf{n}\|=s+2} \frac{c_{\mathbf{mn}}^{(s-1)}}{\sum_j (m_j - n_j)\omega_j} \prod_j (a_j^+)^{m_j} (a_j)^{n_j} \tag{3.6}$$

(note that $S^{(s)}$ is indeed anti-hermitian). We now have all the theoretical tools for applying CPT to the study of the highly excited dynamics of semi-rigid molecules handy. Let us however emphasize, as noted by Sibert [9], that "a crucial feature of the computational procedure is that all the operators be expressed in a single form". Like Sibert, we have chosen to write all the creation operators first, as in Eqs. (3.4)-(3.6). Evaluation of the commutators in Eq. (2.10) requires that many terms of the form $(a_j^+)^{m_j}(a_j)^{n_j}(a_j^+)^{m'_j}(a_j)^{n'_j}$ be rewritten in the standard form. This is readily accomplished by using Sibert's formula in Eq. (2.11) of Ref. [9].

The principal point one can play with to favor the convergence of the perturbation series is the choice, at each order s of the perturbation procedure, of the terms of $H^{(s-1,s)}$ to keep in $H^{(s,s)}$ or, conversely, to put in $R^{(s-1)}$ to be cancelled. Examination of Eq. (3.6) shows that terms of $H^{(s-1,s)}$ with $\mathbf{m} = \mathbf{n}$ must necessarily be kept in $H^{(s,s)}$ in order for the denominator not to diverge. The simplest perturbative Hamiltonian is obtained by putting all the other terms in $R^{(s-1)}$. After s transformations, one is thus left with a perturbative Hamiltonian of the form

$$K^{(s)} = \sum_{\|\mathbf{m}\|\le s/2+1} h_{\mathbf{mm}}^{(s)} \prod_j (a_j^+)^{m_j} (a_j)^{m_j} \,. \tag{3.7}$$

Upon linear expansion of each $(a_j^+)^{m_j}(a_j)^{m_j}$ operator in terms of the $(a_j^+ a_j)^{m_j}$ ones, the perturbative Hamiltonian writes

$$K^{(s)} = K_D^{(s)} = \sum_j \nu_j^{(s)} (a_j^+ a_j) + \sum_{j\le k} x_{jk}^{(s)} (a_j^+ a_j)(a_k^+ a_k) + \ldots \tag{3.8}$$

where the right-hand side of the equation contains terms with total degree up to s+2. This is just the well-known Dunham polynomial expansion. Since

$a_j^+ a_j |v_j\rangle = v_j |v_j\rangle$, the Dunham expansion is diagonal in the direct product basis of harmonic oscillators. The convergence properties of the series of Dunham Hamiltonians are illustrated in Fig. 1, where the arithmetic average error between the energies of the exact states of HCP [50,51] and those obtained from perturbation procedure are plotted as a function of the perturbation order s. Included in the calculations are the first 323 states of HCP, with energies up to 17700 cm^{-1} above the quantum mechanical ground state, that is more than 75% of the energy of the CPH saddle. These levels contain up to 30 quanta of excitation in the bend degree of freedom. It is seen in Fig. 1 that perturbation calculations diverge for orders s larger than 3, the average arithmetic error at order s=3 being still as large as 159 cm^{-1}.

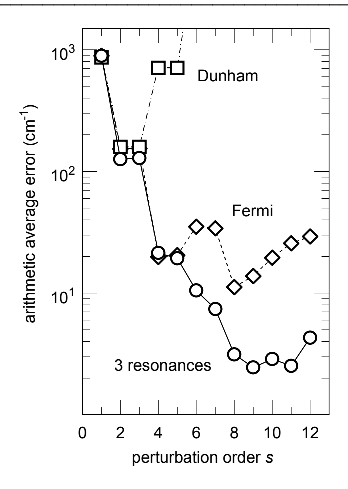


Figure 1 : *Plot, as a function of the perturbation order s, of the arithmetic average error between the energies of the eigenstates of HCP obtained from "exact" variational calculations [50,51] and from perturbative ones. The results for the Dunham expansions of Eq. (3.8) are indicated with squares, those for the Fermi resonance Hamiltonians of Eq. (3.10) with losanges and those for the Hamiltonians with three resonances with circles. These later Hamiltonians include the Fermi resonance $2\omega_2 - \omega_3 \approx 0$, its first harmonics $4\omega_2 - 2\omega_3 \approx 0$ and the additional resonance $2\omega_2 \approx 0$. Included in the calculations are the first 323 states of HCP, with energies up to 17700 cm^{-1} above the quantum mechanical ground state, i.e. more than 75% of the energy of the CPH saddle. These levels contain up to $v_2 = 30$ quanta of excitation in the bend degree of freedom.*

When looking at the shape of the wave functions [50,51] and at the fundamental frequencies of HCP (ω_1=3479 cm^{-1}, ω_2=650 cm^{-1}, ω_3=1256 cm^{-1}), one realizes that this early divergence of the perturbation series is probably due to a Fermi resonance between the bend (mode 2) and the CP stretch (mode 3). One says that the fundamental frequencies are approximately resonant if there exist two vectors $\mathbf{m}^*$ and $\mathbf{n}^*$ of positive integers, such that

$$\sum_j (m_j^* - n_j^*)\omega_j \approx 0 \tag{3.9}$$

According to Eq. (3.6), the operators $S^{(s)}$ and the perturbation series diverge if the terms of $H^{(s-1,s)}$ such that $\mathbf{m}-\mathbf{n} = \pm(\mathbf{m}^* - \mathbf{n}^*)$ are put in $R^{(s-1)}$ when the resonance condition of Eq. (3.9) is satisfied. Therefore, these terms must necessarily be kept in $H^{(s,s)}$. After linear expansion of each $(a_j^+)^{m_j}(a_j)^{m_j}$ operator in terms of the $(a_j^+ a_j)^{m_j}$ ones, the perturbative Hamiltonian is thus obtained in the form

$$\begin{aligned} K^{(s)} &= K_D^{(s)} + K_R^{(s)} \\ K_R^{(s)} &= \left\{\prod_j (a_j^+)^{m_j^*}\right\} \times \\ &\quad \left\{k^{(s)} + \sum_j k_j^{(s)}(a_j^+ a_j) + \ldots\right\}\left\{\prod_j (a_j)^{n_j^*}\right\}, \end{aligned} \tag{3.10}$$

where $K_D^{(s)}$ is the Dunham expansion of Eq. (3.8) and the right-hand side of the second equation again contains terms with total degree up to s+2. It is of course possible to take two (or more) resonances simultaneously into account. When doing so, the perturbative Hamiltonian $K^{(s)}$ consists of the Dunham expansion $K_D^{(s)}$ plus two (or more) resonance terms $K_R^{(s)}$. It should however be kept in mind that each additional linearly independent resonance destroys one good quantum number and consequently increases the size of the matrices to diagonalize. Moreover, from the dynamical point of view, the Hamiltonians with two (or more) independent resonances are at least partially chaotic, while those with zero or one resonance are completely integrable and

therefore best suited for the purpose of semiclassical investigations.

Because of the degeneracy of the bending motion, the Fermi resonance $2\omega_2 - \omega_3 \approx 0$ between the bend (mode 2) and the CP stretch (mode 3) of HCP is described by the vectors $\mathbf{m}^* = (m_1^*, m_{2g}^*, m_{2d}^*, m_3^*) = (0,1,1,0)$ and $\mathbf{n}^* = (n_1^*, n_{2g}^*, n_{2d}^*, n_3^*) = (0,0,0,1)$. Since both v_1 (the number of quanta in the CH stretch) and $P = v_2 + 2v_3$ (P is called the polyad number) are good quantum numbers for the Fermi resonance Hamiltonian (*i.e.* the perturbative Hamiltonian with the $2\omega_2 - \omega_3 \approx 0$ resonance), the eigenstates are obtained from the diagonalization of very small matrices of size $P/2+1$ [13,15,53]. The convergence properties of the series of Fermi resonance Hamiltonians are illustrated in Fig. 1. It is seen that they perform much better than the Dunham expansions, because convergence is obtained up to 8th order of the theory. At this order, the average arithmetic error is 11.2 cm^{-1}. A closer examination of exact and perturbative energies reveals that a vast majority of states is accurately reproduced by the Fermi resonance Hamiltonian, while a dozen states with $v_2 \geq 22$ have considerably larger errors that range up to 394 cm^{-1}.

A systematic search for additional resonances must next be undertaken to improve the calculation of the states with the largest values of v_2. It turns out that excellent results are obtained upon simultaneous introduction in the perturbative Hamiltonian of the first harmonics $4\omega_2 - 2\omega_3 \approx 0$ of the Fermi resonance, which is characterized by the vectors $\mathbf{m}^* = (0,2,2,0)$ and $\mathbf{n}^* = (0,0,0,2)$, and the $2\omega_2 \approx 0$ resonance with vectors $\mathbf{m}^* = (0,1,1,0)$ and $\mathbf{n}^* = (0,0,0,0)$. When taking the three resonances into account, there is only one good quantum number left, namely v_1, the number of quanta in the CH stretch, but the size of the matrices to diagonalize still remains very small compared to exact quantum calculations. As can be checked in Fig. 1, the convergence properties of the three-resonance Hamiltonians are again substantially better than those of the Fermi resonance Hamiltonians. As shown in the upper panel of Fig. 2, an average error as small as 2.45 cm^{-1} is obtained at order s=9, with only one error larger than 20 cm^{-1}, that for the state with the maximum number of quanta (v_2=30) in the bend. Comparison of the two panels of Fig. 2 further shows that the errors for most states are again substantially reduced when s increases from s=9 to s=11. Unfortunately, the errors for the four states with the largest values of v_2 diverge again, so that the average error remains nearly constant. The divergence for the states with the largest values of v_2 is here principally due to the fact that the polynomial Taylor expansion fails to reproduce correctly the potential energy surface for the largest values of the bending angle.

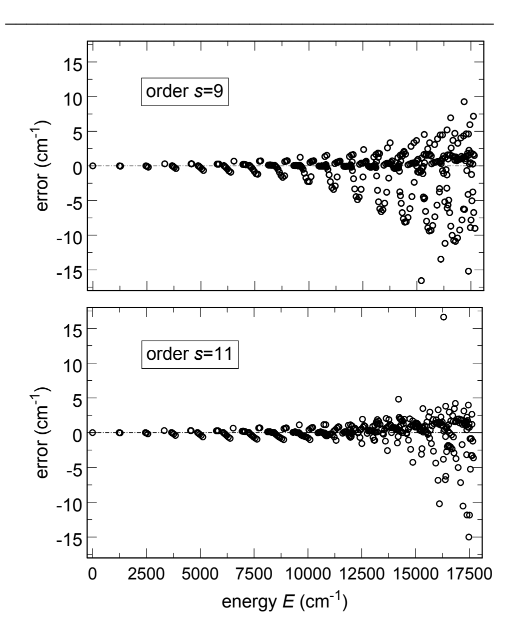


Figure 2 : *Plot, as a function of the energy of each state, of the difference between exact and perturbative quantum energies for the first 323 states of HCP at 9th (top plot) and 11th (bottom plot) order of the theory. The perturbative Hamiltonians take the three resonances $2\omega_2 - \omega_3 \approx 0$, $4\omega_2 - 2\omega_3 \approx 0$ and $2\omega_2 \approx 0$ into account. At order s=9, the error for the lowest state of polyad $[v_1, P]$=[0,30], which is calculated at 95 cm^{-1}, lies out of the plotting range. At order s=11, the errors for the lowest state of polyads [0,26], [0,28], [0,30] and [1,24], as well as for the second lowest state of polyad [0,30], which are calculated at 36, 111, 191, 20 and 51 cm^{-1}, respectively, lie out of the plotting range.*

It is interesting to note that convergence properties very close to those of the three-resonance Hamiltonians are obtained when computing the eigenstates of the Fermi resonance Hamiltonians, but with the parameters $\nu_j^{(s)}$, $x_{jk}^{(s)}$,..., $k^{(s)}$, $k_j^{(s)}$,... of the three-resonance Hamiltonians [17]. The semiclassical analysis of this later Fermi resonance Hamiltonian provides unparalleled insight into the highly excited vibrational dynamics of HCP and particularly the saddle-node bifurcation, which is the first step of the HCP↔CPH isomerization process [13,15,16,53].

4 – APPLICATION TO FLOPPY MOLECULES

This section is devoted to the application of CPT to the study of the highly excited vibrational dynamics of floppy molecules. The procedure described below is an improved version of the work published in Refs [14,18]. As in this earlier work, the *ab initio* surface for HCN computed by Murrell, Carter and Halonen [54] and the corresponding rotationless bound states calculated by Bacic [55] will be used for the purpose of illustration.

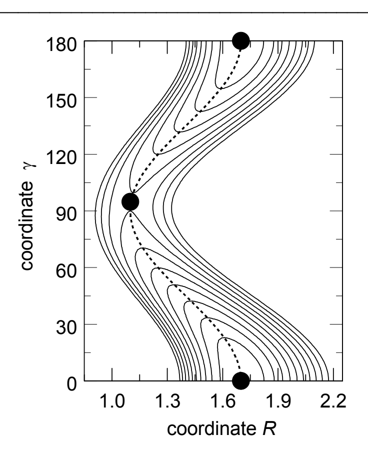


Figure 3 : *Contour plot of the typical potential energy surface of a floppy molecule. The black dots at γ=0° and γ=180° denote the two equilibrium positions, while the black dot around γ=95° indicates a saddle. The dotted line is the minimum energy path (MEP), which connects the three extrema. The coordinate γ (vertical axis) is called a reactive coordinate and the coordinate R (horizontal axis) an inactive one.*

The typical potential energy surface of floppy molecules is schematized in Fig. 3. It is characterized by the existence of at least two equilibrium positions, which are separated by saddle points. A "minimum energy path" (MEP), also called "reaction pathway", connects the different equilibrium positions and the saddles. In Fig. 3, the equilibrium positions are the two black dots at γ=0° and γ=180°, the saddle is the black dot at about γ=95° and the reaction pathway is the dotted line. The perturbative Hamiltonian we are looking for must reproduce accurately the states of the initial Hamiltonian in both wells up to and above the isomerization barrier. It is clearly seen in Fig. 3 that the vibrational degrees of freedom can be separated into two different families. The first family includes those coordinates, whose variation leads from one well to another well, and which will therefore be called "reactive coordinates". The second family includes all the other coordinates, whose variation remains localized in one well, and which will henceforth be described as "inactive coordinates". Coordinate γ of Fig. 3 is a reactive coordinate, while *R* is an inactive one. In most cases, the dynamics of small floppy molecules involves a single reactive coordinate (generally an angle) and several inactive ones. For example, the two Jacobi coordinates *r* and *R* behave as inactive coordinates for the HCN↔CNH isomerization reaction, while the Jacobi angle γ is the reactive coordinate (*r* is the CN bond length, *R* the distance between H and the center of mass G of CN, and γ the HGN angle).

There exist at least two reasons, why the procedure described in the previous section cannot be used to study the dynamics of floppy molecules. First, the Taylor expansion in the neighbourhood of one equilibrium position is expected to describe correctly the corresponding well, but certainly not two (or more) of them. Moreover, treating a reactive mode as if it were an harmonic oscillator is bound to fail, since it behaves much more like an hindered rotor in the neighbourhood of the isomerization saddle and like a free rotor largely above the saddle. Inspired by previous work of Marcus [56-58], Miller and co-workers [59-61] and Chapuisat and co-workers [62-66], we have found that an excellent approximation of the *ab initio* Hamiltonian is obtained

from a mixed expansion of the *ab initio* Hamiltonian around the MEP. The first step for obtaining this expansion consists of a canonical transformation, according to

$$q_j \to q_j^0(\gamma) + z_j$$
$$\frac{\partial}{\partial\gamma} \to \frac{\partial}{\partial\gamma} - \sum_j \frac{\mathrm{d}q_j^0(\gamma)}{\mathrm{d}\gamma}\frac{\partial}{\partial z_j} \quad , \qquad (4.1)$$

where a single reactive coordinate γ has been assumed and the index j is restricted to inactive coordinates q_j. $q_j^0(\gamma)$ is the value of q_j on the MEP for each particular value of γ. The obtained Hamiltonian is then Taylor-expanded relative to the z_j's and Fourier-expanded relative to the reactive coordinate γ (for more details on the technical procedure, see Ref. [18]). Practically, the *ab initio* Hamiltonian for the HCN↔CNH system [54] was Fourier expanded up to $\cos(10\gamma)$. The obtained expression was next rewritten in terms of powers of $\cos\gamma$. Note that all the powers of $\cos\gamma$ that appear in the course of the calculations must be retained, even when larger than 10, in order for the perturbative Hamiltonian to remain hermitian. With the initial partition described below, the maximum power of $\cos\gamma$ increases like $10(s-2)$. After conversion of the z_j's and their conjugate momenta to creation-annihilation operators (*cf* Eqs. (3.1)-(3.2)), the initial Hamiltonian is thus of the form

$$H^{(0)} = \sum_{M,P,N,\mathbf{m},\mathbf{n}} h^{(0)}_{MPN\mathbf{mn}} (\cos\gamma)^M \sigma^P (J^2)^N \times \prod_j (a_j^+)^{m_j} (a_j)^{n_j} \quad , \qquad (4.2)$$

where j is restricted to inactive coordinates. The $h^{(0)}_{MPN\mathbf{mn}}$'s are real coefficients. σ denotes the operator $\sin\gamma\frac{\partial}{\partial\gamma}$. The associated exponent P can take only the values 0 and 1. J^2 stands for the operator

$$J^2 = -\frac{1}{\sin\gamma}\frac{\partial}{\partial\gamma}\sin\gamma\frac{\partial}{\partial\gamma} - \frac{1}{(\sin\gamma)^2}\frac{\partial^2}{\partial\varphi^2} \quad , \qquad (4.3)$$

where φ is the rotation angle around the axis of inertia with smallest momentum. The matrix elements of these operators in the basis of the spherical functions $|\ell,m\rangle = Y_\ell^m(\gamma,\varphi)$ are easily obtained from

$$J^2|\ell,m\rangle = \ell(\ell+1)|\ell,m\rangle$$
$$\sigma|\ell,m\rangle = \ell\sqrt{\frac{(\ell-m+1)(\ell+m+1)}{(2\ell+1)(2\ell+3)}}|\ell+1,m\rangle - (\ell+1)\sqrt{\frac{(\ell-m)(\ell+m)}{(2\ell-1)(2\ell+1)}}|\ell-1,m\rangle \qquad (4.4)$$
$$\cos\gamma|\ell,m\rangle = \sqrt{\frac{(\ell-m+1)(\ell+m+1)}{(2\ell+1)(2\ell+3)}}|\ell+1,m\rangle + \sqrt{\frac{(\ell-m)(\ell+m)}{(2\ell-1)(2\ell+1)}}|\ell-1,m\rangle \quad .$$

The form of $H^{(0)}$ in Eq. (4.2) is thus particularly suitable for energy level calculations and will be preserved for each $H^{(s)}$ by the successive transformations. Note that the major advantage of the method presented here precisely lies in the fact that states with different values of the vibrational angular momentum m are treated simultaneously and on the same footing, while the older version of Refs. [14,18] required additional hard work for the states with m>0. As for semi-rigid molecules, it is of practical importance to express all the operators in a single standard form, which is chosen to be that of Eq. (4.2). Evaluation of the commutators in Eq. (2.10) then requires that many terms of the form $(\cos\gamma)^M\sigma^P(J^2)^N(\cos\gamma)^{M'}\sigma^{P'}(J^2)^{N'}$ be rewritten in the standard form. We did not try to derive a general formula, like Sibert's one for creation-annihilation operators [9]. Each product is instead iteratively recast in the normal form by using the following fundamental relations

$$\begin{aligned}
J^2(\cos\gamma)^M &= (\cos\gamma)^M J^2 + 2M(\cos\gamma)^{M-1}\sigma + M(M+1)(\cos\gamma)^M - M(M-1)(\cos\gamma)^{M-2}\\
J^2(\cos\gamma)^M\sigma &= (\cos\gamma)^M\sigma J^2 + 2(M+1)(\cos\gamma)^{M+1}J^2 - 2M(\cos\gamma)^{M-1}J^2 + M(M+1)(\cos\gamma)^M\sigma - M(M-1)(\cos\gamma)^{M-2}\sigma\\
\sigma(\cos\gamma)^M &= (\cos\gamma)^M\sigma + M(\cos\gamma)^{M+1} - M(\cos\gamma)^{M-1}\\
\sigma(\cos\gamma)^M\sigma &= (\cos\gamma)^{M+2}J^2 - (\cos\gamma)^M J^2 + M(\cos\gamma)^{M+1}\sigma - M(\cos\gamma)^{M-1}\sigma \quad .
\end{aligned} \qquad (4.5)$$

A crucial question concerns the partition of the initial Hamiltonian $H^{(0)}$ into the various $H^{(0,k)}$'s and

particularly the terms to be put into $H^{(0,0)}$. Since the resolution of Eq. (2.11) turns out to be quite difficult if $H^{(0,0)}$ depends on the reactive coordinate, $H^{(0,0)}$ must be chosen to contain only the sum of the harmonic oscillators associated with the inactive modes, that is

$$H^{(0,0)} = \sum_j \omega_j (a_j^+ a_j) \quad , \tag{4.6}$$

where the index j is however restricted to inactive coordinates. When doing so, the solution of Eq. (2.11) is very similar to Eqs. (3.5)-(3.6). Indeed, if

$$R^{(s-1)} = \sum_{M,P,N,\mathbf{m},\mathbf{n}} c_{MPN\mathbf{mn}}^{(s-1)} (\cos\gamma)^M \sigma^P (J^2)^N \times \prod_j (a_j^+)^{m_j} (a_j)^{n_j} \quad , \tag{4.7}$$

then the solution of Eq. (2.11) is just

$$S^{(s)} = \sum_{M,P,N,\mathbf{m},\mathbf{n}} \frac{c_{MPN\mathbf{mn}}^{(s-1)}}{\sum_j \omega_j (m_j - n_j)} (\cos\gamma)^M \times \sigma^P (J^2)^N \prod_j (a_j^+)^{m_j} (a_j)^{n_j} \quad , \tag{4.8}$$

where the index j is again restricted to inactive modes. There is more freedom for the ordering of the other terms. We found that a good choice, which warrants both rapid calculations and convergence up to high orders, consists in putting each term with indices *M*, *P*, *N*, **m** and **n** into $H^{(0,k)}$, where $k = \|\mathbf{m}+\mathbf{n}\| + P + 2N - 2$ if $M = 0$ and $k = \|\mathbf{m}+\mathbf{n}\| + P + 2N$ if $M > 0$. An exception obviously occurs for the pure bending terms J^2 and $\cos^M(\gamma)$, which are put into $H^{(0,1)}$ instead of $H^{(0,0)}$. Each $H^{(0,k)}$ is symmetrized after partition has been completed. Be careful that σ is not exactly antisymmetric, but satisfies instead

$$\sigma^+ = -\sigma - 2\cos\gamma \quad . \tag{4.9}$$

One now has all the necessary tools for studying floppy molecules handy. The question that naturally arises concerns the form of the perturbative Hamiltonian, that is, of the terms of $H^{(s-1,s)}$ to keep in $H^{(s,s)}$ or, conversely, to put in $R^{(s-1)}$ to be cancelled by the perturbation procedure. The simplest perturbative Hamiltonian is the one for which the number of quanta in each inactive mode remains a good quantum number. It is obtained by putting each term with indices *M*, *P*, *N*, **m** and **n**, such that $\mathbf{m} \neq \mathbf{n}$, into $R^{(s-1)}$. After linear expansion of each $(a_j^+)^{m_j}(a_j)^{m_j}$ operator in terms of the $(a_j^+ a_j)^{m_j}$ ones, the perturbative Hamiltonian is thus obtained in the form

$$K^{(s)} = \sum_{M,P,N,\mathbf{m}} k_{MPN\mathbf{m}}^{(s)} (\cos\gamma)^M \sigma^P (J^2)^N \prod_j (a_j^+ a_j)^{m_j} \tag{4.10}$$

Eq. (4.10) is the counterpart, for floppy molecules, of the Dunham expansion of Eq. (3.8). The convergence properties of this perturbative series are illustrated in Fig. 4, where the arithmetic average error between the energies of the exact states of HCN [55] and those obtained from the perturbative Hamiltonians of Eq. (4.10) are plotted as a function of the perturbation order *s*.

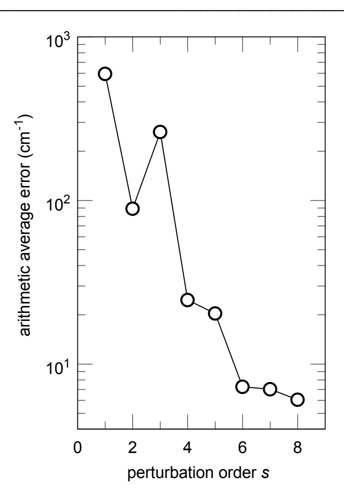


Figure 4 : *Plot, as a function of the perturbation order s, of the arithmetic average error between the energies of the eigenstates of HCN obtained from exact variational calculations [55] and from perturbative ones. The perturbative Hamiltonian, defined in Eq. (4.10), is formally a one-dimensional Hamiltonian (in the reactive coordinate γ) parametrized by the number of quanta in the CH and CN stretches. Included in the calculations are the first 111 states of the HCN↔CNH system, with energies up to 11770 cm^{-1} above the quantum mechanical ground state, that is, slightly above the isomerization saddle for pure bending states. These levels contain up to $v_2 = 44$ quanta of excitation in the bend degree of freedom.*

Included in the calculations are the first 111 states of the HCN↔CNH system, with energies up to 11770 cm^{-1} above the quantum mechanical ground state, that is, slightly above the barrier to linearity for pure bending states (two states are almost uniformly delocalized over the two wells). Note that we stopped comparison with exact quantum results at this energy because of the lack of reliable quantum results for larger values of the bend quantum number – not because of an abrupt degradation of the accuracy of the perturbative Hamiltonian. It is seen in Fig. 4 that the perturbation series converges rapidly up to order s=6 before remaining stationary at orders s=7 and s=8. At order s=6, very small $|\ell, m\rangle$ bases with $0 \le \ell \le 48$ and $m = 0$ are sufficient to converge the first 111 rotationless states of the perturbative Hamiltonian to better than 10^{-3} cm^{-1}. It can furthermore be checked in Fig. 5 that the error between the energies of exact and perturbative (6th order) quantum states increases smoothly with energy, although a few pairs of more resonantly coupled states are observed at the highest energies, *i.e.* close to the isomerization saddle for pure bending states.

The perturbative Hamiltonian of Eq. (4.10) is formally a one-dimensional system (in the reactive coordinate) parametrized by the number of quanta $v_j = a_j^+ a_j$ in the inactive modes j=1 (CH stretch) and j=3 (CN stretch). An illustration thereof is provided in Fig. 6, which shows the pseudo-potential curve and the probability density for the pure bending states of HCN. The pseudo-potential curve is obtained by setting J, σ, $v_1 = a_1^+ a_1$ and $v_3 = a_3^+ a_3$ to zero in Eq. (4.10). Being one-dimensional, the perturbative Hamiltonian is necessarily integrable (*i.e.* non chaotic). From the physical point of view, it is interesting to note that the "exact" HCN↔CNH system remains very close to the integrable perturbative Hamiltonian, even in the region close to the saddle where the classical dynamics is known to be largely chaotic. A similar situation was encountered while studying the dynamics of HOCl close to the dissociation threshold [67]. It was indeed found that an integrable Fermi resonance Hamiltonian accurately reproduces the dynamics of the exact system in this

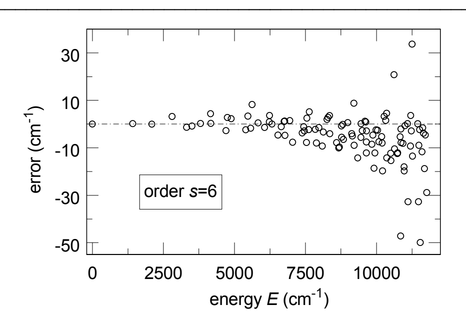


Figure 5 : *Plot, as a function of the energy of each state, of the difference between exact and perturbative quantum energies for the first 111 states of HCN at 6th order of the theory. The perturbative Hamiltonian is that of Eq. (4.10).*

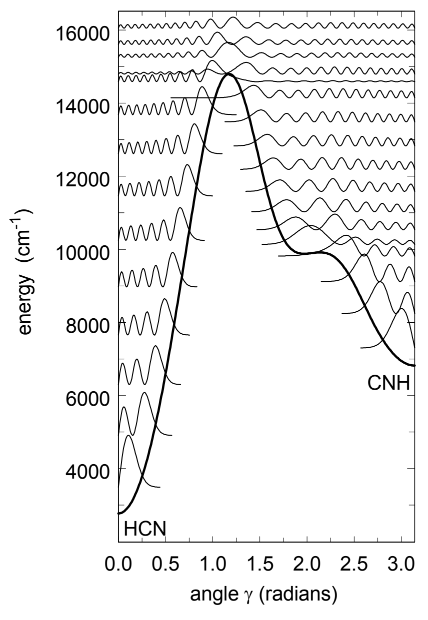


Figure 6 : *Plot, as a function of the bending angle γ, of the pseudo-potential (thick line) and the probability density (thinner lines) for the pure bending states ($v_1 = v_3 = 0$) of the HCN↔CNH system. These results are obtained by applying 6th order CPT to the ab initio surface of Murrell, Carter and Halonen [54]. The energies on the vertical axis are plotted relative to the minimum of the PES. The vertical scale is the same for all the probability plots and the baseline for each plot coincides, on the vertical axis, with the energy of the corresponding state.*

largely chaotic region of the phase space (see also Refs. [16,23,44-49]).

5 – APPLICATION TO NON-BORN-OPPENHEIMER DYNAMICS

This section is devoted to the application of CPT to the study of non-Born-Oppenheimer dynamics, that is, of vibrationally excited molecules on coupled electronic surfaces. The procedure described below is a simplified version of the work published in Ref. [19]. A still different scheme was presented in Ref. [20] but will not be discussed in this article, because it does not follow the general lines of Sect. 2. As in Refs. [19,20], a simple model with two 2-dimensional diabatic electronic surfaces coupled by a linear term will serve for the purpose of illustration, although the conclusions derived from Refs. [19,20] have recently been used to get a precise model of the conical intersection in NO_2 [68].

The diabatic vibronic Hamiltonian of a molecular system with two coupled electronic surfaces writes

$$\mathbf{H} = \begin{pmatrix} T+V_e & V_c \\ V_c & T+V_g \end{pmatrix} , \qquad (5.1)$$

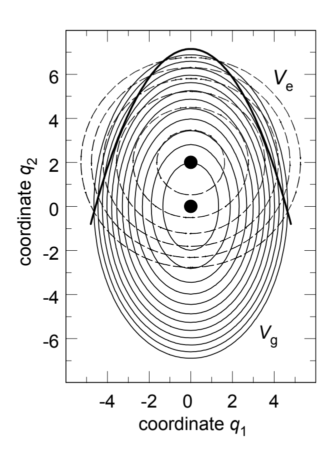


Figure 7 : *Contour plot of the ground V_g (solid lines) and excited V_e (dashed lines) diabatic surfaces of Eqs. (5.1)-(5.2). q_1 and q_2 are the dimensionless coordinates of the ground surface V_g. The contours range from 1500 to 18000 cm^{-1} for V_g and from 10500 to 18000 cm^{-1} for V_e, with increments of 1500 cm^{-1}. The two black dots indicate the minimum of each surface. Note that the minimum of the excited electronic surface V_e lies inside the well of the ground surface V_g. The thicker line indicates the crossing seam between the two surfaces.*

where T is the kinetic energy of the molecule and V_g, V_e and V_c are the diabatic ground, excited and coupling surfaces, respectively. As in Refs. [19,20], one takes

$$\begin{aligned} T &= \frac{1}{2}\omega_{1g} p_1^2 + \frac{1}{2}\omega_{2g} p_2^2 \\ V_g &= \frac{1}{2}\omega_{1g} q_1^2 + \frac{1}{2}\omega_{2g} q_2^2 \\ V_e &= \Delta E + \frac{1}{2}\frac{\omega_{1e}^2}{\omega_{1g}}(q_1 - q_{10}) + \frac{1}{2}\frac{\omega_{2e}^2}{\omega_{2g}}(q_2 - q_{20})^2 \\ V_c &= \lambda\, q_1 , \end{aligned} \qquad (5.2)$$

that is, the ground and excited surfaces are the sum of two uncoupled harmonic oscillators with centre shift and frequency mismatch, while the coupling surface is just the linear term, which is known to dominate the conical intersection of NO_2 and several other polyatomic molecules [69-74]. Note that the Hamiltonian in Eq. (5.2) is written in terms of the normal coordinates of the ground electronic surface V_g. As in Refs. [19,20], numerical values are ω_{1g}=1669 cm^{-1}, ω_{2g}=759 cm^{-1}, ω_{1e}=1000 cm^{-1} and ω_{2e}=745 cm^{-1} for the fundamental frequencies of V_g and V_e, ΔE=9700 cm^{-1} for the energy shift between the bottoms of the two surfaces, q_{10}=0 and q_{20}=2 for the center shift, and λ=700 cm^{-1} for the diabatic coupling (except for q_{20}, these values are close to those for the antisymmetric stretch and bend degrees of freedom of NO_2 in the two lowest electronic states). The contour plots of V_g and V_e are displayed in Fig. 7. Note that the bottom of the excited surface V_e lies inside the ground state well. Fig. 8 shows how the states of the uncoupled ground (circles) and excited (losanges) surfaces are shifted upon switching on of the diabatic coupling. The vertical line locates the energy of the bottom of V_e. It is observed in this figure that the ground state of V_g is already shifted to lower energies by more than 20 cm^{-1} and that shifts may reach about 500 cm^{-1} close to the bottom of V_e. This is due to the fact that each zero-order state of the uncoupled ground surface V_g is

coupled through V_c to a large number of high-energy zero-order states of the uncoupled excited surface V_e, so

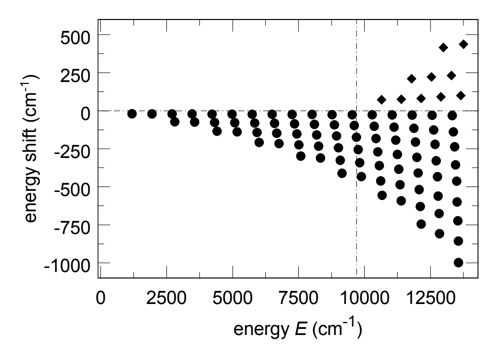


Figure 8 : *Plot, as a function of the absolute energy E of each state, of the energy shifts of the states belonging to the ground (circles) and excited (losanges) diabatic surfaces caused by the coupling (through V_c) to the other surface. The vertical line indicates the energy of the bottom of the excited surface V_e (E=9700 cm^{-1}).*

---

that switching on the diabatic coupling V_c results in large shifts for all of the states of V_g and V_e, including those states of V_g located far below the bottom of V_e. Nonetheless, these shifts appear to be quite regular, which indicates that, in the investigated energy range, switching on the diabatic coupling V_c principally modifies the harmonic frequencies and the anharmonicities in each well. The goal of the remainder of this section is to show how these harmonic and anharmonic corrections are obtained from CPT.

For the sake of clarity, the case for n=2 coupled electronic surfaces is handled explicitly here, but the procedure extends readily to larger values of n. One defines a n^2-dimensional basis $(\mathbf{g}, \mathbf{e}, \mathbf{j}_+, \mathbf{j}_-)$ of $n*n$ matrices

$$\mathbf{g} = \begin{pmatrix} 0 & 0 \\ 0 & 1 \end{pmatrix}, \qquad \mathbf{e} = \begin{pmatrix} 1 & 0 \\ 0 & 0 \end{pmatrix}, \qquad \mathbf{j}_+ = \begin{pmatrix} 0 & 1 \\ 0 & 0 \end{pmatrix}, \qquad \mathbf{j}_- = \begin{pmatrix} 0 & 0 \\ 1 & 0 \end{pmatrix}, \tag{5.3}$$

where $\mathbf{g}$ and $\mathbf{e}$ are the projections on the ground and excited surfaces, respectively, and $\mathbf{j}_+$ and $\mathbf{j}_-$ are raising- and lowering-like operators. Each operator $\mathbf{A}$ is decomposed on this basis according to

$$\mathbf{A} = \begin{pmatrix} A_e & A_+ \\ A_- & A_g \end{pmatrix} = A_g\,\mathbf{g} + A_e\,\mathbf{e} + A_+\,\mathbf{j}_+ + A_-\,\mathbf{j}_- , \tag{5.4}$$

and the commutator $\mathbf{C} = [\mathbf{A}, \mathbf{B}] = \mathbf{AB} - \mathbf{BA}$ of two operators $\mathbf{A}$ and $\mathbf{B}$ writes

$$\begin{aligned} C_g &= [A_g, B_g] + A_- B_+ - B_- A_+ \\ C_e &= [A_e, B_e] + A_+ B_- - B_+ A_- \\ C_+ &= A_+ B_g - B_+ A_g + A_e B_+ - B_e A_+ \\ C_- &= A_- B_e - B_- A_e + A_g B_- - B_g A_- \quad . \end{aligned} \tag{5.5}$$

As for the dynamics on a single electronic surface, the initial Hamiltonian $\mathbf{H}$ of Eqs. (5.1)-(5.2) must be partitioned into $\mathbf{H}^{(0,0)}$ plus higher order terms $\mathbf{H}^{(0,k)}$ ($k \geq 1$) and the rules for obtaining the successive operators $\mathbf{S}^{(s)}$ from the unwanted terms of $\mathbf{H}^{(s-1,s)}$ must be found for each perturbation order s – except that all operators are now matrix quantities. In order for the transformations of Eq. (2.6) to be unitary ones, $S_g^{(s)}$ and $S_e^{(s)}$ must be anti-hermitian, while $S_+^{(s)}$ and $S_-^{(s)}$ must satisfy

$$S_+^{(s)} = -S_-^{(s)+} , \tag{5.6}$$

where $S_g^{(s)}$, $S_e^{(s)}$, $S_+^{(s)}$ and $S_-^{(s)}$ are the components of $\mathbf{S}^{(s)}$ in the $(\mathbf{g}, \mathbf{e}, \mathbf{j}_+, \mathbf{j}_-)$ basis. These conditions are automatically fulfilled by the procedure proposed below. Examination of the matrix version of Eq. (2.11), *i.e.*

$$[\mathbf{S}^{(s)}, \mathbf{H}^{(0,0)}] = -\mathbf{R}^{(s-1)} , \tag{5.7}$$

shows that $\mathbf{H}^{(0,0)}$ must satisfy severe constraints in order for this equation to be easy to solve. The best choice probably consists in taking

$$\begin{aligned} \mathbf{H}^{(0,0)} &= \left(\frac{\omega_{1g}}{2} a_1^+ a_1 + \frac{\omega_{2g}}{2} a_2^+ a_2\right)\mathbf{g} \\ &\quad + \left(\delta E + \frac{\omega_{1g}}{2} a_1^+ a_1 + \frac{\omega_{2g}}{2} a_2^+ a_2\right)\mathbf{e} , \end{aligned} \tag{5.8}$$

where

$$\delta E = \Delta E + \frac{\omega_{1e} + \omega_{2e}}{2} - \frac{\omega_{1g} + \omega_{2g}}{2} \tag{5.9}$$

is the energy gap between the ground states of V_g and V_e, and the (a_j^+, a_j) creation and annihilation operators are obtained from the normal coordinates (p_j, q_j) of the ground electronic surface V_g according to Eq. (3.1). All

other terms, which describe the diabatic coupling as well as the frequency mismatch and the center shift between the two electronic surfaces, are put in $\mathbf{H}^{(0,1)}$. Investigation of more complex systems will probably require the ordering of (here missing) higher-order terms of V_g, V_e and V_c as in the lowest equation of Eq. (3.4). The fact that all operators are expressed in terms of the creation and annihilation operators of the ground electronic surface V_g is the principal advantage of the formulation presented in this article when compared to the first version of Ref. [19]. Indeed, in this earlier work, creation and annihilation operators referred to a virtual average surface $(V_g + V_e)/2$. Eq. (5.7) is very easy to solve when $\mathbf{H}^{(0,0)}$ is taken as in Eq. (5.8). Indeed, if the Hermitian subset $\mathbf{R}^{(s-1)}$ of $\mathbf{H}^{(s-1,s)}$ to be cancelled at order *s* of the perturbation procedure is of the form

$$\begin{aligned}\mathbf{R}^{(s-1)} &= \mathbf{g} \sum_{\mathbf{m},\mathbf{n}} a_{\mathbf{mn}}^{(s-1)} \prod_j (a_j^+)^{m_j} (a_j)^{n_j} \\ &+ \mathbf{e} \sum_{\mathbf{m},\mathbf{n}} b_{\mathbf{mn}}^{(s-1)} \prod_j (a_j^+)^{m_j} (a_j)^{n_j} \\ &+ \mathbf{j}_+ \sum_{\mathbf{m},\mathbf{n}} c_{\mathbf{mn}}^{(s-1)} \prod_j (a_j^+)^{m_j} (a_j)^{n_j} \\ &+ \mathbf{j}_- \sum_{\mathbf{m},\mathbf{n}} d_{\mathbf{mn}}^{(s-1)} \prod_j (a_j^+)^{m_j} (a_j)^{n_j} \quad ,\end{aligned} \tag{5.10}$$

then the solution of Eq. (5.7) is just

$$\begin{aligned}\mathbf{S}^{(s)} &= \mathbf{g} \sum_{\mathbf{m},\mathbf{n}} \frac{a_{\mathbf{mn}}^{(s-1)}}{\Sigma_{\mathbf{mn}}} \prod_j (a_j^+)^{m_j} (a_j)^{n_j} \\ &+ \mathbf{e} \sum_{\mathbf{m},\mathbf{n}} \frac{b_{\mathbf{mn}}^{(s-1)}}{\Sigma_{\mathbf{mn}}} \prod_j (a_j^+)^{m_j} (a_j)^{n_j} \\ &+ \mathbf{j}_+ \sum_{\mathbf{m},\mathbf{n}} \frac{c_{\mathbf{mn}}^{(s-1)}}{\Sigma_{\mathbf{mn}} - \delta E} \prod_j (a_j^+)^{m_j} (a_j)^{n_j} \\ &+ \mathbf{j}_- \sum_{\mathbf{m},\mathbf{n}} \frac{d_{\mathbf{mn}}^{(s-1)}}{\Sigma_{\mathbf{mn}} + \delta E} \prod_j (a_j^+)^{m_j} (a_j)^{n_j} \quad ,\end{aligned} \tag{5.11}$$

where $\Sigma_{\mathbf{mn}} = \sum_j (m_j - n_j)\,\omega_{jg}$. The simplest perturbative Hamiltonian one can think of consists of two Dunham expansions (one for the electronic ground state and one for the excited state) with no coupling between the two surfaces, that is

$$\mathbf{K}^{(s)} = H_g^{(s)}\,\mathbf{g} + H_e^{(s)}\,\mathbf{e} \quad , \tag{5.12}$$

where

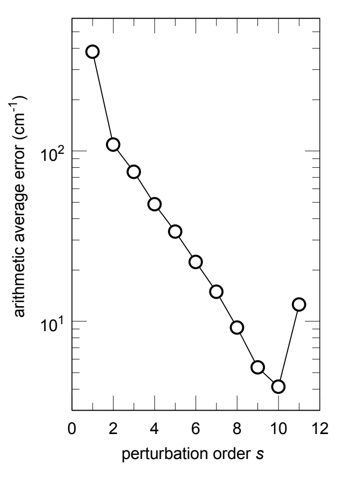


Figure 9 : *Plot, as a function of the perturbation order s, of the arithmetic average error between the exact energies of the model Hamiltonian of Eqs. (5.1)-(5.2) and those obtained from the perturbative Hamiltonian of Eqs. (5.12)-(5.13). The perturbative Hamiltonian consists of two uncoupled Dunham expansions, one for the ground electronic surface and one for the excited surface. Included in the calculations are the first 91 states of the system shown in Fig. 8, with energies up to 14000 cm^{-1} above the minimum of V_g. Among these 91 states, 81 are principally localized on the V_g surface and 10 on the V_e surface. These states contain up to $v_2 = 16$ quanta of excitation in mode 2.*

$$K_\xi^{(s)} = \sum_j \nu_{j\xi}^{(s)} (a_j^+ a_j) + \sum_{j \le k} x_{jk\xi}^{(s)} (a_j^+ a_j)(a_k^+ a_k) + \ldots \tag{5.13}$$

$(\xi = g, e)$. Such a perturbative Hamiltonian is obtained by keeping into $\mathbf{H}^{(s,s)}$ only the **g** and **e** components of $\mathbf{H}^{(s-1,s)}$ such that $\mathbf{m} = \mathbf{n}$ and by putting all the other components into $\mathbf{R}^{(s-1)}$ to let them be cancelled by the perturbation procedure at order *s*. Note that the maximum power in the right-hand side of Eq. (5.13) increases here like 2*s*+2, compared to *s*+2 for the procedure for semi-rigid molecules with a single electronic surface (*cf.* Eq. (3.8)). The convergence properties of this perturbation series are illustrated in Fig. 9, where the arithmetic average error between the energies of the states of the exact Hamiltonian in Eqs. (5.1)-(5.2) and those obtained from the perturbative Hamiltonians in Eqs. (5.12)-(5.13)

is plotted as a function of the perturbation order s. Included in the calculations are the first 91 states of the system, whose shifts induced by the diabatic coupling V_c are shown in Fig. 8. 81 states out of these 91 ones are principally localized in the electronic ground state, while the remaining 10 states are principally localized in the electronic excited state. It is seen in Fig. 9 that the series converges exponentially up to 10th order but diverges for $s \geq 11$. Average error at order s=10 is as small as 4.1 cm^{-1}, which is particularly impressive when reminding that states are shifted by up to 1000 cm^{-1} upon switching on of V_c. The reason for the divergence at order s=11 is easily understood when looking at Fig. 10, which shows the errors between the energies of exact and perturbative (10th order) quantum states as a function of energy. Indeed, it is seen in this figure that errors remain negligible below the energy of the bottom of V_e, which is indicated by a vertical line, while they increase sharply above this energy. Examination of Eq. (5.11) shows that this divergence is most likely due to vibronic resonances, *i.e.* to resonances between states of the electronic ground and excited surfaces, which cause some of the $\Sigma_{\mathbf{mn}} \mp \delta E$ denominators to become too small and the corresponding terms to diverge.

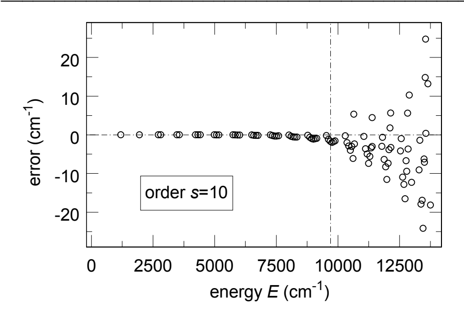


Figure 10 : *Plot, as a function of the energy of each state, of the difference between exact and perturbative quantum energies for the first 91 states of the model Hamiltonian of Eqs. (5.1)-(5.2) at 10th order of the theory. The perturbative Hamiltonian, shown in Eqs. (5.12)-(5.13), consists of two uncoupled Dunham expansions, one for the ground electronic surface and one for the excited surface. The vertical line indicates the energy of the bottom of the excited electronic surface* V_e. *Notice the sharp increase of the differences above this threshold.*

6 – CONCLUSION

This article has focused on practical recipes for applying CPT to various situations encountered at high vibrational energies (resonances, isomerization and electronic couplings) and on numerical examples, which demonstrate the efficiency of the proposed procedures. How the obtained perturbative Hamiltonians are next handled to extract the physical information encoded therein, is a question that was deliberately skipped. The interested reader is referred, for example, to Refs. [13-16] for more information on this topic. Before concluding, we would like to mention a few points, which, to our mind, deserve further attention.

First, it should be emphasized that an accurate initial expansion is a *sine qua non* condition for successful perturbative calculations. For example, it was pointed out in Sect. 3 that convergence of the perturbative series for HCP is limited to 9th order, because of the poor accuracy of the Taylor expansion at large bending angles (see Fig. 2). This is here of little consequence, since the average error is already as small as 2.4 cm^{-1}. It however sometimes happens that the Taylor expansion is too poor an approximation to be amenable to perturbative calculations, although this remains an exception rather than being the rule. A striking example is the second potential energy surface for HCP computed by Schinke and co-workers [75], which is in better agreement with experimental calculations than the first one [50,51] discussed in Sect. 3. It turns out that the Taylor expansion computed from this second surface is such a bad approximation that perturbative calculations based thereon are unable to reproduce the energies of all but the lowest quantum states. This is all the more surprising as the dynamics encoded in both spectra are rather similar [13,15,16,50,51,53]. It would therefore be interesting to find polynomial expressions, which would be more reliable than Taylor expansions for the purpose of subsequent perturbative calculations.

The second remark concerns dissociation, which was not discussed in this article. Any realistic description of the dissociation dynamics of triatomic molecules necessitates at least two large-amplitude coordinates, namely the dissociating stretch coordinate and the bend.

One can think of a procedure similar to that described in Sect. 4, where both the dissociating stretch (described by exponential functions) and the bend (described by trigonometric functions) would be handled as reactive coordinates. Upon application of the procedure described in Sect. 4, there would then remain only one good quantum number left in the perturbative Hamiltonian, which would quantize the inactive coordinate, *i.e.* the motion along the non-dissociating stretch degree of freedom. Another more complex possibility, which would however result in a larger number of good quantum numbers, would be to use Morse functions to describe the dissociating coordinate, as suggested recently by Child and co-workers [76]. Everything still has to be done in this domain.

At last, it is worth mentioning that, while in this article all physically "non-important" terms have systematically been dropped from the perturbative Hamiltonian (*cf.* Eq. (2.12)), one is not obliged to do so. When keeping all terms in the final Hamiltonian – or more precisely all terms up to a maximum order much larger than the perturbation order *s* – one virtually recovers the exact Hamiltonian [20], provided, of course, that the expansion is accurate enough (see above). The perturbative Hamiltonian however has one great advantage compared to the initial one, namely that the physically non-important terms have been strongly reduced by the perturbation procedure. Consequently, the size of the matrices which must be diagonalized to get converged eigenvalues can be substantially smaller for the perturbative Hamiltonian than for the initial one [20]. In order to get, with more limited numerical effort, the exact eigenvalues of systems which lie today at the limit of usual diagonalization procedures , one can therefore think to apply this technique (*i.e.* CPT without neglect) to the MEP expansion described in Sect. 4, the mixed Taylor/Fourier expansion being usually more precise and more adapted to the description of complex surfaces than Taylor's one. We plan to test this procedure against the vibrational states of H_2O_2 [77,78] in a close future.

REFERENCES

[1] E.C. Kemble, *The fundamental principles of quantum mechanics*, Mc Graw-Hill, New York, 1937
[2] E. Schrödinger, Ann. d. Physik 80, 437 (1926)
[3] M.R. Aliev and J.K.G. Watson, in *Molecular spectroscopy : modern research*, vol. III, edited by K.N. Rao, Academic Press, San Diego,1985
[4] J.H. Van Vleck, Phys. Rev. 33, 467 (1929)
[5] W.H. Shaffer and H.H. Nielsen, Phys. Rev. 56, 188 (1939)
[6] W.H. Shaffer, H.H. Nielsen and L.H. Thomas, Phys. Rev. 56, 895 (1939)
[7] W.H. Shaffer, H.H. Nielsen and L.H. Thomas, Phys. Rev. 56, 1051 (1939)
[8] H.H. Nielsen, Rev. Mod. Phys. 23, 90 (1951)
[9] E.L. Sibert, J. Chem. Phys. 88, 4378 (1988)
[10] X. Wang and E.L. Sibert, J. Chem. Phys. 111, 4510 (1999)
[11] X. Wang, E.L. Sibert and J.M.L. Martin, J. Chem. Phys. 112, 1353 (2000)
[12] X. Wang and E.L. Sibert, J. Chem. Phys. 113, 5384 (2000)
[13] M. Joyeux, S.Y. Grebenshchikov and R. Schinke, J. Chem. Phys. 109, 8342 (1998)
[14] D. Sugny, M. Joyeux and E.L. Sibert, J. Chem. Phys. 113, 7165 (2000)
[15] H. Ishikawa, R.W. Field, S.C. Farantos, M. Joyeux, J. Koput, C. Beck and R. Schinke, Annu. Rev. Phys. Chem. 50, 443 (1999)
[16] M. Joyeux, S.C. Farantos and R. Schinke, J. Phys. Chem. A, in press
[17] M. Joyeux, J. Chem. Phys. 109, 2111 (1998)
[18] D. Sugny and M. Joyeux, J. Chem. Phys. 112, 31 (2000)
[19] D. Sugny and M. Joyeux, Chem. Phys. Letters 337, 319 (2001)
[20] D. Sugny and M. Joyeux, Chem. Phys. Letters 352, 99 (2002)
[21] G.D. Birkhoff, *Dynamical systems*, AMS Colloquium, New-York, 1966, vol. 9
[22] F.G. Gustavson, Astron. J. 71, 670 (1966)
[23] R.T. Swimm and J.B. Delos, J. Chem. Phys. 71, 1706 (1979)
[24] T. Uzer, D.W. Noid and R.A. Marcus, J. Chem. Phys. 79, 4412 (1983)
[25] J.H. Van Vleck, Rev. Mod. Phys. 23, 213 (1951)
[26] I. Shavitt and L.T. Redmon, J. Chem. Phys. 73, 5711 (1980)
[27] D. Papousek and M.R. Aliev, *Molecular vibrational-rotational spectra*, Elsevier, Amsterdam, 1982
[28] A.B. McCoy and E.L. Sibert, in *Dynamics of molecules and chemical reactions*, edited by R.E. Wyatt and J.Z.H. Zhang, Dekker, New-York, 1996
[29] K. Sarka and J. Demaison, in *Computational molecular spectroscopy*, edited by P. Jensen and P.R. Bunker, Wiley, Chichester (England), 2000
[30] K. Nakagawa, S. Tsunekawa and T. Kojima, J. Mol. Spectrosc. 126, 329 (1987)
[31] J. Tang and K. Takagi, J. Mol. Spectrosc. 161, 487 (1993)
[32] Y.-B. Duan, H.-M. Zhang and K. Takagi, J. Chem. Phys. 104, 3914 (1996)
[33] Y.-B. Duan and K. Takagi, J. Chem. Phys. 104, 7395 (1996)
[34] Y.-B. Duan, Z.-D. Sun and K. Takagi, J. Chem. Phys. 105, 5348 (1996)
[35] Y.-B. Duan, L. Wang and K. Takagi, J. Mol. Spectrosc. 193, 418 (1999)
[36] R. Meyer and H.H. Günthard, J. Chem. Phys. 49, 1510 (1968)
[37] D. Sugny, *PhD thesis*, Grenoble (France), 2002
[38] E.L. Sibert, J. Chem. Phys. 90, 2672 (1989)
[39] A.B. Mc Coy and E.L. Sibert, J. Chem. Phys. 92, 1893 (1990)
[40] A.B. Mc Coy and E.L. Sibert, J. Chem. Phys. 95, 3476 (1991)
[41] A.B. Mc Coy and E.L. Sibert, J. Chem. Phys. 95, 3488 (1991)
[42] A.B. Mc Coy, D.C. Burleigh and E.L. Sibert, J. Chem. Phys. 95, 7449 (1991)
[43] Y. Pak, E.L. Sibert and R.C. Woods, J. Chem. Phys. 107, 1717 (1997)
[44] C. Jaffé and W.P. Reinhardt, J. Chem. Phys. 71, 1862 (1979)
[45] W.P. Reinhardt, J. Phys. Chem. 86, 2158 (1982)
[46] C. Jaffé and W.P. Reinhardt, J. Chem. Phys. 77, 5191 (1982)
[47] R.B. Shirts and W.P. Reinhardt, J. Chem. Phys. 77, 5204 (1982)
[48] W.P. Reinhardt and D. Farrelly, J. Phys. (France) 43, C2 (1982)
[49] K. Sohlberg and R.B. Shirts, J. Chem. Phys. 101, 7763 (1994)
[50] S.C. Farantos, H.-M. Keller, R. Schinke, K. Yamashita and K. Morokuma, J. Chem. Phys. 104, 10055 (1996)
[51] C. Beck, H.-M. Keller, S.Y. Grebenshchkov, R. Schinke, S.C. Farantos, K. Yamashita and K. Morokuma, J. Chem. Phys. 107, 9818 (1997)
[52] E.B. Wilson, J.C. Decius and P.C. Cross, *Molecular vibrations*, Dover, New-York, 1955

[53] M. Joyeux, D. Sugny, V. Tyng, M. Kellman, H. Ishikawa, R.W. Field, C. Beck and R. Schinke, J. Chem. Phys. 112, 4162 (2000)
[54] J.N. Murrell, S. Carter and L.O. Halonen, J. Mol. Spectrosc. 93, 307 (1982)
[55] Z. Bacic, J. Chem. Phys. 95, 3456 (1991)
[56] R.A. Marcus, J. Chem. Phys. 45, 4493 (1966)
[57] R.A. Marcus, J. Chem. Phys. 46, 959 (1967)
[58] R.A. Marcus, J. Chem. Phys. 49, 2610 (1968)
[59] W.H. Miller, N.C. Handy and J.E. Adams, J. Chem. Phys. 72, 99 (1980)
[60] S.K. Gray, W.H. Miller, Y. Yamaguchi and H.F. Schaefer, J. Chem. Phys. 73, 2733 (1980)
[61] T. Carrington, L.M. Hubbard, H.F. Schaefer and W.H. Miller, J. Chem. Phys. 80, 4347 (1984)
[62] C. Saint-Espès, X. Chapuisat and F. Schneider, Chem. Phys. 159, 377 (1992)
[63] X. Chapuisat and C. Saint-Espès, Chem. Phys. 159, 391 (1992)
[64] C. Saint-Espès, X. Chapuisat and C. Zuhrt, Chem. Phys. 188, 33 (1994)
[65] X. Chapuisat, C. Saint-Espès, C. Zuhrt and L. Zülicke, Chem. Phys. 217, 43 (1997)
[66] F. Gatti, Y. Justum, M. Menou, A. Nauts and X. Chapuisat, J. Mol. Spectrosc. 181, 403 (1997)
[67] M. Joyeux, D. Sugny, M. Lombardi, R. Jost, R. Schinke, S. Skokov and J. Bowman, J. Chem. Phys. 113, 9610 (2000)
[68] R. Jost, M. Joyeux and M. Jacon, Chem. Phys., in press
[69] H. Köppel, W. Domcke and L.S. Cederbaum, Adv. Chem. Phys. 57, 59 (1984)
[70] W. Domcke and G. Stock, Adv. Chem. Phys. 100, 1 (1997)
[71] I.B. Bersucker and V.Z. Polinger, *Vibronic interactions in molecules and crystals*, Springer, Berlin, 1989
[72] G. Herzberg and H.C. Longuet-Higgins, Discuss. Faraday Soc. 35, 77 (1963)
[73] T. Carrington, Discuss. Faraday Soc. 53, 27 (1972)
[74] D.R. Yarkony, Rev. Mod. Phys. 68, 985 (1996)
[75] C. Beck, R. Schinke and J. Koput, J. Chem. Phys. 112, 8446 (2000)
[76] M.S. Child, M.P. Jacobson and C.D. Cooper, J. Phys. Chem. A 105, 10791 (2001)
[77] B. Kuhn, T. Rizzo, D. Luckhaus, M. Quack and M.A. Suhm, J. Chem. Phys. 111, 2565 (1999)
[78] R. Chen, G. Ma and H. Guo, Chem. Phys. Letters 320, 567 (2000)

4.2 Hamiltonian monodromy from a Gauss-Manin connexion

Corresponding articles : [1, 17]
This work has been done in collaboration with P. Mardesic and M. Pelletier of the *Institut de Mathématiques de Bourgogne* in Dijon, H. R. Jauslin and K. Efstathiou of the *Laboratory of mathematics of Gröningen* in the Netherlands. We also acknowledge fruitful discussions with D. A. Sadovskií and B. I. Zhilinskií of the *Université du Littoral* in Dunkerque.

Introduced by Duistermaat in 1980 [55] for completely integrable systems, Hamiltonian monodromy is the simplest topological obstruction to the existence of global action-angle variables in Hamiltonian integrable systems [49]. The phase space of an integrable system is foliated into combined level sets of first integrals or fibres. Under certain general conditions, the Liouville-Arnold theorem [38] tells us that regular fibres are (disjoint unions of) tori, and furthermore, the torus bundle is locally trivial and is described by local action-angle variables. Due to the presence of certain isolated singular fibres such as pinched tori (see below for a picture), regular tori are forced to fit together with a twist which prevents extending these action-angle variables to the whole bundle. The system has then a nontrivial monodromy [49]. A typical example is given by the 1 :-1 resonant oscillator [87]. The quantum analog of this concept was formulated by S. Vu Gnoc [120]. In order to render this notion more accessible, we have written an article on Hamiltonian monodromy for non specialist readers [1].

The theory of monodromy has known recent important developments both from the mathematical and physical perspectives. Other global structures of toric fibrations have been discovered. This resulted in the concept of generalized or fractional monodromy [87, 88, 89, 57] and bidromy [104]. Fractional monodromy was at the origin of my work [17] on the relation between this concept and the Gauss-Manin connexion of Riemann surfaces. These generalizations are associated to other singular tori such as curled tori for fractional monodromy and bitori for bidromy. A curled torus can be viewed, in the simplest case, as two cylinders glued along a line, whose extremities corresponding to a figure eight are identified after a half-twist. The construction of a bitorus is very similar, except there is no half-twist.

Different singular and regular tori are represented in Fig. 4.1.

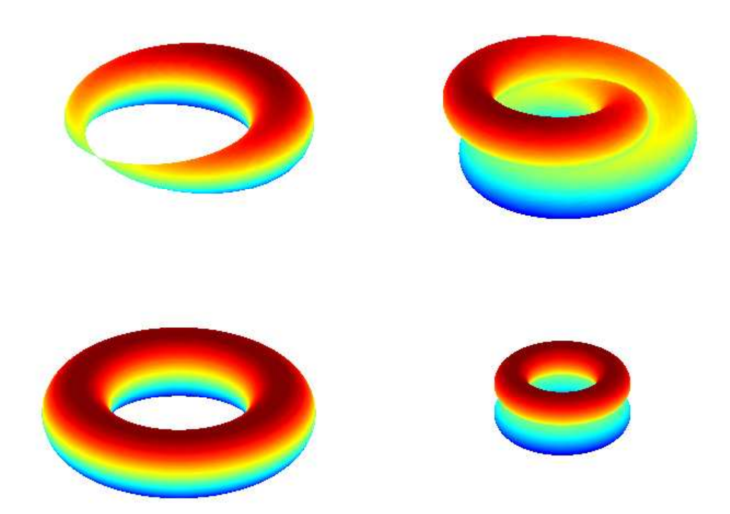


FIGURE 4.1 – Regular and singular tori : (left top) a pinched torus, (right top) a curled torus, (left bottom) a regular torus, (right bottom) a bitorus.

The fundamental problem solved by Duistermaat was the generalization of action-angle variables to the whole phase space when the set of regular points of the image of the energy-momentum map is not simply connected. This occurs when this image has an isolated singularity associated to a pinched torus. Such a system has a non-trivial monodromy. This implies that after a loop around the singularity, the action variables are changed. The relation between the new and the old action coordinates is given by the monodromy matrix which is, for a two-degrees of freedom system, a 2×2 matrix with integer coefficients and with a determinant equal to 1. The definition of Hamiltonian monodromy can be extended [87, 88, 89, 57] to characterize not only isolated singularities but also particular types of non isolated singularities corresponding to a line of weak singularities associated to curled tori. In addition, we consider loops which cross the line of singularities. For such loops, it can be shown that the notion of Hamiltonian monodromy can still be defined in a restrictive way [17]. A formal extension of this generalization leads to a monodromy matrix with fractional coefficients and to the denomination fractional monodromy. The original idea of the work [17] was to study fractional monodromy through a complexification of the phase space which allows to bypass the line of singularities and

to define a complex continuation of the action variables. In particular, we show that the Hamiltonian monodromy can be defined from a Gauss-Manin monodromy of a Riemann surface constructed from the energy-momentum map. We computed the monodromy matrices for $1 : -n$ and $m : -n$ resonant systems from the real approach introduced in [57] and the complex one based on Riemann surfaces [17]. We reproduce here the article [17]. We are currently working on the application of the complex approach to the bidromy phenomenon introduced in [104]. In this case, we consider loops of the image of the energy-momentum map which cross a line of bitori.

In [9], we show the role played by singular tori in the counterpropagating dynamics of waves in a nonlinear media. Using numerical simulations, we conjecture that these tori appear as an attractor for the spatio-temporal dynamics of the non-linear wave systems. More precisely, the wave system exhibits a relaxation process towards a stationary state which lies on the singular torus in the limit of an infinite medium. This torus is associated to an integrable Hamiltonian constructed from the spatio-temporal nonlinear system. These Hamiltonians are very similar to the ones which can be encountered in classical and quantum physics for systems with a finite number of degrees of freedom. This remark can be illustrated by the example of the counterpropagative three-wave interaction [9] which exhibits the same Hamiltonian as the one in the Fermi model of the CO_2 molecule. The robustness properties of the stationary state can also be determined from the topology of the singular torus.

JOURNAL OF MATHEMATICAL PHYSICS 49, 042701 (2008)

Fractional Hamiltonian monodromy from a Gauss–Manin monodromy

D. Sugny,[1,a)] P. Mardešić,[2] M. Pelletier,[2] A. Jebrane,[2] and H. R. Jauslin[1]
[1]*Institut Carnot de Bourgogne, UMR 5209 CNRS-Université de Bourgogne, BP 47870, 21078 Dijon, France*
[2]*Institut de Mathématiques de Bourgogne, UMR CNRS 5584, BP 47870, 21078 Dijon, France*

(Received 17 September 2007; accepted 24 January 2008; published online 3 April 2008)

Fractional Hamiltonian monodromy is a generalization of the notion of Hamiltonian monodromy, recently introduced by [Nekhoroshev, Sadovskií, and Zhilinskií, C. R. Acad. Sci. Paris, Ser. 1 **335**, 985 (2002); Ann. Henri Poincare **7**, 1099 (2006)] for energy-momentum maps whose image has a particular type of nonisolated singularities. In this paper, we analyze the notion of fractional Hamiltonian monodromy in terms of the Gauss–Manin monodromy of a Riemann surface constructed from the energy-momentum map and associated with a loop in complex space which bypasses the line of singularities. We also prove some propositions on fractional Hamiltonian monodromy for $1:-n$ and $m:-n$ resonant systems. © *2008 American Institute of Physics.* [DOI: 10.1063/1.2863614]

I. INTRODUCTION

We consider an integrable system on a four dimensional symplectic manifold defined by an energy-momentum map. For a proper map, the Liouville–Arnold theorem allows to foliate the phase space by tori or a disjoint union of tori over the regular values of the image of the map. The Hamiltonian monodromy describes the possible nontriviality of a 2-torus bundle over a loop in the set of regular values of the image of the energy-momentum map. The monodromy matrix is the matrix with integer coefficients of an automorphism of the first homology group H_1 of the torus.[1,2] The word *Hamiltonian* is added to distinguish this monodromy from the Gauss–Manin monodromy of Riemann surfaces which is also used in this paper.[29,30] A nontrivial monodromy can be expected if the set of regular values of the image of the energy-momentum map is not simply connected. Hamiltonian monodromy has profound implications both in classical and quantum mechanics[3] since it is the simplest topological obstruction to the existence of global action-angle variables[1] and thus of *global good quantum numbers*.[3] The phenomenon of Hamiltonian monodromy has been exhibited in a large variety of physical systems both in classical and quantum mechanics.[4–13]

The presence of nontrivial monodromy in energy-momentum maps with isolated singularities of focus-focus type is now well established. For example, the nontrivial monodromy in the spherical pendulum is due to this singularity.[1,2] Recently, the definition of Hamiltonian monodromy has been extended to characterize not only isolated singularities but also some types of nonisolated singularities, leading to the concept of fractional Hamiltonian monodromy.[14–17] More precisely, one considers an energy-momentum map with a one-dimensional set C of *weak critical values* defined by the property that each point of this set lifts to a particular type of singular torus, a curled torus, i.e., for the simplest case, two cylinders glued together along a line whose extremities corresponding to a figure eight are identified after a half-twist (see Fig. 16). Fractional monodromy can appear if the set of admissible paths is enlarged to include loops which cross the singular line

---

[a)]Electronic mail: dominique.sugny@u-bourgogne.fr.

C. For such paths, the singularity of C being sufficiently weak, it can be shown that the monodromy action can still be defined but only on a subgroup of H_1. The formal extension of this action to the whole group leads to monodromy matrices with fractional coefficients and to the denomination fractional monodromy. One of the main motivations for the introduction of this new concept is given by the quantum manifestation of monodromy in the discrete joint spectrum of the energy-momentum map.[3,15] This spectrum can be represented as a lattice of points with defects in $\mathbb{R}^2$. The focus-focus singularity can be detected by a point defect of this lattice which prevents it to be a regular lattice isomorphic to $\mathbb{Z}^2$. In the same way, fractional monodromy can be interpreted as a line defect of the lattice and appears therefore as a natural generalization of standard Hamiltonian monodromy.[15]

The presence of fractional monodromy has been shown in a system of coupled oscillators in $m:-n$ resonance with m or n different from 1. Two constructions have been given based on geometric[15,18] or analytic[17] arguments to define rigorously the crossing of C. The geometric construction consists in following a basis of cycles of a regular torus through the crossing of C. Not all the cycles can cross continuously the singularity, only those corresponding to a subgroup of H_1 can. When C is crossed, one allows cycles to break up and reconnect, the orientation of the cycles being preserved. The second construction uses, as in the original paper of Duistermaat and Cushman and Bates,[2] the period lattice of the torus[19] which is, however, not defined on the singular line C. The period lattice is defined through two functions Θ and T at each point of the regular values of the image of the energy-momentum map. Some regularizations of these functions can be made in order to cross continuously the line of singularities.[17] Note that the preceding geometric point of view can be reconstructed from this analytic approach since the basis of cycles can be determined from the functions Θ and T.

The goal of this work is to study fractional monodromy by complexifying the phase space in order to bypass the line of singularities. Somewhat similar studies for the Lagrange top and the spherical pendulum have already been published[20–22] and have highlighted the relation between the Hamiltonian and complex monodromy. An extension to the complex domain has also been used in Refs. 9–11 to show that the action variables are not differentiable for particular regular points of the bifurcation diagram. A parallel can finally be made with Bohr–Sommerfeld rules for semiclassical quantization. Such calculations can be undertaken in the C^∞ (Refs. 23–25) or in the analytic context.[26–28] The real approach needs regularization of the subprincipal term, whereas the complex approach avoids such problems by avoiding the singularity. In this paper, we show that fractional Hamiltonian monodromy can be defined from a Gauss–Manin monodromy[29,30] of a Riemann surface constructed from the energy-momentum map. The construction can be made in the reduced phase space[2] which is well suited to the introduction of Riemann surfaces. The Gauss–Manin connection is defined along a real loop which is locally deformed near C to bypass the line of singularities. The bypass is a semicircle around C. The Gauss–Manin connection can be calculated by studying the motion of the ramification points of the Riemann surface, as is done in the Picard–Lefschetz theory. We also introduce the complex extension of the functions Θ and T which are viewed as integrals of rational forms over a cycle of the Riemann surface. In other words, the regularizations of Θ and T in the real approach are replaced by a complex continuation of these functions. The variations of Θ and T along the bypass in the complex domain are deduced from the Gauss–Manin monodromy. The functions Θ and T allow us to go back to the real approach and to define a real monodromy. We show that this monodromy corresponds to fractional Hamiltonian monodromy in the limit where the radius of the semicircle goes to 0. Using this construction, we recover the results of the real approach obtained in Refs. 14–17 for the $1:-2$ resonance and Refs. 18 and 31 for $m:-n$ resonance. Moreover, for $1:-n$ and $m:-n$ resonant systems, we give new proofs of these results from the real and the complex approaches. A geometric point of view of the Gauss–Manin monodromy can be given by inspecting the motion of the branching points of the Riemann surface along the semicircle around C. For $1:-n$ resonant systems, the Riemann surface has locally n complex branching points in a neighborhood of C lying on a circle around the origin with an angle of $2\pi/n$ between each other. Along a semicircle

around C, the n points turn by an angle of $2\pi/n$ and exchange their positions. The variation of Θ near C is then calculated as a residue of a given 1-form. This characterizes the line of singularities C and fractional monodromy.

The organization of this article is as follows. We first consider the real approach and we determine the monodromy matrices for $1:-2$, $1:-n$, and $m:-n$ resonances in Sec. II. We next show in Sec. III how fractional monodromy can be defined in the complex approach and we detail its geometric interpretation. We recover the different results obtained in the real approach. Concluding remarks and perspectives are given in Sec. IV. Appendixes A and B present a schematic representation of the geometric construction of fractional monodromy for $1:-2$ and $1:-n$ resonant systems in the real approach and in the semiclassical point of view for $1:-n$ and $m:-n$ resonances. The material of these appendixes complements the existing literature on these two points. Appendix C finally deals with the reduction procedure in the complex approach.

II. THE REAL APPROACH

The goal of this section is to furnish a short overview of the fractional Hamiltonian monodromy in the real approach. Starting from the example introduced in Refs. 16 and 17 for the $1:-2$ resonance, we extend it to $1:-n$ and $m:-n$ resonances. The core of the results presented in this section is already contained in Refs. 14–17 We describe it in some detail since we need the results for the complex approach. Furthermore, we present analytic computations in this section and a geometric construction in Appendix A which are slightly different from the original ones and give a new view on the fractional Hamiltonian monodromy. The originality of the analytical computation for the $1:-2$ resonance lies in the introduction of a local description of the energy-momentum map near the origin of the bifurcation diagram which considerably simplifies the computation of the monodromy matrix. Since these arguments are generalizable to $1:-n$ and $m:-n$ resonances, they allow us to prove some propositions stated in Refs. 15, 16, 18, and 31. For the geometric description, we introduce the standard representation of a torus, i.e., a rectangle whose edges are identified. This geometric construction can be extended straightforwardly to $1:-n$ resonant systems.

A. The $1:-2$ resonance

We consider the symplectic manifold $M=T^*\mathbb{R}^2$ with standard symplectic form $\omega=dq_1\wedge dp_1+dq_2\wedge dp_2$. We introduce the energy-momentum map $F=(H,J):M\to\mathbb{R}^2$, where the two functions J and H have zero Poisson brackets $\{J,H\}=0$. Following Refs. 14–17, we choose a system corresponding to the $1:-2$ resonance defined by

$$H=\sqrt{2}[(q_1^2-p_1^2)p_2+2q_1p_1q_2]+2\varepsilon(q_1^2+p_1^2)(q_2^2+p_2^2),$$
$$J=\tfrac{1}{2}(q_1^2+p_1^2)-(q_2^2+p_2^2), \tag{1}$$

where ε is a nonzero positive real number. We denote by $\mathcal{R}$ the image of F and by $\mathcal{R}_{\rm reg}$ the regular values of $\mathcal{R}$. We recall that a point $M\in\mathcal{R}$ is regular if the 1-forms dH and dJ are linearly independent at all points of $F^{-1}(h,j)$.

The flow of J defines an S^1-action on the phase space but this action is not principal since the isotropy groups of the points $\{p_1=0,\ q_1=0,\ p_2,q_2\}$ are isomorphic to $\mathbb{Z}/2\mathbb{Z}$. The reduced phase space $J^{-1}(j)/S^1$ can be constructed by using the algebra of invariant polynomials with values in $\mathbb{R}$ which is generated by[2,16]

$$J(\mathbf{p},\mathbf{q})=\tfrac{1}{2}(q_1^2+p_1^2)-(q_2^2+p_2^2),$$
$$\pi_1(\mathbf{p},\mathbf{q})=\tfrac{1}{2}(q_1^2+p_1^2)+(q_2^2+p_2^2), \tag{2}$$
$$\pi_2(\mathbf{p},\mathbf{q})=\sqrt{2}[(q_1^2-p_1^2)q_2-2q_1p_1p_2],$$

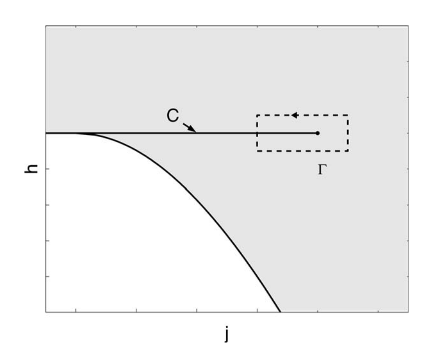


FIG. 1. Image $\mathcal{R}$ of the energy-momentum map F (in gray). The singular line C is represented by the horizontal solid line. The small full dot indicates the position of the image of the pinched-curled torus. A loop Γ transversally crossing C is depicted by dashed lines.

$$\pi_3(\mathbf{p},\mathbf{q}) = \sqrt{2}[(q_1^2 - p_1^2)p_2 + 2q_1p_1q_2],$$

with the constraint $|J| \leq \pi_1$. The reduced phase spaces $P_j = J^{-1}(j)/S^1$ are defined in the space $\mathbb{R}^3 = (\pi_1, \pi_2, \pi_3)$ by the equations

$$\pi_2^2 + \pi_3^2 = (\pi_1 - j)(\pi_1 + j)^2 \tag{3}$$

and correspond to noncompact surfaces with a conical singularity for $j < 0$. Having introduced the invariant polynomials, some comments can be made on the choice of H. Since $\{H, J\} = 0$, it can be shown that if H is polynomial in (p_i, q_i), then it can be written as a polynomial function in J, π_1, π_2, and π_3. We also notice that since the reduced phase space for the $1:-2$ resonance is noncompact, not every choice of H leads to a proper map for the energy-momentum map $F = (H, J)$. This explains why a term of degree 4 has been added to H [see Eq. (1)]. The image of the energy-momentum map defined by Eq. (1) has the particularity to present a line of singularities C; each point of this line except the origin lifts to a singular curled torus (the origin lifts to a pinched-curled torus). The topology of these singular tori can be determined by the intersection of the reduced phase space P_j with the level set $H_j = h$ (see Sec. II D). H_j is the reduced Hamiltonian, i.e., a map from P_j to $\mathbb{R}$ that sends a point of P_j to $H(\pi_1, \pi_2, \pi_3, j)$. Moreover, since the two energy-momentum maps $F = (H, J)$ and $F' = (H - f(J), J)$, where f is a polynomial function, define up to a diffeomorphism the same fibration of the phase space, we can consider an example such that $H = 0$ for the line of singularities C. Figure 1 displays the bifurcation diagram of F (see Refs. 16 and 17 for details on this construction). Singular points (i.e., not regular) are represented by solid lines in Fig. 1. C is a line of weak singularities. The word *weak* means that for each point of C, there exist points of the corresponding preimage such that the rank of F is 1. We recall that for a regular point, the rank of F is always equal to 2 and that the rank of F is 0 for one point of $F^{-1}(0,0)$.

B. Fractional Hamiltonian monodromy

We begin this section by recalling some basic facts about integer and fractional monodromies. The word *Hamiltonian* in Hamiltonian monodromy will be omitted when confusion is unlikely to occur.

In the standard or integer case, we assume that the preimage of each point $(h, j) \in \mathcal{R}_{\text{reg}}$ is a torus $T^2(h, j)$. This allows to define a 2-torus bundle over $\mathcal{R}_{\text{reg}}$ which is locally trivial. Monodromy is the simplest obstruction for it to be globally trivial.[1,2] An explicit construction of the monodromy matrix can be done as follows. Let Γ be a loop along regular values of $\mathcal{R}$. We consider a point (h, j) of Γ which lifts to a torus $T^2(h, j)$. We fix a basis of the homology group $H_1(T^2(h, j), \mathbb{Z})$. We then deform continuously this basis along Γ.[2,32] After a loop when returning back to the initial point (h, j), the basis may have changed and the monodromy matrix, which is the matrix of an automorphism of H_1, describes this modification. The monodromy matrix only

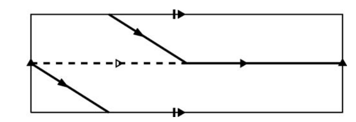


FIG. 2. Schematic representation on the torus $F^{-1}(h,j)$ of the cycles β_1 and β_2 depicted, respectively, by dashed and solid lines.

depends on the homotopy class of the loop Γ. Fractional monodromy is obtained by extending the possible loops, allowing them to cross some particular type of weak singular lines such as C. The preceding construction can be generalized to fractional monodromy but only a subgroup of $H_1(T^2(h,j),\mathbb{Z})$ can be transported continuously across line C.[15,17] These remarks can be understood by the following construction. Let $(h,j)\in\mathcal{R}_{\text{reg}}$. Denoting by φ_J and φ_H the flows associated with the Hamiltonians J and H, the period lattice of F at a point (h,j) is the set

$$\{(t_1,t_2)\in\mathbb{R}^2|\varphi_J^{t_1}\circ\varphi_H^{t_2}(z)=z\},\tag{4}$$

for all $z\in F^{-1}(h,j)$. A basis for this period lattice, which is isomorphic to $\mathbb{Z}^2$, is given by the vectors $v_1=(2\pi,0)$ and $v_2=(-\Theta,T)$, where Θ is the rotation angle and T the first return time of the flow φ_H defined as follows.[1,2] The Hamiltonian J generates an S^1-action on $F^{-1}(h,j)$. We denote by θ an angle conjugated to the action J. Following φ_J which is parametrized by θ, one goes back to the starting point when θ increases by 2π, which gives v_1. If we consider now φ_H from a point of an orbit of the flow φ_J, one sees that the first intersection of these two flows takes places at time T. The two points of intersection of the two flows define two angles θ_f and θ_i and the twist $\Theta=\theta_f-\theta_i$ which is determined with respect to the direction of φ_J. Note that a different choice of the angle θ leads to a different basis for the period lattice. The corresponding rotation angles Θ differ by a multiple of 2π. The monodromy matrix associated with a loop lying in the regular values of the image of the energy-momentum map is related to the behavior of the functions Θ and T along this loop. For the standard monodromy, after a counterclockwise loop around an isolated critical value (focus-focus singularity), it can be shown that the rotation angle is increased by 2π, whereas the first return time is unchanged. As a consequence, v_1, is transformed into v_1 and v_2 into $-v_1+v_2$, and thus the monodromy matrix M written in the local basis (v_1,v_2) is equal to

$$M=\begin{pmatrix}1 & 0\\ -1 & 1\end{pmatrix}.\tag{5}$$

The two functions Θ and T allow to define a basis of cycles for the homology group $H_1(F^{-1}(h,j),\mathbb{Z})$ and thus to recover a more geometric point of view. A basis $([\beta_1],[\beta_2])$ of $H_1(F^{-1}(h,j),\mathbb{Z})$ is given by the cycles associated, respectively, to the flows of the vector fields

$$\begin{aligned}X_1&=2\pi X_J,\\ X_2&=-\Theta(h,j)X_J+T(h,j)X_H.\end{aligned}\tag{6}$$

The flows $\varphi_{X_1}^t$ $(t\in[0,1])$ and $\varphi_{X_2}^t$ $(t\in[0,1])$ generate, respectively, the closed cycles β_1 and β_2. These two cycles are schematically represented in Fig. 2 for $\Theta=-\pi$. In the basis $([\beta_1],[\beta_2])$, the monodromy matrix is given by the same matrix as Eq. (5) obtained for the period lattice.

The situation is slightly more complicated for fractional monodromy. The analytic construction of fractional monodromy follows the same steps as for the standard case.[17] Returning to the example of Eq. (1) and considering the loop Γ of Fig. 1, the question which naturally arises is the definition of the crossing of line C since Θ has a discontinuity of size π on this line and T diverges. The idea of the method proposed in Ref. 17 consists in extending by continuity the function Θ (the continuous function is called $\tilde{\Theta}$) and in rescaling the time to obtain a finite first return time denoted as τ. Note that this rescaling does not modify the definition of the cycles but

only the time to cover them. This leaves therefore the monodromy matrix unchanged. $\tilde{\Theta}$ is defined by $\tilde{\Theta}(h,j)=\Theta(h,j)$ for points (h,j) of Γ before the crossing of line C and by $\tilde{\Theta}(h,j)=\Theta(h,j)+\pi$ for points after the crossing.[17] A basis of the period lattice is given by the vectors $v_1=(2\pi,0)$ and $v_2=(-\tilde{\Theta},\tau)$, and the cycles β_1 and β_2 are now associated with the vector fields

$$X_1 = 2\pi X_J,$$
$$\tilde{X}_2 = -\tilde{\Theta}(h,j)X_J + \tau(h,j)X_H. \tag{7}$$

The construction of these cycles has, however, to be carefully examined. $\varphi^t_{X_1}$ $(t\in[0,1])$ generates a cycle β_1 for all points of Γ. Before the crossing, $\varphi^t_{\tilde{X}_2}$ $(t\in[0,1])$ generates a closed cycle β_2, but after the crossing, $\varphi^t_{\tilde{X}_2}$ $(t\in[0,1])$ generates only half of a cycle. To get a complete cycle, we thus have to take $t\in[0,2]$. This means geometrically that only a cycle β_2 covered twice can be transported continuously across line C. Thus, not all cycles in the homology group can be transported along Γ. Only a subgroup corresponding to the cycles that are run twice by $\tilde{X}_2$ can be transported. In terms of the period lattice, the crossing of C is only possible for the sublattice generated by v_1 and $2v_2$. We can then define the monodromy matrix for a counterclockwise loop transversally crossing C once. The monodromy matrix M reads in the basis $(v_1,2v_2)$ or in the basis $([\beta_1],[2\beta_2])$,

$$M = \begin{pmatrix} 1 & 0 \\ -1 & 1 \end{pmatrix}. \tag{8}$$

Extending *formally* the definition of M to the whole homology group or the whole period lattice, we obtain in the basis (v_1,v_2) or in the basis $([\beta_1],[\beta_2])$,

$$M = \begin{pmatrix} 1 & 0 \\ -\frac{1}{2} & 1 \end{pmatrix}. \tag{9}$$

We finally note that this *generalized* monodromy is still topological in the sense that it depends only on the homotopy equivalence class of the loop considered. We also point out that these cycles prolonged continuously to the curled torus allow to recover the geometric construction of fractional monodromy described in Appendix A.

C. Local computation of the monodromy matrix

The determination of the monodromy matrix is based on the behavior of the functions Θ and τ on the line of singularities C. More precisely, the monodromy matrix can be constructed uniquely from the size of the discontinuity of Θ and from the fact that τ is continuous. In Ref. 17, the computation was done by using global expressions for Θ and τ in terms of elliptic integrals. It is clear that such a global calculation can be expected to be done explicitly only for simple energy-momentum maps.

We propose a computation of the fractional monodromy matrix based on local expansions in h and j around $(h=0,\ j=0)$. This expansion is not trivial because a particular dissymmetry in h and j has to be preserved.

Lemma 1: In the variables (π_1,π_2,π_3,J) and for a point $(h,j)\in\mathcal{R}_{\mathrm{reg}}$, the functions Θ and τ are given by the following expressions:

$$\Theta(h,j) = h\int_{\pi_1^-}^{\pi_1^+} \frac{d\pi_1}{(j+\pi_1)\sqrt{Q(\pi_1)}} \tag{10}$$

and

$$\tau(h,j) = \frac{1}{2}\int_{\pi_1^-}^{\pi_1^+} \frac{j+\pi_1}{\sqrt{Q(\pi_1)}} d\pi_1, \tag{11}$$

where $Q(\pi_1)$ is a polynomial given by

$$Q(\pi_1) = (\pi_1 - j)(\pi_1 + j)^2 - [h - \varepsilon(\pi_1^2 - j^2)]^2. \tag{12}$$

π_1^+ and π_1^- are the two largest real roots of Q with $\pi_1^- < \pi_1^+$.

Proof: See Ref. 17 and Sec. II E for a more general construction. We recall that τ is the first return time of the flow of the rescaled vector field $[1/(q_1^2+p_1^2)]X_H$. □

Proposition 1: The monodromy matrix for a counterclockwise oriented loop Γ transversally crossing line C once at a point different from the origin (see Fig. 1) is given by

$$M = \begin{pmatrix} 1 & 0 \\ -\frac{1}{2} & 1 \end{pmatrix}. \tag{13}$$

Proof: The monodromy matrix is given by the behavior of Θ and τ in the neighborhood of line C. Taking $j<0$ fixed and finite, the limits $\lim_{h\to 0^\pm} \Theta(h,j)$ and $\lim_{h\to 0^\pm} \tau(h,j)$ have been calculated in Ref. 17. Elliptic integrals and asymptotic expansions of these integrals were used.

We propose a simpler computation by considering the limit $j\to 0$. For this purpose, we analyze the roots of the polynomial Q as h and j go to zero. Since a qualitative change of the functions Θ and τ is expected when the polynomial Q has a multiple complex root, we determine the complex discriminant locus of Q near the origin $h=j=0$. This point will be made clearer with the introduction of Riemann surfaces in Sec. III but here it gives the way in which the two limits $h\to 0$ and $j\to 0$ should be taken. The discriminant locus in the real approach with the constraint $\pi_1 \geqslant |j|$ has already been calculated since it corresponds to the line of singularities of the bifurcation diagram, i.e., to the points where the 1-forms dH and dJ are linearly dependent (see Fig. 1). We introduce the variable $x=j+\pi_1$, and h, j, and x are taken complex. Three roots of Q vanish for $h=j=0$. We use the Newton polyhedron to determine an expansion of these three roots as power series in h and j (see Ref. 33 for a complete description of this method). We recall that given a polynomial $Q(x,h,j)$ such that $Q(0,0,0)=0$, one associates with each monomial $x^m j^k h^n$ in Q with nonzero coefficient the point (m,k,n) in $\mathbb{R}^3$ and the set $K_{(m,k,n)}=\{(u,v,w) | u\geqslant m, v\geqslant k, w\geqslant n\}$. The Newton polyhedron is the convex envelope of the union of all these sets. The Newton polyhedron procedure states, in first approximation, that terms which are not in the boundary of the Newton polyhedron can be neglected. In the two-dimensional case, the Newton polyhedron becomes the Newton polygon.

Let us assume that x, j, and h go to zero. Constructing the Newton polyhedron associated with Q, we obtain the principal part Q_N of Q corresponding to terms of the boundary of the polyhedron, which can be written as

$$Q_N = x^3 - 2jx^2 - h^2. \tag{14}$$

We notice that this principal part is symmetric with respect to h which is not the case for the polynomial Q. Simple algebra leads to the following asymptotic discriminant locus:

$$h = \pm\sqrt{j^3\left(-\frac{32}{27}\right)}, \qquad h = 0, \tag{15}$$

denoted as Δ. This complex locus is displayed for $j\in\mathbb{R}$ in Fig. 7. Equation (14) also shows that the weights 2, 2, and 3 can, respectively, be attributed to x, j, and h. In other words, if we introduce the small parameter r, the principal parts of x, j, and h can be written as

$$x_N = \bar{x}r^2,$$
$$j_N = \bar{j}r^2, \quad (16)$$
$$h_N = \bar{h}r^3.$$

The monodromy can be computed along a small loop in $\mathcal{R}$ around the origin. This loop can be parametrized by $(\bar{h},\bar{j}) \in S^1$ which allows to derive a local version of the computation of fractional monodromy. We thus let $\bar{h}\to 0$ while keeping $\bar{j}$ fixed and finite. Note that it is equivalent to consider the limits $h,j\to 0$ with the condition $h=o(j^{3/2})$ since on Δ, we have asymptotically $h=O(j^{3/2})$. In order to determine the leading terms of the roots of Q in this case, we construct the Newton polygon of Q_N. The approximate solutions fulfill

$$-2\bar{j}\bar{x}^2 - \bar{h}^2 = 0. \quad (17)$$

Since the sum of the three roots of Q that go to zero when $h,j\to 0$ is $2j$, and the sum of the four roots is $1/\varepsilon^2$, one deduces that the principal parts of the roots are given in the original variables by

$$x_1 = 2j,$$
$$x_2 = \frac{-h}{\sqrt{-2j}},$$
$$x_3 = \frac{h}{\sqrt{-2j}}, \quad (18)$$
$$x_4 = \frac{1}{\varepsilon^2}.$$

These expressions can be compared with the ones given in Ref. 17 where $j<0$ is fixed and $h\to 0$,

$$x_1 = 2j,$$
$$x_2 = \frac{-h}{\sqrt{-2j}+2\varepsilon j},$$
$$x_3 = \frac{h}{\sqrt{-2j}-2\varepsilon j}, \quad (19)$$
$$x_4 = 2j + \frac{1}{\varepsilon^2} + \frac{2\varepsilon h}{1+2\varepsilon^2 j}.$$

We now calculate $\lim_{\bar{h}\to 0^\pm,\bar{j}<0}\Theta(h,j)$ and $\lim_{\bar{h}\to 0,\bar{j}<0}\tau(h,j)$. We consider first $h>0$ and $j<0$. $\Theta(h,j)$ can be written as

$$\Theta(h,j) = \frac{h}{i\varepsilon}\int_{x_3}^{x_4} \frac{dx}{x\sqrt{(x-x_1)(x-x_2)(x-x_3)(x-x_4)}}. \quad (20)$$

We determine only the principal term of the asymptotic expansion of Θ. The symbol $\sim$ represents the equivalence in the limit $h\to 0$, $j\to 0$, and $h=o(j^{3/2})$. From Eq. (18), we obtain

$$\Theta(h,j) \sim \frac{h}{i\varepsilon}\int_{h/\sqrt{-2j}}^{1/\varepsilon^2} \frac{dx}{x\sqrt{(x-2j)(x+h/\sqrt{-2j})(x-h/\sqrt{-2j})(x-1/\varepsilon^2)}}. \tag{21}$$

We decompose the preceding integral into three integrals by introducing the terms k and k' which go to 0 such that $|h|/\sqrt{-2j} \ll k \ll -2j \ll k' \ll 1$. k and k' are chosen, for instance, as j^{α}. The notation $a \ll b$ means that the ratio $a/b \to 0$ as a and b go to 0. The three integrals are taken over the intervals $[|h|/\sqrt{-2j},k]$, $[k,k']$, and $[k',1/\varepsilon^2]$. It can be shown that the limit of the last two integrals is zero. The first integral reads

$$\Theta(h,j) \sim \frac{h}{i\varepsilon}\int_{h/\sqrt{-2j}}^{k} \frac{dx}{x\sqrt{(-2j)(x^2-h^2/(-2j))(-1/\varepsilon^2)}}, \tag{22}$$

which can be rewritten as

$$\Theta(h,j) \sim h\int_{h/\sqrt{-2j}}^{k} \frac{dx}{x\sqrt{(-2j)(x^2-h^2/(-2j))}}. \tag{23}$$

The change of variables $x=h/\sqrt{-2j}u$ leads to

$$\Theta(h,j) \sim \int_{1}^{+\infty} \frac{du}{u\sqrt{u^2-1}}. \tag{24}$$

Using the fact that

$$\int \frac{du}{u\sqrt{u^2-1}} = \arctan[\sqrt{u^2-1}], \tag{25}$$

one finally arrives to

$$\lim_{h\to 0^+, j\to 0^-, h=o(j^{3/2})} \Theta(h,j) = \frac{\pi}{2}. \tag{26}$$

Similar calculations for $h<0$ give

$$\lim_{h\to 0^-, j\to 0^-, h=o(j^{3/2})} \Theta(h,j) = \frac{-\pi}{2}. \tag{27}$$

We then deduce that the discontinuity of Θ is equal to π.

τ can be calculated along the same lines. This time, the first two terms go to zero and we only determine the last one,

$$\tau(h,j) \sim \frac{1}{2i\varepsilon}\int_{k'}^{1/\varepsilon^2} \frac{xdx}{\sqrt{(x-x_1)(x-x_2)(x-x_3)(x-x_4)}}. \tag{28}$$

Simple algebra leads to

$$\tau(h,j) \sim \frac{1}{2i\varepsilon}\int_{k'}^{1/\varepsilon^2} \frac{dx}{\sqrt{x(x-1/\varepsilon^2)}}, \tag{29}$$

and using the fact that

$$\int \frac{dx}{\sqrt{x(x-1/\varepsilon^2)}} = 2\ln[\sqrt{x}+\sqrt{x-1/\varepsilon^2}], \tag{30}$$

one obtains that

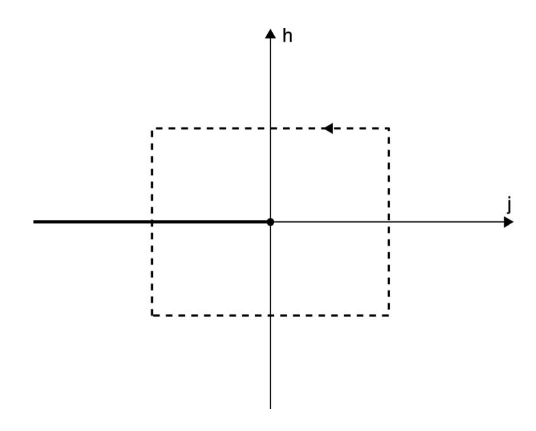


FIG. 3. Local bifurcation diagram in the neighborhood of the origin ($h=0$, $j=0$) for the $1:-n$ resonant system. The singular locus is represented by the large solid line. The small full dot indicates the position of the origin. The dashed line depicts a loop used to calculate the fractional monodromy matrix.

$$\lim_{h\to 0^{\pm}, j\to 0^{-}, h=o(j^{3/2})} \tau(h,j) = \frac{-\pi}{2\varepsilon}. \tag{31}$$

τ is therefore continuous on line C. The monodromy matrix is finally deduced from the behavior of Θ and τ in the neighborhood of C. We follow for that purpose the construction of Ref. 17 which is briefly recalled in Sec. II B. □

Remark 1: The preceding computation being local does not show the topological character of fractional monodromy, i.e., its independence with respect to the homotopically equivalent loops considered or more simply with respect to j. This point has been proved in the real approach in Ref. 17 and will be proved in the complex approach in Sec. III.

D. 1:−*n* resonant system

We consider the energy-momentum map $F=(H,J)$, where J is given by

$$J = \tfrac{1}{2}[(p_1^2+q_1^2) - n(q_2^2+p_2^2)], \tag{32}$$

with $n \geqslant 2$. We assume that the bifurcation diagram of F is locally in the neighborhood of the origin given by Fig. 3. The singular locus corresponds to ($h=0$, $j\leqslant 0$). Each point of this locus lifts to a singular torus, i.e., a pinched-curled torus for the origin and an n—curled torus for the other points. A k-curled torus is a singular torus for which one cycle is covered k-times, while the others only once. Its transverse section can be represented as a flower with k petals. We now restrict the discussion to a particular family of energy-momentum maps having locally the bifurcation diagram of Fig. 3. This family corresponds to simple models where fractional monodromy is expected to be present. Note that similar energy-momentum maps have been used in, Ref. 18. As in Sec. II B, the first step to construct this family consists in determining the invariant polynomials associated with the momentum J. We have[16]

$$\begin{aligned}
J(\mathbf{p},\mathbf{q}) &= \tfrac{1}{2}[m(q_1^2+p_1^2) - n(q_2^2+p_2^2)],\\
\pi_1(\mathbf{p},\mathbf{q}) &= \tfrac{1}{2}[m(q_1^2+p_1^2) + n(q_2^2+p_2^2)],\\
\pi_2(\mathbf{p},\mathbf{q}) &= \sqrt{n^m m^n}\,\Re[(q_1+ip_1)^n(q_2+ip_2)^m],\\
\pi_3(\mathbf{p},\mathbf{q}) &= \sqrt{n^m m^n}\,\Im[(q_1+ip_1)^n(q_2+ip_2)^m],
\end{aligned} \tag{33}$$

for $m \geqslant 1$ and $n \geqslant 1$. The reduced phase space P_j is defined by

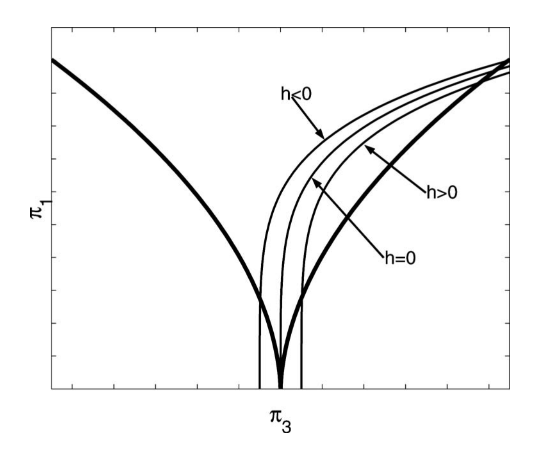


FIG. 4. Intersections of the reduced phase space P_j (in large solid lines) with the level sets $H_j=h$ for $h>0$, $h=0$, and $h<0$ in the plane $\pi_2=0$. The energy-momentum map corresponding to this diagram is given by Eq. (36).

$$\pi_2^2+\pi_3^2=(\pi_1+j)^n(\pi_1-j)^m, \tag{34}$$

with the condition $\pi_1 \geqslant |j|$.

Definition 1: We consider the set $\mathcal{F}$ of energy-momentum maps $F=(J,H)$ which can be written as

$$F=\begin{cases} J \\ H=\pi_3+R(\pi_1,J), \end{cases} \tag{35}$$

where R is a polynomial so that F is a proper map. π_1, π_3, and J are given by Eq. (33) for $m=1$.

Note that we do not search to determine or characterize the set $\mathcal{F}$. Only some properties of the elements of $\mathcal{F}$ will be sufficient to compute the monodromy matrix. Simple examples can be exhibited to show that $\mathcal{F}$ is not empty. For instance, for the $1:-3$ resonance, we can choose

$$F=\begin{cases} J \\ H=\pi_3-(\pi_1-J)(\pi_1+J)^4. \end{cases} \tag{36}$$

We are interested in the local behavior of R near the origin or, in other words, under which conditions on R, the image of the corresponding energy-momentum map is given by Fig. 3.

Lemma 2: The energy-momentum map given by Eq. (35) has locally the bifurcation diagram of Fig. 3 in a neighborhood of the origin if the polynomial R is of the form

$$R(\pi_1,J)=(\pi_1+J)^{n'}(\pi_1-J)^{m'}\tilde{R}(\pi_1,J), \tag{37}$$

where n' and m' are positive integers such that $n'>n/2$ and $n'+m'>(n+1)/2$. $\tilde{R}$ is a polynomial in π_1 and J such that the two smallest real positive roots of the polynomial Q which are larger than j for $(h,j)\in\mathcal{R}_{\mathrm{reg}}$ are simple roots. Q is the polynomial defined by

$$Q=(\pi_1+j)^n(\pi_1-j)-[h-R(\pi_1,j)]^2. \tag{38}$$

The two roots are denoted as π_1^- and π_1^+ with $\pi_1^-<\pi_1^+$.

Proof: The proof is based on the nature of the intersection of the reduced phase space P_j with the level sets $\{H_j=h\}$ of equations $h=\pi_3+R(\pi_1,j)$ as h and j vary. Figure 4 displays these intersections for three different values of h, $j<0$ being fixed. The case considered in this figure is the $1:-3$ resonance and the energy-momentum map of Eq. (36). Figure 4 represents the generic topology of the level sets $\{H_j=h\}$ which we are going to characterize. We recall that each point of the reduced phase space lifts in the original phase space to a circle except for the point of

coordinates ($\pi_1=-j$, $\pi_2=0$, $\pi_3=0$) which lifts either to a circle covered n times, if $j<0$, or to a point, if $j=0$. One deduces from the bifurcation diagram of F that the intersection of the level set $\{H_j=h\}$ with P_j contains a circle passing through the singular point $S=(\pi_1=-j,\pi_2=0,\pi_3=0)$, for $j\leq 0$ and $h=0$. We set $y=\pi_3$, $x=\pi_1+j$, and $x'=\pi_1-j$. The local behavior near the point S of the two surfaces is given by

$$y = \pm x^{n/2}x'^{1/2}, \tag{39}$$

for P_j, and by

$$y = -R(\pi_1,j), \tag{40}$$

for $\{H_j=0\}$. It is then straightforward to show that the local behavior expected is obtained if $R(\pi_1,j)=x^{n'}x'^{m'}\tilde{R}(\pi_1,j)$ with the conditions $n'>n/2$ and $n'+m'>(n+1)/2$, $m'\geq 0$. The first and second inequalities result, respectively, from the conditions for $j<0$ and $j=0$. □

Remark 2: The inequalities of Lemma 2 are strict to ensure that a multiplication by a constant factor of the term R does not modify the local behavior of the image of the energy-momentum map. This point has not been assumed for the $1:-2$ *resonance; the parameter* ε *is thus chosen sufficiently small in this case. Here, this hypothesis simplifies the computation of the monodromy matrix, as can be seen in the proofs of Lemma 4 and Proposition 2.*

Proposition 2: The monodromy matrix of a $1:-n$ *resonant system of the form (35) is given for a loop turning counterclockwise around the origin (see Fig. 3) and transversally crossing line C once by*

$$M = \begin{pmatrix} 1 & 0 \\ -1/n & 1 \end{pmatrix}. \tag{41}$$

Remark 3: Propositions 2 and 3 (see Sec. II E) were formulated as conjectures in Refs. 15 and 16. They are based on the analysis of the quantum joint spectrum of the energy-momentum maps. They have been recently proved in Ref. 18 from a geometrical construction. Note also that our starting point here and in Sec. II E is more general than in Sec. II B in the sense that only a local structure of the bifurcation diagram of the energy-momentum map $F=(H,J)$ *is assumed.*

As was done for the $1:-2$ resonance, we have to determine the expressions of the functions Θ and τ in terms of the invariant polynomials, the monodromy matrix being given by the behavior of these two functions in the neighborhood of C.

Lemma 3: The functions Θ *and* τ *are given for a point* $(h,j)\in\mathcal{R}_{\rm reg}$ *by the following integrals:*

$$\begin{aligned}\Theta(h,j) &= \int_{\pi_1^-}^{\pi_1^+} \frac{h}{j+\pi_1}\frac{d\pi_1}{\sqrt{Q}} + \Theta_0(h,j),\\ \tau(h,j) &= \frac{1}{n}\int_{\pi_1^-}^{\pi_1^+} \frac{(j+\pi_1)^{n-1}}{\sqrt{Q}}d\pi_1.\end{aligned} \tag{42}$$

Θ_0 *is a function over* $\mathcal{R}$ *which is continuous on the line of singularities C and which therefore gives a trivial contribution to the monodromy matrix.* τ *is the first return time of the rescaled vector field* $X=[1/(p_1^2+q_1^2)^{n-1}]X_H$.

Proof: For a point $(h,j)\in\mathcal{R}_{\rm reg}$, $\Theta(h,j)$ can be written as[17]

$$\Theta(h,j) = \int_0^T \dot{\theta}dt, \tag{43}$$

where θ is an angle variable conjugate to J. It can be expressed in terms of the variables (q_1,p_1) by

$$\theta = \arg(p_1 + iq_1). \tag{44}$$

This corresponds to a particular choice of the angle θ. Other choices lead to the same monodromy matrix. This point will be detailed in Sec. II E for the $m:-n$ resonance. Differentiating Eq. (44) and using Hamilton's equations, one arrives to

$$\dot{\theta} = \frac{n\pi_3 + \frac{\partial R}{\partial p_1}p_1 + \frac{\partial R}{\partial q_1}q_1}{q_1^2 + p_1^2}, \tag{45}$$

which simplifies into

$$\dot{\theta} = \frac{1}{j + \pi_1}\left(nh - nR + \frac{\partial R}{\partial p_1}p_1 + \frac{\partial R}{\partial q_1}q_1\right). \tag{46}$$

The integral of Eq. (43) can be rewritten as an integral in the reduced phase space P_j,[17]

$$\Theta(h,j) = 2\int_{\pi_1^-}^{\pi_1^+} \dot{\theta}\frac{d\pi_1}{\pi_1}. \tag{47}$$

Using the particular form of the polynomial R (see Lemma 2), it can be shown that the last three terms of Eq. (46) give a continuous contribution to the function Θ denoted as Θ_0. Since $\dot{\pi}_1 = 2n\pi_2$,[16] we finally obtain that

$$\Theta(h,j) = \int_{\pi_1^-}^{\pi_1^+} \frac{h}{j + \pi_1}\frac{d\pi_1}{\sqrt{Q}} + \Theta_0(h,j). \tag{48}$$

The term π_2 has been replaced in Eq. (48) by combining Eqs. (34) and (36).

The determination of τ is straightforward if we remark that

$$\tau(h,j) = \int_0^{\tau} ds = \int_0^T \frac{ds}{dt}dt = \int_0^T (p_1^2 + q_1^2)^{n-1}dt, \tag{49}$$

where s and t are, respectively, the rescaled and the original times. The rest of the proof consists, as we did for Θ, in rewriting the integral of Eq. (49) in the reduced phase space P_j and leads to

$$\tau(h,j) = \frac{1}{n}\int_{\pi_1^-}^{\pi_1^+} \frac{(j + \pi_1)^{n-1}}{\sqrt{Q}}d\pi_1. \tag{50}$$

□

The last technical point to be discussed is the behavior of the roots of Q as h goes to zero.

Lemma 4: The complex discriminant locus Δ of Q near the origin ($h=0$, $j=0$) *is given by*

$$\Delta = \begin{cases} h = 0 \\ h = \pm\sqrt{-n^n j^{n+1}\frac{2^{n+1}}{(n+1)^{(n+1)}}}. \end{cases} \tag{51}$$

The polynomial Q as a function of x and in the limit $h \to 0$, $j<0$ fixed, has n roots x_k whose leading term reads

$$x_k = \frac{h^{2/n}}{(-2j)^{1/n}}e^{2i\pi k/n}, \tag{52}$$

with $k \in \{0,1,2,\ldots,n-1\}$. *The other roots of Q have a nonzero finite limit.*

Proof: We first determine the complex discriminant locus Δ of Q near the point ($h=0$, $j=0$).

Constructing the Newton polyhedron of Q and taking into account only the terms of lower degrees, the principal part Q_N of Q can be written as

$$Q_N(x) = x^{n+1} - 2jx^n - h^2. \tag{53}$$

A straightforward calculation then leads to Δ.

In the limit $h \to 0$, $j < 0$ fixed, we construct the Newton polygon associated with Q. The roots of the principal part of Q_N satisfy $-2jx^n = h^2$ which allows to deduce the n roots x_k ($k \in \{0,1,\ldots,n-1\}$). □

We have now all the tools ready to prove Proposition 2.

Proof: We first consider the cases $h > 0$ and $j < 0$. We recall some of the properties of the roots of the polynomial Q viewed as a function of x which will be used in the calculation. We assume that Q has N roots with $N > n$, denoted as x_i ($i \in \{0,1,\ldots,N-1\}$). $x_n, x_{n+1}, \ldots, x_{N-1}$ are the roots of Q of order 1 in the limit $h \to 0$, $j < 0$ fixed. x_n is the smallest real positive root of Q with a nonzero limit. Since the polynomial R is defined up to a multiplicative constant, we can write Q without loss of generality as follows: $Q(x) = \Pi_{i=0}^{i=N-1}(x - x_i)$. Examination of the coefficients of Q leads to the following relations:

$$\prod_{i=0}^{i=N-1} x_i = (-1)^{N+1} h^2,$$

$$\prod_{i=0}^{n-1} x_i = (-1)^{n-1} \frac{h^2}{(-2j)}, \tag{54}$$

$$\prod_{i=n}^{N-1} x_i = 2j(-1)^{N-n+1}.$$

We determine only an equivalent of the function $\Theta - \Theta_0$. We obtain

$$\Theta(h,j) - \Theta_0(h,j) \sim h \int_{|h|^{2/n}/(-2j)^{1/n}}^{x_n} \frac{dx}{x\sqrt{\prod_{i=0}^{i=N-1}(x - x_i)}}, \tag{55}$$

where $|h|^{2/n}/(-2j)^{1/n}$ is the smallest positive real root of Q. We introduce the function k such that $|h|^{2/n}/(-2j)^{1/n} \ll k \ll 1$ when $h \to 0$. We then proceed as in the proof for the $1:-2$ resonance by decomposing the integral of Eq. (55) into two integrals. Only the first integral from $|h|^{2/n}/(-2j)^{1/n}$ to k has a limit different from zero. We then have

$$\Theta(h,j) - \Theta_0(h,j) \sim h \int_{|h|^{2/n}/(-2j)^{1/n}}^{k} \frac{dx}{x\sqrt{(-2j)\left(x^n - \frac{h^2}{-2j}\right) \times 1}}. \tag{56}$$

The change of variables $x = [|h|^{2/n}/(-2j)^{1/n}]u$ leads to the following expression for $\Theta - \Theta_0$:

$$\Theta(h,j) - \Theta_0(h,j) \sim \int_1^{+\infty} \frac{du}{u\sqrt{u^n - 1}}. \tag{57}$$

Using the fact that

$$\int \frac{du}{u\sqrt{u^n - 1}} = \frac{2}{n} \arctan[\sqrt{u^n - 1}], \tag{58}$$

one finally arrives to

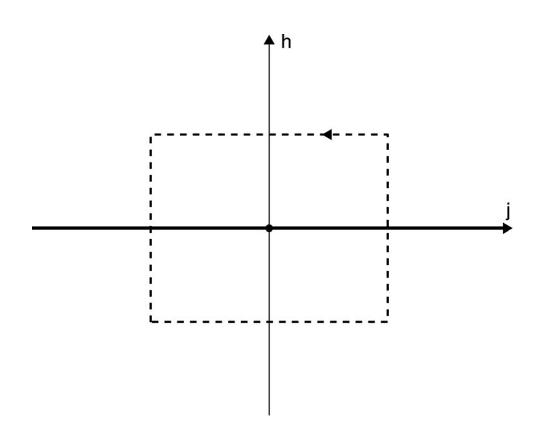


FIG. 5. Same as Fig. 3 but for the $m:-n$ resonant system.

$$\lim_{h\to 0^+, j<0} \Theta(h,j) - \Theta_0(h,j) = \frac{\pi}{n}. \tag{59}$$

It can also be shown that

$$\lim_{h\to 0^-, j<0} \Theta(h,j) - \Theta_0(h,j) = \frac{-\pi}{n}. \tag{60}$$

Following the same arguments, we can calculate the limit of τ. We decompose τ into two integrals but we only examine the last one denoted as τ_2. The calculation of the other integral can be done along the same lines. An equivalent of τ_2 is given by

$$\tau_2(h,j) \sim \frac{1}{n}\int_k^{x_n} \frac{x^{n-1}dx}{\sqrt{\prod_{i=0}^{N-1}(x-x_i)}}, \tag{61}$$

which can be rewritten as

$$\tau_2(h,j) \sim \frac{1}{n}\int_k^{x_n} \frac{dx}{\sqrt{x^{-n+2}(x^{N-n}-2j)}}, \tag{62}$$

which has the same finite and nonzero limit as $h\to 0^{\pm}$ with $j<0$ fixed. □

E. Generalization to $m:-n$ resonances

For the $m:-n$ resonant case, the momentum J reads

$$J = \tfrac{1}{2}[m(p_1^2+q_1^2) - n(q_2^2+p_2^2)], \tag{63}$$

where $m\geqslant 2$ and $n\geqslant 2$ are relatively prime integers. The bifurcation diagram corresponding locally near the origin to an $m:-n$ resonant system is displayed in Fig. 5. The equation of the singular locus is $h=0$. Each point of this line lifts for $j<0$ to an n-curled torus, whereas the points of C with $j>0$ lift to an m-curled torus. The origin corresponds to a pinched-curled torus.

Proposition 3: The monodromy matrix of an $m:-n$ resonant system of the form (35) is given for m and n relatively prime and for a counterclockwise loop around the origin (see Fig. 4) by

$$M = \begin{pmatrix} 1 & 0 \\ -1/mn & 1 \end{pmatrix}. \tag{64}$$

The proof of Proposition 3 follows the same lines as for the $1:-n$ resonance. As in Sec. II D, we consider the family of energy-momentum maps given by Eq. (35), where π_1, π_3, and J are given by Eq. (33) with $m>1$. Some lemmas are required before the final proof.

Lemma 5: The energy-momentum map F of Eq. (35) has locally the bifurcation diagram of Fig. 5 in a neighborhood of the origin if R is of the form

$$R(\pi_1,J) = (\pi_1 + J)^{n'}(\pi_1 - J)^{m'}\tilde{R}(\pi_1,J), \tag{65}$$

where $n'>n/2$, $m'>m/2$. $\tilde{R}$ is a polynomial such that the two smallest real positive roots of Q which are larger than j are simple roots for $(h,j)\in\mathcal{R}_{\text{reg}}$. Q is the following polynomial:

$$Q = (\pi_1 + j)^n(\pi_1 - j)^m - (h - R(\pi_1,j))^2. \tag{66}$$

The two roots are denoted as π_1^- and π_1^+.

Proof: The proof is similar to the proof of Lemma 2. □

Lemma 6: The functions Θ and τ are defined for a point $(h,j)\in\mathcal{R}_{\text{reg}}$ by the following integrals:

$$\Theta(h,j) = \int_{\pi_1^-}^{\pi_1^+}\left[\frac{hu}{j+\pi_1} + \frac{hv}{\pi_1 - j}\right]\frac{d\pi_1}{\sqrt{Q}} + \Theta_0(h,j),$$
$$\tau(h,j) = \frac{1}{mn}\int_{\pi_1^-}^{\pi_1^+}\frac{(j+\pi_1)^{n-1}(\pi_1 - j)^{m-1}}{\sqrt{Q}}d\pi_1. \tag{67}$$

Θ_0 is a function over $\mathcal{R}$ which is continuous on the line of singularities C. u and v are two integers such that $mu-nv=1$. τ is the first return time of the rescaled vector field $X=[1/(p_1^2+q_1^2)^{n-1}(p_2^2+q_2^2)^{m-1}]X_H$ defined such that τ has a nonzero finite limit on C.

Remark 4: One can obtain the expression given by Eq. (42) corresponding to the case $1:-n$ as a special case of Eq. (67) with $u=1$ and $v=0$, which is a particular solution of $mu-nv=1$ for $m=1$.

Proof: The determination of Θ is based on the dependence of the angle θ as a function of the coordinates (p_1,q_1,p_2,q_2). To clarify this question, we introduce the canonical conjugate coordinates (I_1,φ_1) and (I_2,φ_2) which are defined as follows:

$$q_k = \sqrt{2I_k}\sin\varphi_k,$$
$$p_k = \sqrt{2I_k}\cos\varphi_k. \tag{68}$$

Note that the polar coordinates (I_k,φ_k) are only defined if $p_k^2+q_k^2>0$,[19] which is not the case on line C. By definition, the angles φ_1 and φ_2 vary in an interval of length 2π. We look for a linear canonical transformation which transforms the two angles φ_1 and φ_2 into θ and ψ, where the angle θ is canonically conjugate to J. The angular dependence of H in the variables $(I_1,\varphi_1,I_2,\varphi_2)$ is given by the term π_3 and is equal to $n\varphi_1+m\varphi_2$. We then set

$$\theta = u\varphi_1 + v\varphi_2,$$
$$\psi = n\varphi_1 + m\varphi_2, \tag{69}$$

where u and v are integers such that $mu-nv=1$, which ensures that the determinant of the linear canonical transformation is 1 and that θ and ψ are two angles varying in an interval of length 2π. Since m and n are relatively prime, the Bezout theorem states that this equation has a solution (u_0,v_0). There are an infinite number of solutions which can be written (u_0+kn,v_0+km) with $k\in\mathbb{Z}$. We denote by (u,v) one of these solutions. A choice of a couple (u,v) is associated with a choice of a particular basis of the homology group.

The generating function F_2 of type 2 (Ref. 19) associated with the canonical transformation is given by

$$F_2 = (u\varphi_1 + v\varphi_2)\tilde{J} + (n\varphi_1 + m\varphi_2)\mathcal{I}, \tag{70}$$

where $\tilde{J}$ and $\mathcal{I}$ are the momenta conjugated, respectively, to θ and ψ. From the definition of F_2, one deduces that

$$\begin{aligned} \tilde{J} &= mI_1 - nI_2, \\ \mathcal{I} &= uI_2 - vI_1, \end{aligned} \tag{71}$$

and that as expected $\tilde{J}=J$. We will drop the tilde in the rest of the proof.

The angle θ can therefore be written as

$$\theta = u \arg(p_1 + iq_1) + v \arg(p_2 + iq_2). \tag{72}$$

Differentiating Eq. (71) with respect to time and using the Hamilton equations, one obtains that

$$\dot{\theta} = \frac{u\left(n\pi_3 + \frac{\partial R}{\partial p_1}p_1 + \frac{\partial R}{\partial q_1}q_1\right)}{q_1^2 + p_1^2} + \frac{v\left(m\pi_3 + \frac{\partial R}{\partial p_2}p_2 + \frac{\partial R}{\partial q_2}q_2\right)}{q_2^2 + p_2^2}, \tag{73}$$

which leads to

$$\dot{\theta} = \frac{u\left(nmh - nmR + m\frac{\partial R}{\partial p_1}p_1 + m\frac{\partial R}{\partial q_1}q_1\right)}{j + \pi_1} + \frac{v\left(nmh - nmR + n\frac{\partial R}{\partial p_2}p_2 + n\frac{\partial R}{\partial q_2}q_2\right)}{\pi_1 - j}. \tag{74}$$

The last step consists in rewriting this integral as an integral in the reduced phase space P_j. The R-dependent part of Θ gives a continuous contribution on line C denoted Θ_0. Since $\dot{\pi}_1 = 2mn\pi_2$, one finally obtains

$$\Theta(h,j) = \int_{\pi_1^-}^{\pi_1^+} \left[\frac{hu}{j + \pi_1} + \frac{hv}{\pi_1 - j}\right]\frac{d\pi_1}{\pi_2} + \Theta_0(h,j). \tag{75}$$

For τ, the proof is straightforward and similar to the one of Lemma 3. □

Lemma 7: The complex discriminant locus Δ *near the origin is given by*

$$\Delta = \begin{cases} h = 0 \\ h = \pm\sqrt{(-1)^m 2^{m+n} m^m n^n j^{m+n}/(m+n)^{m+n}}. \end{cases} \tag{76}$$

In the limit $h \to 0$, $j<0$ *fixed, the polynomial* Q *as a function of* x *has* n *roots* x_k *whose leading term is*

$$x_k = \frac{h^{2/n}}{(-2j)^{m/n}} e^{2i\pi k/n}, \tag{77}$$

with $k \in \{0,1,\ldots,n-1\}$, *the other roots having a finite limit different from zero.*

In the limit $h \to 0$, $j>0$ *fixed, the polynomial* Q *as a function of* x' *has* m *roots* x'_k *whose leading term is*

$$x'_k = \frac{h^{2/m}}{(2j)^{n/m}} e^{2i\pi k/m}, \tag{78}$$

with $k \in \{0,1,\ldots,m-1\}$, *the other roots having a finite limit different from zero.*

Remark 5: We notice that the cases $j>0$ and $j<0$ give the same expressions but with m and n interchanged.

Proof: Let us assume that $j<0$. As for the $1:-n$ resonance, we calculate the complex discriminant locus of Q near the origin as a function of x. The construction of the Newton polyhedron gives the principal part Q_N of Q,

$$Q_N(x) = (x-2j)^m x^n - h^2. \tag{79}$$

Simple algebra leads to the discriminant locus Δ.

In the limit $h \to 0$, $j<0$ fixed, the construction of the Newton polygon of Q leads to the following equation for the roots of the principal part of Q:

$$(-2j)^m x^n = h^2, \tag{80}$$

and to the n roots x_k of Eq. (77). Exchanging the role of m and n and taking $j>0$, a similar proof gives the roots of Eq. (78). □

Having established Lemmas 5, 6, and 7, we can pass to the proof of Proposition 3.

Proof: Since line C is crossed two times by the loop Γ, the monodromy matrix M has two contributions denoted as M_- for $j<0$ and M_+ for $j>0$. We first consider the case $j<0$. The case $j>0$ will be deduced from the calculation for $j<0$ by exchanging the role of m and n. The calculation is based on the analysis of the roots of the polynomial Q. Q has N roots denoted as x_i with $i \in \{0,1,\ldots,N-1\}$. The roots $x_n,\ldots,x_{N-1}$ are of order 1. A simple analysis of the polynomial Q leads to the following relations:

$$\prod_{i=0}^{N-1} x_i = h^2(-1)^{N+1},$$

$$\prod_{i=0}^{n-1} x_i = \frac{h^2}{(-2j)^m}(-1)^{n-1}, \tag{81}$$

$$\prod_{i=n}^{N-1} x_i = (-1)^{N-n+m}(-2j)^m.$$

Following the same steps as in the proof for the $1:-n$ resonance, one arrives to

$$\Theta(h,j) - \Theta_0(h,j) \sim uh \int_{|h|^{2/n}/(-2j)^{m/n}}^{k} \frac{dx}{x\sqrt{(-2j)^m\left(x^n - \frac{h^2}{(-2j)^m}\right) \times 1}}, \tag{82}$$

where $|h|^{2/n}/(-2j)^{m/n} \ll k \ll 1$. For $h>0$, Eq. (82) simplifies into

$$\Theta(h,j) - \Theta_0(h,j) \sim u \int_1^{+\infty} \frac{dx}{x\sqrt{x^n-1}}. \tag{83}$$

We finally obtain that

$$\lim_{h\to 0^{\pm}, j<0} = \Theta(h,j) - \Theta_0(h,j) = \pm u\frac{\pi}{n}. \tag{84}$$

A similar proof leads to

$$\lim_{h\to 0^{\pm},j>0} = \Theta(h,j) - \Theta_0(h,j) = \pm v\frac{\pi}{m}. \tag{85}$$

The calculation of τ uses the same arguments and shows that τ is continuous on C.

One then deduces that the matrices M_- and M_+ are, respectively, given by

$$M_- = \begin{pmatrix} 1 & 0 \\ -\dfrac{u}{n} & 1 \end{pmatrix} \tag{86}$$

and

$$M_+ = \begin{pmatrix} 1 & 0 \\ \dfrac{v}{m} & 1 \end{pmatrix}, \tag{87}$$

where we have taken into account for M_+ the fact that line C is crossed from $h<0$ to $h>0$. The total monodromy matrix is given by the product of the matrices M_- and M_+,

$$M = \begin{pmatrix} 1 & 0 \\ -\dfrac{u}{n} & 1 \end{pmatrix}\begin{pmatrix} 1 & 0 \\ \dfrac{v}{m} & 1 \end{pmatrix} = \begin{pmatrix} 1 & 0 \\ -\dfrac{1}{mn} & 1 \end{pmatrix}, \tag{88}$$

where the relation $mu-nv=1$ has been used. □

III. EXTENSION TO THE COMPLEX DOMAIN

A. Idea of the method

In this section, we reformulate the notion of the fractional Hamiltonian monodromy by deforming the loop Γ close to line C, such that it bypasses line C through the complex domain. The bypass Γ_C is a semicircle around line C. The starting point of the complex approach is given by the expressions of the functions Θ and τ as real one-dimensional integrals [see, for instance, Lemma 1 and Eqs. (10) and (11) for the $1:-2$ resonance case]. If we consider the complexified variables h, j, and π_1, then $\Theta(h,j)$ and $\tau(h,j)$ can be interpreted as integrals of rational 1-forms over a cycle δ on the Riemann surface defined by $\pi_2^2=Q(\pi_1)$. This allows the use of topological properties of the Riemann surfaces.

More precisely, we first introduce a Riemann surface constructed from the energy-momentum map F and we determine the Gauss–Manin connection along the loop Γ bypassing line C of singularities. The Gauss–Manin connection is determined by following the motion of the ramification points of the Riemann surface. The Gauss–Manin monodromy is calculated for a base point $(-h_0,j)$ with $j<0$ and $h_0>0$. As explained below, we can then construct the extension to the complex domain of the functions Θ and τ. The monodromy matrix is determined as in the real approach by the variation of the functions Θ and τ along the loop Γ. The regularizations of the functions Θ and τ to cross line C are replaced by their continuations along the semicircle Γ_C. Fractional monodromy is obtained in the limit where the radius h_0 of the semicircle Γ_C tends to 0 and the base point $(-h_0,j)$ goes to line C.

B. Extension to the complex domain of the 1:−2 resonant system

Remark 6: All that has been established in Sec. II A for the real approach can be done exactly in the same way for the complexified phase space $T^*\mathbb{C}^2$, where $(J,\pi_1,\pi_2,\pi_3)\in\mathbb{C}^4$, except for the fact that there is no restriction on the values of J and π_1. The quotient is taken to be $\mathbb{C}^*\sim S^1\times\mathbb{R}^*$. The reduction in the complex approach is described in AppendixC. The manifold $\mathbb{C}^4/S^1\times\mathbb{R}^*$ has real dimension 6.

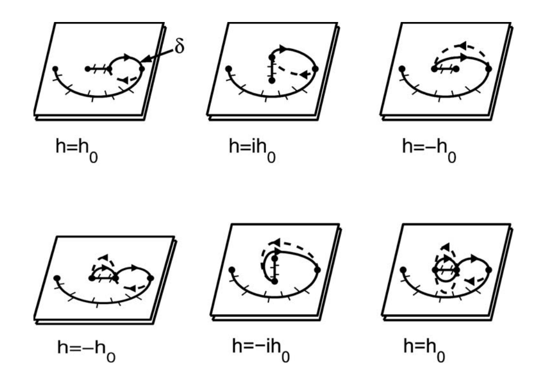


FIG. 6. Transport of the cycle δ along a path around line C. The path is a semicircle of radius $h_0>0$. The solid lines without arrows represent arbitrary branch cuts of the Riemann surfaces, and the full dots the ramification points (see text). The parts in solid and dashed lines of the loop lie, respectively, in the upper and lower leaves of the Riemann surface. For the first figure, the ramification points are from left to right x_1, x_2, x_3, and x_4.

We begin by recalling some of the basic elements of the theory of complex algebraic curves which will be used throughout this section (see Ref. 33 for a comprehensive introduction).

Let $P:\mathbb{C}^2\to\mathbb{C}$ be a polynomial function. The fibers $P^{-1}(z)$ are complex algebraic curves (hence two-dimensional real surfaces). There exists a finite set $\Sigma\subset\mathbb{C}$ (essentially critical values of P) such that all fibers $P^{-1}(z)$, $z\in\mathbb{C}\setminus\Sigma$, look alike. Moreover, the mapping $P:\mathbb{C}^2\setminus(P^{-1}(\Sigma))\to\mathbb{C}\setminus\Sigma$ is a locally trivial fibration. The local triviality of the fibration can be shown by pushing a generic fiber to nearby fibers using the gradient flow associated with the polynomial P. This construction is not defined in critical points where the gradient vanishes, which explains why the critical points have to be eliminated from the base space of the fibration. Hence, given any path $\gamma:[z_0,z_1]\to\mathbb{C}\setminus\Sigma$, one can identify the fibers $P^{-1}(\gamma(z_0))$ and $P^{-1}(\gamma(z_1))$. This identification is not unique but induces a unique identification between the homology groups of the two fibers. For $z_0\in\mathbb{C}\setminus\Sigma$, a cycle $\delta(z_0)\in H_1(P^{-1}(z_0))$ can be transported along any path γ in $\mathbb{C}\setminus\Sigma$ starting at z_0 giving thus a family of cycles $\delta(z)$. The transport depends only on the homotopy class of the path γ in $\mathbb{C}\setminus\Sigma$. This is the classical Gauss–Manin connection.[29,30] To each loop in $\mathbb{C}\setminus\Sigma$, the Gauss–Manin monodromy is defined from the Gauss-Manin connection as an automorphism of the homology group H_1.

For the $1:-2$ resonance (see Sec. II B), the energy-momentum map of Eq. (1) can be treated in the formalism of complex algebraic curves even if the situation is more complicated than described above. The difficulty here lies in the fact that the *fibration* is defined only implicitly by

$$F^{\mathbb{C}}:=\pi_2^2-[(\pi_1-j)(\pi_1+j)^2-(h-\varepsilon(\pi_1^2-j^2))^2]=0, \tag{89}$$

i.e., $\pi_2^2=Q(\pi_1,j,h)$.

For fixed generic values of (h,j), Eq. (89) defines a torus from which two points at infinity have been deleted. The corresponding complex algebraic curve is schematically represented in Fig. 6. This representation can be understood by solving Eq. (89) with respect to π_2. Generically, there are four values of π_1 for which $Q(\pi_1,j,h)=0$, giving each a single solution for $\pi_2=0$. These points are the ramification points of the complex algebraic curve. For all other points π_1, there are two solutions π_2 of Eq. (89) represented by the two leaves in Fig. 6. We denote by $F^{\mathbb{C}}_{(j,h)}$ the set of points $(\pi_1,\pi_2)\in\mathbb{C}^2$ such that (π_1,π_2,j,h) verify Eq. (89). Note that for two different values $(h,j)\neq(h',j')$, the fibers $F^{\mathbb{C}}_{(j,h)}$ and $F^{\mathbb{C}}_{(j',h')}$ intersect. Nevertheless, it is possible to generalize the Gauss–Manin connection to this case. Consider for that the mapping $G:\mathbb{C}^4\to\mathbb{C}^3$, given by

$$G(\pi_1,\pi_2,h,j)=(\pi_2^2-Q(\pi_1,h,j),h,j). \tag{90}$$

The mapping G defines a fibration on the complement $\mathbb{C}^3\setminus\Sigma$ of the set $\Sigma\in\mathbb{C}^3$, where its rank is not maximal. We use here the Ehresmann fibration theorem.[34] We take as basis of our fibration denoted as $\mathcal{B}\in\mathbb{C}^2$ the set $(\{0\}\times\mathbb{C}^2)\cap(\mathbb{C}^3\setminus\Sigma)$ which is viewed as a set in the (h,j)-space $\mathbb{C}^2$. As in

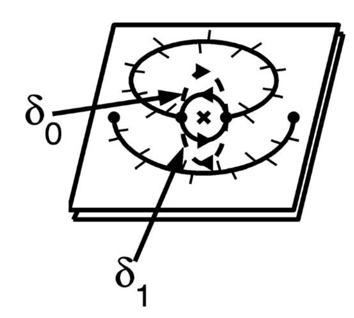


FIG. 7. Definition of the cycles δ_0 and δ_1 for the $1:-2$ resonance. The position of the pole of Θ is represented by a cross.

the real approach, we introduce the variable $x=j+\pi_1$ and we set $y=\pi_2$. The singular locus of the fibration is the set of points $(h,j)\in\mathbb{C}^2$, where the polynomial Q has multiple complex roots. This set is given by Eq. (15) and is displayed for $j\in\mathbb{R}$ in Fig. 7. We notice that for $(h,j)=(0,0)$, the fibration is singular and that the singularity $(x=0,y=0)$ is not of Morse type.

In the reduced phase space P_j, the original real torus projects to a cycle $\delta(h,j)$ delimited by π_1^- and π_1^+ (see, for instance, Fig. 4). π_1^- and π_1^+ are the two largest real roots of the polynomial Q as a function of π_1. Returning back to the Riemann surface and following notations of Eq. (18), the roots of Q, which are simple ramification points of the Riemann surface, are denoted as x_k ($k=1,\ldots,4$). One can introduce cuts along the segment x_2x_3 and along a simple curve joining x_1 and x_4 and avoiding the segment x_2x_3. For $(h,j)\in\mathcal{R}_{\text{reg}}$, the cycle $\delta(h,j)$ is represented by the real oval between the two largest real ramification points which correspond, respectively, to $j+\pi_1^-$ and $j+\pi_1^+$. To be coherent with the real approach, this cycle is oriented from $x=j+\pi_1^-$ to $x=j+\pi_1^+$ in the upper leaf and from $x=j+\pi_1^+$ to $x=j+\pi_1^-$ in the lower one. All these notations are displayed in Fig. 6.

C. Computation of fractional monodromy from the Gauss–Manin monodromy

We pursue in this section the construction for the $1:-2$ resonant system to arrive to the computation of fractional monodromy at the end of the section. Let Γ be a loop around the origin. We recall that the computation of the monodromy matrix associated with Γ is based on the difference of the values of the functions Θ and τ at each side of C as h goes to 0. The goal here is to compute the variations of these functions using their extensions to the complex domain near C.

Definition 2: Starting with the result of Lemma 1, we introduce the complex continuation of the functions Θ and τ defined by

$$\Theta(h,j)=\frac{h}{2i\varepsilon}\int_{\delta(h,j)}\frac{dx}{xy},$$
$$\tau(h,j)=\frac{1}{4i\varepsilon}\int_{\delta(h,j)}\frac{xdx}{y}, \tag{91}$$

where $(h,j)\in\mathcal{B}$ and $y^2=(x-x_1)(x-x_2)(x-x_3)(x-x_4)$. The positive and negative determinations of the square root y have been chosen, respectively, for the upper and the lower leaves of the Riemann surface. We have added a factor $\frac{1}{2}$ in the definition of Θ and τ to coincide with the real case.

We locally deform in a neighborhood of line C the loop Γ. We denote by Γ_C this complex deformation and by Γ_R the rest of the loop. Γ, Γ_C, and Γ_R are represented in Figs. 7 and 8.

Remark 7: In this work, we have considered deformations of the real loop in the half-plane $\Im[h]>0$ but they could be equivalently done in the half-plane $\Im[h]<0$.

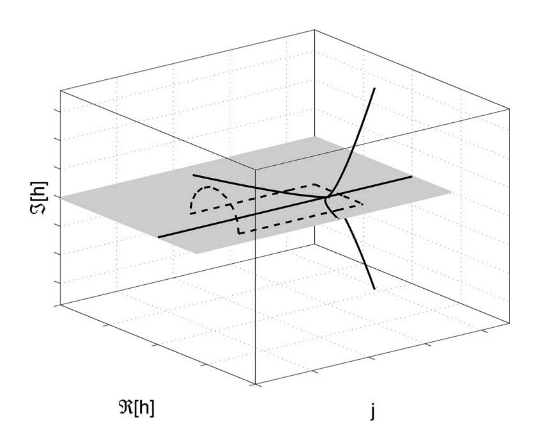


FIG. 8. Complex discriminant locus Δ (solid lines) of the energy-momentum map of Eq. (1) for $j \in \mathbb{R}$ and $h \in \mathbb{C}$. The gray plane corresponds to the real bifurcation diagram. The different branches of Δ are given by Eq. (15) near the origin. The six branches intersect at the origin. Four of the branches are real and lie in the gray plane. The dashed lines represent the loop Γ locally deformed near C to the complex domain. The semicircle which corresponds to Γ_C (see text) is in a complex *h-plane* with j fixed.

The bypass $\Gamma_C(h_0)$ is a semicircle of radius h_0 in a plane with $j_0 < 0$ fixed around line C. The corresponding real path completing $\Gamma_C(h_0)$ is denoted as $\Gamma_R(h_0)$. From Eq. (15) and for a small j_0, one deduces that if $h_0 < \sqrt{\frac{-32}{27} j_0^3}$, then x_2 and x_3 exchange their positions along $\Gamma_C(h_0)$, whereas if $h_0 > \sqrt{\frac{-32}{27} j_0^3}$, then three ramification points of the Riemann surface (x_1, x_2, and x_3) move and exchange their positions. The change of the ramification points is displayed in Fig. 9. It can also be deduced from the asymptotic expansions of the roots of Q [see Eq. (18)]. This can be seen by parametrizing the loop $\Gamma_C(h_0)$ as

$$h = h_0 e^{it},$$
$$j = j_0, \tag{92}$$

where $t \in [0, \pi]$. There is thus a qualitative difference of the result depending on the value of h_0. h_0 must be chosen sufficiently small to be in the first case since for each fixed j_0, we are interested in the limit $h_0 \to 0$.

The family of cycles $\delta(h,j)$ can be obtained by transport of the cycle $\delta(h_0,j_0)$ along Γ_R. Examining Fig. 10, one sees that the lines of singularities crossed by Γ_R have no incidence on the ramification points defining the cycle δ. This means that for the lines considered, the ramification points associated with δ do not collide with other ramification points. This is not the case on line C since x_2 and x_3 collide on this line. The parallel transport of δ along $\Gamma_C(h_0)$ is given by the change of the ramification points along $\Gamma_C(h_0)$. In accordance with the Picard–Lefshetz theory[29,30] (see Figs. 6), one can show that the cycle $\delta(h_0,j_0)$ when transported along the bypass $\Gamma_C(h_0)$ is transformed into $\delta(-h_0,j_0)+\delta_0(-h_0,j_0)$, where δ_0 is a vanishing cycle around the ramification points x_2 and x_3 of the fiber $F^{\mathbb{C}}_{(-h_0,j_0)}$. x_2 and x_3 are defined by Eq. (19). For the position of the cuts of Fig. 6, the cycle $\delta_0(-h_0,j_0)$ is composed of a path from x_3 to x_2 on the upper leaf followed by the lift of the same path to the lower leaf run in the opposite direction. The vanishing cycles δ_0 and

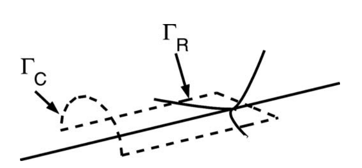


FIG. 9. Decomposition of the loop Γ into the paths Γ_C and Γ_R.

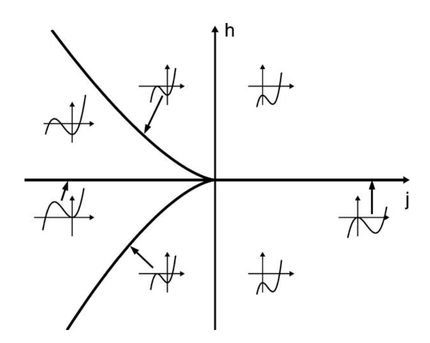


FIG. 10. Schematic representation of three of the roots of the polynomial Q as a function of h and j. These roots are the roots of the principal part Q_N of Q defined by Eq. (14). The polynomial Q has another root larger in module which is not represented here as it undergoes no bifurcation. The small insets depict the graph of Q_N as a function of x for different values of h and j. The position of the insets gives the corresponding values of h and j. The solid lines are real lines of singularities of Δ.

δ_1 are represented in Fig. 7. The cycle δ_1 will be used in Lemma 8. Note the different choices of cuts for the Riemann surface between Fig. 6 and Fig. 7. Hence, an Abelian integral $I(h_0,j_0) = \int_{\delta(h_0,j_0)}\omega$ becomes, after going once around the semicircle $\Gamma_C(h_0)$, the sum $I(-h_0,j_0) + \int_{\delta_0(-h_0,j_0)}\omega$, which gives the variation of the function I over $\Gamma_C(h_0)$. This latter remark can be applied to the functions Θ and τ. However, due to the presence of a pole at $x=0$ for the function Θ, the cycle δ_0 has to be positioned with respect to $x=0$. The counterclockwise turning of the ramification points x_2 and x_3 implies that the cycle δ_0 avoids the singularity $x=0$ from above.

From the analysis of the behavior of the cycle δ along Γ, we can determine the variations of the functions Θ and τ along this loop. These variations are denoted as $\Delta\Theta_\Gamma(h_0)$ and $\Delta\tau_\Gamma(h_0)$ and defined as follows.

Definition 3: For the energy-momentum map of Eq. (1), $\Delta\Theta_\Gamma(h_0)$ *and* $\Delta\tau_\Gamma(h_0)$ *are given in the complex approach by*

$$\begin{aligned}\Delta\Theta_\Gamma(h_0) &= \Delta\Theta_{\Gamma_C}(h_0) + \Delta\Theta_{\Gamma_R}(h_0),\\ \Delta\tau_\Gamma(h_0) &= \Delta\tau_{\Gamma_C}(h_0) + \Delta\tau_{\Gamma_R}(h_0).\end{aligned} \tag{93}$$

The base point of the loop Γ is here the point $(-h_0,j_0)$ (with $j_0<0$ and $h_0>0$) which belongs to the intersection of Γ_R and Γ_C. A simple calculation allows to simplify the expressions of $\Delta\Theta_\Gamma(h_0)$ and $\Delta\tau_\Gamma(h_0)$. Since

$$\Delta\Theta_R(h_0) = \frac{h_0}{2i\varepsilon}\int_{\delta(h_0,j_0)}\frac{dx}{xy} - \frac{-h_0}{2i\varepsilon}\int_{\delta(-h_0,j_0)}\frac{dx}{xy} \tag{94}$$

and

$$\Delta\Theta_C(h_0) = \frac{-h_0}{2i\varepsilon}\int_{\delta(-h_0,j_0)}\frac{dx}{xy} + \frac{-h_0}{2i\varepsilon}\int_{\delta_0(-h_0,j_0)}\frac{dx}{xy} - \frac{h_0}{2i\varepsilon}\int_{\delta(h_0,j_0)}\frac{dx}{xy}, \tag{95}$$

one deduces, for $j_0<0$ fixed, that

$$\Delta\Theta_\Gamma(h_0) = -\frac{h_0}{2i\varepsilon}\int_{\delta_0(-h_0,j_0)}\frac{dx}{xy},$$
$$\Delta\tau_\Gamma(h_0) = \frac{1}{4i\varepsilon}\int_{\delta_0(-h_0,j_0)}\frac{xdx}{y}. \quad (96)$$

We introduce for the function Θ the following quantities:

$$\Delta\Theta_\Gamma = \lim_{h_0\to 0}\Delta\Theta_\Gamma(h_0),$$
$$\Delta\Theta_{\Gamma_C} = \lim_{h_0\to 0}\Delta\Theta_{\Gamma_C}(h_0), \quad (97)$$
$$\Delta\Theta_{\Gamma_R} = \lim_{h_0\to 0}\Delta\Theta_{\Gamma_R}(h_0),$$

and the same for τ.

Different results have to be established before computing the monodromy matrix. The variation of Θ around C can be viewed as a residue.

Lemma 8: The sum of the integrals of the 1-form $(h_0/2i\varepsilon)(dx/xy)$ over δ_0 and δ_1 is independent of h_0 and j_0 and equal to

$$\frac{h_0}{2i\varepsilon}\int_{\delta_0(h_0,j_0)}\frac{dx}{xy} + \frac{h_0}{2i\varepsilon}\int_{\delta_1(h_0,j_0)}\frac{dx}{xy} = 2\pi. \quad (98)$$

In this equation, h_0 is taken sufficiently small and $j_0<0$.

Proof: We use the notations of Fig. 7. The union of δ_0 and δ_1 corresponds to two loops around the pole $x=0$ lying, respectively, in the upper and the lower leaves of the Riemann surface. The orientation of these two loops is on the lower leaf, opposite to the one on the upper leaf. The same applies to the determination of the square root y for the two leaves of the Riemann surface. Hence, the sum of the left hand side of Eq. (98) is given by two times the residue of the 1-form dx/xy at $x=0$. One deduces that

$$\frac{h_0}{2i\varepsilon}\int_{\delta_0(h_0,j_0)}\frac{dx}{xy} + \frac{h_0}{2i\varepsilon}\int_{\delta_1(h_0,j_0)}\frac{dx}{xy} = \frac{h_0}{2i\varepsilon}4\pi i \,\mathrm{Res}\left(\frac{1}{xy},x=0\right). \quad (99)$$

Simple algebra leads to

$$\mathrm{Res}\left(\frac{1}{xy},x=0\right) = \frac{\varepsilon}{h_0}, \quad (100)$$

which completes the proof. □

Lemma 9: The variations of the functions Θ and τ along Γ are

$$\Delta\Theta_\Gamma = \pi,$$
$$\Delta\tau_\Gamma = 0. \quad (101)$$

Proof: We use Eq. (96) and we calculate these two quantities in the limit $h_0\to 0$ and $j_0<0$ fixed. The asymptotic expansion of the roots x_i for $h\to 0$ and $j<0$ fixed is given by Eq. (19) (see Ref. 17 for the explicit computation).

We begin by the computation of $\Delta\Theta_\Gamma$. We first notice that x_2 and x_3 are real. δ_0 can thus be viewed as a real loop which is locally deformed in a neighborhood of $x=0$ to avoid the pole in $x=0$. Since the path δ_0 is oriented in the opposite direction and the sign of y is the opposite in the

lower leaf with respect to the upper leaf, it is straightforward to see that the contributions of the upper and lower leaves of the Riemann surface coincide. $\Delta\Theta_\Gamma$ can be written as follows:

$$\Delta\Theta_\Gamma = \lim_{h_0\to 0}\left[\mathrm{PV}\frac{-h_0}{i\varepsilon}\int_{x_3}^{x_2}\frac{dx}{xy} + \frac{h_0}{i\varepsilon}\frac{1}{2}2\pi i\,\mathrm{Res}\left(\frac{1}{xy},x=0\right)\right], \tag{102}$$

where PV denotes the principal value of the integral. The introduction of the principal value is due to the presence of the pole at $x=0$. The residue is calculated with the positive determination of the square root y. The factor $\frac{-1}{2}$ in front of the residue corresponds to the fact that the integral is taken on a semicircle which is oriented in a clockwise manner. The contribution of the residue term to $\Delta\Theta_\Gamma$ is equal to π. Following Ref. 17, the computation of the principal value term can be done by using elliptic integrals. It can be shown that this term is zero.

Using the same arguments, we can deduce that $\Delta\tau_\Gamma=0$ since τ has no singularity along the real segment x_2x_3. □

In the limit $h_0\to 0$, δ_0 and δ_1 play a symmetrical role for Θ. More precisely, we have the following.

Corollary 1: The integrals of the 1-form $(h_0/2i\varepsilon)(dx/xy)$ *over* δ_0 *and* δ_1 *are given by*

$$\lim_{h_0\to 0}\frac{h_0}{2i\varepsilon}\int_{\delta_0(h_0,j_0)}\frac{dx}{xy} = \lim_{h_0\to 0}\frac{h_0}{2i\varepsilon}\int_{\delta_1(h_0,j_0)}\frac{dx}{xy} = \pi. \tag{103}$$

Proof: The proof of Lemma 9 has already shown that

$$\lim_{h_0\to 0}\frac{h_0}{2i\varepsilon}\int_{\delta_0(h_0,j_0)}\frac{dx}{xy} = \pi. \tag{104}$$

We conclude for δ_1 by using Lemma 8. □

Remark 8: The semicircle Γ_C *is taken to be asymptotic in order for* $\Delta\Theta_\Gamma$ *and* $\Delta\tau_\Gamma$ *to be independent of h and j and to recover the topological character of fractional monodromy. In contrast, if we consider a loop around line C, then the variation of* Θ *along this loop is topological as it is calculated from a residue (see Lemma 8).*

From Lemma 9, we can finally conclude by the following proposition.

Proposition 4: The monodromy matrix M for the loop Γ *is given by*

$$M = \begin{pmatrix} 1 & 0 \\ -\frac{1}{2} & 1 \end{pmatrix}. \tag{105}$$

Proof: We use Lemma 9 and the fact that the monodromy matrix is determined by the variations $\Delta\Theta_\Gamma$ and $\Delta\tau_\Gamma$. □

Remark 9: In the computation of Lemma 9, we have taken arbitrary j, which shows the topological character of the definition of fractional monodromy.

We note that the real and the complex approach can be related by the following corollary.

Corollary 2: $\Delta\Theta_C=0$ *and hence* $\Delta\Theta_R=\Delta\Theta_\Gamma$.

Proof: We apply Jordan's lemma to show that $\Delta\Theta_C=0$. □

The monodromy matrix in the real approach (complex approach) is given by $\Delta\Theta_R$ and $\Delta\tau_R$ ($\Delta\Theta_\Gamma$ and $\Delta\tau_\Gamma$). Corollary 2 shows that these two approaches are equivalent.

D. Generalization to 1:−*n* resonance

All the arguments used for constructing the extension to the complex domain of $1:-2$ resonant systems can be generalized to $1:-n$ and $m:-n$ resonant systems. As for the real approach, we consider the family $\mathcal{F}$ of energy-momentum maps introduced in Eq. (35).

The Riemann surface is defined from the relation deduced from Eqs. (34) and (35),

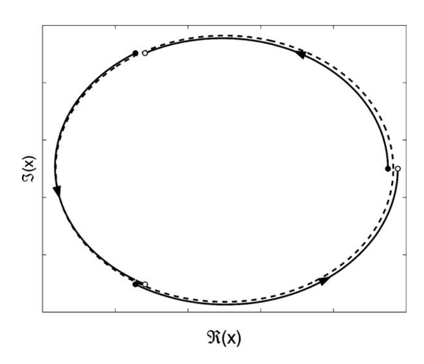


FIG. 11. Evolution of three of the roots (see text) of the polynomial Q from the $1:-3$ resonance and for a semicircle going from $h_0>0$ to $-h_0<0$ ($j_0<0$ fixed). Numerical values are taken to be $h_0=0.005$ and $j_0=-1$. The radius of the semicircle is h_0. The energy-momentum map is given by Eq. (36). The full and open dots represent, respectively, the roots for the starting and the ending points of the path. The dashed line is a circle of radius $h_0^{2/3}/(-2j)^{1/3}$, which corresponds to the leading term of the expansion of the roots as $h_0 \to 0$.

$$y^2 = x^n(x-2j) - [h - R(x-j,j)]^2. \tag{106}$$

The discriminant locus Δ of these systems is given locally by Eq. (51). Note that this locus is qualitatively different according to the parity of n. More precisely, the real lines of singularities for n odd become purely imaginary for n even. This does not change the discussion of this section. Following the preceding case, we consider a loop Γ around the origin which decomposes into a semicircle Γ_C around line C and a real path Γ_R. Along Γ_C, one sees by using the expansion of the roots of Q (Lemma 4) that for $j<0$, n roots in the variable x turn asymptotically around the origin by an angle $2\pi/n$. The other roots stay fixed to first order in h. Figure 11 illustrates this point for the $1:-3$ resonance. Note that only the roots of the principal part are exactly exchanged among themselves. The definition of the cycles δ_0, δ_1, and δ_2 is given in Fig. 12. Following the change of the ramification points, we can transport the cycle δ along Γ_C. $\delta(h,j)$ is a real oval between x_0 and the ramification point of the Riemann surface associated with π_1^+ denoted as x_n. This cycle is oriented from x_0 to x_n in the upper leaf and from x_n to x_0 in the lower one. Figures 13 and 14 display the transport of δ. Not all the ramification points are represented in Figs. 13 and 14. The position of the cuts is arbitrary but indicates on which leaf of the Riemann surface a path lies. We can compare two Riemann surfaces if the cuts of the two surfaces are the same. Since for the $1:-n$ resonance the cuts move after a semicircle, one has to modify the presentation of the surface to recover the initial choice of cuts. An example of this transformation is given in Fig. 13.

We see that after the semicircle $\Gamma_C(h_0)$ around C, $\delta(h_0,j_0)$ is transformed into $\delta(-h_0,j_0) + \delta_0(-h_0,j_0)$. δ_0 is composed of a path from x_0 to x_{n-1} in the upper leaf and of the lift of the same path in the lower leaf but run in the opposite direction.

Definition 4: We define the complex extension of the functions Θ *and* τ *as*

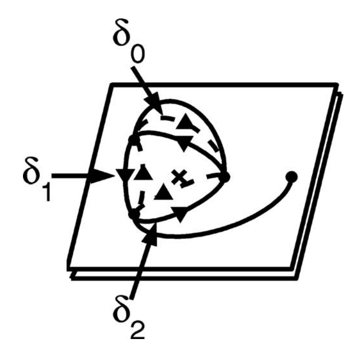


FIG. 12. Definition of the cycles δ_0, δ_1, and δ_2 for the $1:-3$ resonance. The cross indicates the position of the pole of Θ.

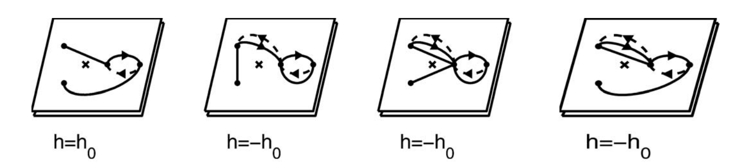


FIG. 13. Transport of the cycle δ along a semicircle around line C. The radius of the semicircle is h_0. The last three figures are equivalent but with different cuts. The cross indicates the position of the pole of Θ.

$$\Theta(h,j) = \frac{h}{2}\int_{\delta(h,j)} \frac{dx}{xy} + \Theta_0(h,j), \tag{107}$$

where the positive determination of the square root y is associated with the upper leaf and

$$\tau(h,j) = \frac{1}{2n}\int_{\delta(h,j)} \frac{x^{n-1}dx}{y}. \tag{108}$$

Θ_0 *is the complex extension of the real function* Θ_0 *introduced in Eq.* (48). Θ_0 *has a trivial contribution to the monodromy matrix.*

We define the variations $\Delta\Theta_\Gamma(h_0)$ and $\Delta\tau_\Gamma(h_0)$ of the functions Θ and τ along Γ as in Definition 3 for the $1:-2$ resonance. These variations are given by integrals over the cycle δ_0. $\Delta\Theta_\Gamma$ and $\Delta\tau_\Gamma$ denote the limits of these variations as $h_0 \to 0$. They are given by

$$\Delta\Theta_\Gamma = \lim_{h_0\to 0} \Delta\Theta_\Gamma(h_0),$$
$$\Delta\tau_\Gamma = \lim_{h_0\to 0} \Delta\tau_\Gamma(h_0). \tag{109}$$

Equivalent lemmas to Lemmas 8 and 9 for the $1:-2$ resonance can be established for the $1:-n$ resonance. We only state the final result.

Proposition 5: The monodromy matrix associated with the loop Γ *is equal to*

$$M = \begin{pmatrix} 1 & 0 \\ -1/n & 1 \end{pmatrix}. \tag{110}$$

Proof: We compute the different integrals in the limit $h_0 \to 0$ with $j_0 < 0$ fixed. $\Delta\Theta_\Gamma(h_0)$ can be written as

$$\Delta\Theta_\Gamma(h_0) = \frac{-h_0}{2}\int_{\delta_0(-h_0,j_0)} \frac{dx}{xy}, \tag{111}$$

where δ_0 is the cycle between x_0 and x_{n-1} which is oriented from x_0 to x_{n-1} in the upper leaf and inversely in the lower leaf. In the limit $h_0 \to 0$, one deduces that

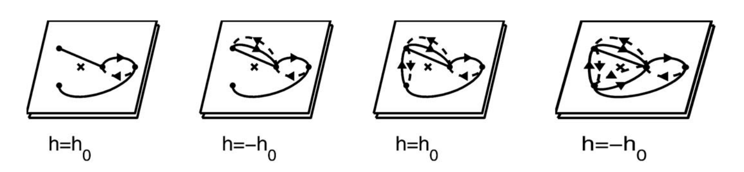


FIG. 14. Same as Fig. 13 but for three semicircles around line C.

$$\Delta\Theta_\Gamma = \lim_{h_0\to 0} h_0 \int_{x_{n-1}}^{x_0} \frac{dx}{x\sqrt{\prod_{k=0}^{N-1}(x-x_k)}}, \tag{112}$$

where the integral is taken along an arc of a circle from x_{n-1} to x_0 of radius $h_0^{2/n}/(-2j)^{1/n}$. Using the change of variables $x=[h_0^{2/n}/(-2j)^{1/n}]e^{i\chi}$, we obtain

$$\Delta\Theta_\Gamma = \int_0^{2\pi/n} \frac{d\chi}{\sqrt{\prod_{k=0}^{n-1}(e^{i\chi}-e^{2i\pi k/n})}}. \tag{113}$$

It is straightforward to check that the integrand is not modified by the translation $\chi'=\chi+2\pi/n$. One then deduces that

$$\Delta\Theta_\Gamma = \lim_{h_0\to 0} -\frac{1}{n}\mathrm{Res}\left[\frac{-h_0}{x\sqrt{\prod_{k=0}^{N-1}(x-x_k)}}, x=0\right]. \tag{114}$$

Simple algebra finally gives

$$\Delta\Theta_\Gamma = \frac{2\pi}{n}. \tag{115}$$

Similar arguments show that $\Delta\tau_\Gamma=0$. We finally construct the monodromy matrix from the variations of Θ and τ along Γ. □

We finish this section by presenting a complementary computation of the fractional Hamiltonian monodromy in the complex approach. The idea here is to use direct asymptotic computations to determine $\Delta\Theta_\Gamma$.

Lemma 10: For $j<0$ *fixed and* $|h|\to 0$, *we have the following asymptotic behavior:*

$$\Theta(h,j)-\Theta_0(h,j) \sim \frac{2}{n}\arctan\left[\frac{k_0}{h}\right], \tag{116}$$

where k_0 *is a function of* h *such that* $\lim_{|h|\to 0}|k_0|/|h|=0$.

Proof: We proceed as in the real approach by using the asymptotic expansions of the roots x_k of the polynomial Q (see Lemma 4). Following computations of the proof of Proposition 2, we obtain

$$\Theta(h,j)-\Theta_0(h,j) \sim h\int_{h^{2/n}/(-2j)^{1/n}}^{x_n} \frac{dx}{x\sqrt{\prod_{i=0}^{i=N-1}(x-x_i)}}, \tag{117}$$

which transforms into

$$\Theta(h,j)-\Theta_0(h,j) \sim h\int_{h^{2/n}/(-2j)^{1/n}}^{k} \frac{dx}{x\sqrt{(-2j)\left(x^n-\frac{h^2}{-2j}\right)}}. \tag{118}$$

The real function k fulfills $\lim_{|h|\to 0}[k(-2j)^{1/n}/|h|^{2/n}]=0$. Introducing the variable u such that $x=[h^{2/n}/(-2j)^{1/n}]u$, one arrives to

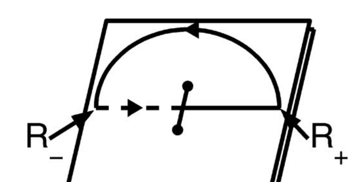


FIG. 15. Riemann surface of the function arctan. The solid and dashed lines, respectively, lie in the upper and the lower leaves. The ramification points correspond to the complex numbers i and $-i$.

$$\Theta(h,j) - \Theta_0(h,j) \sim \int_1^{k(-2j)^{1/n}/h^{2/n}} \frac{du}{u\sqrt{u^n - 1}}, \tag{119}$$

where we have used the fact that $\sqrt{h^2}=h$. One finally obtains that

$$\Theta(h,j) - \Theta_0(h,j) \sim \left[\frac{2}{n}\arctan[\sqrt{u^n - 1}]\right]_1^{k(-2j)^{1/n}/h^{2/n}}, \tag{120}$$

which leads to

$$\Theta(h,j) - \Theta_0(h,j) \sim \frac{2}{n}\arctan\left[\frac{k_0}{h}\right], \tag{121}$$

where $k_0=k^{n/2}\sqrt{-2j}$. □

The behavior of the function Θ near line C is thus related to the complex function arctan. Using the fact that

$$\arctan z = \frac{1}{2i}\ln\left[\frac{1+iz}{1-iz}\right], \tag{122}$$

for $z \in \mathbb{C}$, we can construct the Riemann surface of this function. This surface has infinitely many leaves and a cut between the points $z=i$ and $z=-i$. Figure 15 displays two leaves of this surface in the variable z. We recall that this function has a jump of π along a loop crossing the cut once. Using Eqs. (57) and (58), one sees that the limits of Θ when $h \to 0^{\pm}$ correspond, respectively, to the points R_+ and R_- of the Riemann surface (see Fig. 15). Since these two limit points are the initial and final points of Γ_R, we can associate with Γ_R the real path from R_- to R_+ of the Riemann surface of the function arctan. The complex continuation of the function Θ along the small semicircle Γ_C of the bifurcation diagram is associated with the big circle at infinity of Fig. 15. From Fig. 15, we thus recover that after a real loop Γ locally deformed to the complex domain to bypass line C, the function Θ has a jump of $2\pi/n$. This result is also coherent with the analysis performed with the variation of the cycles δ. We denote by δ_k the cycle between the ramification points x_k and x_{k+1}. The cycle is oriented from x_k to x_{k+1} in the upper leaf and from x_{k+1} to x_k in the lower one. Following the proof of Proposition 5, it can be shown that if we compute Θ along one of these cycles, then we obtain asymptotically the same result. More precisely, we have

$$\frac{h}{2}\int_{\delta_k(h,j)} \frac{dx}{xy} = \frac{2\pi}{n}, \tag{123}$$

for $j<0$ fixed and $h \to 0^-$. We consider now r semicircles around C. The cycle δ is transformed into $\delta+\delta_0-\delta_1+\delta_2-\cdots+(-1)^{r-1}\delta_{r-1}$. This is displayed for $r=3$ in Fig. 14. As expected, we thus see that after an even (odd) number of semicircles, the function Θ has no jump (a jump of $2\pi/n$) which corresponds to the behavior of the complex arctan.

E. Generalization to $m:-n$ resonance

We now study the $m:-n$ resonant system with $m>1$ and m and n relatively prime. We associate with such a system a Riemann surface which can be constructed in the variables $x=\pi_1+j$ or $x'=\pi_1-j$ from

$$y^2 = x^n(x-2j)^m - [h - R(x-j,j)]^2 \tag{124}$$

or

$$y^2 = (x'+2j)^n x'^m - [h - R(x'+j,j)]^2. \tag{125}$$

One passes from one representation to the other by the relation $x=x'-2j$. In particular, the two surfaces have the same ramification points translated by $2j$. Depending on the line of singularities considered, one or the other surface will be used, i.e., the surface in x for $j<0$ and the surface in x' for $j>0$. We next recall that the discriminant locus Δ of such a system is given by Eq. (76). From the expansion of the roots of the polynomial Q in $h=0$ (Lemma 7), we deduce that for $j<0$ ($j>0$), n (m) roots in x (in x') exchange their positions along a loop around line C. We locally deform Γ in a neighborhood of line C and we decompose this loop into four loops, Γ_{R_1}, Γ_{R_2}, Γ_{C_1}, and Γ_{C_2}, where Γ_{C_1} and Γ_{C_2} are, respectively, two semicircles around the lines of singularities $(h=0,j<0)$ and $(h=0,j>0)$. Γ_{R_1} and Γ_{R_2} complete the loop Γ, respectively, for $h<0$ and $h>0$. We define the variations of the functions Θ and τ along Γ as follows:

$$\begin{aligned} \Delta\Theta_\Gamma &= \Delta\Theta_{\Gamma_{C_1}} + \Delta\Theta_{\Gamma_{C_2}} + \Delta\Theta_{\Gamma_{R_1}} + \Delta\Theta_{\Gamma_{R_2}}, \\ \Delta\tau_\Gamma &= \Delta\tau_{\Gamma_{C_1}} + \Delta\tau_{\Gamma_{C_2}} + \Delta\tau_{\Gamma_{R_1}} + \Delta\tau_{\Gamma_{R_2}}, \end{aligned} \tag{126}$$

where the different variations are determined asymptotically, i.e., when the radii of the semicircles C_1 and C_2 go to 0. A simple calculation then shows that the study of the $m:-n$ resonance can be reduced to the study of two cases for $j>0$ and $j<0$ similar to the $1:-n$ resonance. This allows us to compute the jump of the function Θ along Γ and to deduce the monodromy matrix for the real loop Γ. We recover the result of Proposition 3.

IV. CONCLUSION

In this paper, we have investigated the notion of the fractional Hamiltonian monodromy in the $1:-2$, $1:-n$, and $m:-n$ resonant systems. We have presented an asymptotic method to calculate the monodromy matrix in the real approach and we have proposed a definition of fractional monodromy using a complex extension of the bifurcation diagram. From this definition, we have recovered the results of the real approach. At this point, the question which naturally arises is the generalization of this concept to other types of singularities. A part of the answer could be given by applying the complex approach to a new generalization of standard monodromy, the bidromy, which has been recently introduced in Ref. 35.

APPENDIX A: GEOMETRIC CONSTRUCTION

1. $1:-2$ resonance

As stated in the Introduction, the geometric construction of fractional monodromy generalizes the construction of standard monodromy. We propose a schematic representation that is slightly different from the original one proposed in Ref. 15. This representation has the advantage to be easily generalized to $1:-n$ resonant systems. We use a standard representation of a torus, i.e., a rectangle whose edges are identified according to the arrows. The crossing of line C is displayed in Figs. 16 and 17. A curled torus is represented by two rectangles glued along a horizontal edge and with a particular identification of the vertical edges (see Fig. 16, $h=0$). This construction is not limited to a given energy-momentum map but can be applied to any energy-momentum map

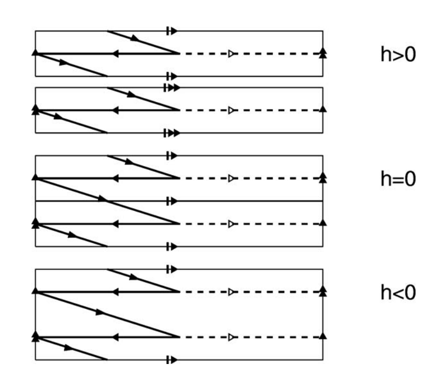


FIG. 16. Schematic representation of the continuous transport of the basic cycles (β_1,β_2) when the singular line C is crossed. γ_1 and γ_2 are, respectively, represented by dashed and solid lines.

having a bifurcation diagram with such a line of singularities. Let β_1 and β_2 be the two cycles associated with the flows of X_1 and X_2 defined in Eq. (6). They are the representatives of the classes of homology $[\beta_1]$ and $[\beta_2]$ which form a basis of $H_1(T^2(h,j),\mathbb{Z})$, where $(h,j)\in\mathcal{R}_{\text{reg}}$. Only a subgroup of H_1 can be transported continuously across line C. We assume that a basis for this subgroup is given by $[\beta_1]$ and $[2\beta_2]$. $2\beta_2$ corresponds to the cycle β_2 covered twice. For $h>0$, as representatives of $[\beta_1]$ and $[2\beta_2]$, we consider the two cycles $\gamma_1=\beta_1$ and γ_2. The cycle γ_2 is the union of two cycles β_2 with starting points belonging to the same orbit of the flow of X_1 but separated by an angle $\theta=\pi$. To make a link with analytical calculations, Θ is taken to be $\pi/2$ in this case. γ_1 can be easily transported across C and it remains unchanged. To transport continuously γ_2, the two cycles forming γ_2 have to be connected in one point in $h=0$ and then merged to form only one cycle covered once for $h<0$. Representatives of the basis of $H_1(F^{-1}(h,j),\mathbb{Z})$ for $h<0$ are given in Fig. 17, note that $\Theta=-\pi/2$ since Θ has a discontinuity of size π on C. The value $\Theta=-\pi/2$ can also be deduced from Fig. 17 by comparing the cycles γ_1 and γ_2. Comparison of Fig. 16 $(h<0)$ and Fig. 17 leads to the conclusion that after one loop, the cycle γ_2 becomes a representative of the equivalence class $[2\beta_2-\beta_1]$ and that the corresponding monodromy matrix written formally in the basis $([\beta_1],[\beta_2])$ is given by

$$M=\begin{pmatrix} 1 & 0 \\ -\frac{1}{2} & 1 \end{pmatrix}. \tag{A1}$$

2. 1:−*n* resonance

The geometric construction of Appendix A 1 can be straightforwardly generalized to other resonances. We consider the 1:−3 resonance but other resonances can be treated along the same lines. The 3-curled torus is represented in Fig. 18 $(h=0)$ by three rectangles glued along a common edge. Note also the particular identification of the vertical edges. Following notations of Appendix A 1, a basis of the subgroup of $H_1(F^{-1}(h,j),\mathbb{Z})$ which can be transported continuously across C is given by $[\beta_1]$ and $[3\beta_2]$. For $h>0$, as a representative of $[3\beta_2]$, we choose three cycles β_2 whose starting points belong to the same orbit of the flow of X_j with an angle θ of $2\pi/3$ between each other. We also assume that $\Theta=\pi/3$ in this case. After crossing C, this cycle belongs for $h<0$ to

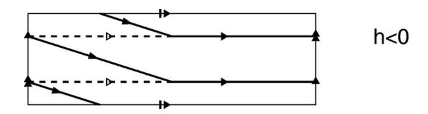


FIG. 17. Schematic representation of the basis cycles for $h<0$. Representatives of $[\beta_1]$ and $[2\beta_2]$ are, respectively, represented by dashed and solid lines.

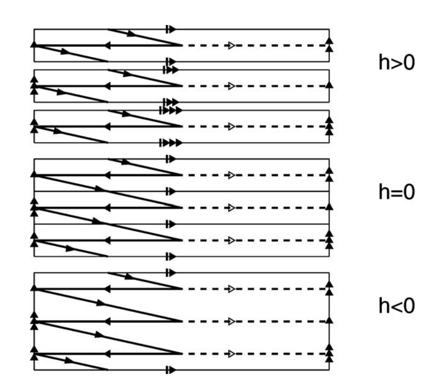


FIG. 18. Same as Fig. 16 but for the $1:-3$ resonance.

the equivalence class $[3\beta_2-\beta_1]$, as shown by Fig. 19. For $h<0$, $\Theta=-\pi/3$ since the discontinuity of Θ on C is equal to $2\pi/3$. In the basis $([\beta_1],[\beta_2])$, the monodromy matrix M is given by

$$M=\begin{pmatrix} 1 & 0 \\ -\frac{1}{3} & 1 \end{pmatrix}. \tag{A2}$$

APPENDIX B: THE SEMICLASSICAL POINT OF VIEW

We illustrate in this section the relation between classical monodromy and its semiclassical counterpart for $1:-n$ and $m:-n$ resonant systems. To our knowledge, this point has not been discussed up to now in the literature. We refer the reader to Refs. 3 and 15 for a rigorous definition of this semiclassical point of view. Here, we consider only the graphical representations of semiclassical monodromy as a pictorial illustration of classical monodromy.

We consider two quantum differential operators $\hat{J}$ and $\hat{H}$ whose classical limits are the Hamiltonians J and H. These two operators commute, i.e., $[\hat{J},\hat{H}]=0$. They thus have a system of common eigenfunctions belonging to $L^2(\mathbb{R}^2,dq_1\wedge dq_2)$. The corresponding eigenvalues form the quantum joint spectrum of the energy-momentum map F which is a two-dimensional lattice of points. We can construct the quantum-classical bifurcation diagram of F by superposing both the quantum joint spectrum and the classical bifurcation diagram. This has been done for the $1:-n$ and $m:-n$ resonant systems in Figs. 20 and 21. Note that the quantum joint spectrum is defined for a given value $\hbar$ viewed here as a parameter. Using Einstein-Brillouin-Keller (EBK) quantification rules, we also introduce the semiclassical joint spectrum which is defined as the set of points $(h,j)\in\mathcal{R}_{\text{reg}}$, where the numbers n_1 and n_2 given by the relation

$$\hbar\left(n_i+\frac{\alpha_i}{4}\right)=\oint_{\gamma_i}\mathbf{pdq} \tag{B1}$$

are integers. In Eq. (B1), $\mathbf{pdq}$ is the Liouville 1-form and α_i the Maslov index associated with the cycle γ_i, where $([\gamma_1],[\gamma_2])$ is a basis of $H_1(T^2(h,j),\mathbb{Z})$. We remark that the semiclassical lattice differs from the quantum lattice by $o(\hbar)$ which is irrelevant in our study. We also point out that the EBK quantification rules are not valid near the line of singularities C and have to be replaced by singular rules.[25] In contrast, the quantum joint spectrum gives a smooth transition of the crossing

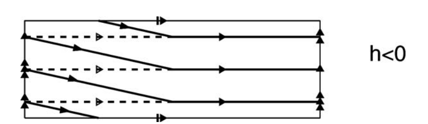


FIG. 19. Same as Fig. 17 but for the $1:-3$ resonance.

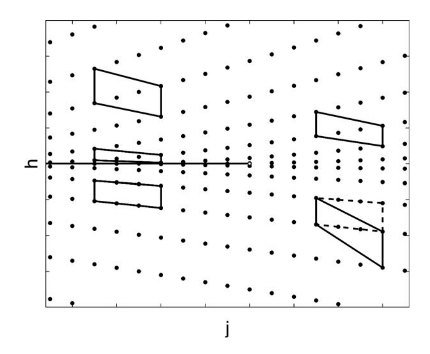


FIG. 20. Semiclassical bifurcation diagram for the 1:−3 resonance and the energy-momentum map of Eq. (36). The line of singularities C is represented by a solid line. The open dot indicates the position of the origin of the bifurcation diagram. The final cell after a counterclockwise closed loop around the origin is depicted by dashed lines.

C. Moreover, locally around a regular value of $\mathcal{R}$, this lattice is regular in the sense that there exists a map which sends this lattice to $\hbar\mathbb{Z}^2$ as $\hbar$ tends to zero. A systematic approach has been developed to check the regularity of the global spectrum. The method consists in taking a cell, i.e., a quadrilateral whose vertices lie on the points of the lattice, transporting continuously this cell along a loop Γ and comparing the final cell with the initial one. If the two cells are different, then the system has a nontrivial quantum monodromy. The rotation matrix which sends the initial cell to the final one is the quantum monodromy matrix M_Q. More precisely, if the cell is supported by the two vectors (w_1,w_2) and if after a loop these vectors are transformed into (w_1',w_2'), then M_Q is defined by the relation

$$\begin{pmatrix} w_1' \\ w_2' \end{pmatrix} = M_Q \begin{pmatrix} w_1 \\ w_2 \end{pmatrix}. \tag{B2}$$

Using the semiclassical joint spectrum, it can be shown that $M_Q=(M_{\rm Cl}^t)^{-1}$, where $M_{\rm Cl}$ is the classical monodromy matrix. We recall that when the system has fractional monodromy, the size of the cell has to be increased to cross the line of singularities. In a way analogous to the classical case, a simple cell cannot be transported continuously across line C. The multiple cell then becomes the basic cell, which is equivalent to consider only a sublattice of the original lattice. Here, the vertical lines of the quantum bifurcation diagram which are parallel to w_1 are labeled by n_1, the quantum number associated with φ_J which is a global quantum number. The cells are thus multiplied in the other direction. For instance, for the 1:−3 resonance, the size is multiplied by 3. This point is displayed in Fig. 20. For a resonance m:$-n$, due to the form of the monodromy matrix, the size is increased from 1 to mn which explains why we have considered cells of size 6 in Fig. 21 for the 2:−3 resonance. Examination of Figs. 20 and 21 shows that in the basis (w_1,w_2), the quantum monodromy matrices are, respectively, equal to

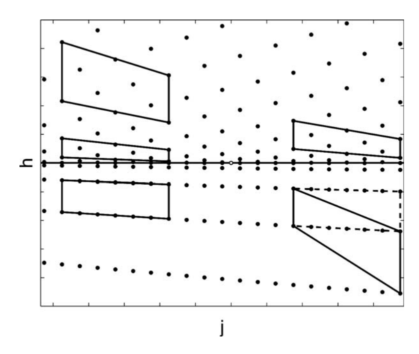


FIG. 21. Same as Fig. 20 but for the 2:−3 resonance. The corresponding energy-momentum map is given by Eq. (B5).

$$\begin{pmatrix} 1 & \frac{1}{3} \\ 0 & 1 \end{pmatrix}, \tag{B3}$$

for the $1:-3$ resonance, and

$$\begin{pmatrix} 1 & \frac{1}{6} \\ 0 & 1 \end{pmatrix}, \tag{B4}$$

for the $2:-3$ resonance. The energy-momentum map used for the $2:-3$ resonance is defined by

$$F = \begin{cases} J \\ \pi_3 + (\pi_1 + J)^2(\pi_1 - J)^2. \end{cases} \tag{B5}$$

APPENDIX C: REDUCTION IN THE COMPLEX APPROACH

We detail in this section the reduction in the complex approach for an $m:-n$ resonant system. This reduction is different from the reduction used in the real approach which is associated with the S^1-action of the flow of the Hamiltonian J. Both reductions leave the polynomials (J, π_1, π_2, π_3) defined by Eq. (33) invariant.

We start from the complexified phase space $T^*\mathbb{C}^2$ with $(p_1, q_1, p_2, q_2) \in \mathbb{C}^4$. The reduction is based on two $SO(2,\mathbb{C})$ actions Φ_1 and Φ_2. We recall that a matrix $R \in SO(2,\mathbb{C})$ is a 2×2 matrix, which reads

$$\begin{pmatrix} a & -b \\ b & a \end{pmatrix}, \tag{C1}$$

where $(a,b) \in \mathbb{C}^2$ and $a^2+b^2=1$. Φ_k $(k \in \{1,2\})$ is a map from $SO(2,\mathbb{C})\times\mathbb{C}^2$ to $\mathbb{C}^2$, which associates with each couple $(R,(q_k,p_k))$ the point of coordinates

$$\begin{pmatrix} a_k & -b_k \\ b_k & a_k \end{pmatrix}\begin{pmatrix} q_k \\ p_k \end{pmatrix} = \begin{pmatrix} a_k q_k - b_k p_k \\ b_k q_k + a_k p_k \end{pmatrix}. \tag{C2}$$

We next introduce new coordinates which can be written as follows:

$$\begin{aligned} \eta_1 &= q_1 - ip_1, \\ \xi_1 &= q_1 + ip_1, \\ \eta_2 &= q_2 - ip_2, \\ \xi_2 &= q_2 + ip_2. \end{aligned} \tag{C3}$$

Under the action of Φ_k, these new coordinates transform into $\lambda_k \xi_k$ and $\lambda_k^{-1}\eta_k$, where $\lambda_k = a_k + ib_k$. Finally, simple algebra shows that the complexified invariant polynomials (J, π_1, π_2, π_3) are invariant under the conjoint action of Φ_1 and Φ_2 if $\lambda_1^n \lambda_2^m = 1$. One can conclude that the reduction is associated with a $\mathbb{C}^*$-action Φ from $\mathbb{C}^* \times \mathbb{C}^4$ to $\mathbb{C}^4$ defined as follows:

$$\Phi:(\lambda,(\xi_1,\eta_1,\xi_2,\eta_2)) \to (\lambda^m \xi_1, \lambda^{-m}\eta_1, \lambda^{-n}\xi_2, \lambda^n \eta_2). \tag{C4}$$

[1] J. J. Duistermaat, Commun. Pure Appl. Math. **33**, 687 (1980).
[2] R. H. Cushman and L. Bates, *Global Aspects of Classical Integrable Systems* (Birkhauser, Basel, 1997).
[3] S. Vü Ngọc, Commun. Math. Phys. **203**, 465 (1999).
[4] C. A. Arango, W. W. Kennerly, and G. S. Ezra, Chem. Phys. Lett. **392**, 486 (2004).
[5] D. A. Sadovskií and R. H. Cushman, Physica D **142**, 166 (2000).
[6] I. N. Kozin and R. M. Roberts, J. Chem. Phys. **118**, 10523 (2003).

[7] M. S. Child, T. Weston, and J. Tennyson, Mol. Phys. **96**, 371 (1999).
[8] D. A. Sadovskií and B. I. Zhilinskií, Phys. Lett. A **256**, 235 (1999).
[9] H. Waalkens, A. Junge, and H. R. Dullin, J. Phys. A **36**, L307 (2003).
[10] H. Waalkens, P. H. Richter, and H. R. Dullin, Physica D **195**, 265 (2004).
[11] H. Waalkens and H. R. Dullin, Ann. Phys. (N.Y.) **295**, 81 (2002).
[12] A. Giacobbe, R. H. Cushman, D. A. Sadovskií, and B. I. Zhilinskií, J. Math. Phys. **45**, 5076 (2004).
[13] K. Efstathiou, M. Joyeux, and D. A. Sadovskií, Phys. Rev. A **69**, 032504 (2004).
[14] N. N. Nekhoroshev, D. A. Sadovskií, and B. I. Zhilinskií, C. R. Acad. Sci. Paris, Ser. 1 **335**, 985 (2002).
[15] N. N. Nekhoroshev, D. A. Sadovskií, and B. I. Zhilinskií, Ann. Henri Poincare **7**, 1099 (2006).
[16] K. Efstathiou, *Metamorphoses of Hamiltonian Systems with Symmetry*, Lecture Notes in Mathematics Series-LNM 1864 (Springer-Verlag, Heidelberg, 2004).
[17] K. Efstathiou, R. H. Cushman, and D. A. Sadovskií, Adv. Math. **209**, 241 (2007).
[18] N. N. Nekhoroshev, Mat. Sb. **198**, 383 (2007).
[19] V. I. Arnol'd, *Mathematical Methods of Classical Mechanics* (Springer-Verlag, New York, 1989).
[20] M. Audin, Commun. Math. Phys. **229**, 459 (2002).
[21] O. Vivolo, J. Geom. Phys. **46**, 99 (2003).
[22] F. Beukers and R. H. Cushman, Contemp. Math. **292**, 47 (2002).
[23] Y. Colin de Verdière and B. Parisse, Commun. Math. Phys. **205**, 459 (1999).
[24] S. Vü Ngọc, Commun. Pure Appl. Math. **53**, 143 (2000).
[25] Y. Colin de Verdière and S. Vü Ngọc, Ann. Sci. Ec. Normale Super. **36**, 1 (2003).
[26] A. Voros, Ann. Inst. Henri Poincare, Sect. A **39**, 211 (1983).
[27] E. Delabaere, H. Dillinger, and F. Pham, J. Math. Phys. **38**, 6126 (1997).
[28] E. Delabaere and F. Pham, Ann. Phys. (N.Y.) **261**, 180 (1997).
[29] V. I. Arnol'd, S. M. Goussein-Zade, and A. N. Varchenko, *Singularities of Differentiable Mappings* (Birkhauser, Boston, 1988).
[30] H. Zoladek, *The Monodromy Group* (Birkhauser, Boston, 2006).
[31] A. Giacobbe, "Fractional monodromy: Parallel transport of homology cycles," Diff. Geom. Applic. (in press).
[32] L. M. Bates, J. Appl. Math. **42**, 837 (1991).
[33] F. Kirwan, *Complex Algebraic Curves* (Cambridge University Press, Cambridge, 1993).
[34] J. A. Wolf, Mich. Math. J. **11**, 65 (1964).
[35] D. A. Sadovskií and B. I. Zhilinskií, Ann. Phys. (N.Y.) **322**, 164 (2007).

4.3 Dynamics of nonlinear wave systems

Corresponding articles : [9, 4]
This work has been done in collaboration with A. Picozzi, H. R. Jauslin and S. Lagrange of the *Institut Carnot de Bourgogne* in Dijon.

In this section, I present a completely different physical and mathematical domain that I began exploring since 2007. The goal is to study the dynamics of waves in non-linear media. As a first problem, we consider the dynamics of counter-propagating waves which is a very interesting and complex phenomenon with potential applications in the polarization of laser beams in non-linear optics.

In the case of the four-wave counter-propagating interaction, different studies have shown the richness of this physical system which can exhibit bistability [60], chaos [59] and polarization domain wall solitons [96]. Recently, a new effect concerning the polarization dynamics for this type of interaction has been observed both theoretically [94] and experimentally [95]. More precisely, it can be shown that the dynamics of this four-wave interaction is governed by a system of four inhomogeneous first order partial differential equations. The complexity of the dynamics is in large part due to the resonant terms coupling the four equations. The originality of this system relies in the boundary conditions imposed to the fields at both ends of the medium. One observes a relaxation process towards a time-independent attractor solution of a Hamiltonian system. It is this asymptotic dynamics which reveals the geometry of this problem and makes the link with ordinary differential equations systems. In addition, the stationary solution obtained presents a robust character when the boundary conditions or the length of the medium are varied. This can find remarkable applications in optics such as the possibility to realize a polarizer with 100% efficiency. The polarization attraction is associated with a transfer of polarization between the counterpropagating waves.

In [9], we have shown numerically that the system converges to a trajectory lying on a singular pinched torus which therefore plays the role of an attractor for the infinite dimensional dynamical system. We have proved that the Hamiltonian system corresponds locally to a $1 : -1$ resonant system very similar to a system of two coupled angular momenta studied in [103]. We have also pointed out that the exchange of polarization between the pump

and the signal along the fiber can be explained by the geometry of the singular torus. In [9], we generalize the observations for the four-wave interaction scheme to other models where the attraction phenomenon is present. A first example is given by the dynamics of two waves in fiber Bragg gratings [115] which is governed by a system of two partial differential equations. Another example is the interaction of three waves in nonlinear media. An analysis of the associated Hamiltonian system shows that the corresponding three-dimensional bifurcation diagram has a line of singularities similar to the one of [62]. When two amplitudes are equal, the bifurcation diagram becomes two-dimensional and possesses a line of curled torus which is also present in systems with non trivial fractional monodromy [87, 88, 89].

We are now working on the following questions. Due to the generality of the resonant four-wave interaction scheme and of other models, we expect that this process can play a role in other domains such as plasma physics [122], hydrodynamics [70], acoustic waves [67] or in Bose-Einstein condensates [113]. The main difficulty will be to determine under which conditions in each domain the attraction phenomenon can appear and its possible physical role. A more ambitious work is to define the notion of dynamical Hamiltonian monodromy in such systems [53]. The origin of this concept comes from the idea of finding dynamical manifestations of the nontrivial topology of integrable Hamiltonians due to the monodromy. In other words, the goal is to determine physical dynamical processes that allow to observe a nontrivial monodromy. One possibility could be to consider physical systems having several accessible external parameters which can be controlled. Using such a control, one then modifies the system to follow the loop around the singularity in the image of the energy-momentum map. The counterpropagating waves systems seem to be particularly well suited to this question since the energy and the momentum of the associated integrable system can be modified by changing adiabatically the boundary conditions of the fiber. The remaining question which naturally arises is the role of dynamical monodromy in the dynamics of laser fields and in particular its role for the attraction phenomenon.

The article [4] is the continuation of the short letter [9]. In this paper, we present a complete overview of the attraction phenomenon on one of the three examples treated in [9], the polarization attraction. This case is the more physically relevant process with experimental applications in op-

tical fibers. We detail every step of our approach, i.e. the determination and the construction of the singular tori, the determination of all the solutions satisfying the boundary conditions and the numerical simulations in the adiabatic approach. This approach consists in slowly modifying the boundary conditions from 0 to their final values. In this case, we show that the system follows an instantaneous stationary state that lies on the corresponding instantaneous singular torus depending upon the values of the boundary conditions. All these points are only briefly mentioned in the letter [9]. This detailed exposition, which cannot be found in the existing optics literature, will help the interested readers to apply such techniques to other examples of counterpropagating nonlinear wave systems. We reproduce here the article [9].

On the role of singular tori in the dynamics of spatio-temporal nonlinear wave systems

D. Sugny,* A. Picozzi, S. Lagrange, and H. R. Jauslin

Institut Carnot de Bourgogne, UMR CNRS 5027, BP 47870, 21078 Dijon, France

(Dated: April 17, 2009)

Abstract

We show that the peculiar topological properties inherent to singular tori play a major role in the spatio-temporal dynamics of counterpropagating nonlinear waves. Under rather general conditions, these Hamiltonian wave systems exhibit a relaxation process towards a stationary state. On the basis of recently developed mathematical techniques, we show that this stationary state converges exponentially towards the singular torus of the associated Liouville integrable Hamiltonian system in the limit of an infinite medium. The singular torus then appears as an *attractor* for the infinite dimensional dynamical system, a feature which is illustrated by several key models of spatio-temporal wave interactions. The properties of the stationary state and the robustness of the spatio-temporal dynamics can be deduced from the topology of the singular torus.

PACS numbers: 02.30.Ik,45.05.+x,05.45.-a

*Electronic address: `dominique.sugny@u-bourgogne.fr`

Hamiltonian integrable systems have a long history dating back to Liouville in the mid 19th century. The modern mathematical foundations of this domain have been established in particular by Arnold [1] one hundred years later. In these last decades, while the physics community of dynamical systems was mainly concerned with the theory of chaos, novel methods were introduced in mathematics to study integrable systems [2–4]. More recently, the relevance of these mathematical structures has been analyzed in the context of mechanical systems characterized by a small number of degrees of freedom [5–10]. This Letter is aimed at describing a novel class of infinite dimensional dynamical systems in which these novel mathematical concepts find a remarkable physical application.

We consider a Hamiltonian H with two degrees of freedom defined on the four dimensional phase-space $\mathbb{R}^4$. The Hamiltonian H is said Liouville-integrable if it has as many independent constants of motion as the number of degrees of freedom. Since H does not depend on time, it will be integrable if there exists a function K which Poisson-commutes with H, i.e. $\{H, K\} = 0$. From our perspective, the essential object in the study of integrable systems is not the Hamiltonian H but the energy-momentum map $\mathcal{F} : (p_1, q_1, p_2, q_2) \rightarrow (H, K)$ [2] where (p_1, q_1, p_2, q_2) are coordinates of $\mathbb{R}^4$. The image of $\mathcal{F}$ is called the energy-momentum set or bifurcation diagram. The Liouville-Arnold theorem states that the inverse image $\mathcal{F}^{-1}(h, k)$ of a point $(H = h, K = k)$ of the energy-momentum set is a two-dimensional torus. This theorem assumes that this preimage is connected and compact, and that the two gradient vectors of the phase-space $\nabla H = (\frac{\partial H}{\partial p_1}, \frac{\partial H}{\partial q_1}, \frac{\partial H}{\partial p_2}, \frac{\partial H}{\partial q_2})$ and ∇K are not parallel for any point of the torus. Under these conditions, the corresponding point (h, k) is a regular point of the image of $\mathcal{F}$. At a regular point, action-angle variables can be introduced [1]. However, if the two vectors $(\nabla H, \nabla K)$ are parallel for some points of the torus, then the preimage $\mathcal{F}^{-1}(h, k)$ is no longer a regular torus, but a *singular torus*. The topology of the singular torus can be of different types: a point (for an equilibrium), a circle (for a periodic orbit) or a pinched torus, to cite a few. A pinched torus is a regular torus whose radius has been pinched to zero in one point, as illustrated in Fig. 1a. Simple integrable Hamiltonians with pinched tori may be constructed with the momentum $K = (p_1^2 + q_1^2 - p_2^2 - q_2^2)/2$, which corresponds to a $1 : -1$ resonance, i.e., two harmonic oscillators of +1 and -1 frequencies [3]. The positions and the geometry of singular tori are determined through a global analysis of the energy-momentum map $\mathcal{F}$. In general, a singular pinched torus is associated to an isolated singularity of the energy-momentum set (see Fig. 1b-c for an example).

The analysis of the geometry of singular tori and their importance in the dynamics of integrable Hamiltonians have been established only recently in the mathematical community. The fundamental problem was the generalization of action-angle variables to the whole phase-space when the set of regular points (H, K) is not simply connected. This precisely occurs when the image of $\mathcal{F}$ possesses an isolated singularity associated to a pinched torus. Duistermaat solved this problem in 1980 by introducing the concept of monodromy [2, 4]. Non-trivial monodromy implies that after a loop in the regular values of the energy-momentum set, the action variables are changed. Different examples of monodromy in classical and quantum physics have been subsequently discovered [3, 5], in particular in the rovibrational spectrum of the CO_2 molecule [6], in the hydrogen atom in electric and magnetic fields [7] or in the problem of scattering by a central potential [8].

Our aim in this Letter is to show that singular tori play a major role in a novel class of physical systems. We deal here with the counterpropagating spatio-temporal dynamics of a nonlinear wave system which is ruled by Partial Differential Equations (PDE), i.e., a dynamical system with an infinite number of degrees of freedom. The numerical simulations reveal that, under rather general conditions, the spatio-temporal dynamics relaxes towards a *stationary* state. This property allows us to establish a relation between the original PDE and the corresponding integrable Hamiltonian dynamics ruled by the stationary Ordinary Differential Equation (ODE). As a remarkable result, the spatio-temporal dynamics of the nonlinear wave system is attracted towards a stationary state which is shown to *converge exponentially* to the singular torus of the associated ODE's phase-space.

The peculiar topological property inherent to the singular torus manifests itself by a robust character of the stationary solution of the PDE, i.e. the stationary solution preserves its global form regardless of the considered system size L. This feature may appear counterintuitive if one considers that an integrable Hamiltonian system exhibits in general quasi-periodic oscillations. A consequence of this robust character is that the Hamiltonian system exhibits an *attraction* process: A wave injected from one side of the medium is attracted, independently of its initial state, towards a unique state determined by the properties of the singular torus. The space-time relaxation phenomenon and the associated process of attraction are exemplified by several key models of nonlinear wave interactions.

Let us begin to consider the evolution of a nonlinear wave in a periodic potential. This problem is encountered in a variety of physical disciplines such as optics, condensed matter

physics or Bose-Einstein condensates [11–13], in which the behavior of atoms mimics those of electrons in crystals or photons in optical gratings. Because of Bragg-reflections inherent to wave propagation in a periodic potential, these systems are generally characterized by a counterpropagating wave interaction. More specifically, we analyze the one-dimensional model that rules nonlinear wave propagation around a forbidden frequency band-gap

$$\begin{aligned} \frac{\partial u}{\partial t} + \frac{\partial u}{\partial z} &= i\kappa v + i\gamma(|u|^2 + 2|v|^2)u, \\ \frac{\partial v}{\partial t} - \frac{\partial v}{\partial z} &= i\kappa u + i\gamma(|v|^2 + 2|u|^2)v, \end{aligned} \tag{1}$$

where κ and γ refer to the linear and nonlinear coefficients, u and v being the forward and backward complex wave amplitudes. In optics, Eqs. (1) may be derived from Maxwell's equations, while in Bose-Einstein condensates they may be derived from the nonlinear Schrödinger equation with a periodic potential [12, 13].

The counterpropagating nature of the interaction imposes the following boundary conditions $u(0,t) = u_0$, $v(L,t) = v_L$. The numerical integration of (1) reveals that, after a complex transient, the two fields relax towards a stationary state associated to a singular torus (see Figs. 1-2). Indeed, to analyze the stationary solutions of Eqs. (1), we remark that the corresponding ODE's system is Hamiltonian with respect to the canonically conjugate real coordinates (p_u, q_u, p_v, q_v) defined by $u = q_u + ip_u$ and $v = q_v - ip_v$,

$$H = \kappa(p_u p_v - q_u q_v) - \gamma|u|^2|v|^2 - \gamma(|u|^4 + |v|^4)/4. \tag{2}$$

The momentum $K = (|u|^2 - |v|^2)/2$ being a constant of motion, this system is Liouville-integrable. We underline that the invariant K corresponds to a $1 : -1$ resonance that originates in the counterpropagating nature of the wave interaction. The bifurcation diagram (H, K) of this system has been constructed by using the mathematical tools of Ref.[3] (see Fig. 1b). Each point of the gray region lifts to a regular torus in the phase-space, whereas singular points are indicated by solid lines and full dots lift to singular tori. The numerical simulations show that the spatio-temporal dynamics is attracted towards a stationary state associated to a pinched torus, whose image is located at $H = K = 0$. This relaxation process is illustrated in Fig. 1b and Fig. 2c, which show the temporal evolutions of $\tilde{H}(t) = \frac{1}{L}\int_0^L H(z,t)\,dz$ and $\tilde{K}(t) = \frac{1}{L}\int_0^L K(z,t)\,dz$. In a loose sense, $\tilde{H}$ and $\tilde{K}$ may be regarded as the *instantaneous* Hamiltonian and momentum averaged over the length L. The *trajectories* in Fig. 1b and Fig. 2c thus represent the spatio-temporal relaxation of the system towards the pinched torus ($H = K = 0$). Note that, for a finite length L, the relaxation occurs

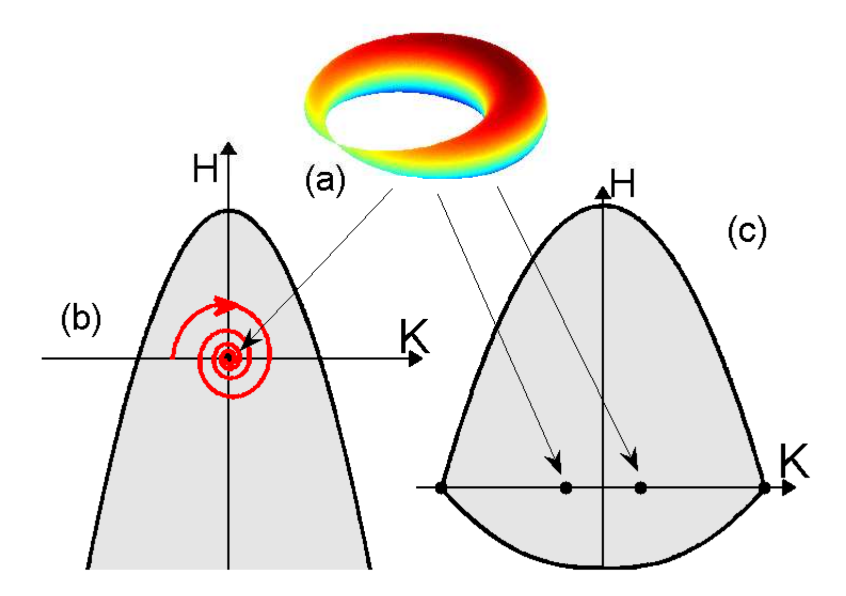


FIG. 1: (Color online) Image of the energy-momentum map $\mathcal{F}$ (gray) for the Hamiltonian (2) (b) and the Hamiltonian (4) (c). The singular points are represented by solid lines and black full dots. The dots indicate the positions of the image of the pinched tori (a). The red-path in (b) schematically represents the evolution $[\tilde{H}(t), \tilde{K}(t)]$ of the PDE system (1) during the space-time relaxation process (also see Fig. 2c-d).

to a point in the *neighborhood* of the pinched torus $H \simeq K \simeq 0$ (see Fig. 2c). Actually, the numerical simulations reveal that the stationary state converges exponentially towards the pinched torus in the limit $L \to +\infty$, as illustrated in Fig. 2d. We conjecture that this exponential law originates in the logarithmic divergence of one of the periods of the torus as the distance between this torus and the pinched torus tends to zero.

This process of attraction towards a singular torus allows to interpret a recent experiment realized in optical fibers [14]. This effect was called *polarization attraction* due to its role in the dynamics of wave polarizations. Note that the generality of the attraction process and its relation to the existence of singular tori were not identified in these previous works. Let us consider the counterpropagating Four-Wave Interaction (FWI) ruled by the following

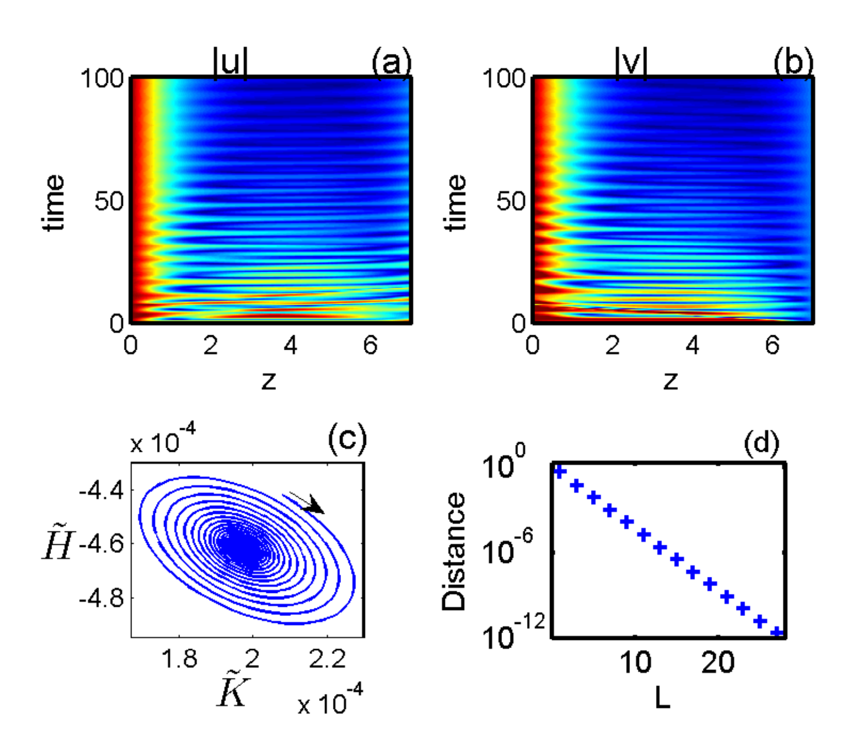


FIG. 2: (Color online) (a)-(b) Numerical simulations of the PDE (1) showing the spatio-temporal evolution of the fields $|u|$ (a) and $|v|$ (b): after a transient the two waves relax to the stationary state associated to the singular pinched torus located at $H = K = 0$ (see Fig. 1b). (c) Corresponding trajectory $[\tilde{H}(t), \tilde{K}(t)]$ in the energy-momentum set (H, K). The small arrow in (c) indicates the temporal evolution of the trajectory [$\kappa = 1$, $\gamma = 0.5$, $u_0 = 1$ (red), $v_L = 0.25$ (blue)]. (d) Evolution of the distance $\rho = \sqrt{H^2 + K^2}$ between the singular torus and the regular torus on which lies the stationary state for a given length L: the stationary state converges exponentially towards the singular torus as $L \to +\infty$.

PDE:

$$\begin{array}{l} \frac{\partial \vec{S}}{\partial t} + \frac{\partial \vec{S}}{\partial z} = [\vec{S} \times \mathcal{J}\vec{S} + 2\vec{S} \times \mathcal{J}\vec{J}], \\ \frac{\partial \vec{J}}{\partial t} - \frac{\partial \vec{J}}{\partial z} = [\vec{J} \times \mathcal{J}\vec{J} + 2\vec{J} \times \mathcal{J}\vec{S}]. \end{array} \tag{3}$$

In the Poincaré-Stokes formalism, $\vec{S} = (S_x, S_y, S_z)$ and $\vec{J} = (J_x, J_y, J_z)$ respectively represent the polarizations of the forward and backward waves, while $\mathcal{J}$ denotes the diagonal matrix diag$(-1, 0, -1)$ [15]. Note that, besides optics, the phenomenology of Eqs. (3) is also relevant to ferromagnetic materials ruled by the Landau-Lifshitz equation.

The phase-space of the stationary ODEs (3) is the product of two spheres, $\mathbb{S}^2 \times \mathbb{S}^2$. The

dynamics of the stationary state is governed by an integrable Hamiltonian

$$H = 2(S_x J_x + S_z J_z) - (S_y^2 + J_y^2)/2, \tag{4}$$

and the momentum $K = S_z + J_z$. In spite of the deep differences between this physical system and wave propagation in periodic potentials discussed above [Eq. (1)], both systems exhibit the same phenomenology. Indeed, on the basis of Ref. [9], we constructed the corresponding bifurcation diagram illustrated in Fig. 1c. The space-time dynamics of the PDEs (3) is shown to be attracted towards one of the two singular pinched tori [16]. As for the model (1), the convergence towards the singular torus follows an exponential law (data not shown). This exponential convergence plays an essential role for the experimental applications of the attraction process, in particular, it permitted the observation of polarization attraction within a very short nonlinear medium of length L [14]. Furthermore, the geometry of the singular torus shows that the process of polarization attraction is not restricted to the particular case of *circularly* polarized waves [14], but may be generalized to any state of polarization [16].

Remarking that the pinched torus is a particular example of singular torus encountered in integrable Hamiltonians [3], one may wonder whether other kinds of singular tori could be relevant to nonlinear wave systems. We illustrate this aspect by considering the example of the Three-Wave Interaction (TWI), which is known to occur in any weakly nonlinear medium whose lowest order nonlinearity is quadratic in terms of the wave amplitudes. For this reason the TWI is encountered in such diverse fields as plasma physics, hydrodynamics, acoustics and nonlinear optics [17]. In its counterpropagating configuration, the TWI model takes the form

$$\begin{aligned} \frac{\partial u}{\partial t} + \frac{\partial u}{\partial z} &= -vw, \\ \frac{\partial v}{\partial t} + \frac{\partial v}{\partial z} &= uw^*, \\ \frac{\partial w}{\partial t} - \frac{\partial w}{\partial z} &= uv^*, \end{aligned} \tag{5}$$

where u and v (w) refer to the forward (backward) propagating waves. Introducing the canonically conjugated real coordinates $u = q_u + ip_u$, $v = q_v + ip_v$ and $w = q_w - ip_w$, the three-degrees of freedom Hamiltonian associated to the stationary PDEs (5) reads

$$H = -q_v q_w p_u - p_v p_w p_u - q_v p_w q_u + p_v q_w q_u. \tag{6}$$

The constants of motion are $J = (|w|^2 - |u|^2)/2$ and $N = (|u|^2 + |w|^2 + 2|v|^2)$, which respectively correspond to the 1:-1 and 1:1:2 resonances. This Hamiltonian system exhibits

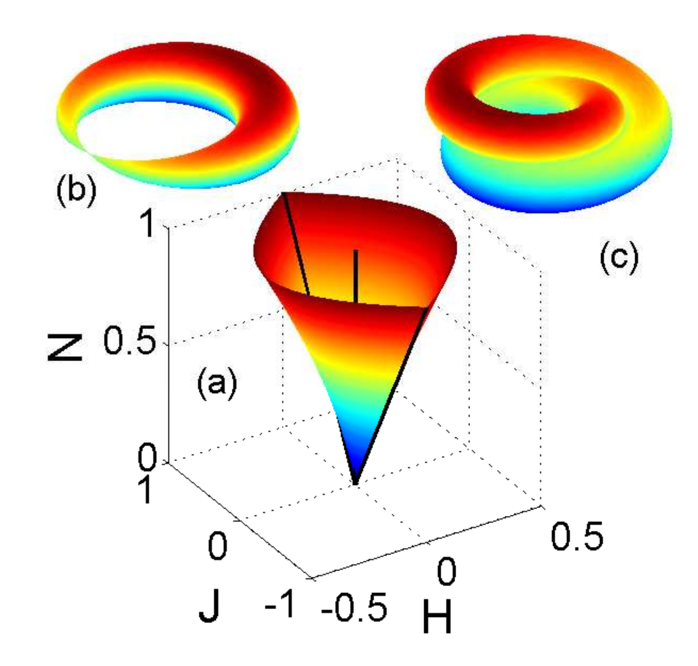


FIG. 3: (Color online) (a) Bifurcation diagram of the energy-momentum map $\mathcal{F}$: $(q_u, p_u, q_v, p_v, q_w, p_w) \to (H, N, J)$. Each point of the singular line ($H = J = 0$) lifts in phase-space to a singular torus which is both pinched (b) and curled (c).

a rather complex three-dimensional bifurcation diagram that can be constructed using the mathematical techniques recently developed in Ref. [10]. We remark that this set is also encountered in the classical dynamics of the Fermi model of the CO_2 molecule [6]. It is characterized by a line of singularities for $J = H = 0$, whose preimage is a singular torus that is both pinched and curled: In the subspace $N = const$ the torus is pinched, whereas it is curled in the subspace $J = const$, as illustrated in Fig. 3. Note that a curled torus can be constructed by gluing together two cylinders along a line and identifying the extremities after a half-twist.

The numerical simulations of the PDEs (5) reveal that the space-time dynamics is attracted towards a stationary state, in a way akin to the relaxation process illustrated in Fig. 2a-b. The stationary state lies on a regular torus, which is shown to converge exponentially towards the singular torus at ($J = 0, H = 0$) when the interaction length $L \to \infty$ (see Fig. 4a). Accordingly, the stationary solution satisfies $|u(z)| = |w(z)|$, which means that the backward wave w is attracted towards the state $u_0 = u(z = 0)$, regardless of its initial

condition at $w_L = w(z = L)$. This attraction process is clearly visible in the numerical simulations of the PDEs (5), as illustrated in Fig. 4b. Note that the attraction process takes place irrespective of the boundary condition $v_0 = v(z = 0)$, as revealed by Fig. 4c. We underline that, because of the singular nature of the torus, the global form of the stationary solutions reported in Figs. 4b-c is preserved for larger nonlinear interaction lengths L. This remarkable robustness is illustrated in Fig. 4d, in which we report the *output* values of the fields $[u_L = u(z = L),\ v_L = v(z = L),\ w_0 = w(z = 0)]$ for increasing lengths (L) of interaction, keeping fixed the boundary conditions $[u_0 = 1,\ v_0 = 0.1,\ w_L = 0.5]$. For large L, the fields asymptotically reach the values predicted by the singular torus, i.e., $u_L^2 = w_L^2,\ w_0^2 = N - u_0^2 - 2v_0^2,\ v_L^2 = N/2 - w_L^2$ with $N = 2(u_0^2 + v_0^2)$.

In summary, this work reveals that the peculiar topological properties of singular tori could play a previously unrecognized fundamental role in the spatio-temporal dynamics of nonlinear waves. In this way, we also show that the dynamics of a system with infinite number of degrees of freedom may be captured by a low-dimensional dynamical system [18]. Given the ubiquitous character of the considered model equations, the phenomenon of attraction reported here is relevant to a large variety of physical domains.

---

[1] V. I. Arnol'd, *Mathematical Methods of Classical Mechanics* (Springer-Verlag, New York, 1989).

[2] R. H. Cushman and L. Bates, *Global Aspects of Classical Integrable Systems* (Birkhauser, Basel, 1997).

[3] K. Efstathiou, *Metamorphoses of Hamiltonian Systems with Symmetry* (Springer-Verlag, Lecture Notes in Mathematics series- LNM 1864, Heidelberg, 2004).

[4] J. J. Duistermaat, Commun. Pure Appl. Math. **33**, 687 (1980).

[5] D. Sugny, P. Mardešić, M. Pelletier, A. Jebrane, and H. R. Jauslin, J. Math. Phys. **49**, 042701 (2008).

[6] R. H. Cushman, H. R. Dullin, A. Giacobbe, D. D. Holm, M. Joyeux, D. A. Sadovskií, and B. I. Zhilinskií, Phys. Rev. Lett. **93**, 024302 (2004).

[7] K. Efstathiou, O. Lukina, and D. A. Sadovskií, Phys. Rev. Lett. **101**, 253003 (2008).

[8] H. R. Dullin and H. Waalkens, Phys. Rev. Lett. **101**, 070405 (2008).

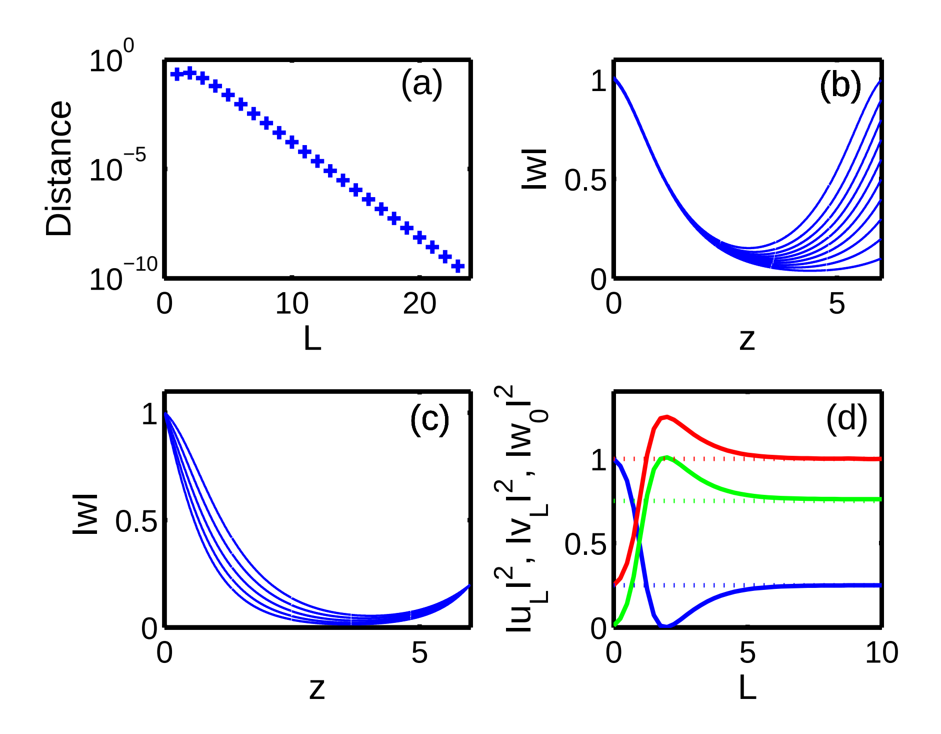


FIG. 4: (Color online) Properties of the stationary solutions obtained by solving numerically the PDEs (5). (a) Exponential convergence of the stationary solution towards the pinched-curled torus as $L \to \infty$ (the distance between the regular and the singular torus is given by $\rho = \sqrt{J^2 + H^2}$). (b) The field w is attracted towards 1 regardless of its boundary condition w_L $[u_0 = 1,\ v_0 = 0.2]$. (c) Stationary states of w for different boundary conditions v_0 ranging from 0 to 1 $[u_0 = 1]$. (d) Dependence on L of u_L (blue), v_L (green) and w_0 (red), keeping fixed the boundary conditions $[u_0 = 1,\ v_0 = 0.1,\ w_L = 0.5]$: The fields asymptotically reach the values corresponding to the singular torus (horizontal dashed lines).

[9] D. A. Sadovskií and B. I. Zhilinskií, Phys. Lett. A **256**, 235 (1999).

[10] A. Giacobbe, R. H. Cushman, D. A. Sadovskií, and B. I. Zhilinskií, J. Math. Phys. **45**, 5076 (2004).

[11] O. Morsch and M. Oberthaler, Rev. Mod. Phys. **78**, 179 (2006).

[12] See, e.g., C. Conti and S. Trillo, Phys. Rev. Lett. **92**, 120404 (2004).

[13] G. P. Agrawal, *Nonlinear Fiber Optics* (Academic Press, 2001).

[14] S. Pitois et al., Europhys. Lett. **70**, 88 (2005). S. Pitois, J. Fatome, and G. Millot, Opt. Express **16**, 6643 (2008).

[15] D. David, D. D. Holm, and M. V. Tratnik, Phys. Rep. **187**, 281 (1990).

[16] D. Sugny, S. Lagrange, A. Picozzi, and H. R. Jauslin, in preparation (2009).

[17] D. J. Kaup, A. Reiman, and A. Bers, Rev. Mod. Phys. **51**, 275 (1979).

[18] See, e.g., N. Akhmediev, and J. M. Soto-Crespo, Phys. Lett. A **317**, 287 (2003).

Chapitre 5

Control of quantum systems

5.1 Control of molecular orientation and alignment

Corresponding articles : [6, 8, 13, 15, 16, 21, 23, 24, 25, 27]
This work has been done initially with the group of Osman Atabek of the *Laboratoire de Photophysique Moléculaire* in Orsay and then with local collaborators both theoreticians (S. Guérin and H. R. Jauslin) and experimentalists (O. Faucher, B. Lavorel, E. Hertz and F. Chaussard). The control of molecular orientation is a part of the PhD work of the student R. Tehini.

Molecular orientation and alignment is a well-established topic in quantum control [107, 109] both experimentally and theoretically. Controlling the molecular rotation has several possible applications which extend from the control of chemical reactions (enhancement of reactive cross sections) to nanoscale design and quantum computing. For a linear molecule, alignment means an increased probability distribution along the polarization direction axis of the control field whereas orientation requires, in addition, the same (or opposite) direction as the polarization vector. Several theoretical methods to reach a high degree of alignment or orientation have been proposed using adiabatic techniques [58, 65], optimal control schemes or genetic algorithms [54, 43, 106], trains of short pulses [82, 83, 42], two-color laser fields [119, 75]. The experimental control of molecular alignment is also well understood [107] and generalizations to nonlinear molecules [93, 68], three-dimensional alignment [81, 114, 80], or to more complex dynamics [52] have also been considered. With the presently available technology, the control of molecular orientation is however more difficult to achieve. The difficulties lie

in the generation of the laser pulses or in the low temperature required to obtain a high efficiency. Nevertheless, new techniques combining electrostatic fields and nonresonant femtosecond laser pulses seem to be a promising road [61].

To be more precise, we consider now the simple case of a linear molecule at zero temperature. The equations can be straightforwardly generalized to nonlinear molecules (symmetric and asymmetric tops) and to nonzero temperatures. We assume that the molecule is controlled by a non-resonant (with respect to vibronic frequencies) linearly polarized laser field $E(t)$. The dynamics of the system is governed by the Schrödinger equation written in atomic units :

$$i\frac{\partial}{\partial t}|\psi(t)\rangle = [BJ^2 - \mu_0 \cos\theta E(t) - \frac{1}{2}(\Delta\alpha\cos^2\theta + \alpha_\perp)E(t)^2$$
$$-\frac{1}{6}((\beta_\parallel - 3\beta_\perp)\cos^3\theta + 3\beta_\perp\cos\theta)E(t)^3]|\psi(t)\rangle$$

where B is the rotational constant, μ_0 the permanent dipole moment, $\alpha_\parallel$ and $\alpha_\perp$ the parallel and perpendicular components of the polarizability tensor, $\Delta\alpha = \alpha_\parallel - \alpha_\perp$ and $\beta_\parallel$ and $\beta_\perp$ the parallel and perpendicular components of the hyperpolarizability tensor.

My contribution is this domain is two-fold. I first introduce the notion of target states which are the states maximizing the orientation or the alignment in a given finite-dimensional Hilbert space spanned by the first rotational levels. The dimension of this space is related to the temperature and to the intensity of the field used. This dimension has to be chosen in each practical case. We recall that a basis of the Hilbert space is given by the spherical harmonics. Let θ be the polar angle between the molecular axis and the field polarization direction. The degree of orientation and alignment of the molecular system are respectively given by the expectation values $\langle\cos\theta\rangle$ and $\langle\cos^2\theta\rangle$. At zero temperature, the target state is simply the eigenvector of maximum eigenvalue of the projection of the operators $\cos\theta$ or $\cos^2\theta$ onto the finite dimensional Hilbert space. The target states have been introduced in [28, 25], extended to non zero temperatures in [23] and to dissipative media in [21]. My other contribution has consisted in constructing control strategies in the sudden regime. The sudden regime of control is characterized by pulses of short duration with respect to the rotational period of the molecule. It is well suited to experimental applications using femtosecond laser fields. In this framework, we have shown that a train of short pulses is

an efficient way to produce orientation or alignment or equivalently to get close to the target state [28, 25, 23, 21]. The delay and the intensity of each pulse can be optimized by genetic algorithms or fixed to a given value in a systematic strategy of maximization of orientation or alignment [25, 23]. More complex strategies using for instance a laser pulse with few optical cycles or a two-color laser field can also be designed [27, 24, 15].

The dissipation effect on alignment due to molecular collisions has been recently discussed in different works [98, 99]. It has been proposed that the dynamics is then governed by the Lindblad equation. In [16], a first work done in collaboration with the group of O. Faucher and B. Lavorel shows experimentally that it is indeed the case. The question of the precise determination of the dissipative parameters describing the interaction between the system and the environment has not been completely solved in particular when the pressure of the gas is high. In [21], we have shown how to modify the strategy of a train of laser pulses to reach a high degree of alignment even in presence of dissipation.

In [8] and [13], we consider optimal control theory (OCT) to determine the different control fields both for molecular orientation [13] and molecular alignment [8]. We do not consider the sudden regime but an intermediary regime with a control duration equal to one or several rotational periods. In the sudden regime, numerical simulations show that the optimal solution is very close to a gaussian pulse. Monotonically convergent algorithms have been used to solve the optimal equations. Molecular orientation and alignment correspond to nonstandard situation in OCT. In [13], we show how to generalize monotonic algorithms to nonlinear interaction with the control field, which is the case if polarizability and hyperpolarizability terms are considered in the Hamiltonian. We also propose in [8] a new formulation of these algorithms to take into account spectral constraints and we apply it to molecular alignment. In particular, we consider spectral constraints which mimic experimental pulse shaping techniques. This allows to determine optimal solutions which are experimentally implementable. In other words, since there exists no unique optimal solution for such control problems, we can select it using spectral filters control fields satisfying particular constraints. Control experiments use liquid crystal pulse shapers which work in the frequency domain by tailoring the spectral phase and amplitude of the electric field [69, 102]. Only a piecewise constant function in phase and in ampli-

tude over a given bandwidth in the frequency domain can be produced by such techniques. The number of pixels is usually of the order of 640. We have shown in [8] that 128 pixels (both in phase and in amplitude) is a sufficient number to produce molecular orientation or alignment. The pixels that discretize the Fourier transform are taken equally spaced in the frequency interval defined by the bandwidth of the pulse shaper.

We reproduce here the article [25].

Laser control for the optimal evolution of pure quantum states

D. Sugny,[1,*] A. Keller,[2] O. Atabek,[2] D. Daems,[3] C. M. Dion,[4] S. Guérin,[1] and H. R. Jauslin[1]
[1]*Laboratoire de Physique de l'Université de Bourgogne, UMR CNRS 5027, Boîte Postale 47870, 21078 Dijon, France*
[2]*Laboratoire de Photophysique Moléculaire du CNRS, Université Paris-Sud, Bâtiment 210, Campus d'Orsay, 91405 Orsay Cedex, France*
[3]*Center for Nonlinear Phenomena and Complex Systems, Université Libre de Bruxelles, 1050 Brussels, Belgium*
[4]*Department of Physics, Umeå University, SE-90187 Umeå, Sweden*
(Received 27 October 2004; published 7 June 2005)

Starting from an initial pure quantum state, we present a strategy for reaching a target state corresponding to the extremum (maximum or minimum) of a given observable. We show that a sequence of pulses of moderate intensity, applied at times when the average of the observable reaches its local or global extremum, constitutes a strategy transferable to different control issues. Among them, postpulse molecular alignment and orientation are presented as examples. The robustness of such strategies with respect to experimentally relevant parameters is also examined.

DOI: 10.1103/PhysRevA.71.063402 PACS number(s): 32.80.Qk, 33.80.−b, 32.80.Lg, 42.50.Hz

I. INTRODUCTION

Recent advances in laser technology have opened up large possibilities for the control of quantum processes playing a role in a variety of problems encompassing chemical reactivity [1,2], high-order harmonic generation [3], or logical gates with applications in quantum information [4–6]. Several advances have been achieved in this context, from the discovery of elementary basic mechanisms of strong-field-induced molecular dynamics, to optimal control strategies bringing together sophisticated numerical algorithms (such as evolutionary algorithms) [3,7]. Parallel to these works, a systematic study of quantum systems in either pure or mixed (statistical) states has been undertaken using control theory [8]. Upper and lower bounds corresponding to kinematical constraints have been established for the expectation value of arbitrary observables of driven quantum systems [9,10], with a particular attention paid to their dynamical realizability [11,12]. This latter question, which is related to their complete controllability, has been solved for linear control, i.e., for Hamiltonians depending in a linear way on the control functions, of nondissipative finite-level quantum systems [11].

The aim of this study, which is a continuation of our previous paper [13], is to show how a strategy worked out for the laser control of a specific observable can be transposed to a generic system. An essential feature of the control scheme we propose is to reduce the physical Hilbert space to a subspace $\mathcal{H}^{(N)}$, of finite dimension N. A target state $|\chi^{(N)}\rangle$, which maximizes (or minimizes) the expectation value of an observable $\mathcal{O}$, is then defined in this subspace. The first obvious advantage of the finite dimensionality is that $|\chi^{(N)}\rangle$ appears, through a variational principle, to be the eigenvector (for the nondegenerate case) associated to $\mathcal{H}^{(N)}$ with the highest or lowest eigenvalue of the restriction of the observable $\mathcal{O}$. These bounds being kinematic, they only indicate to which extent the system can be dynamically controlled by application of time-dependent external fields. Moreover, in the finite-dimensional case, the complete or noncomplete controllability can be determined and related (for a linear control system) to the dimension of the Lie algebra generated by the unperturbed Hamiltonian and the interaction operator [11,12].

Assuming the dynamical realizability of the target state, the remaining question consists in explicitly finding a suitable scheme in terms of a unitary evolution operator $U(t)$ which, starting from an initial pure state of the molecular system, dynamically brings it close to the state $|\chi^{(N)}\rangle$. Several control strategies have already been proposed using, for instance, adiabatic passage techniques [14,15], factorizations of unitary operators [16], or optimal control schemes [7,17]. Here, we pursue another approach, and we show that a sequence of short pulses of moderate intensity can be devised for reaching these target states. A generalization to models incorporating fluctuating environmental effects such as temperature, via statistically mixed initial states, is still an open question on which work is in progress.

The strategy is exemplified by two illustrative cases, the alignment and the orientation control of rigid-rotor molecules. We show that either complete or close to complete control is achieved after the application of a finite number of pulses. More precisely, the alignment and orientation control processes, aiming at both efficiency and maximal duration within a rotational period, require few kicks to get close to the target, while remaining in the conventionally fixed finite-dimensional Hilbert subspace. We note that in all the dynamical mechanisms under consideration, we are interested in controlling the postpulse behavior of the observables. The motivations for such processes are now well established in a wide variety of applications extending from chemical reaction dynamics to surface processing, catalysis, nanoscale design, and quantum computing [2,18–21].

The paper is organized as follows. A mathematical setup is given in Sec. II for the general control strategy, which is then applied to the case of molecular alignment and orienta-

*Electronic address: dominique.sugny@u-bourgogne.fr

tion. These processes are taken on a parallel footing in Sec. III by considering either the polarizability or the permanent dipole moment of the molecular system. Section IV collects the results with a special emphasis on the robustness with respect to control parameters and the experimental feasibility. Concluding remarks and prospective views are presented in Sec. V. Some details of the calculations and some proofs are presented in Appendices A–D.

II. METHODOLOGY

The field-free Hamiltonian acting on the physical Hilbert space $\mathcal{H}$ is denoted H_0. The initial pure quantum state of interest $|\psi_n(t=0)\rangle$ is taken as one of the eigenstates of H_0 corresponding to the eigenvalue E_n. One considers an observable $\mathcal{O}$ which, through the dynamical behavior of its expectation value $\langle\mathcal{O}(t)\rangle$, describes the physical property to be controlled by the external field. $\mathcal{O}$ is a self-adjoint operator which does not commute with H_0. The aim of the control is to find an evolution operator $U(t)$, within a class of experimentally realizable processes, such that the time evolution of the initial state under the action of $U(t)$ leads to an average $\langle\psi_n(t)|\mathcal{O}|\psi_n(t)\rangle$ that is maximized or minimized. This goal is achieved in three steps.

A. Finite-dimensional subspace

We first select a finite N-dimensional subspace $\mathcal{H}^{(N)}$ of the physical Hilbert space. For instance, in the case of alignment and orientation such a subspace is generated by the first N eigenstates $|n\rangle$ of H_0 with eigenvalues E_n [13]. The mathematical advantage of this reduction is twofold when considering the reduced operator

$$\mathcal{O}^{(N)} = P^{(N)}\mathcal{O}P^{(N)}, \tag{1}$$

$P^{(N)}$ being the projector on the subspace $\mathcal{H}^{(N)}$. The first advantage, of kinematical nature [9,10], is related to the fact that $\mathcal{O}^{(N)}$ has now an upper- and lower-bounded discrete spectrum, as opposed to the possibly continuous or unbounded spectrum of $\mathcal{O}$. The second is that the controllability of the system can be completely analyzed (see Sec. II D for details), whereas such results are limited for the infinite-dimensional case [22].

Finally, we assume that all the fundamental frequencies of H_0 in $\mathcal{H}^{(N)}$ are commensurate, i.e., integer multiples of a fundamental frequency ω, which implies that the motion is periodic in time, with period $T=2\pi/\omega$.

Apart from these mathematical considerations, which will be used in Sec. II D, the reduction of the Hilbert space may also lead to other physical advantages in specific cases. Indeed, for postpulse alignment and orientation control, the finite dimensionality of the molecular rotational space, involving low momenta, leads to longer alignment and orientation dynamics as a result of the slower oscillation of $\langle\mathcal{O}(t)\rangle$ after interaction with the field. It is precisely this behavior that roughly constitutes the basis of the compromise between efficiency and long duration of such control issues. Reciprocally, the justification of the dimensionality reduction is related to the fact that moderate perturbations, i.e., a moderate number of applied pulses and amplitude, can only transfer finite amounts of energy to the molecule, confining the system to a finite-dimensional subspace [13].

B. Controllability

The control is exerted through the application of a time-dependent external field described by the Hamiltonian

$$H(t) = H_0 + V(t), \tag{2}$$

where $V(t)$ is the molecule-field interaction potential. The general structure of $V(t)=V(\vec{\xi},\vec{\mathcal{E}}(t))$ involves the field vector $\vec{\mathcal{E}}(t)$ (amplitude and polarization direction) together with molecular vectorial characteristics $\vec{\xi}$ that may, in some cases, be field induced (an example of such a behavior, through the polarizability interaction, is given in Sec. III). Moreover, in order to apply the results of control theory, we also assume that the system is control linear, which means here that V can be written in the form

$$V(t) = -v(t)H_I, \tag{3}$$

where v is a real control function (that can be chosen at will) and H_I the interaction operator. If a system of the form (3) is completely controllable [11,12] then there exists a function $v(t)$ such that the corresponding propagator $U(t)$ brings the initial state to the target state. A simple example of a noncontrollable system is a decoupled one. In this case, the matrix representation of H is block diagonal and the Hilbert space can be decomposed as a direct sum of at least two orthogonal subspaces. However, for nondecoupled systems, the question of dynamical realizability is more difficult and an investigation of the structure of the Lie algebra is needed. A Lie algebra of matrices is a subspace of the vector space (over the field of reals) of $N\times N$ matrices (with complex entries) which is stable under the commutation operation [11]. Two cases of particular relevance here are the Lie algebra of $N\times N$ skew-Hermitian matrices denoted by $\mathrm{u}(N)$ and whose dimension is N^2, and the Lie algebra $\mathrm{su}(N)$ of $N\times N$ zero-trace skew Hermitian matrices, whose dimension is N^2-1. We recall [11,12] that a necessary and sufficient condition for the complete controllability of the Hamiltonian system defined by H [Eq. (2)] is that the Lie algebra generated by iH_0 and iH_I be $\mathrm{u}(N)$. In the rest of this section, we will assume the dynamical realizability of the target states.

C. Target state

The state $|\chi^{(N)}\rangle$ which maximizes (or minimizes) $\mathcal{O}^{(N)}$ in the subspace $\mathcal{H}^{(N)}$ is nothing but the eigenstate of $\mathcal{O}^{(N)}$ corresponding to its upper (or lower) eigenvalue. This provides a clear description of the target state in terms of a linear combination of states $|n\rangle$ in direct relation with the observable to control. If N is large enough, the upper (or lower) eigenvalue of $\mathcal{O}^{(N)}$ will be close to the corresponding bound of $\mathcal{O}$ (if this operator is bounded) and an efficient control could be achieved (assuming complete controllability). Once again, it is worth noting that large N allows for higher values of $|\langle\mathcal{O}^{(N)}\rangle|$, but leads to higher energy transfer from the ex-

ternal field to the molecular system and consequently results in shorter durations as the postpulse average $\langle \mathcal{O}(t) \rangle$ is done over a superposition involving many more eigenstates of H_0.

D. Control strategy

We shall now present in detail two control schemes. The first one, which was first proposed in [23] and further developed in [13], consists in applying pulses each time $\langle \mathcal{O}^{(N)} \rangle$ reaches its maximum value within a period T of the field-free dynamics. An individual pulse perturbs the molecule by an effective evolution operator $U_{\tilde{A}}$, where $\tilde{A}$ is a real parameter related to the field amplitude: Eq. (7) gives, for instance, the expression of $\tilde{A}$ in the sudden approximation. The system remains in the subspace $\mathcal{H}^{(N)}$, up to negligible corrections, if the field amplitude $\tilde{A}$ is small enough. Between two successive pulses, the molecule evolves following its field-free motion, governed by $U_{H_0}(\Delta t) = \exp(-iH_0 \Delta t)$. An important hypothesis of our strategy is that the system is to be perturbed according to a unitary operator $U_{\tilde{A}}$, which commutes with $\mathcal{O}^{(N)}$, such that its application does not alter $\langle \mathcal{O}^{(N)} \rangle = \langle U_{\tilde{A}}^{-1} \mathcal{O}^{(N)} U_{\tilde{A}} \rangle$. Furthermore, the optimal target state $|\chi^{(N)}\rangle$ is an eigenfunction of both $\mathcal{O}^{(N)}$ and $U_{\tilde{A}}$.

We now consider that pulses are applied at times t_i when $\langle \mathcal{O}^{(N)}(t) \rangle$ reaches its global maximum $\mathcal{O}_i = \langle \mathcal{O}^{(N)}(t_i) \rangle$. The sequence of $\mathcal{O}_i$'s is increasing (possibly constant) but bounded and is therefore convergent. Due to the hypothesis on the fundamental frequencies (Sec. II A) and the fact that $\langle \mathcal{O}^{(N)} \rangle = \langle U_{\tilde{A}}^{-1} \mathcal{O}^{(N)} U_{\tilde{A}} \rangle$, $\langle \mathcal{O}^{(N)}(t) \rangle$ is a periodic, continuous, and differentiable (under free evolution) function. It is then easy to verify that the limit of the preceding sequence is a fixed point $\mathcal{O}_i = \mathcal{O}_{i+1}$, for any value of the parameter $\tilde{A}$, corresponding to a wave function $|\psi_f\rangle$ (or a family of wave functions) such that $\langle \psi_f | \mathcal{O}^{(N)} | \psi_f \rangle = \langle \psi_f | U_{\tilde{A}}^{-1} \mathcal{O}^{(N)} U_{\tilde{A}} | \psi_f \rangle = \mathcal{O}_i$ is a global maximum within a period T.

The description of this control strategy raises several questions which are not completely resolved. The first one is the set of limits (corresponding to the fixed points) of the process. It can readily be shown that this set contains some of the eigenvectors of the operator $\mathcal{O}^{(N)}$, but we can look for the conditions on H_0, $U_{\tilde{A}}$, and $\mathcal{O}^{(N)}$ such that these wave functions be the unique fixed points of the strategy. Appendix A provides a sufficient condition on these operators. The second question deals with the determination of the domain of attraction of each fixed point and, more precisely, the domain of the target state. The domain of attraction of $|\psi_f\rangle$ can be defined as the set of initial states $|\psi\rangle$ such that, for some choice of the parameters $\tilde{A}_i$ (the pulses being labeled by i), the process, starting from $|\psi\rangle$ converges to $|\psi_f\rangle$. The last open question concerns the reduction to a finite-dimensional space of the dynamics. In this paper, the fact that the dynamics resides within the subspace $\mathcal{H}^{(N)}$ is only numerically justified (see Sec. III for details). Work is in progress on these open questions.

The second control scheme that can be used is a strategy similar in its spirit to the first one. Up to now, we have searched for a sequence of perturbations that maximize the average value of the observable $\langle \mathcal{O}^{(N)}(t) \rangle$. Another relevant optimization would be to get closer to the target state $|\chi^{(N)}\rangle$. This can be done in practice by applying pulses each time the modulus of the projection on the target state, $|\langle \chi^{(N)} | \psi_n(t) \rangle|$, reaches a maximum. The relative merits of the two control schemes will be discussed in Sec. IV.

To conclude, we mention an alternative that can favor the convergence of the control scheme. The general strategy is based on global maxima of the field-free dynamics, but local maxima can also be used. This will be illustrated numerically for the control of molecular alignment in Sec. IV, where it will be shown that a better convergence is obtained with local maxima.

E. The sudden approximation

Depending on the duration τ of the radiative interaction $V(t)$ as compared to molecular characteristic times T, we may be in the adiabatic ($\tau \gg T$) or in the sudden ($\tau \ll T$) limits. Long laser pulses have been shown to yield very efficient adiabatic molecular control [24–27], but with the caveat of it disappearing after the pulse, as the molecule returns to its initial state when the turnoff is adiabatic. As we are rather concerned with the postpulse behavior of $\langle \mathcal{O}(t) \rangle$, we hereafter use short pulses, assuming the sudden limit. Following the derivation of the lowest-order impulsive approximation given in Refs. [28,29], the time-dependent Schrödinger equation, written in the interaction representation as

$$i\hbar \frac{\partial}{\partial t} \tilde{\psi}_\lambda(t) = [e^{iH_0 t/\hbar} V(t) e^{-iH_0 t/\hbar}] \tilde{\psi}_\lambda(t), \tag{4}$$

with $\tilde{\psi}_n(t) = e^{iH_0 t/\hbar} \psi_n(t)$, is integrated on the total pulse duration τ to yield

$$\tilde{\psi}_n(\tau) = -\frac{i}{\hbar} \int_0^\tau [e^{iH_0 t/\hbar} V(t) e^{-iH_0 t/\hbar}] \tilde{\psi}_n(t) dt + \tilde{\psi}_n(t=0). \tag{5}$$

At the lowest order in τ/T, one can substitute $e^{iH_0 t/\hbar}$ with $\mathbf{1}$ in Eq. (5) and, using $V(t) = v(t) H_I$ [Eq. (3)], the integral equation (5) can be solved as

$$\tilde{\psi}_n(\tau) = \exp(i\tilde{A} H_I) \tilde{\psi}_n(t=0), \tag{6}$$

with

$$\tilde{A} = \frac{1}{\hbar} \int_0^\tau v(t) dt. \tag{7}$$

Finally, returning to the Schrödinger representation, one obtains

$$\psi_n(t \geq \tau) = U_{H_0}(t) U_{\tilde{A}} \psi_n(t=0), \tag{8}$$

where the evolution operators are given by

$$U_{H_0}(t) = \exp(-iH_0 t/\hbar) \tag{9}$$

and

$$U_{\tilde{A}} = \exp(i\tilde{A} H_I). \tag{10}$$

We are now in a position to examine the conditions (choice of the parameters N, A, and t_i's) under which the mentioned

strategies work in the control of alignment and orientation processes.

III. CONTROL OF THE MOLECULAR ALIGNMENT AND ORIENTATION

Laser-induced alignment and orientation are important issues in controlling molecular dynamics [2]. For a diatomic molecule driven by a linearly polarized laser field, alignment means an increased probability distribution along the polarization axis whereas orientation requires in addition the same (or opposite) direction as the polarization vector. In a variety of applications, extending from chemical reaction dynamics to surface processing, catalysis, and nanoscale design [2,18,19,21], noticeable orientation that persists after the end of the pulse is of special importance. This is why the identification of target states that satisfy these two requirements (i.e., efficiency and persistence) is the basis of the construction presented in Ref. [13].

The time evolution of the molecule, hereafter described in a three-dimensional rigid-rotor approximation, interacting with a linearly polarized field is governed by the time-dependent Schrödinger equation (TDSE), expressed in atomic units,

$$i\frac{\partial}{\partial t}\psi(\theta,\phi;t) = [BJ^2 - \vec{\mu}(\vec{\mathcal{E}})\cdot\vec{\mathcal{E}}(t)]\psi(\theta,\phi;t), \qquad (11)$$

where J is the angular momentum operator, B the rotational constant, $\vec{\mu}(\vec{\mathcal{E}})$ the total dipole moment, and $\vec{\mathcal{E}}$ the electric field. θ denotes the polar angle between the molecular axis and the polarization direction of the applied field. The motion related to the azimuthal angle ϕ can be separated due to cylindrical symmetry. The field-induced dipole is expanded in powers of $\vec{\mathcal{E}}(t)$,

$$\vec{\mu} = \vec{\mu}_0 + \bar{\bar{\alpha}}\cdot\vec{\mathcal{E}}(t) + \cdots, \qquad (12)$$

where the two first terms (to which our approximation is limited) are, respectively, the permanent dipole $\vec{\mu}_0$ and the polarizability tensor $\bar{\bar{\alpha}}$. We notice that only very intense lasers may require the inclusion in Eq. (12) of higher-order terms. The electric field is written as

$$\vec{\mathcal{E}}(t) = f(t)\cos(\omega t)\vec{\epsilon}, \qquad (13)$$

$\vec{\epsilon}$ being the unit polarization vector, ω the carrier wave frequency, and $f(t)$ the laser pulse envelope. In a high-frequency regime, which is often referred to in models dealing with alignment [2], the permanent dipole interaction, i.e., $\vec{\mu}_0\cdot\vec{\mathcal{E}}(t)$, averages to zero due to the term $\cos(\omega t)$, whereas the polarizability interaction corresponding to $\bar{\bar{\alpha}}\cdot\vec{\mathcal{E}}^2(t)$, involves a $\cos^2(\omega t)$ term which contributes an average $1/2$. Finally, in a high-frequency approximation [26,30], the TDSE [Eq. (11)] is written as

$$i\frac{\partial}{\partial t}\psi(\theta,\phi;t) = \left[BJ^2 - \frac{1}{4}f^2(t)(\Delta\alpha\cos^2\theta + \alpha_\perp)\right]\psi(\theta,\phi;t), \qquad (14)$$

where $\Delta\alpha=\alpha_\parallel-\alpha_\perp$ is the difference between the parallel $\alpha_\parallel$ and perpendicular $\alpha_\perp$ components of the polarizability tensor. While excellent alignment can be obtained through adiabatic transport on so-called pendular states [26] resulting from field dressing, only sudden pulses offer the possibility of alignment that persists after the field is over [2]. As opposed to alignment, orientation requires spatial symmetry breaking, and therefore cannot be obtained from a radiative interaction in $\cos^2\theta$ such as the one depicted in Eq. (14) resulting from polarizability. It has recently been shown that very short pulses combining a frequency ω and its second harmonic 2ω (in resonance with a vibrational transition), excite, through the combined effect of μ_0 and α, a mixture of even and odd rotational levels and have the ability to produce postpulse orientation [31]. But even more efficient orientation is obtained using half-cycle pulses (HCPs), that, through their highly asymmetrical shape, induce a very sudden momentum transfer to the molecule which orients under such a kick after the field is off [28,32]. It is worth noting that both the $(\omega+2\omega)$ and the kick mechanisms have received confirmation from optimal control schemes [7]. In a moderate-field approximation where the polarizability interaction is neglected as compared to the permanent dipole one, the TDSE which governs the orientation process can be written as

$$i\frac{\partial}{\partial t}\psi(\theta,\phi;t) = [BJ^2 - f(t)\mu_0\cos\theta]\psi(\theta,\phi;t). \qquad (15)$$

As the two processes (i.e., postpulse alignment and orientation) require short-duration pulses, from now on, we assume a sudden approximation based on the shortness of the pulse duration τ as compared to the molecular rotational period $T_{rot}=\pi/B$. For relatively low j (where j labels the eigenstates of J^2), this amounts to the definition of a dimensionless, small perturbative parameter $\varepsilon=\tau B$. This definition, together with a rescaling of time $s=t/\tau$ (such that $s\in[0,1]$ during the pulse) leads to a TDSE that can be treated by time-dependent unitary perturbation theory [33,34],

$$i\frac{\partial}{\partial s}\psi(\theta,\phi;s) = [H_0 - V_{a;o}(s)]\psi(\theta,\phi;s), \qquad (16)$$

with $H_0=\varepsilon J^2$ and $V_{a;o}(s)$ the radiative interaction depending on the process to be described. More precisely, we have for alignment

$$V_a(s) = E_a^2(s)\cos^2\theta + F_a^2(s) \qquad (17)$$

and for orientation

$$V_o(s) = E_o(s)\cos\theta. \qquad (18)$$

The time-dependent functions are defined as

$$E_a^2(s) = \Delta\alpha\tau f^2(\tau s)/2, \qquad (19)$$

$$F_a^2(s) = \alpha_\perp\tau f^2(\tau s)/2, \qquad (20)$$

$$E_0(s) = \mu_0 \tau f(\tau s). \tag{21}$$

Returning now to the successive steps of our approach as detailed in the mathematical setup (Sec. II), we have to define an initial pure quantum state and the observables adequately describing both processes. The initial state of the molecule is taken as the ground state of the rigid rotor,

$$|\psi_{n=0}(t=0)\rangle = |j=0,m=0\rangle. \tag{22}$$

We remark that any other rotational state of the rotor, i.e., $|j \geqslant m,m\rangle$, cannot be taken, by observing that the projection quantum number m is invariant upon the application of linearly polarized pulses. The two observables we consider are $\mathcal{O}_a = \cos^2\theta$ for alignment and $\mathcal{O}_o = \cos\theta$ for orientation. The goal of the field-driven molecular alignment (or orientation) is then to maximize (or to minimize, depending the choice of the orientation) for the largest time duration, the expectation values

$$\langle \mathcal{O}_{a;o}(s)\rangle = \langle \psi(\theta,\phi;s)|\mathcal{O}_{a;o}|\psi(\theta,\phi;s)\rangle, \tag{23}$$

after the pulse is over.

The second step consists in the reduction of the dimensionality of the infinite physical Hilbert space by considering a finite subspace $\mathcal{H}^{(N)}_{m=0}$ generated by the first N eigenvectors of J^2, i.e., $|j,m=0\rangle$ $(j=0,1,\ldots,N-1)$. The observables are projected in this subspace according to

$$\mathcal{O}^{(N)}_{a;o} = P^{(N)}_{m=0}\mathcal{O}_{a;o}P^{(N)}_{m=0}, \tag{24}$$

with the projectors explicitly given by

$$P^{(N)}_{m=0} = \sum_{j=0}^{N-1} |j,m=0\rangle\langle j,m=0|. \tag{25}$$

It is clear from Eq. (24) that $\mathcal{O}^{(N)}_{a;o}$ has, as opposed to $\cos^2\theta$ or $\cos\theta$, a purely discrete spectrum. The target states $|\chi^{(N)}_{a;o}\rangle$ that maximize the alignment (or the orientation) in the subspace $\mathcal{H}^{(N)}_{m=0}$ are simply the eigenstates of $\mathcal{O}^{(N)}_{a;o}$ with the highest eigenvalue. Their calculation in terms of the appropriate expansion coefficients $c^{a;o}_j$ in the $|j,m=0\rangle$ basis,

$$|\chi^{(N)}_{a;o}\rangle = \sum_{j=0}^{N-1} c^{a;o}_j |j,m=0\rangle, \tag{26}$$

involves the diagonalization of the $N\times N$ matrices of $\mathcal{O}^{(N)}_{a;o}$ [Eq. (24)] written in the same basis. For instance, in the simplest case of orientation, a tridiagonal matrix of the operator $\mathcal{O}^{(N)}_o$ results (when using the approximation $\langle j,m=0|\cos\theta|j\pm1,m=0\rangle = 1/2$, valid for $j \gg m$) in the analytical expression

$$|\chi^{(N)}_o\rangle \simeq \left(\frac{2}{N+1}\right)^{1/2}\sum_{j=0}^{N-1}\sin\left(\pi\frac{j+1}{N+1}\right)|j,m=0\rangle, \tag{27}$$

with the corresponding maximal orientation found in this subspace

$$\langle \chi^{(N)}_o|\cos\theta|\chi^{(N)}_o\rangle \simeq \cos\left(\frac{\pi}{N+1}\right). \tag{28}$$

Having determined the kinematical constraints, we can now analyze the dynamical realizability of these target states. This kind of Hamiltonian (involving a dipole interaction with the control field) has already been investigated by Schirmer and co-workers [12] and it was shown that the Lie algebra generated by $iH^{(N)}_0$ and $i\mathcal{O}^{(N)}_{a;o}$ is $\mathrm{u}(N)$ (Theorem 1 of Ref. [12]). The system is therefore completely controllable.

The next step consists in applying our control strategy. For doing so, we determine the evolution operator for individual pulses. This is done in the impulsive sudden limit [28,29]. The interaction term of the alignment process $V_a(s)$ [Eq. (17)] involves the square of the electric field amplitude. The time evolution can be expressed in terms of a free evolution combined with

$$U_a = \exp[iA_a\cos^2\theta], \tag{29}$$

where

$$A_a = \int_0^1 E^2_a(s)ds \tag{30}$$

is the total pulse square area. We note that we have not taken into account the θ-independent contribution $F^2_a(s)$ to $V_a(s)$ as it would only contribute a pure phase factor. For the case of orientation, we get as the instantaneous evolution operator describing the kick

$$U_o = \exp[iA_0\cos\theta], \tag{31}$$

with

$$A_o = \int_0^1 E_o(s)ds \tag{32}$$

the total pulse area. Between pulses, the molecule evolves under the effect of its field-free rotation, described by the evolution operator

$$U_{H_0} = \exp[-i\varepsilon J^2 s]. \tag{33}$$

One can easily check the necessary commutation relations

$$[\mathcal{O}^{(N)}_{a;o}, U_{a;o}] = 0, \tag{34}$$

implying that the target states $|\chi^{(N)}_{a;o}\rangle$ are eigenfunctions of both $\mathcal{O}^{(N)}_{a;o}$ and $U_{a;o}$. Note that all quantities $(s,\varepsilon,E^2_a,E_o)$ are dimensionless, and hence do not depend on a specific molecular system. Times can be expressed in terms of fractions of the molecular rotational period T_{rot}. Moreover, the molecule-laser interaction characteristics (E^2_a or E_o) combine the field strength $\mathcal{E}$ with molecular constants α or μ_0, in such a way that the same values may be considered for different molecules at other, adequately chosen laser intensities. The final step for the control scheme consists in applying the instantaneous perturbations at specific times. More precisely, as has been discussed in the mathematical setup (Sec. II), two distinct strategies are adopted for the determination of these times. The first one ($S1$) consists in taking the series of s_i when $\langle \mathcal{O}^{(N)}_{a;o}\rangle(s)$ reaches its successive maxima (global or local) during the free evolution following a kick. The second one ($S2$) consists in taking the s_i's as times when the modulus of the projection of the wave function on the target states

$|\langle\psi_\lambda(s)|\chi_{a;o}^{(N)}\rangle|$ reaches a maximum during the free evolution. The numerical results obtained by both strategies are presented in Sec. IV.

We now discuss the relative merits of the two schemes from a theoretical point of view. For the strategy $S1$, the slope after the pulse can be explicitly determined in the infinite-dimensional case, as shown in Appendix C,

$$\frac{d}{ds}\langle\cos\theta\rangle\bigg|_{s_i+0} = 2\varepsilon A(\mathbf{1} - \langle\cos^2\theta\rangle) \tag{35}$$

for orientation, and

$$\frac{d}{ds}\langle\cos^2\theta\rangle\bigg|_{s_i+0} = 2A\varepsilon\langle\sin^2 2\theta\rangle \tag{36}$$

for alignment. As $\langle\cos^2\theta\rangle < 1$ and $\langle\sin^2 2\theta\rangle > 0$, one deduces that, in both cases, the slope takes a nonzero value after the application of the kick, whatever the pulse area A of the field. This point proves that the control scheme can be iterated for the alignment and orientation processes. In the finite-dimensional case, the corresponding expression for orientation derived in Appendix C is slightly different. We obtain for $\cos^{(N)}\theta$

$$\frac{d}{ds}\langle\cos^{(N)}\theta\rangle\bigg|_{s_i+0} = 2\varepsilon A[\mathbf{1} - \langle(\cos^{(N)}\theta)^2\rangle + B] + O(A^2), \tag{37}$$

B being a boundary term which is of the form

$$B = -\frac{N^2 + 2N + 1}{2N + 1}|a_N|^2, \tag{38}$$

where the a_n's are the coefficients of the wave function in the basis $|0 \leqslant j \leqslant N-1, m=0\rangle$. Here, we notice that we cannot conclude as above and arguments of dimensionality have to be used. In this way, Appendixes A and B show that the unique fixed point of strategy $S2$ is the target state $|\chi^{(N)}\rangle$ whereas scheme $S1$ can possess several fixed points as the eigenfunctions of the operator $\mathcal{O}^{(N)}$. However, the strategy $S1$ has the advantage that the target state can be selected during the dynamical process by appropriately choosing the intensities and the number of laser pulses. This is not the case for the scheme $S2$ because the target state has to be selected *a priori*.

IV. RESULTS

The results are presented in a general way, transferable to any particular molecule (characterized by its rotational period, its permanent dipole and its polarizability) interacting with any pulsed field (characterized by its moderate amplitude and its short duration as compared to the molecular rotational period). The relevant parameters, which gather both molecule and field constants, are taken to be $A_a=1.5$, $A_o=1$, and $\varepsilon=0.03$. They are compatible with any molecule, provided that the field amplitude is adequately chosen. For LiCl, for instance, this amounts to a pulse duration of about 0.3 ps and a field amplitude of 1.5×10^5 V cm^{-1} [28] in the case of the orientation. Time is indicated in fractions of the molecular rotational period. The presentation of the results follows the different steps of the control strategy. Analytical estimations of the dynamical parameters are reported in Appendix D.

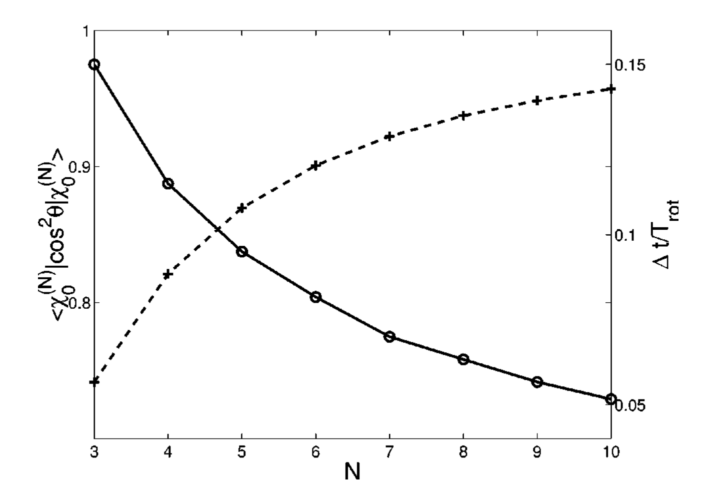


FIG. 1. Maximum alignment efficiency (crosses) and associated duration (open circles) as a function of N, the dimension of the rotationally excited subspace $\mathcal{H}_{m=0}^{(N)}$ (see text). The solid and dashed lines are just to guide the eye.

A. The finite-dimensional subspace

Relevant information for the characterization of alignment and orientation in the finite subspace $\mathcal{H}_{m=0}^{(N)}$ as a function of its dimensionality N are displayed in Figs. 1 and 2. The maximum efficiency [approximately given by Eq. (28) for the case of orientation] that can ideally be expected for a process that stays confined within $\mathcal{H}_{m=0}^{(N)}$ is given as $\langle\chi_0^{(N)}|\mathcal{O}_{a;o}^{(N)}|\chi_0^{(N)}\rangle$. The maximum duration, measuring the relative duration of the alignment and orientation processes over which $\langle\mathcal{O}_{a;o}^{(N)}(s)\rangle$ remains larger than 0.5 during the field-free evolution, is indicated in terms of a fraction of the rotational period as $\Delta t/T_{rot}$. The information displayed is crucial for the choice of the dimensionality N of the reduced subspace:

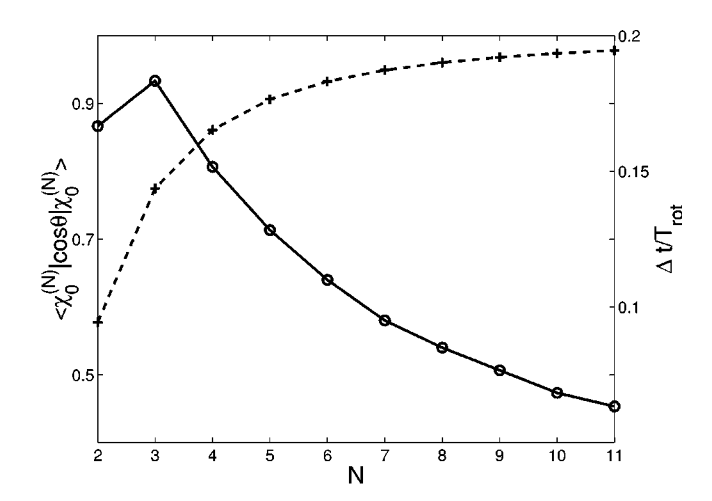


FIG. 2. Same as Fig. 1, but for orientation.

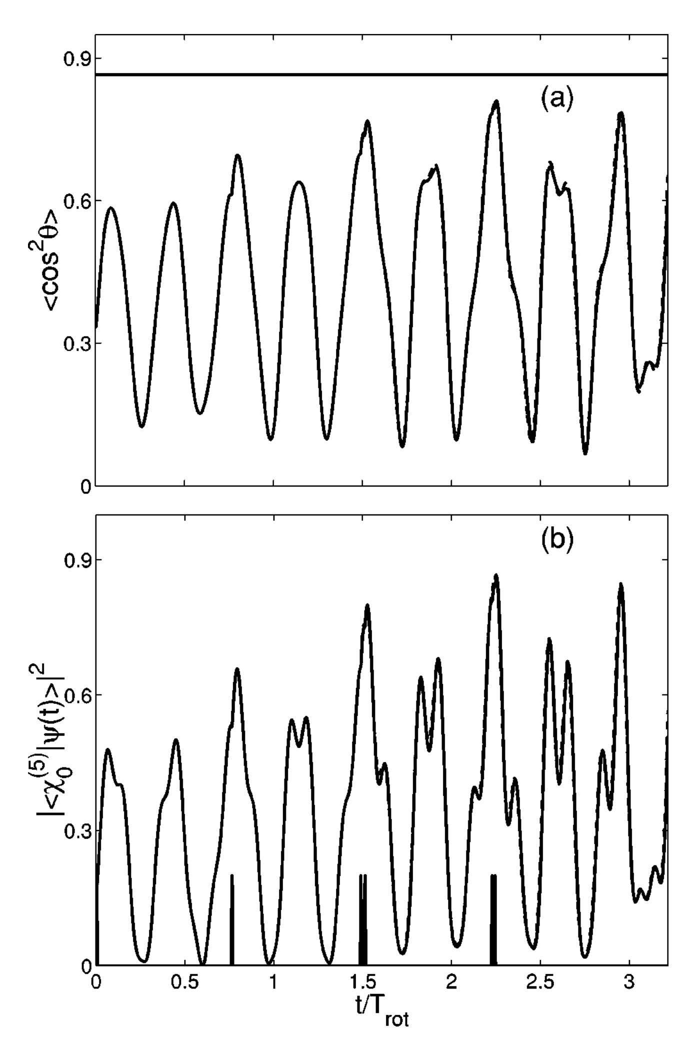


FIG. 3. Alignment dynamics during and after the train of pulses determined by strategy $S1$ of perturbing at the global maxima of $\langle\cos^2\theta\rangle$: (a) for $\langle\psi_\lambda(s)|\cos^2\theta|\psi_\lambda(s)\rangle$ and (b) for $|\langle\chi_a^{(5)}|\psi_\lambda(s)\rangle|^2$. The solid line corresponds to the exactly propagated wave function $\psi_\lambda(s)$ and the dashed line to the propagation of $\psi_\lambda(s)$ in the subspace $\mathcal{H}_{m=0}^{(5)}$. The train of pulses is displayed on (b) and the optimal alignment in $\mathcal{H}_{m=0}^{(5)}$ is indicated by the horizontal line on (a).

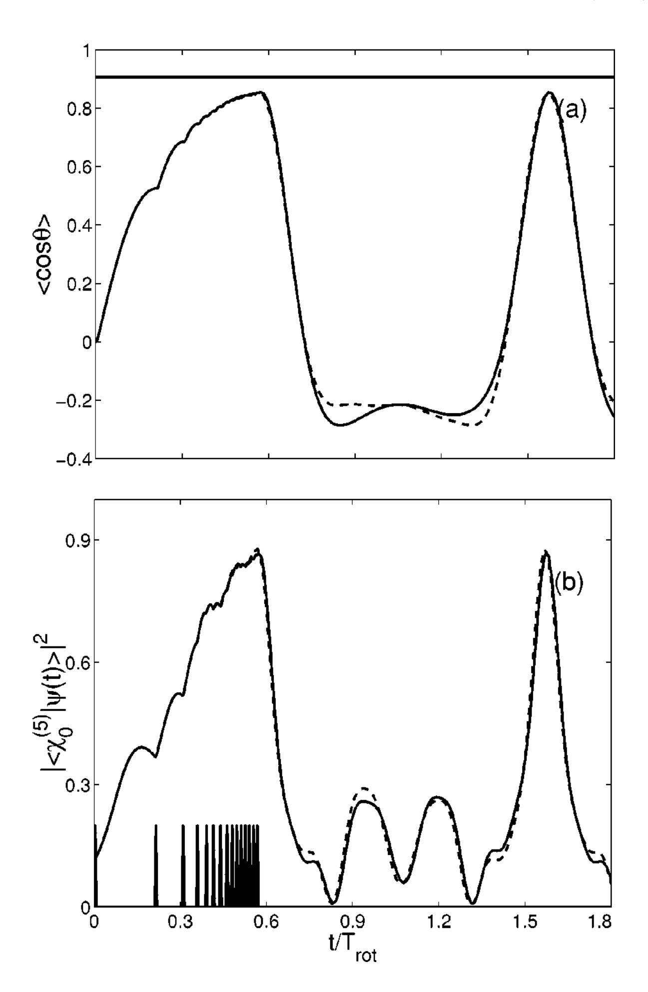


FIG. 4. Same as Fig. 3, but for the orientation dynamics.

a larger N is more suitable for a better efficiency of alignment or orientation, but leads to a shorter duration. The compromise between maximum efficiency and duration is to be done at that step. In order to keep an alignment or orientation duration of the order of one-tenth of the rotational period (amounting to durations exceeding 10 ps for heavy diatomic molecules such as NaI), N has to be limited to 5, as can be observed from Figs. 1 and 2. This may seem rather limiting in view of the moderate molecular rotational excitation, but even such a low dimension ($N=5$) turns out to be sufficient for very efficient alignment (about 0.85) or orientation (about 0.9). This fixes completely the target states [approximately given by Eq. (27) in the case of orientation] for both processes.

B. Dynamics controlled by the two strategies

The two strategies, denoted $S1$ and $S2$, can be exploited in the same way, the time delays between the successive pulses being defined following one of the two processes [maxima of $\langle\mathcal{O}_{a;o}^{(5)}\rangle$ for $S1$, or maxima of $|\langle\chi_{a;o}^{(5)}|\psi_\lambda(t)\rangle|^2$ for $S2$]. We look for the dynamical behavior of the two quantities, namely, the expectation value of the observables $\langle\mathcal{O}_{a;o}^{(5)}\rangle$ and the projections on the target states $|\langle\chi_{a;o}^{(5)}|\psi_\lambda(t)\rangle|^2$. All results are displayed with the first pulse taken as the origin of time and extend at least one rotational period T_{rot} after the last pulse. This helps to show the complete field-free behavior of the dynamics, which repeats periodically, leading to revival structures. Figures 3 and 4 illustrate the results of applying strategy $S1$ to the alignment and orientation processes, respectively. Noticeably different behavior is obtained for the two processes: clearly, a smaller number of pulses is necessary to control alignment (i.e., six pulses for alignment instead of 15 for orientation). The first pulse already provides an alignment efficiency of 0.75, whereas it only yields 0.5 orientation efficiency. Conversely, the overall dynamics (conditioning the delays between successive pulses) is much more oscillatory with complex structures in the case of alignment as compared to orientation where it progressively increases up to 0.89, which is almost the optimal limit as found from Fig. 2. In all cases, a comparison of the observables and the projections calculated using the exact wave function $\psi_\lambda(s)$ with the one propagated in the subspace $\mathcal{H}_{m=0}^{(5)}$ supports the claim that the rotational dynamics actually resides within $\mathcal{H}_0^{(5)}$. In both cases, the panels (b) show the way the wave

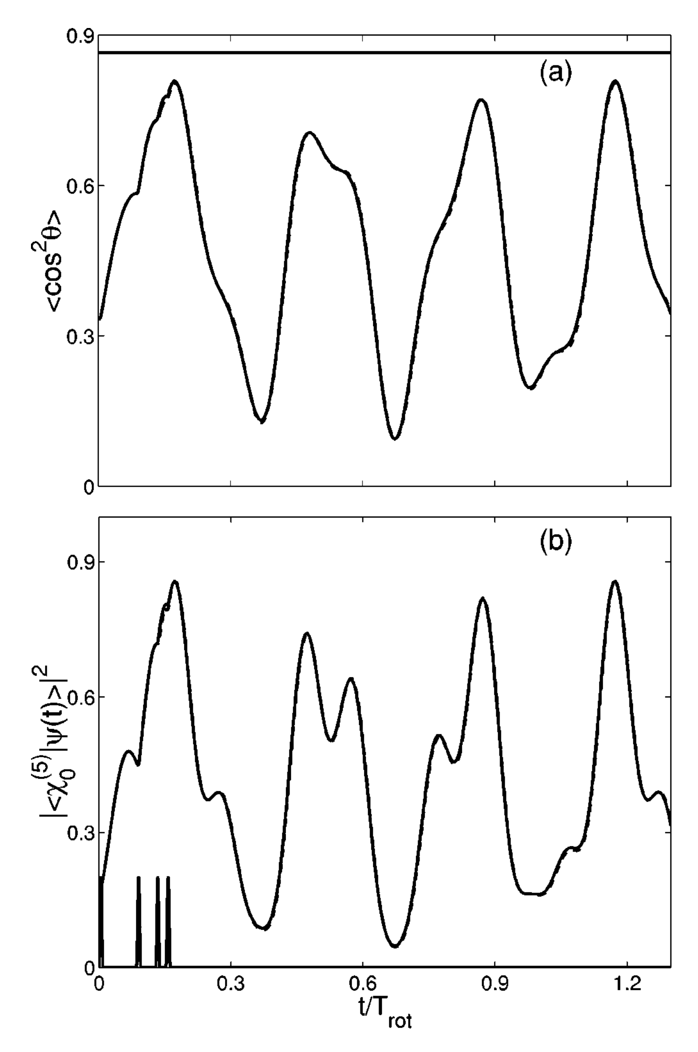


FIG. 5. Same as Fig. 3, but local maxima (the first maximum after the pulse) have been used.

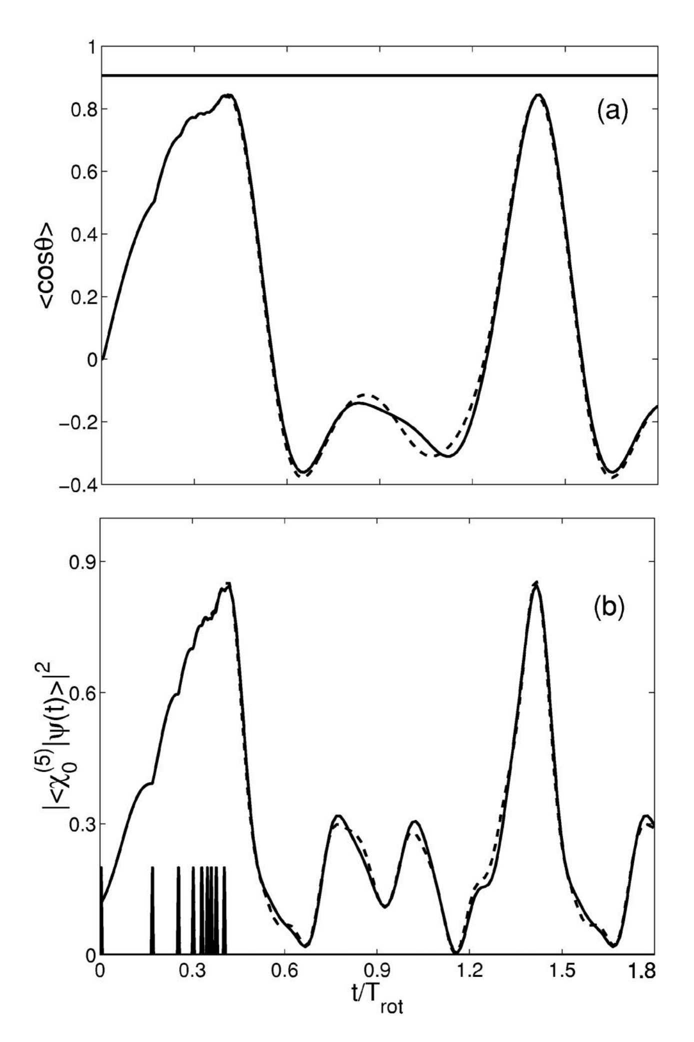


FIG. 6. Same as Fig. 4, but referring to strategy $S2$, perturbing the system at the maxima of $|\langle\chi_o^{(5)}|\psi_\lambda(s)\rangle|^2$.

function $\psi_\lambda(s)$ gets close to the target state $\chi_{a;o}^{(5)}$, illustrating the successful outcome of the control strategy with a coherent choice of parameters A, N, and the number of pulses for appropriately describing the dynamics. Finally, the postpulse dynamics leads to results particularly remarkable with respect to previous proposals. An efficiency of about 0.85 with a duration of 1/10 of the rotational period is achieved for alignment, with even better results for orientation, i.e., 0.89 efficiency and 2/10 of the rotational period duration (which corresponds to about 2 ps for a light molecule like LiCl and 20 ps for a heavy one like NaI).

We next notice a series of local maxima in Fig. 3 (for instance, just after the first kick), which could be used for the control strategy. This point is illustrated in Fig. 5 for strategy $S1$. It turns out that excellent results are obtained for the alignment process using in the control scheme the local maxima (the next one after the application of the pulse). More unexpectedly, this leads to a better result than the use of the global maxima, as optimal alignment is almost achieved after only four kicks (while six are used in Fig. 3). In this example, it is clear that the best choice for the convergence of the process is to kick at a local maximum. However, we did not manage to establish general rules for this degree of freedom and it thus seems that numerical tests have to be undertaken for each practical case.

The outcome of the calculation when applying strategy $S2$ to the orientation, taken as an example, is displayed in Fig. 6. The results obtained are very similar to those using strategy $S1$, with a smaller number of pulses (viz., nine) but leading to slightly less efficient orientation. This suggests a great similarity between the two strategies from a numerical point of view, as can be seen when comparing Figs. 4 and 6.

C. Robustness

The robustness of the overall strategy has in principle to be checked against two variables: the time delays between successive pulses and the total energy delivered by individual pulses. Figure 7 illustrates the robustness against the most sensitive parameter, i.e., the time delays s_i, where $\langle\mathcal{O}_o^{(N)}(s_i)\rangle$ is maximum. This is given for the orientation process only, by considering again the two strategies $S1$ and $S2$. Strategy $S2$ seems here more robust, but this is only due to the smaller number of pulses which are necessary for reaching the target state (nine for $S2$, instead of 15 for $S1$).

As for experimental feasibility, the accuracy of the light paths followed by successive pulses is of the order of

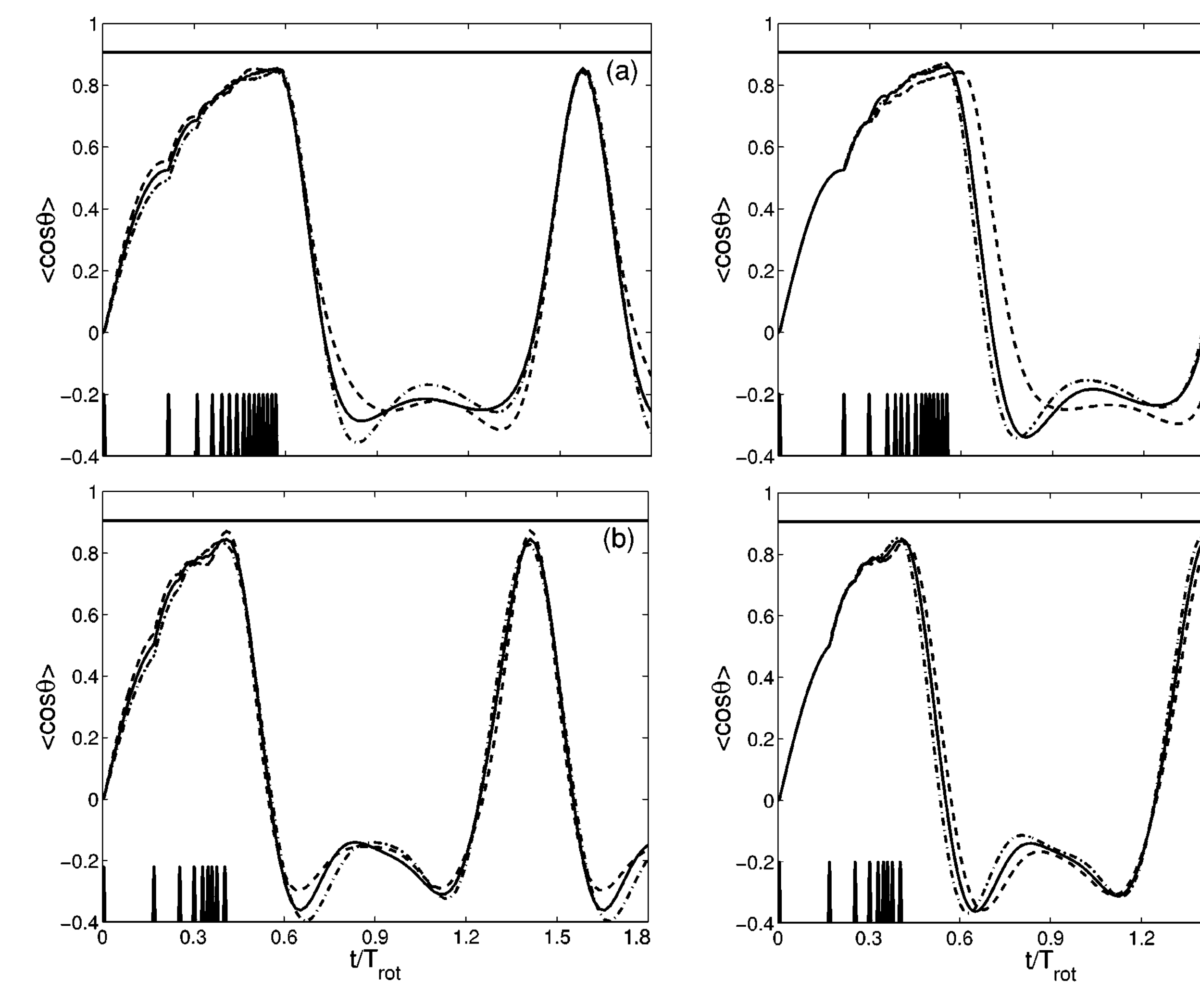


FIG. 7. Robustness of the orientation dynamics when shifting the time delays between pulses systematically by ±0.1% of the rotational period (the dashed line corresponds to overestimates by +0.1% whereas the dot-dashed one to underestimates by −0.1%, the solid line corresponding to the calculation of Fig. 4). The strategy *S*1 is displayed on (a) and *S*2 on (b).

FIG. 8. Robustness of the orientation dynamics varying the pulse energy by 10%. The full line corresponds to $A=1$, i.e., the calculation of Fig. 4, the dotted and dot-dashed lines are for $A=1.1$ and 0.9, respectively. The strategy *S*1 is displayed on (a) and *S*2 on (b).

0.2 μm, corresponding to 0.6 fs. This is, for instance for a light diatomic molecule like LiCl, less than 1/10 of the inaccuracies considered when varying the time delays, in Fig. 7. In other words, both strategies are very robust with respect to such inaccuracies affecting the molecule-pulse interaction terms. On the contrary, the measure of the total energy per pulse is affected by a more severe inaccuracy. This is checked in Fig. 8, by varying *A* by 10%, for both strategies *S*1 and *S*2. Remarkable robustness is achieved, advocating for an experimental feasibility of the control scheme: a few short pulses (say five to six), with a moderate total energy determined within 10% of accuracy, applied with time delays of the order of 1 ps with an accuracy of 1 fs, leads to an excellent control of the orientation for any molecular system.

V. CONCLUSIONS

In this work, we have developed a laser control strategy for a molecular system initially in a pure quantum state, aiming at the maximalization (or minimalization) of an observable $\mathcal{O}$ given by an operator, not commuting with the molecular field-free Hamiltonian. The strategy consists of four steps: reduction of the dimensionality of the original physical Hilbert space; definition of a target state as an eigenvector of the reduced observable in the finite subspace; analysis of the controllability of the system; application of a train of sudden perturbations *U*, commuting with $\mathcal{O}$, at times where the expectation value of $\mathcal{O}$ reaches a maximum during its field-free evolution. A process similar in its spirit consists in applying the pulses at times when the projection of the time-evolved wave function on the target states reaches maximum values. This latter strategy yields comparable numerical results even if, from a theoretical point of view, its set of fixed points (which corresponds only to the target state) can be smaller than (or equal to) the one of the first process. Moreover, it is worth noting that such general strategies are not only independent of the particular molecule, but are also transferable to different control issues and different observables. Finally, we have checked the robustness with respect to inaccuracies

in the time delays between pulses or the total pulse energies, and found it to be remarkably good, as long as moderate intensity and short radiative interactions are considered.

Control strategies based on pure states are however subject to important modifications when dealing with temperature effects. Orientation, for instance, drastically decreases for increasing temperatures [32,35–37]. This is basically due to the fact that, at nonzero temperature, the initial state is in general not a pure state, but a mixed one, i.e., a superposition of a statistical ensemble of rotational states with $m \neq 0$, which tend to misalign the molecule. The dynamics of such mixed states is described by a density operator $\rho(t)$ (instead of a wave function) evolving according to the von Neuman equation (instead of the Schrödinger equation). Following the dimensionality reduction of the Hilbert space, the control strategy looks now for the optimal density operator $\rho^{(N)}$, which maximizes the observable $\mathcal{O}^{(N)}$ in the same subspace. This amounts to maximizing $\mathrm{Tr}[\rho^{(N)}\mathcal{O}^{(N)}]$, with the commutation relation $[\rho^{(N)},\mathcal{O}^{(N)}]=0$. It has been shown [9,10] that such a goal can be achieved by a unitary operator U that appropriately orders the common eigenvectors of $\rho^{(N)}$ and $\mathcal{O}^{(N)}$, such that the one corresponding to the highest eigenvalue of $\rho^{(N)}$ is associated with the one corresponding to the highest eigenvalue of $\mathcal{O}^{(N)}$, and so forth. An even more sophisticated generalization of the control strategy is to be looked for when the particular system under consideration evolves while interacting with a physical environment describing collisional processes in a gas, or friction in a liquid [38,39]. The strategies that have to be worked out would involve nonunitary perturbations U, and special attention has to be paid to decoherence [40,41]. Work in these directions is in progress.

ACKNOWLEDGMENT

Support from the Conseil Régional de Bourgogne is gratefully acknowledged.

APPENDIX A: ANALYSIS OF THE SET OF FIXED POINTS: THE GENERAL CASE

The goal of this appendix is to determine the set of fixed points of the control strategy $S1$. Indeed, as mentioned in Sec. II, a crucial question for the convergence of the control scheme is the set $\mathcal{F}$ of its fixed points. In general, we are not able to exactly determine $\mathcal{F}$, but only a larger set $\mathcal{S}$. The latter contains the wave functions $|\psi_s\rangle$, which satisfy the requirements

$$\langle\psi_s|[H_0,\mathcal{O}^{(N)}]|\psi_s\rangle = 0 \tag{A1}$$

and

$$\langle\psi_s|U_{\tilde{A}}^{-1}[H_0,\mathcal{O}^{(N)}]U_{\tilde{A}}|\psi_s\rangle = 0, \tag{A2}$$

for all values of the real parameter $\tilde{A}$. As mentioned above, we can show that $\mathcal{F}$ is a subset of $\mathcal{S}$. For the purpose of proving this result, we observe that just before the pulse at t_i-0 one has

$$\frac{d}{dt}\langle\mathcal{O}^{(N)}\rangle\bigg|_{t_i-0} = i\langle[H_0,\mathcal{O}^{(N)}]\rangle|_{t_i-0} = 0, \tag{A3}$$

whereas just after the pulse at t_i+0

$$\frac{d}{dt}\langle\mathcal{O}^{(N)}\rangle\bigg|_{t_i+0} = i\langle U_{\tilde{A}}^{-1}[H_0,\mathcal{O}^{(N)}]U_{\tilde{A}}\rangle|_{t_i+0} \tag{A4}$$

$$= i\langle[U_{\tilde{A}}^{-1}H_0U_{\tilde{A}},\mathcal{O}^{(N)}]\rangle_{t_i+0}. \tag{A5}$$

We can conclude by arguing that if there exists a value of the parameter $\tilde{A}$ such that the slope undergoes a change from zero [Eq. (A3)] to a nonzero finite value [Eq. (A4)], then $\langle\mathcal{O}^{(N)}(t)\rangle$ will reach within the period T a maximum strictly larger than the one obtained prior the application of the pulse.

We are now in a position to state the following theorem: $\mathcal{S}=\{|\chi^{(n)}\rangle\}$ (the $|\chi^{(n)}\rangle$'s being the eigenstates of $\mathcal{O}^{(N)}$) if and only if the dimension of the vector space $\mathcal{V}$ generated by $[H_0,\mathcal{O}^{(N)}]$ and the elements of the form $U_{\tilde{A}}^{-1}[H_0,\mathcal{O}^{(N)}]U_{\tilde{A}}$, where $\tilde{A}\in\mathbb{R}$, is equal to $N(N-1)$. The proof goes as follows.

We first recall that the complete controllability of the system is assumed. This condition is equivalent to requiring that the Lie algebra $\mathcal{L}$ generated by iH_0 and iH_I is $\mathrm{u}(N)$ or that the dimension of this vector space is N^2. Moreover, $U_{\tilde{A}}^{-1}[H_0,\mathcal{O}^{(N)}]U_{\tilde{A}}$ being a skew-Hermitian operator, it can be shown that $\mathcal{V}$ is a subspace of $\mathcal{L}$. The starting point for the following computations will be the standard basis of $\mathrm{u}(N)$ [12],

$$x_{mn} = e_{mn} - e_{nm},$$

$$y_{mn} = i(e_{mn} + e_{nm}),$$

$$d_{nn} = ie_{nn}, \tag{A6}$$

where $e_{mn}=|\chi^{(m)}\rangle\langle\chi^{(n)}|$, $1\leq n\leq N-1$, and $n<m\leq N$. We denote D the dimension of $\mathcal{V}$. This vector space is generated by the set v_k $(k=1,\ldots,D)$, which can be written as a linear combination of elements of the basis given by Eq. (A6). Expanding $[H_0,\mathcal{O}^{(N)}]$ and $U_{\tilde{A}}^{-1}[H_0,\mathcal{O}^{(N)}]U_{\tilde{A}}$ with respect to the previous set v_k and taking the mean value of these operators over a wave function $|\psi_s\rangle\in\mathcal{S}$, we obtain a system of linear equations. Inverting the system, one gets D equations of the form

$$\langle\psi_s|v_k|\psi_s\rangle = 0. \tag{A7}$$

As $|\chi^{(n)}\rangle\in\mathcal{S}$ and $\langle\chi^{(n)}|d_{nn}|\chi^{(n)}\rangle=1$ for any $n=1,\ldots,N$, it is clear that $\mathcal{V}$ does not contain any linear combination of the d_{nn}'s, which shows that the dimension of $\mathcal{V}$ is at most $N(N-1)$. Hence, if we assume that, for instance, $x_{mn}\in\mathcal{V}$ and $y_{mn}\in\mathcal{V}$, we obtain by introducing the wave function $|\psi\rangle=\sum_{n=1}^{N}c_n|\chi^{(n)}\rangle$ into Eq. (A7)

$$c_m^* c_n - c_n^* c_m = 0,$$

$$c_m^* c_n + c_n^* c_m = 0. \quad (A8)$$

From Eqs. (A8), one deduces that $c_m=0$ or $c_n=0$. By repeating this procedure for each couple (m,n), it can be shown that the states $|\chi^{(n)}\rangle$, for which for some n_0

$$c_{n_0} = 1,$$

$$c_{m;m\neq n_0} = 0, \quad (A9)$$

are the unique elements of $\mathcal{S}$ if and only if the dimension of $\mathcal{V}$ is $N(N-1)$. Numerical calculations of this dimension and complementary results are presented in Appendix B. Finally, a conclusion regarding this theorem is that if the dimension of $\mathcal{V}$ is $N(N-1)$, then the set $\mathcal{F}$ of fixed points of the control strategy is a subset of $\{|\chi^{(n)}\rangle\}$, the set of eigenvectors of the impulsive propagator $U_{\tilde{A}}$, which are also the ones of $\mathcal{O}^{(N)}$ as the two operators commute.

APPENDIX B: ANALYSIS OF THE SET OF FIXED POINTS IN THE SUDDEN APPROXIMATION

This appendix particularizes the general arguments of Appendix A to the sudden approximation. We first consider the strategy $S1$. In this case, we have to determine the dimension of the vector space $\mathcal{V}$ defined in Appendix A. In the sudden approximation, we recall that the evolution operator $U_{\tilde{A}}$ can be written as [Eq. (10)]

$$U_{\tilde{A}} = e^{i\tilde{A}H_I}, \quad (B1)$$

and $\mathcal{V}$ is then generated by the elements of the form $e^{-i\tilde{A}H_I}[H_0,\mathcal{O}^{(N)}]e^{i\tilde{A}H_I}$, where $\tilde{A}\in\mathbb{R}$. For the sake of clarity, we now consider that $H_I=\mathcal{O}^{(N)}$ (this assumption is satisfied for the alignment and orientation processes). Using the Campbell-Hausdorf formula [42], simple algebra shows that $\mathcal{V}$ is also spanned by the operators $ad^n(H_0,\mathcal{O}^{(N)})$ $(n\geq 1)$. The notation $ad^n(B,C)$ for the operators B and C is defined by the recurrence formula

$$ad^n(B,C) = \begin{cases} B, & n=0, \\ [ad^{n-1}(B,C),C], & n\geq 1. \end{cases} \quad (B2)$$

From a practical point of view, owing to the complexity of analytical calculations, a numerical algorithm, which closely follows the one for complete controllability [43], can be used to determine the dimension of $\mathcal{V}$. The first step consists in rewriting the matrix of each operator $ad^n(H_0,\mathcal{O}^{(N)})$ $(n\geq 1)$ as an N^2 column vector obtained by concatenating its columns. We next construct a new matrix R with these vectors, each vector corresponding to a column of R. Finally, the dimension of $\mathcal{V}$ is given by the rank of R.

We apply this method to the orientation process in a finite-dimensional space. The results of these computations are presented in Table I, where the notation $\dim(\mathcal{V})$ corresponds to the dimension of the vector space $\mathcal{V}$. For the orientation, as $\dim(\mathcal{V})<N(N-1)$, one deduces that $\mathcal{S}\neq\{|\chi^{(n)}\rangle\}$.

TABLE I. Dimensions of the vector spaces $\mathcal{L}$ and $\mathcal{V}$ as a function of N for the orientation dynamics. The third column indicates the maximum of the dimension of $\mathcal{V}$.

N	$\dim(\mathcal{L})$	Max. of $\dim(\mathcal{V})$	$\dim(\mathcal{V})$
3	9	6	4
4	16	12	8
5	25	20	12

This point can also be understood through the following calculation.

We introduce the operator $C=[H_0,\mathcal{O}^{(N)}]$ and we denote by C_{mn} its matrix elements in the basis $\{|\chi^{(n)}\rangle\}$,

$$C_{nm} = \langle\chi^{(n)}|C|\chi^{(m)}\rangle. \quad (B3)$$

For operators $H_0=J^2$ and $\mathcal{O}^{(N)}=\cos^{(N)}\theta$, it can furthermore be checked that $C_{mn}=0$ if $m=n$ and $C_{mn}\neq 0$ otherwise. Assuming that the slope is zero before and after the pulse, we can easily show that

$$\sum_{m,n=1}^{N} c_m^* c_n C_{mn} = 0,$$

$$\sum_{m,n=1}^{N} e^{i\tilde{A}(\chi_m-\chi_n)} c_m^* c_n C_{mn} = 0, \quad (B4)$$

where the c_n's are the weighting coefficients of the wave function just before the pulse in the basis of the eigenstates of $\mathcal{O}^{(N)}$, and the χ_n's the eigenvalues of $\mathcal{O}^{(N)}$. From Eqs. (B4), one then deduces that

$$\sum_{m\neq n} e^{i\tilde{A}(\chi_m-\chi_n)} c_m^* c_n C_{mn} = \sum_{m\neq n} c_m^* c_n C_{mn}. \quad (B5)$$

To conclude, we will use the following notion. A group of energy levels of $\mathcal{O}^{(N)}$ is said to be equally spaced if there exists a set of integers $\{p,q,r,s\}\in\{1,2,\ldots,N\}^4$ such that

$$\chi_p - \chi_q = \chi_r - \chi_s. \quad (B6)$$

We next suppose that the spectrum of $\mathcal{O}^{(N)}$ is not equally spaced (according to the previous definition) and that the coefficients $C_{mn;m\neq 0}\neq 0$. Using the fact that the left-hand side of Eq. (B5) is a regular function of the parameter $\tilde{A}$ that is constant if and only if all its coefficients $c_m^* c_n C_{mn}$ are zero, we see that the unique solutions of Eq. (B5) are the eigenvectors $|\chi^{(n)}\rangle$ of $\mathcal{O}^{(N)}$ for which

$$c_n = 1,$$

$$c_{m;m\neq n} = 0. \quad (B7)$$

It is interesting to note that the two previous hypotheses also give practical conditions on $\mathcal{O}^{(N)}$ and H_0 in order to determine the set $\mathcal{S}$. Indeed, for the orientation process, we notice that the spectrum of $\cos^{(N)}\theta$ being equally spaced (the spectrum is symmetric), the dimension of $\mathcal{V}$ is not equal to the maximum dimension $N(N-1)$.

Let us now determine the set $\mathcal{F}$ of fixed points for the strategy $S2$ in the sudden approximation. In this case, we first clarify the definition of $\mathcal{S}$. It can be shown that $\mathcal{S}$ contains the wave functions $|\psi\rangle$ which satisfy

$$\mathrm{Im}[\langle\chi^{(N)}|e^{i\tilde{A}\mathcal{O}^{(N)}}|\psi\rangle\langle\psi|e^{-i\tilde{A}\mathcal{O}^{(N)}}H_0|\chi^{(N)}\rangle]=0 \tag{B8}$$

for any value of $\tilde{A}$, with Im corresponding to the imaginary part. Equation (B8) can be rewritten as

$$\sum_{m=1}^{N}\mathrm{Im}[c_N c_m^* h_{mN} e^{-iA(\chi_m-\chi_N)}]=0, \tag{B9}$$

the h_{mn}'s being the matrix coefficients of H_0 in the basis $\{|\chi^{(n)}\rangle\}$. If the spectrum of $\mathcal{O}^{(N)}$ is completely nondegenerate, one deduces from Eq. (B9) that

$$\mathrm{Im}[c_N c_m^* h_{mN} e^{-iA(\chi_m-\chi_N)}]=0 \tag{B10}$$

for any value of m ($m\neq N$). Simple algebra shows that

$$c_N c_m^* h_{mN}=0. \tag{B11}$$

If we now assume that $h_{mN}\neq 0$, one obtains that $c_N=0$ or $c_m=0$. The case $c_N=0$ corresponds to the minimum of the projection $|\langle\psi|\chi^{(N)}\rangle|^2$, which is not relevant here. Finally, in the other case, we can conclude that the unique element of $\mathcal{S}$ is $|\chi^{(N)}\rangle$. We also remark that these two conditions are satisfied for the orientation process. In this example, we have therefore shown that the limit of the sequence is $|\chi^{(N)}\rangle$.

APPENDIX C: THE MOLECULAR ALIGNMENT AND ORIENTATION CONTROL STRATEGY: THE INFINITE- AND THE FINITE-DIMENSIONAL CASES

In this appendix, we shall focus on the convergence of the sequence in an infinite- and a finite-dimensional Hilbert space, as only the finite case has been treated in Appendixes A and B. We first consider the infinite-dimensional case. We will explicitly derive Eqs. (35) and (36). For doing so, we recall the following fundamental commutation relations [44], which will be used below:

$$[J^2,\cos\theta]=2(\sigma_\theta+\cos\theta),$$

$$[\sigma_\theta,\cos\theta]=\cos^2\theta-\mathbf{1},$$

$$[J^2,\cos^2\theta]=4\cos\theta\sigma+6\cos^2\theta-2,$$

$$[\sigma,\cos^2\theta]=2\cos^3\theta-2\cos\theta,$$

$$[\cos\theta\sigma_\theta,\cos^2\theta]=2\cos^4\theta-2\cos^2\theta, \tag{C1}$$

where $\sigma_\theta=\sin\theta(\partial/\partial\theta)$. We notice that such identities are not satisfied in a finite-dimensional subspace. We consider the strategy $S1$ for the alignment and the orientation processes. We assume that the average $\langle\cos^m\theta\rangle$ reaches a maximum at a time s_i,

$$\left.\frac{d}{ds}\langle\cos^m\theta\rangle\right|_{s_i-0}=i\langle[\varepsilon J^2,\cos^m\theta]\rangle=0, \tag{C2}$$

where $m=1$ for the orientation and $m=2$ for the alignment. A sudden pulse being applied at the time s_i, we have to calculate the slope

$$\left.\frac{d}{ds}\langle\cos^m\theta\rangle\right|_{s_i+0}=i\langle e^{-iA\cos^m\theta}\varepsilon[J^2,\cos^m\theta]e^{iA\cos^m\theta}\rangle. \tag{C3}$$

Using Eqs. (C1) and (C3), one readily obtains for the orientation

$$\left.\frac{d}{ds}\langle\cos\theta\rangle\right|_{s_i+0}=i\langle\varepsilon[J^2,\cos\theta]\rangle+2\varepsilon A(\mathbf{1}-\langle\cos^2\theta\rangle). \tag{C4}$$

For the alignment process, we have

$$\left.\frac{d}{ds}\langle\cos^2\theta\rangle\right|_{s_i+0}=i\langle\varepsilon[J^2,\cos^2\theta]\rangle-4A\varepsilon\langle[\cos\theta\sigma_\theta,\cos^2\theta]\rangle, \tag{C5}$$

which can be rewritten as

$$\left.\frac{d}{ds}\langle\cos^2\theta\rangle\right|_{s_i+0}=i\langle\varepsilon[J^2,\cos^2\theta]\rangle+2A\varepsilon\langle\sin^2 2\theta\rangle. \tag{C6}$$

From Eq. (C2) and from the fact that $\langle\cos^2\theta\rangle<1$ and $\langle\sin^2 2\theta\rangle>0$, one deduces that, in both cases, the slope undergoes a change from zero to a finite nonzero value when a pulse is applied, for any amplitude A and any maximum of the average of $\cos^m\theta$. Note that the sign of the slope and the position of the next local maximum depend on the sign of A.

We address now the case of finite dimensionality. In such a space, the commutation relations of Eq. (C1) cannot be used and we have to introduce the following standard basis of su(N) [12] (related here to the eigenstates of H_0),

$$x_{mn}=e_{mn}-e_{nm},$$

$$y_{mn}=i(e_{mn}+e_{nm}),$$

$$h_n=i(e_{nn}-e_{n+1,n+1}), \tag{C7}$$

where $e_{mn}=|m\rangle\langle n|$, $1\leqslant n\leqslant N-1$, and $n<m\leqslant N$. $|n\rangle$ is the eigenvector of H_0 with eigenvalue E_n [Eq. (2)]. H_0 and the interaction term H_I can be rewritten with respect to this basis as

$$H_0=\sum_{n=1}^{N}E_n e_{nn},$$

$$H_I=\sum_{n=1}^{N-1}d_n(e_{n,n+1}+e_{n+1,n}), \tag{C8}$$

where

$$E_{n+1} = n(n+1) \quad \text{(C9)}$$

and

$$d_{n+1} = \frac{n+1}{\sqrt{(2n+1)(2n+3)}}. \quad \text{(C10)}$$

Assuming that $\langle [H_0, H_I] \rangle = 0$, we now calculate

$$\frac{d}{dt}\langle H_I \rangle = \langle e^{-iAH_I}[H_0, H_I] e^{iAH_I} \rangle, \quad \text{(C11)}$$

i.e., the derivative of the function $\langle H_I \rangle (t)$ after a sudden pulse.

A straightforward calculation leads to the identities

$$[H_0, H_I] = -\sum_{n=1}^{N-1} \mu_n d_n x_{n,n+1}, \quad \text{(C12)}$$

where $\mu_n = E_{n+1} - E_n$, and

$$\frac{1}{2}[[H_0, H_I], H_I] = H_I^2 + \sum_{n=1}^{N-1} (2n+1) d_n^2 e_{n+1,n+1} - \sum_{n=1}^{N} (2n+3) d_n^2 e_{nn}. \quad \text{(C13)}$$

From Eq. (C10), one can rewrite Eq. (C13) as

$$\frac{1}{2}[[H_0, H_I], H_I] = H_I^2 - 1 + \frac{N^2 + 2N + 1}{2N+1} e_{NN}. \quad \text{(C14)}$$

After expansion according to Campbell-Hausdorf's formula, one gets for the derivative of Eq. (C11)

$$\frac{d}{dt}\langle H_I \rangle = 2A\left(1 - \langle V^2 \rangle - \frac{N^2 + 2N + 1}{2N+1}|a_N|^2\right) - i\frac{(N^2 + 2N + 1)N}{(2N+1)^{3/2}\sqrt{2N-1}} A^2 (a_N^* a_{N-1} - a_{N-1}^* a_N) + O(A^3), \quad \text{(C15)}$$

where the a_n's are the coefficients of the wave function in the basis of $|n\rangle$'s. We notice that Eq. (C15) is very similar to Eq. (C4) except for a few terms. If A is small enough, the evolution of the average $\langle H_I \rangle$ will depend on the boundary population $|a_N|^2$.

APPENDIX D: ANALYTICAL ESTIMATIONS OF DYNAMICAL PARAMETERS

In Sec. IV, the dynamics were investigated through numerical tests. In this appendix, we give a few analytical estimations of dynamical parameters such as the time between pulses. Nevertheless, it is noted that, owing to the complexity of complete analytical calculations, only rough estimations can be obtained.

We consider the orientation dynamics and the strategy $S1$. The time Δt between two pulses is assumed to be small enough, which means that only the last kicks of the sequence will be correctly described (this point is clearly illustrated in Fig. 4). We now analyze the evolution of $\langle \cos \theta \rangle (s)$ between the times s_i (taken as 0 for simplicity) and s_f, a sudden pulse being applied at s_i. We have

$$\langle \cos \theta \rangle (s) = \langle e^{-iA \cos \theta} e^{i\varepsilon J^2 s} \cos \theta e^{-i\varepsilon J^2 s} e^{iA \cos \theta} \rangle, \quad \text{(D1)}$$

where $s = t/\tau$ is the rescaled time. Expanding the two time exponentials and neglecting terms of order greater than 2 in s, $\langle \cos \theta \rangle$ can be rewritten in the form

$$\langle \cos \theta \rangle (s) = \langle \cos \theta \rangle (0) + i\varepsilon s \langle e^{-iA \cos \theta}[J^2, \cos \theta] e^{iA \cos \theta} \rangle - \frac{1}{2}\varepsilon^2 s^2 \langle e^{-iA \cos \theta}[J^2, [J^2, \cos \theta]] e^{iA \cos \theta} \rangle. \quad \text{(D2)}$$

As $\langle [J^2, \cos \theta] \rangle (0) = 0$, the proof of Appendix B shows that

$$i\varepsilon s \langle e^{-iA \cos \theta}[J^2, \cos \theta] e^{iA \cos \theta} \rangle = 2\varepsilon As(1 - \langle \cos^2 \theta \rangle). \quad \text{(D3)}$$

We next simplify the third term of Eq. (D2). Using the commutation relations [44]

$$[J^2, \sigma_\theta] = 2 \cos \theta J^2,$$

$$[J^2, \cos \theta] = \sigma_\theta + \cos \theta, \quad \text{(D4)}$$

where $\sigma_\theta = \sin \theta \partial / \partial \theta$, one arrives at

$$\langle e^{-iA \cos \theta}[J^2, [J^2, \cos \theta]] e^{iA \cos \theta} \rangle = 4\langle \cos \theta J^2 \rangle + 8iA \langle \sigma_\theta \cos \theta \rangle + 4A^3 \langle \cos \theta - \cos^3 \theta \rangle + 4iA(1 + \langle \cos^2 \theta \rangle). \quad \text{(D5)}$$

Introducing the operators

$$\mathrm{Re}[\langle \sigma_\theta \cos \theta \rangle] = -\frac{1}{2}(1 + \langle \cos^2 \theta \rangle),$$

$$\mathrm{Im}[\langle \sigma_\theta \cos \theta \rangle] = \frac{1}{2i}\langle \sigma_\theta \cos \theta + \cos \theta \sigma_\theta + 2 \cos^2 \theta \rangle, \quad \text{(D6)}$$

where Re and Im correspond to the real and the imaginary parts of a complex number, respectively, Eq. (D2) becomes

$$\langle \cos \theta \rangle (s) = \langle \cos \theta \rangle (0) + 2\varepsilon As(1 - \langle \cos^2 \theta \rangle) - \frac{1}{2}\varepsilon^2 s^2 \times [4\langle \cos \theta J^2 \rangle - 8A\, \mathrm{Im}(\langle \sigma_\theta \cos \theta \rangle) + 4A^2 \langle \cos \theta - \cos^3 \theta \rangle]. \quad \text{(D7)}$$

Equation (D7) allows us to explicitly determine the time s_f:

$$\Delta s = s_f - s_i = \frac{2A(1 - \langle \cos^2 \theta \rangle)}{\varepsilon[4\langle \cos \theta J^2 \rangle - 8A\, \mathrm{Im}(\langle \sigma_\theta \cos \theta \rangle) + 4A^2 \langle \cos \theta - \cos^3 \theta \rangle]}. \quad \text{(D8)}$$

Up to this point, the calculation involves no approximation on the area of the field A, as only the time delays between the pulses are assumed to be small. In order to highlight different

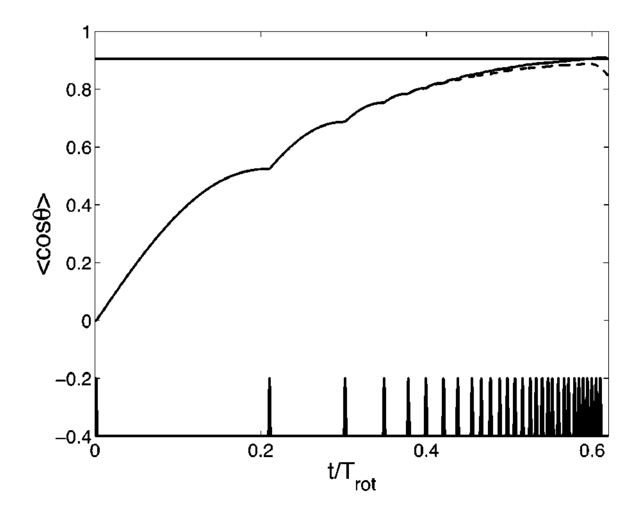


FIG. 9. Orientation dynamics during a train of 30 HCPs. ε is taken to be 0.01.

dynamical behaviors, we now consider the two limits $A \gg 1$ and $A \ll 1$. It can be shown that

$$\Delta s = \frac{1 - \langle \cos^2 \theta \rangle}{2\varepsilon A(\langle \cos \theta - \cos^3 \theta \rangle)} = \frac{k_>}{A} \quad \text{(D9)}$$

if $A \gg 1$ and

$$\Delta s = \frac{A(1 - \langle \cos^2 \theta \rangle)}{2\varepsilon \langle \cos \theta J^2 \rangle} = k_< A \quad \text{(D10)}$$

if $A \ll 1$. $k_>$ and $k_<$ are two constants that do not depend on A. They can be estimated by assuming that the wave function is close enough to the optimal state $|\chi^{(N)}\rangle$. The first limit corresponds to the strategy suggested in Ref. [23], where the area A increases with the number of kicks. From Eq. (D9), we note that the expression of the focusing time [23,45,46] is derived via a quantum calculation, this time being obtained in Ref. [46] through classical or semiclassical analyses.

Due to the moderate intensity of the pulses used in our strategy (for instance, $A=1$ in Fig. 4), it can be approximately described by Eq. (D10). We recall that the choice of the strength of the kicks is crucial for remaining in the finite-dimensional subspace $\mathcal{H}_{m=0}^{(N)}$. This point is clearly illustrated in Fig. 9, which gives a view of the orientation dynamics under the effect of a train of 30 HCPs of area $A=1$. For the last ten pulses, the arithmetic average of the time delays between successive kicks is of the order of $\Delta t/T_{rot} \simeq 5.6 \times 10^{-3}$. This result can also be derived from the analytical formula of Eq. (D10). Using the eigenstate $|\chi^{(5)}\rangle$, we obtain $k_< \simeq 5 \times 10^{-3}$ and

$$\frac{\Delta t}{T_{rot}} = \frac{\varepsilon}{\pi} \Delta s = k_< A = 5 \times 10^{-3}, \quad \text{(D11)}$$

as $A=1$. Finally, it is noted that we can also estimate the difference $\Delta\langle \cos \theta \rangle = \langle \cos \theta \rangle(s_f) - \langle \cos \theta \rangle(s_i)$ between two successive maxima. Straightforward calculation leads to

$$\Delta \langle \cos \theta \rangle = \frac{(1 - \langle \cos^2 \theta \rangle)^2 A^2}{2\langle \cos \theta J^2 \rangle}, \quad \text{(D12)}$$

in the hypothesis that $A \ll 1$.

[1] W. Warrer, H. Rabitz, and M. Dahleh, Science **259**, 1581 (1993).
[2] H. Stapelfeldt and T. Seideman, Rev. Mod. Phys. **75**, 543 (2003).
[3] O. Atabek, C. M. Dion, and A. B. H. Yedder, J. Phys. B **36**, 4667 (2003).
[4] M. A. Nielsen and I. L. Chuang, *Quantum Computation and Quantum Information* (Cambridge University Press, Cambridge, U.K., 2000).
[5] J. I. Cirac and P. Zoller, Phys. Rev. Lett. **74**, 4091 (1995).
[6] K. M. F. Romera, G. U. Laverde, and F. T. Ardila, J. Phys. A **36**, 841 (2003).
[7] C. M. Dion, A. B. H. Yedder, E. Cancès, A. Keller, C. L. Bris, and O. Atabek, Phys. Rev. A **65**, 063408 (2002).
[8] H. Rabitz, R. de Vivie-Riedle, M. Motzkus, and K. Kompa, Science **288**, 824 (2000).
[9] M. D. Girardeau, M. Ina, S. Schirmer, and T. Gulsrud, Phys. Rev. A **55**, R1565 (1997).
[10] M. D. Girardeau, S. G. Schirmer, J. V. Leahy, and R. M. Koch, Phys. Rev. A **58**, 2684 (1998).
[11] V. Ramakrishna, M. V. Salapaka, M. Dahleb, H. Rabitz, and A. Peirce, Phys. Rev. A **51**, 960 (1995).
[12] H. Fu, S. G. Schirmer, and A. I. Solomon, J. Phys. A **34**, 1679 (2001).
[13] D. Sugny, A. Keller, O. Atabek, D. Daems, C. M. Dion, S. Guérin, and H. R. Jauslin, Phys. Rev. A **69**, 033402 (2004).
[14] N. V. Vitanov, T. Halfmann, B. W. Shore, and K. Bergmann, Annu. Rev. Phys. Chem. **52**, 763 (2001).
[15] S. Guérin and H. R. Jauslin, Adv. Chem. Phys. **125**, 147 (2003).
[16] S. G. Schirmer, A. D. Greentree, V. Ramakrishna, and H. Rabitz, J. Phys. A **35**, 8315 (2002).
[17] W. Zhu and H. Rabitz, J. Chem. Phys. **110**, 7142 (1999).
[18] P. R. Brooks, Science **193**, 11 (1976).
[19] T. Seideman, Phys. Rev. A **56**, R17(1997).
[20] T. Seideman, J. Chem. Phys. **111**, 4397 (1999).
[21] F. J. Aoiz, Chem. Phys. Lett. **289**, 132 (1998).
[22] S. Lloyd and S. L. Braunstein, Phys. Rev. Lett. **82**, 1784 (1999).
[23] I. S. Averbukh and R. Arvieu, Phys. Rev. Lett. **87**, 163601 (2001).
[24] M. J. J. Vrakking and S. Solte, Chem. Phys. Lett. **271**, 209 (1997).
[25] S. Guérin, L. P. Yatsenko, H. R. Jauslin, O. Faucher, and B. Lavorel, Phys. Rev. Lett. **88**, 233601 (2002).
[26] B. Friedrich and D. Herschbach, Phys. Rev. Lett. **74**, 4623

(1995).
[27] N. Sangouard, S. Guérin, M. Amniat-Talab, and H. R. Jauslin, Phys. Rev. Lett. **93**, 223602 (2004).
[28] C. M. Dion, A. Keller, and O. Atabek, Eur. Phys. J. D **14**, 249 (2001).
[29] N. E. Henriksen, Chem. Phys. Lett. **312**, 196 (1999).
[30] A. Keller, C. M. Dion, and O. Atabek, Phys. Rev. A **61**, 023409 (2000).
[31] C. M. Dion, A. D. Bandrauk, O. Atabek, A. Keller, H. Umeda, and Y. Fujimura, Chem. Phys. Lett. **302**, 215 (1999).
[32] M. Machholm and N. E. Henriksen, Phys. Rev. Lett. **87**, 193001 (2001).
[33] D. Sugny, A. Keller, O. Atabek, D. Daems, S. Guérin, and H. R. Jauslin, Phys. Rev. A **69**, 043407 (2004).
[34] D. Daems, A. Keller, S. Guérin, H. R. Jauslin, and O. Atabek, Phys. Rev. A **67**, 052505 (2003).
[35] M. Machholm, J. Chem. Phys. **115**, 10724 (2001).
[36] J. Ortigoso, M. Rodriguez, M. Gupta, and B. Friedrich, J. Chem. Phys. **110**, 3870 (1999).
[37] A. B. H. Yedder, A. Auger, C. M. Dion, E. Cancès, A. Keller, C. Le Bris, and O. Atabek, Phys. Rev. A **66**, 063401 (2002).
[38] S. E. Sklarz, D. J. Tannor, and N. Khaneja, Phys. Rev. A **69**, 053408 (2004).
[39] D. J. Tannor and A. Bartana, J. Phys. Chem. A **103**, 10359 (1999).
[40] A. Beige, D. Braun, B. Tregenna, and P. L. Knight, Phys. Rev. Lett. **85**, 1762 (2000).
[41] D. A. Lidar, D. Bacon, J. Kempe, and K. B. Whaley, Phys. Rev. A **63**, 022307 (2001).
[42] E. Merzbacher, *Quantum Mechanics* (Wiley, New York, 1970).
[43] S. G. Schirmer, H. Fu, and A. I. Solomon, Phys. Rev. A **63**, 063410 (2001).
[44] M. Joyeux and D. Sugny, Can. J. Phys. **80**, 1459 (2002).
[45] M. Leibscher, I. S. Averbukh, and H. Rabitz, Phys. Rev. Lett. **90**, 213001 (2003).
[46] M. Leibscher, I. S. Averbukh, P. Rozmej, and R. Arvieu, Phys. Rev. A **69**, 032102 (2004).

5.2 Control of chemical systems by laser fields

Corresponding articles : [7, 18, 20, 22]
This work has been done in collaboration with the group of theoretical chemists of M. Desouter-Lecomte of the *Laboratoire de Chimie-Physique* in Orsay.

The control of the dynamics of chemical processes is a challenging question both from the experimental and theoretical points of view [41, 84, 126]. In control experiments, adaptative laser pulse shaping techniques are currently used and coupled in general with genetic algorithms [74]. Adaptative techniques mean that the outcome of the experiment is analyzed by a computer and modified to optimize the yield of the control. In this context, powerful theoretical methods have been also developed such as the direct optimization of a few pulse parameters [101, 110], the Brumer-Shapiro coherent control [108], adiabatic passage techniques (APT) like the STIRAP method [117, 66], the genetic algorithms and the optimal control theory (OCT).

In this section, we present the control of different chemical processes that we have studied. The control field is tailored by using either optimal control theory (in particular monotonically convergent algorithms, see the corresponding section for details) and optimized adiabatic passage techniques [117, 66]. We now briefly explain the way to construct efficient adiabatic solutions to control the dynamics of molecular systems. Adiabatic methods are usually achieved by using a series of intense pulses which can be frequency chirped. The modification of the shape of the pulse envelope and the chirping rate are sufficiently slow to satisfy adiabatic conditions. An example of adiabatic process is the STIRAP technique which involves a counterintuitive sequence of two pulses in a three-level system with specific couplings. A complete population transfer can be achieved with this strategy. Adiabatic processes are robust in the sense that they are not sensitive to small variations of laser parameters. Such processes have been applied with success in the control of simple chemical processes [79, 118]. However, for complex chemical systems, the efficiency of adiabatic processes is worse. A chemical system is not an ideal system as assumed in adiabatic techniques. For instance, the three-level system of a STIRAP strategy is coupled to background states. This coupling can deteriorate noticeably the efficiency of the scheme

in particular if these states are resonant or almost resonant with the laser fields. Another negative aspect is the duration of these processes which is very long in order to ensure the adiabatic property of the scheme. To overcome these difficulties, the idea is to combine adiabatic processes with an optimization of a finite number of parameters characterizing the different pulses (intensity, duration, delay between the pulses). This strategy is called an optimized adiabatic passage technique. The optimization allows to decrease the control duration and to cancel the effect of background states. With the optimization, we lose however a part of the robustness of the adiabatic processes [22]. This method has the advantage to design simple control fields with respect to the ones obtained from OCT. The results of the two approaches are qualitatively different with simpler control fields for the adiabatic processes but at the price of a more energetic control [22]. Note also that we have found complex systems where the adiabatic techniques do not work whereas the optimal control techniques remain efficient. This strategy can also be used to implement quantum gates in molecular systems. We use for that the adiabatic processes introduced in [77, 64]. The qubits are constructed from the normal modes of the molecule or from particular molecular symmetries [22]. Recently even more complex schemes such as a full adder [44], the Deutsch-Jozsa [112, 116, 90] or Shor algorithms [121] have been considered in molecular systems and implemented using APT or OCT.

We reproduce here the article [22]. In this paper, we use OCT to determine a field controlling the isomerization reaction $H_3CO \rightarrow H_2COH$. We use also APT and OCT to control the passage from one conformer of H_2COH to the other. This reaction is locally described by a one dimensional double-well potential. APT are only efficient in this second case. In [20], we consider the same reaction but with a coupling with a dissipative environment. The dissipation models here the interaction with the degrees of freedom which are not taken into account in the system. We have next applied these techniques to control a cis-trans photoisomerization via a conical intersection in [18] and to implement quantum gates using rovibrational levels [7]. In [18], we consider a one-dimensional vibronic hamiltonian with two electronic surfaces in a model of the retinal in rhodospin. Dissipation effects are included in the model to simulate the other degrees of freedom. The system is coupled to a bath of oscillators. The dynamics is carried out in the Markovian approximation since we assume that the bath correlation

time scale is smaller than the pulse duration. In [7], we show how to choose rovibrational states to construct quantum gates in diatomic ($NaCs$) and polyatomic ($SCCl_2$) molecules. We illustrate in particular the difficulty of encoding quantum gates in pure rotational states.

Laser control in a bifurcating region

D. Sugny,[1] C. Kontz,[1] M. Ndong,[2] Y. Justum,[2] G. Dive,[3] and M. Desouter-Lecomte[4,*]
[1]*Laboratoire de Physique de l'Université de Bourgogne, Unité Mixte de Recherches 5027 CNRS et Université de Bourgogne, BP 47870, 21078 Dijon, France*
[2]*Laboratoire de Chimie Physique, Unité Mixte de Recherches 8000, CNRS et Université de Paris-Sud-11, 91405 Orsay Cedex, France*
[3]*Centre d'Ingéniérie des Protéines, Université de Liège, Sart Tilman B6, B-4000 Liège, Belgium*
[4]*Laboratoire de Chimie Physique, Unité Mixte de Recherches 8000, CNRS et Université de Paris-Sud-11, 91405 Orsay Cedex, France and Département de Chimie, Université de Liège, Institut de Chimie B6, Sart-Tilman, B-4000, Liège 1, Belgium*
(Received 28 April 2006; revised manuscript received 13 July 2006; published 27 October 2006)

We present a complete analysis of the laser control of a model molecular system using both optimal control theory and adiabatic techniques. This molecule has a particular potential energy surface with a bifurcating region connecting three potential wells which allows a variety of processes such as isomerization, tunneling, or implementation of quantum gates on one or two qubits. The parameters of the model have been chosen so as to reproduce the main features of H_3CO which is a molecule benchmark for such dynamics. We show the feasibility of different processes and we investigate their robustness against variations of laser field. We discuss the conditions under which each method of control gives the best results. We also point out the relation between optimal control theory and local control.

DOI: 10.1103/PhysRevA.74.043419 PACS number(s): 32.80.Qk, 82.50.Nd

I. INTRODUCTION

Control of physicochemical processes by ultrashort laser pulses remains nowadays an attractive and challenging domain. The aim of this kind of control is to design a laser pulse which drives the system from an initial state to a specific target state or even better, to find laser fields able to perform unitary transformations on molecular qubits. By this way, shaped laser pulses have become new reagents for chemical reactions. Some of the most important experimental contributions to this field have been reviewed recently [1]. On the other hand, different control schemes have been proposed, among others we can cite the Brumer-Shapiro coherent control [2,3], the Tannor-Rice-Kosloff local control approach [4,5], the Rabitz optimum control theory (OCT) based on learning algorithms or closed-loop control procedures [6–9], or the simulated Raman adiabatic passage (STIRAP) scheme [10–12].

This paper is devoted to a theoretical analysis of different scenarios based on STIRAP (or extension of this process as f-STIRAP [13]) and OCT by working only in the infrared domain, i.e., without transitions *via* excited electronic states. We consider a two-dimensional (2D) model of a bifurcating region in the ground potential energy surface of a polyatomic system. Such a region connects three non equivalent wells. A deep reactant well is connected to a symmetric double well. One passes from the reactant well to the double basin with a large amplitude bending mode of a migrating hydrogen atom around a given bond. The double well corresponds to an internal rotation of this atom around the axis defined by the particular bond. This three-well bifurcating region is an interesting pinball topography which suggests different processes of control:

(1) transformation of a delocalized state into a localized state in the double-well potential [14]

(2) transformation of a localized state of the double-well potential into the other. This has been already proposed in the spirit of Cope rearrangement [15] or enantiomer selection [16]

(3) isomerization from the reactant well to a given basin of the surface like in hydrogen transfer in organic molecules [17]. In our case, this reaction involves a break of symmetry.

(4) realization of one or two qubits systems [18–23]. The double-well region offers different possibilities for the choice of the quantum numbers which allow to define the qubits (parity or excitation) [24].

We address different control issues: the efficiency of various strategies which depend on the shape of the dipolar surface or, equivalently on the structure of the dipolar matrix and the robustness of the control with respect to the process used and the duration of the pulse. In each case, we also analyze the different pathways which are enforced by the laser field. Finally we briefly discuss the relationship between local control and OCT in the particular case where the objective is to maximize the average value of the projector on a superposed state.

II. MODEL

We consider a model recently proposed which reproduces the main features of a bifurcating region connecting three potential energy wells [25]. Isoenergy contours are presented in Fig. 1. The model is calibrated on an *ab initio* computation at the QCISD level [25] of the isomerization of the methoxy radical into hydroxymethyl which is a molecule benchmark for such energy landscapes [26]. We should emphasize that we do not intend to control dynamics of this particular radical moiety, but we are rather interested in this particular topography for which a convenient analytical expression has been proposed.

*Corresponding author. Electronic address: mdesoute@lcp.u-psud.fr

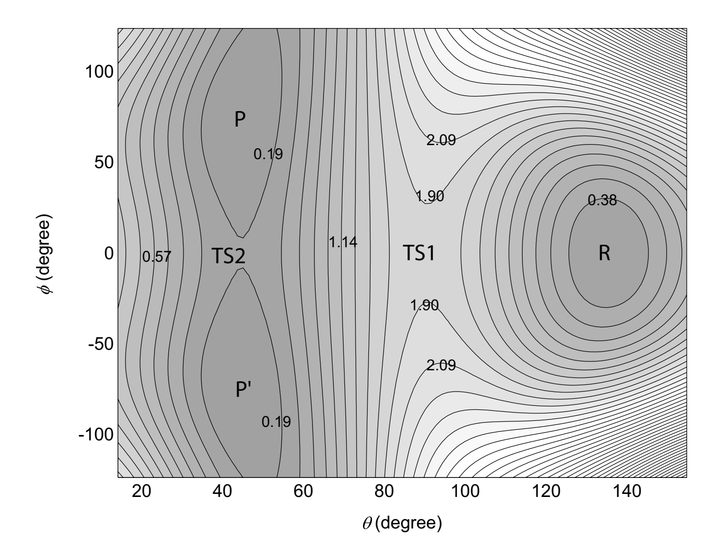


FIG. 1. Isoenergy contours (in eV) in the model potential energy surface of the isomerization $H_3CO \rightarrow H_2COH$ as a function of two active angular coordinates (see Fig. 2). The zero of energy is at the bottom of the product well (P or P'); R=0.181 eV, $TS1$=1.854 eV, and $TS2$=0.195 eV.

The model describes the rotation of the hydrogen atom around a polar bond connecting two atoms (here CO) in different chemical environments (see Fig. 2). The two active coordinates $\theta \in [0,\pi]$ and $\phi \in [-\pi,\pi]$ are the spherical angles of the migrating hydrogen atom with respect to the center of the bond. In C_S geometry (ϕ=0), the first active bending coordinate θ connects the reactant well R to a second well through a first transition state $TS1$ (the barrier height from the reactant is 1.673 eV). This second well is a transition state $TS2$ according to a second symmetry breaking active coordinate ϕ. $TS2$ is the top of the small barrier (0.195 eV) of the double well corresponding to rotational conformers P and P'. Between $TS1$ and $TS2$ lies a valley ridge inflexion point (VRI). Mathematical definitions of a VRI point can be found in different works [27–30]. Roughly speaking, it is a point where a valley corresponding to a particular internal mode becomes an unstable ridge. We point out that field-free dynamics has already been carried out in such bifurcating regions by assuming that initial wave packets can be prepared in the valley uphill from the VRI [31,32]. In the quasiharmonic regime, one can introduce vibrational quantum numbers for θ and ϕ oscillators. The ground state of the R well is denoted by $|0,0\rangle_R$. The delocalized states of the double well are of parity even and odd and are thus noted $|n+,m\rangle$ and $|n-,m\rangle$. The splitting of the first level $|0+,0\rangle$, $|0-,0\rangle$ is 4.3×10^{-5} eV. This corresponds to a rather long tunneling time of about 95 ps much longer than the duration of the pulses used in the control. The first localized states coming from the in phase and out of phase superposition are $|n\mathrm{L},0\rangle=(|n+,0\rangle+|n-,0\rangle)/\sqrt{2}$ and $|n\mathrm{R},0\rangle=(|n+,0\rangle-|n-,0\rangle)/\sqrt{2}$. They are associated to m=0 for the θ vibrator. We recall that the notations R and L do not refer to enantiomers in this example (R is P and L is P').

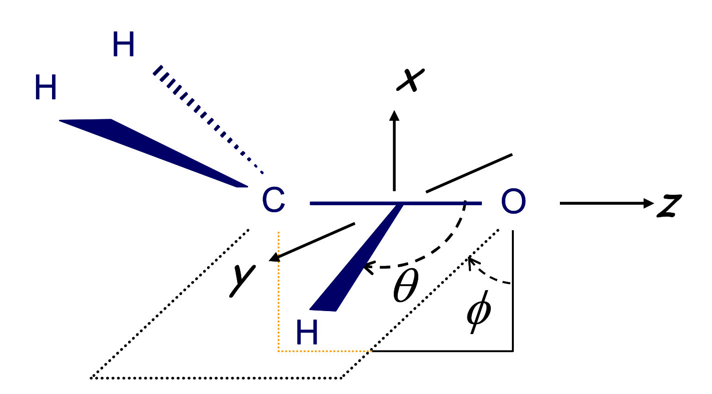


FIG. 2. (Color online) Active coordinates θ and ϕ for the isomerization $H_3CO \rightarrow H_2COH$ and polarization directions for aligned molecules.

In the dipolar approximation, the reduced 2D Hamiltonian takes the form

$$\hat{H} = \hat{H}_0 - \sum_k \hat{\mu}_k E_k(t), \quad (1)$$

where $\hat{H}_0=\hat{T}+\hat{V}$ is the field free Hamiltonian and k denotes the polarization direction. The exact constrained 2D kinetic energy operator can be numerically computed by the TNUM algorithm [33] by freezing the inactive coordinates at the $TS1$ geometry. We extract an approximate kinetic energy operator by fitting the standard angular momentum expression in spherical coordinates. In Euclidian normalization convention, $\hat{T}$ is then equal to

$$\hat{T}_{Eucl} = -\frac{\hbar^2}{2I_\theta}\left(\frac{\partial^2}{\partial\theta^2} + \mathrm{cotan}\,\theta\frac{\partial}{\partial\theta}\right) - \frac{\hbar^2}{2I_\phi}\frac{1}{\sin^2\theta}\frac{\partial^2}{\partial\phi^2},$$

where constant inertia moments I_θ=6160 a.u. and I_ϕ=4430 a.u. are estimated from the TNUM grids. In the Wilson normalization convention in which the volume element is $d\theta d\phi$, $\hat{T}$ becomes

$$\hat{T}_{Wil} = -\frac{\hbar^2}{2I_\theta}\frac{\partial^2}{\partial\theta^2} - \frac{\hbar^2}{2I_\phi \sin^2\theta}\frac{\partial^2}{\partial\phi^2} + v(\theta),$$

where $v(\theta)$ is an extra potential term. This analytical expression is particularly suited to the use of the split operator algorithm [34] which is needed to propagate the wave packets. This point is due to the fact that the coefficient of a given differential operator $\partial/\partial q^k$ does not depend on q^k but only on the other coordinates. We assume that the molecules are aligned in the laboratory frame with the polar bond oriented along the $\vec{e}_z$ axis (see Fig. 2). This could be obviously an important constraint [35]. We consider linear polarizations with directions $\vec{e}_x$ in the C_S plane and $\vec{e}_y$ perpendicular to the C_S plane.

To pursue the construction of the model, we also propose a simple form for dipolar surfaces based on a chemical analysis of the molecule. Indeed, the system can be roughly described as the rotation of a charged particle around a polar bond. The dipolar components $\mu_x(\theta,\phi)$ and $\mu_y(\theta,\phi)$ are larger on the P,P' side ($\theta<\pi/2$) when the particle is close to the most electronegative atom. They decrease quickly for $\theta>\pi/2$, when the particle enters a region near the weakly electronegative atom. The analytical model is given in the

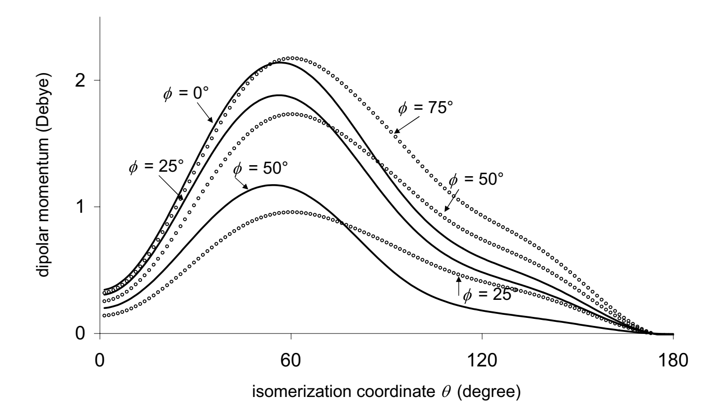


FIG. 3. Cuts in the model dipolar momentum surface (see Appendix) for different values of the torsion angle ϕ. Full lines: $\mu_x(\theta,\phi)$ (symmetric), open circles: $\mu_y(\theta,\phi)$ (antisymmetric).

Appendix. $\mu_x(\theta,\phi)$ and $\mu_y(\theta,\phi)$ are respectively symmetric and antisymmetric with respect to ϕ. Some cuts are given in Fig. 3.

III. CONTROL METHODOLOGIES

A. Local and optimal methods

The control algorithms are usually classified as local [4,36–38] or global depending on whether the field is determined from the instantaneous dynamical properties by maximizing a performance index or from the variational calculus of a cost functional. The objective functional can be defined in different manners [7,8] which are strongly connected [9]. The procedure to maximize the cost functional under the constraint of satisfying the time dependent Schrödinger equation is described in details in the literature [39]. The Zhu, Botina, Rabitz formulation [7] leads to three coupled equations: the Schrödinger equation for $|\psi(t)\rangle$ with an initial condition $|\psi_i(t=0)\rangle=|\phi_i\rangle$ (forward propagation), the Schrödinger equation for the Lagrange multiplier $|\psi_f(t)\rangle$ with a final target condition $|\psi_f(T)\rangle=|\phi_f\rangle$ (backward propagation), and an equation for the optimum field

$$E_j(t) = -(1/\hbar\alpha_0)\mathrm{Im}[\langle\psi_i(t)|\psi_f(t)\rangle\langle\psi_f(t)|\mu_j|\psi_i(t)\rangle], \quad (2)$$

where α_0 is a positive penalty factor chosen to weight the significance of the laser fluence. An experimental switching function $s(t)=\sin^2(\pi t/T)$ is usually introduced [39], α_0 is then replaced by $\alpha_0 \to \alpha_0/s(t)$. The equations are solved by an iterative formulation [7] adapted to a discrete implementation based on a second order split operator scheme [34]. We have used the improvement proposed in Ref. [40]. At each iteration, the field is given by $E_j^{(k)}=E_j^{(k-1)}+\Delta E_j^{(k)}$ where $\Delta E_j^{(k)}$ is calculated by [Eq. (2)].

It is worth noting that the local approach is strongly related to the Zhu, Botina, and Rabitz approach when the performance index involves a projection on a nonstationary state. The local control methodology is overviewed in Ref. [38]. The field is chosen in order to maximize the rate of variation of a performance index $y(t)=y(\langle\hat{O}_j(t)\rangle)$ which is a function of expectation values $\langle\hat{O}_j(t)\rangle=\langle\psi_i(t)|\hat{O}_j(t)|\psi_i(t)\rangle$ of Hermitian operators with $j=1,N$. In the case where the target operator is a projector on a nonstationary wave packet at a final time T: $\hat{O}(T)=|\phi_f\rangle\langle\phi_f|$, the rate depends on a single expectation value $dy(t)/dt=d\langle\hat{O}(t)\rangle/dt$. If the time dependence of the operator is fixed by the field free Hamiltonian

$$\hat{O}(t) = e^{-iH^0(t-T)/\hbar}|\phi_f\rangle\langle\phi_f|e^{iH^0(t-T)/\hbar} = |\phi_f(t)\rangle\langle\phi_f(t)|, \quad (3)$$

in other words, when the operator projects down to the wave packet which freely evolves towards the target state at time T, then one obtains [38]

$$dy(t)/dt = -2\,\mathrm{Im}[\langle\hat{O}(t)\hat{\vec{\mu}}\cdot\vec{E}(t)\rangle]. \quad (4)$$

The local control field giving a monotonous increase of the performance index is obtained by setting, for a polarization direction, $E_j(t)=-\lambda_j\,\mathrm{Im}[\langle\hat{O}(t)\hat{\mu}_j\rangle]$. By inserting expression (3) into this last equation, one gets an expression corresponding to the first step (without zero order field) of the iterative optimum control [Eq. (2)], i.e., when $\psi_f(t)$ evolves with the field free Hamiltonian

$$E_j(t) = -\lambda_j\,\mathrm{Im}[\langle\psi_i(t)|\phi_f(t)\rangle\langle\phi_f(t)|\hat{\mu}_j|\psi_i(t)\rangle]. \quad (5)$$

The method focuses on the λ_j coefficient. With few trials, it is possible to find values of λ_j providing an acceptable field. The latter is then used as an initial-guess field to continue the iterative optimum control procedure. This speeds up the rate of convergence of the algorithm by finally choosing the best α_0.

The optimum field able to steer a set of initial states to a set of target states, i.e., to apply a unitary transformation to the 2^N states of N qubits

$$\begin{pmatrix}\phi_f^1\\ \vdots\\ \phi_f^{2^N}\end{pmatrix} = \hat{U}_{gate}\begin{pmatrix}\phi_i^1\\ \vdots\\ \phi_i^{2^N}\end{pmatrix}$$

can be obtained by the multitarget generalization of OCT [18,21]. We have to propagate simultaneously a set of 2^N wave packets forward in time $\psi_i^n(t=0)=\phi_i^n$ with $n=1,\ldots,2^N$ and a set of 2^N Lagrange multipliers wave packets backwards $\psi_f^n(t=T)=\phi_f^n$ with $n=1,\ldots,2^N$. The optimum field is given by a sum of contributions from each state

$$E_j(t) = -(1/\hbar\alpha_0)\mathrm{Im}\left(\sum_{n=1}^{2^N}[\langle\psi_i^n(t)|\psi_f^n(t)\rangle\langle\psi_f^n(t)|\mu_j|\psi_i^n(t)\rangle]\right). \quad (6)$$

A constraint on the phase of the quantum gate could be added [41].

The fidelity of the quantum gate is measured by

$$F = |\mathrm{tr}(\hat{U}_{gate}^{+}\hat{U}_{control})|^2/2^N \quad (7)$$

B. STIRAP and adiabatic processes

The second strategy for the control is based on adiabatic passage (for a recent overview, see [11,12] and references

therein). Such processes are widely used in a variety of fields, extending from nuclear magnetic resonance and quantum information to atomic and molecular excitations. Adiabatic methods are usually achieved by using a series of intense pulses which can be frequency chirped, the frequencies and the chirping being adapted to the structure of the energy levels. However, the modification of the shape of the pulse envelope and the chirping rate must be sufficiently slow so as to fulfill adiabatic conditions. One of the most well-known adiabatic processes is the STIRAP excitation which involves a counterintuitive sequence of two pulses in a three-level system, in which the field of the Stokes pulse precedes and overlaps the field of the pump pulse. These adiabatic techniques allow a complete population transfer from an initial state to a target state which can be either a stationary state, i.e., an eigenstate of the field free Hamiltonian or a coherent superposition of such states. They are also robust in the sense that they are not sensitive to small variations of laser parameters. Due to these remarkable properties, such processes seem to be particularly suitable for the control of chemical reactions. For instance, they have been applied with success for controlling the isomerization of HCN [42,43]. However, the relevance of adiabatic techniques in a complex system can be questioned. We stress that 100% efficiency of the control is generally ensured only for a subset of levels with particular couplings such as the tripod system. If the molecular system is rich in the energy range considered, the effect of coupling to background states can deteriorate noticeably the population transfer in particular if the background states are resonant or almost resonant with laser fields. Another major drawback of these methods is the duration of the pulses which is longer than the time needed by optimal or local control to reach their objective. This point can be problematic if other concurrent chemical processes with time scale of the same order occur during the control.

To avoid the preceding problems, we combine in this paper adiabatic processes which allow determining a simple form for the overall field and optimization of some parameters of the pulse, leading to a shorter (of the order of few picoseconds) and efficient control. The strategy can be summarized as follows. We first select a subset of levels and we determine an adiabatic process in order to achieve the objective of the control. These levels have to be carefully chosen, as otherwise the value of the electric field is too large. More precisely, we recall that the Rabi frequency $\Omega_{12}=|\mu_{12}|E(t)$ between the states 1 and 2 (μ_{12} being the matrix element of the dipole moment) must be sufficiently large so as to fulfilled adiabatic conditions. For instance, a standard condition is $\Omega_{12}T \gg 1$ where T is a characteristic duration of the pulse, which is the full width half maximum for a Gaussian pulse. In addition, in order to avoid other unwanted chemical processes such as ionization, the intensity of the electric field has to be limited to 10^{14} W/cm^2 which roughly leads to a minimum of the order of 0.1 a.u. for matrix elements of the dipole moment. In a second step, considering all the levels of the system, we decrease the pulse duration to few picoseconds and we optimize both the intensities and the delay between the different pulses to keep efficient control.

We now describe the computational details of the method. We have used Gaussian pulses, the pulses being polarized in the $\vec{e}_x$ or the $\vec{e}_y$ direction. The field $E(t)$ is equal to the sum of terms of the following form:

$$E_0 \exp[-(t-t_k)^2/2\gamma^2]\cos(\omega_k t+\varphi_k), \tag{8}$$

where γ, ω_k, E_0, and φ_k are respectively the width, the frequency, the amplitude, and the phase of the pulse. To simplify even more the overall field, we assume that the width and the amplitude are the same for all the pulses (except for the quantum gates). The delay is defined by the difference between the times t_k.

IV. WAVE PACKET CONTROL

A. Double well scenarios

We consider two control schemes in the double well product region (P and P', see Fig. 1): the localization of the ground delocalized state into one localized state, in the spirit of the previous control on H_2POSH [44] and the transformation from a localized state of one well (P) to a localized state of the other well (P') [15,16]. We schematize these processes as follows:

$$|0+,0\rangle \to \frac{1}{\sqrt{2}}(|0+,0\rangle + |0-,0\rangle) = |0\mathrm{L},0\rangle, \tag{9}$$

$$|0\mathrm{L},0\rangle \to \frac{1}{\sqrt{2}}(|0+,0\rangle - |0-,0\rangle) = |0\mathrm{R},0\rangle. \tag{10}$$

1. Description of the adiabatic processes

We first analyze in details the processes $|0+,0\rangle \to |0\mathrm{L},0\rangle$ or $|0+,0\rangle \to |0\mathrm{R},0\rangle$ which consist in preparing one of the conformer from a delocalized state. The presentation of the results follows the different steps of the strategy. We begin by selecting the first three levels of the system, that is $|0+,0\rangle$, $|0-,0\rangle$, and $|1+,0\rangle$. The method for determining the adiabatic process consists in using the particular symmetry of the dipole moment. For instance, we recall that μ_x only couples the levels $|0+,0\rangle$ and $|1+,0\rangle$, the transition $|0-,0\rangle$ to $|1+,0\rangle$ being forbidden. We consider a f-STIRAP scheme which, as the STIRAP technique, only uses two pulses, the pump and the Stokes fields. We choose to fix the frequencies ω_k and the phases φ_k of each pulse as follows:

$$\omega_k = E_{1+,0} - \frac{1}{2}(E_{0+,0}+E_{0-,0}),$$

$$\varphi_k = 0, \tag{11}$$

where $E_{0+,0}$ is, for instance, the energy of the level $|0+,0\rangle$. In the three-state basis $|0+,0\rangle$, $|0-,0\rangle$, and $|1+,0\rangle$, the total Hamiltonian can be written as

$$\begin{pmatrix} E_{0+,0} & \alpha\Omega_S\cos(\omega t) & \Omega_P\cos(\omega t) \\ \alpha\Omega_S\cos(\omega t) & E_{0-,0} & \Omega_S\cos(\omega t) \\ \Omega_P\cos(\omega t) & \Omega_S\cos(\omega t) & E_{1+,0} \end{pmatrix}, \tag{12}$$

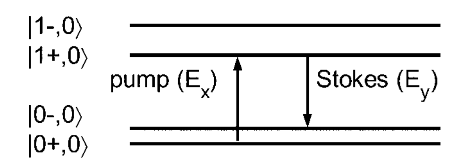
where Ω_P and Ω_S are respectively the Rabi frequencies of the pump and the Stokes pulses for the transitions $|0+,0\rangle$

$\rightarrow|1+,0\rangle$ and $|0-,0\rangle\rightarrow|1+,0\rangle$. The α parameter is equal to $\mu^y{}_{0+0,0-0}/\mu^y{}_{1+0,0-0}$. The pump pulse is polarized along the $\vec{e}_x$ direction whereas the Stokes pulse is polarized along the $\vec{e}_y$ one. Note that the Rabi frequencies are chosen real without loss of generality. Using the RWA approximation [12], the Hamiltonian H_I reads in the interaction representation

$$H_I=\begin{pmatrix} 0 & 0 & \Omega_P \\ 0 & 0 & \Omega_S \\ \Omega_P & \Omega_S & 0 \end{pmatrix}, \qquad (13)$$

where the small detunings $E_{1+,0}-E_{0+,0}-\omega$ and $E_{1+,0}-E_{0-,0}-\omega$ are neglected.

The idea is then to use a f-STIRAP technique. f-STIRAP is an extension of STIRAP which allows the creation of coherent superpositions of states [11]. f-STIRAP is now a well-known process which has already been used in a variety of systems to implement qubit gates or to generate superposed states [45,46]. The process can be schematized by the following diagram:



The extension of the STIRAP technique consists in the fact that the amplitudes of the two pulses are required to have a constant ratio at the end of the pulse. More precisely, if the eigenvector $|\psi_0\rangle$ of eigenvalue 0 of H_I writes

$$|\psi_0\rangle=\frac{1}{\sqrt{\Omega_P{}^2+\Omega_S{}^2}}(\Omega_S|0+,0\rangle-\Omega_P|0-,0\rangle) \qquad (14)$$

then the following conditions have to be fulfilled by the two Rabi frequencies:

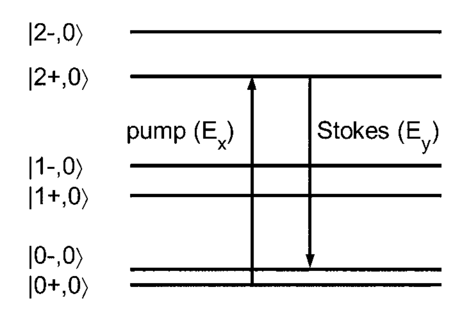
$$\lim_{t\rightarrow-\infty}\frac{\Omega_P}{\Omega_S}=0 \text{ and } \lim_{t\rightarrow+\infty}\frac{\Omega_P}{\Omega_S}=\varepsilon, \qquad (15)$$

where $\varepsilon=\pm1$. One deduces for the two limit cases that

$$|\psi_0(-\infty)\rangle=|0+,0\rangle,$$

$$|\psi_0(+\infty)\rangle=\frac{1}{\sqrt{2}}[|0+,0\rangle-\varepsilon|0-,0\rangle]. \qquad (16)$$

It is then clear that for an adiabatic evolution, the localized state can be obtained from f-STIRAP with $\varepsilon=+1$ for $|0\mathrm{R},0\rangle$ and $\varepsilon=-1$ for $|0\mathrm{L},0\rangle$. Another equivalent scheme can be constructed by replacing the intermediate state $|1+,0\rangle$ of the f-STIRAP process with $|2+,0\rangle$



One can also imagine other mechanisms of the same kind using other intermediate states and the particular symmetry of the dipole moment. Finally, the following points can be noticed. A more complex superposed state can be obtained with f-STIRAP if the ratio Ω_P/Ω_S is different from 1 or -1 when $t\rightarrow+\infty$. Moreover, a process using only one linear polarized laser field but with a frequency ω and its second harmonic 2ω can also be built to control the tunneling [47].

For the transformation $|0\mathrm{L},0\rangle\rightarrow|0\mathrm{R},0\rangle$ from a localized state to the other, we have slightly modified the previous scheme. The limits of [Eq. (15)] become

$$\lim_{t\rightarrow-\infty}\frac{\Omega_P}{\Omega_S}=-\varepsilon \text{ and } \lim_{t\rightarrow+\infty}\frac{\Omega_P}{\Omega_S}=\varepsilon \qquad (17)$$

leading thus to the following limit states:

$$|\psi_0(-\infty)\rangle=\frac{1}{\sqrt{2}}[|0+,0\rangle+\varepsilon|0-,0\rangle],$$

$$|\psi_0(+\infty)\rangle=\frac{1}{\sqrt{2}}[|0+,0\rangle-\varepsilon|0-,0\rangle], \qquad (18)$$

which correspond either to $|0\mathrm{R},0\rangle$ or $|0\mathrm{L},0\rangle$ according to the value of the parameter ε.

Having determined an adiabatic process able to control the specified reaction, we are now in a position to examine the conditions (choice of Rabi frequencies and delay between the pulses) under which the mentioned scheme of control continues to work for a shorter duration of the pulse, i.e., not in the adiabatic limit. The optimized laser field has not been constructed using optimal algorithms in order to preserve as much as possible the robustness of the solution which, as stated above, is one of the most important features of adiabatic processes. For that purpose, we have considered a 2D grid (Rabi frequencies, delay) and we have calculated for each point of the grid, i.e., for particular values of Rabi frequencies and delay, the corresponding time evolution. The Rabi frequency (the same for each pulse) varies from 10^{-5} a.u. to 5×10^{-4} a.u. whereas the limits of the delay are 5×10^{4} a.u. and 5×10^{5} a.u. For our model of H_3CO, this amounts to a pulse duration of about 20 ps and a field amplitude of 5×10^{7} Vm^{-1} that corresponds to a very weak field.

Figure 4 illustrates the results of applying the f-STIRAP strategy for a total duration of 20 ps and for the intermediate state $|1+,0\rangle$. In the adiabatic limit, only states $|0+,0\rangle$ and $|0-,0\rangle$ are expected to be populated. A different behavior is obtained for the process. This is due to coupling to background states and to the fact that adiabatic conditions are not

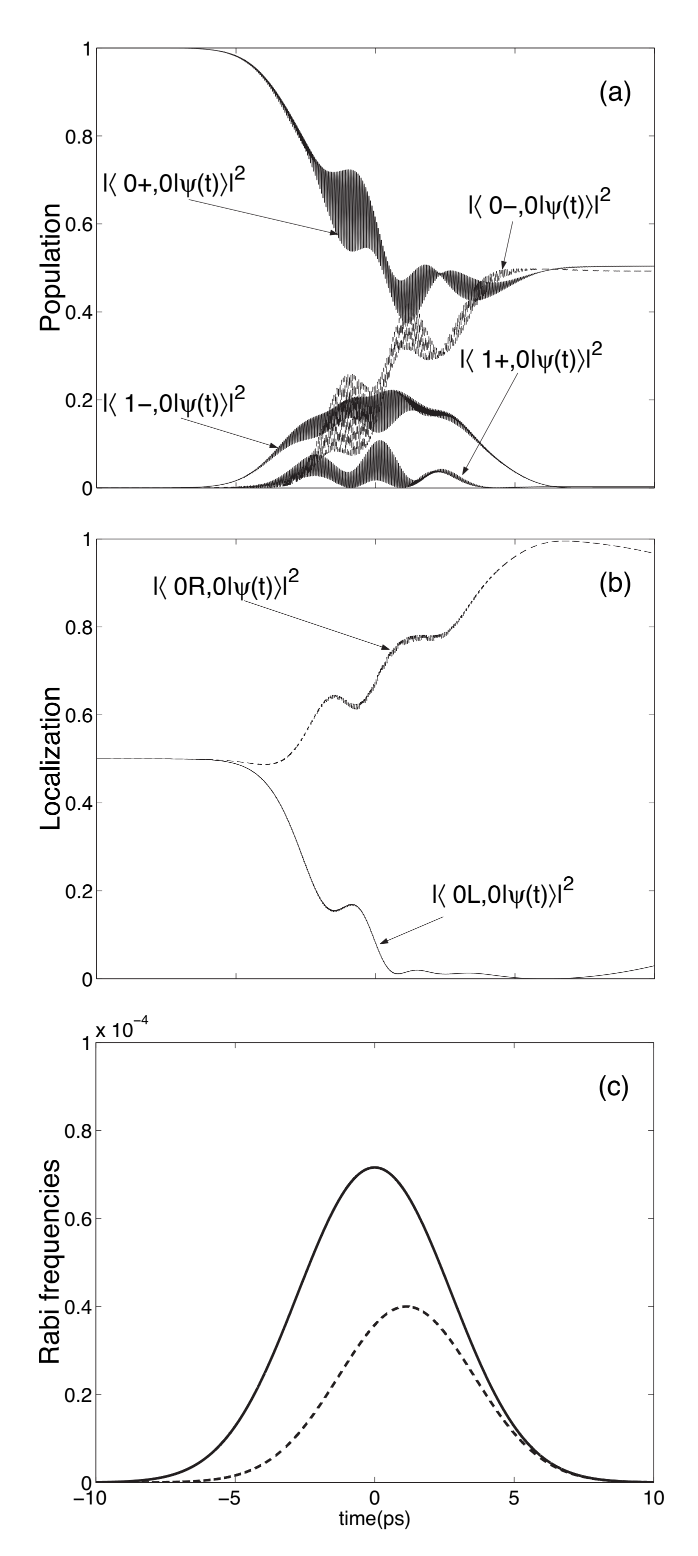


FIG. 4. Dynamics controlled by f-STIRAP strategy for the preparation of the superposed state $|0R,0\rangle$ through the intermediate state $|1+,0\rangle$. Panels (a) and (b) show respectively the evolution of populations in the Hamiltonian eigenbasis and in the superposed states $|0L,0\rangle$ and $|0R,0\rangle$. Populations of other vibrational states remain small during the process. The Rabi frequencies of the different pulses are displayed on panel (c). Rabi frequencies are in atomic units. The solid line corresponds to the Stokes pulse and the dashed line to the pump pulse. The total duration of the pulse is of the order of 20 ps.

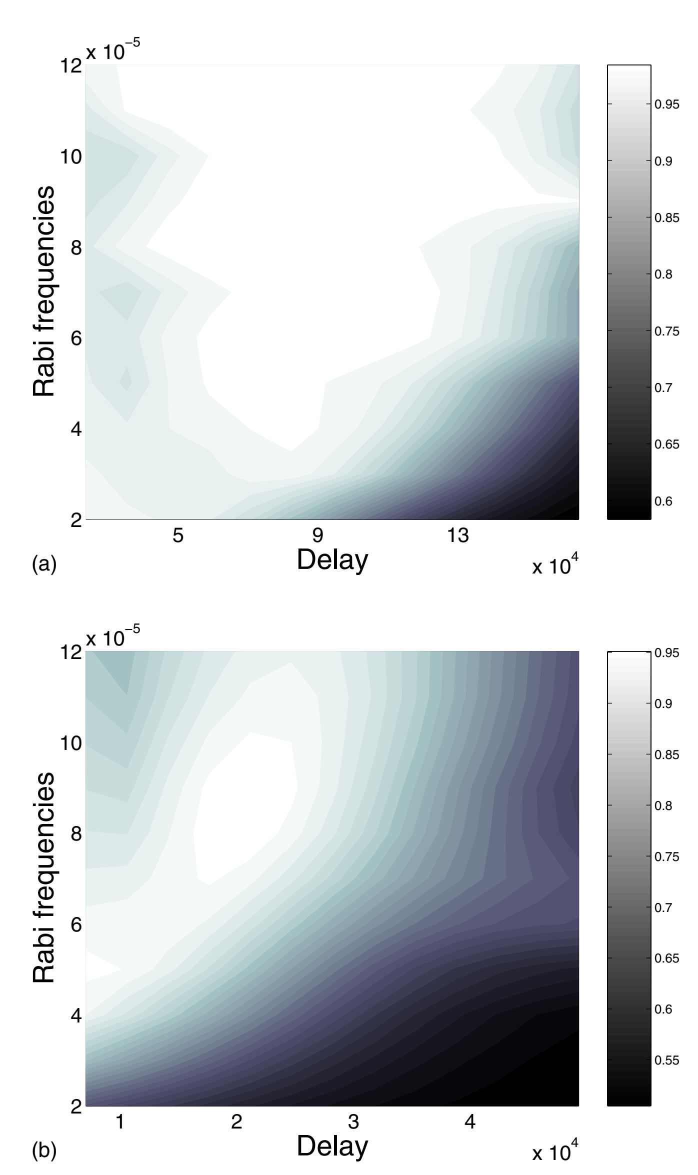


FIG. 5. (Color online) Robustness of the f-STIRAP process as a function of the Rabi frequencies and the delay between the pulses for a total duration of 20 ps (upper part) and 4.5 ps (lower part) of the overall field. Rabi frequencies and delay are in atomic units. The intermediate state is $|2+,0\rangle$.

rigorously fulfilled. For instance, the product Rabi frequencies times duration of the pulse is of the order of 10. However, this deviation from the theoretical description does not decrease its efficiency. The same behavior can be obtained for different intermediate states and different total durations.

The robustness of the strategies has been checked against two parameters: the time delay between successive pulses and the Rabi frequency of each pulse. Figure 5 shows the robustness against these two variables for the f-STIRAP process and for two total durations of about 20 ps (see Fig. 4) and 4.5 ps. Remarkable robustness is achieved, especially for the longer pulse duration, advocating for a possible experimental feasibility of the control scheme. Moreover, it can be clearly seen that the strategy is more robust for longer pulses. This point can be explained by the fact that larger the duration of the pulse is, the more the adiabatic conditions are

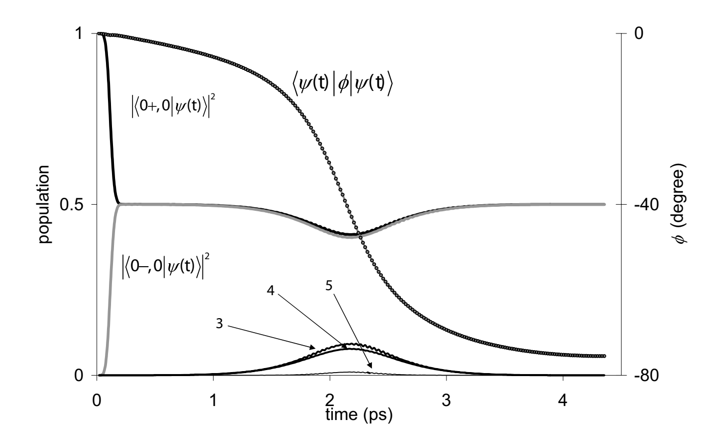


FIG. 6. Dynamics controlled by the optimum field for the preparation of $|0\mathrm{L},0\rangle$. Left axis: evolution of populations in eigenvectors $|0+,0\rangle$ and $|0-,0\rangle$, the excited states 3, 4, 5 nearly correspond to $|1+,0\rangle$, $|1-,0\rangle$, and $|2+,0\rangle$ respectively; right axis: evolution of the average ϕ position.

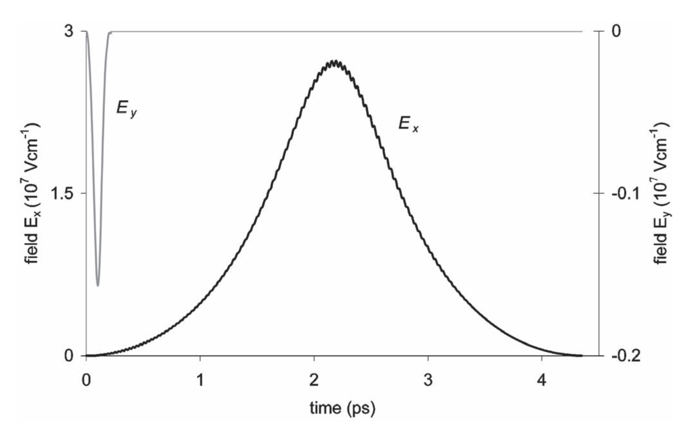


FIG. 7. OCT field obtained for the shortest laser pulse duration studied in the preceding section (f-STIRAP strategy) for the transformation $|0+,0\rangle \rightarrow |0\mathrm{L},0\rangle$ [Eq. (9)].

fulfilled and consequently the more the process is robust [48]. The same study with similar results can be done for the transformation from a localized state to the other. However, we notice that the overall dynamics is generally much more oscillatory with more complex structures as compared to the preceding reaction.

2. Optimal control

Methods based on local or global control allow finding optimum fields with a smaller duration T than fields obtained by the adiabatic approach. Figure 6 displays the evolution of populations in the eigenbasis of $\hat{H}_0$ [Eq. (1)], in particular for the states $|0+,0\rangle$ and $|0-,0\rangle$ and the average value of the operator ϕ showing the localization in the P' well ($\phi = -75°$) at the end of the process, after about 4.5 ps. This time is chosen because it is the shortest time ensuring a good performance index in the STIRAP approach. The objective is reached at 99.99% in 10 iterations with the Rabitz algorithm [Eq. (2)] improved by the correction proposed in Ref. [40] using $\alpha_0 = 1.2$ without any zero order field. Focusing on the first step of the procedure and using local control [Eq. (5)], we obtain a zero order field with $\lambda_x = 8$ and $\lambda_y = 1.2$ leading to a performance index of 91%. The Rabitz algorithm then converges at 99.99% in 3 iterations.

One observes that the populations of the $|0+,0\rangle$ and $|0-,0\rangle$ eigenstates become equal very early but the average ϕ position shows that the equality of populations does not involve the correct phase to form the localized superposition $\frac{1}{\sqrt{2}}(|0+,0\rangle + |0-,0\rangle) = |0\mathrm{L},0\rangle$. Transient excitations help at reaching the target superposition. The OCT field is shown in Fig. 7. A part of the structure of the pulse can be understood as follows. The pulse is composed of two subpulses, one along the $\vec{e}_x$ direction and the other along the $\vec{e}_y$ direction. We consider this latter part. This subpulse can be viewed as a half-cycle pulse (HCP) [49], i.e., only one half of an optical field cycle. HCPs have already been used in different applications; we can cite the control of molecular alignment or orientation [49,50] or the control of tunneling in a double-well system [51]. This pulse, being of short duration with respect to the tunneling time but long in comparison with the period associated to the transitions $|0+,0\rangle \rightarrow |1+,0\rangle$ or $|0-,0\rangle \rightarrow |1+,0\rangle$, produces a superposition of states $|0+,0\rangle$ and $|0-,0\rangle$. Using the sudden approximation [52], the evolution operator U_{HCP} for the HCP can be written as follows in the basis defined by $|0+,0\rangle$ and $|0-,0\rangle$:

$$U_{HCP} = \exp(iA_{HCP}\sigma_x), \tag{19}$$

where A_{HCP} is the area of the pulse times the corresponding matrix element of the dipole moment and σ_x the Pauli matrix. Starting from a delocalized state, it can then be shown that a HCP of area $\pi/4$ and a free evolution of a quarter of the tunneling time lead to a completely localized state [51]. A numerical calculation shows that the area of the optimal pulse along the $\vec{e}_y$ direction is very close to $\pi/4$. Notice that the condition $\Omega_{\max} \ll \Delta$ where $\Omega_{\max}$ is the peak Rabi frequency and Δ the detuning has to be fulfilled to avoid the appearance of other resonances and the transfer of population to excited states. Δ can be roughly estimated by $\Delta = E_{1+,0} - E_{0+,0}$ which leads to the following larger possible value of the electric field $E = 2.5 \times 10^{-3}$ a.u. The second part of the pulse along the $\vec{e}_x$ direction is a more complex field which cannot be explained so simply as it does not respect the condition $\Omega_{\max} \ll \Delta$.

We have also tested the robustness of this process against the area of the different pulses. As can be seen in [Eq. (19)], the area is the main feature of such short pulses. We have observed that the process is robust (of the order of 10%) with respect to such inaccuracies affecting the area of the pulse. It seems that this feature can be attributed to the simple form of the optimal field.

B. Bifurcation scenario

We now investigate the possibility of steering the ground state $|0,0\rangle_R$ of the R well towards the P $|0\mathrm{R},0\rangle$ or P' $|0\mathrm{L},0\rangle$ product basin through the VRI region (see Fig. 1). This control is summarized by the following schematic diagram:

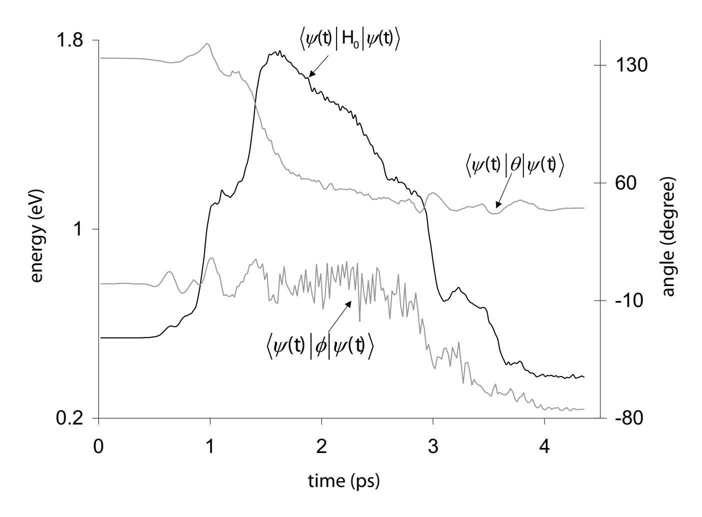


FIG. 8. OCT for the isomerization $R \to P'$. Black line: average unperturbed energy, gray lines: average value of the two active coordinates.

$$|0,0\rangle_R \to |0\mathrm{L},0\rangle \text{ or } |0,0\rangle_R \to |0\mathrm{R},0\rangle. \tag{20}$$

This scenario involves a break of symmetry after a passage over a high barrier (1.67 eV). From a dynamical point of view, it can be wondered which path the controlled wave packet will follow, i.e., whether the bifurcation occurs early (near the VRI) or not (near $TS2$). It should be noted that this example illustrates the extreme sensibility of the control to parameters of the model. This scenario looks like isomerization processes between two wells which have already been discussed in the literature [17,53,37]. However, the topography between $TS1$ and $TS2$ with a change of curvature along ϕ leads to delocalized eigenvectors strongly coupled by the dipolar momentum. This is unfavorable to the STIRAP scheme which needs intermediate states well decoupled from all the others. In OCT, we do not succeed in finding a satisfactory optimum field for the current model inspired from the QCISD *ab initio* level with a $TS1$ barrier of 1.67 eV. The algorithm finds a path involving a too high excitation $\langle\Psi(t)|\hat{H}_0|\Psi(t)\rangle$ of several eV up to 7 eV which is completely unrealistic. We adopt another potential energy surface inspired from other ab initio calculations (MP2) with a smaller energy barrier from the reactant (1.56 eV) at $TS1$ ($R=0.451$ eV, $TS1=1.911$ eV, and $TS2=0.216$ eV) and a slightly different profile along ϕ for $\phi>80°$. We use the same dipolar momentum model. In this case, the OCT gives a reasonable field leading to an average unperturbed energy of the order of E_{TS1} as shown in Fig. 8. For a pulse duration of 4.5 ps, the target is reached with 95.3% in 240 iterations starting with two zero order fields $E_j^0(t)=E_0\cos(\omega_j t)$ where $E_0=0.02$ a.u. and the ω_j are the harmonic frequencies of the two θ and ϕ vibrators in the R well. Figure 8 shows the average value of the two active coordinates during the process. The controlled break of symmetry occurs in a sequential manner. The θ angle first reaches the $TS2$ value before the break of symmetry and the cooling occurs in the double well region.

Figures 9 and 10 give the optimal fields and the corresponding Gabor transforms

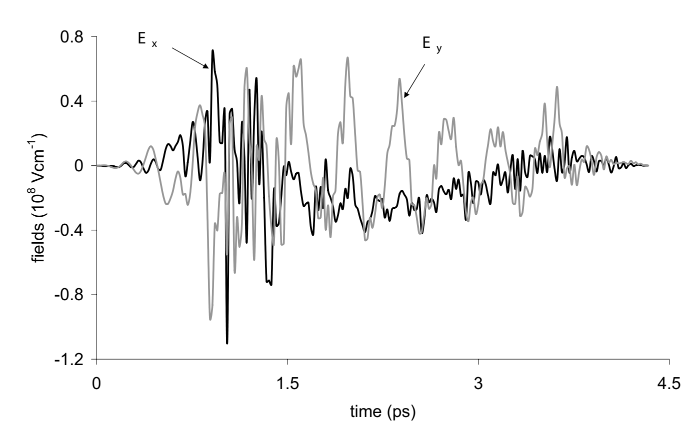


FIG. 9. OCT fields for the izomerization $R \to P'$. Black line: $E_x(t)$, gray lines: $E_y(t)$

$$F(\omega,t) = \left| \int_{-\infty}^{+\infty} H(s-t,\tau)E(s)e^{i\omega s}ds \right|^2, \tag{21}$$

where $H(s,\tau)$ is the Blackman window [54]

$$H(s,\tau) = 0.08\cos\left(\frac{4\pi}{\tau}s\right) + 0.5\cos\left(\frac{2\pi}{\tau}s\right) + 0.42 \quad \text{if } |s| \leq \frac{\tau}{2},$$

$$H(s,\tau) = 0 \text{ elsewhere},$$

and τ is the time resolution. Here we have fixed $\tau=0.2$ ps.

The Gabor transforms contain the zero order frequencies (1715 cm^{-1} for E_x and 1578 cm^{-1} for E_y). A lot of frequencies are used during the time interval [0.8, 1.5] ps. They permit to increase the unperturbed energy above $TS1$. The intermediate states playing a significant role in this heating are the low excitations of the θ vibrator (nearly $|0,1\rangle_R$, $|0,2\rangle_R$, and $|0,3\rangle_R$) and the first excitation in the ϕ vibrator $|1,0\rangle_R$. Between 1.5 ps and 3 ps, a lot of delocalized states are populated with a weight smaller than 5%. At this point, the OCT path involves a large number of intermediate states. Note that this is the extreme opposite of the situation favorable for applying the STIRAP technique. The cooling occurs after 3 ps and mainly involves two states of the double well region (nearly $|0+,1\rangle$ and $|0-,1\rangle$). In this example, cooling is easier than heating probably because the dipolar momentum is very different in the two regions.

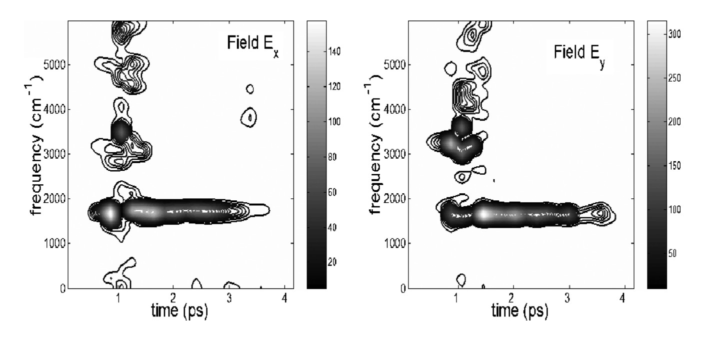


FIG. 10. Gabor transforms [Eq. (21)] of the OCT fields (Fig. 9) for the izomerization $R \to P'$.

We have also tried without any success the local approach [37] which consists in heating and cooling the wave packet according to the average θ position. Besides the difficulty of the expected break of symmetry, the average θ position does not reach the $TS1$ value during the heating but remains in the corresponding well excluding an efficient cooling.

V. LOGICAL GATES

We examine the possibility of realizing logical gates on one or two qubits. We recall that a quantum computation can be described as a sequence of logical gates which determine a unitary transformation $\hat{U}_{gate}$ [55]. Different molecular systems such as vibrationally excited molecules [18–24] have already been proposed for the implementation of one and two-qubits gates and several control schemes using either π-pulses [22] or optimal control theory [18–22] have been constructed. In the present case, the low lying states can be thought of as a qubit $|0\rangle = |0+,0\rangle$ and $|1\rangle = |0-,0\rangle$. The previous transformation $|0+,0\rangle \to |0\text{R},0\rangle$ is obviously related to the well known Hadamard transformation

$$\hat{U}_{\text{HAD}}\begin{pmatrix}|0+,0\rangle\\|0-,0\rangle\end{pmatrix} = (1/\sqrt{2})\begin{pmatrix}1 & 1\\1 & -1\end{pmatrix}\begin{pmatrix}|0+,0\rangle\\|0-,0\rangle\end{pmatrix} = \begin{pmatrix}|0\text{L},0\rangle\\|0\text{R},0\rangle\end{pmatrix}.$$

Following this idea, it can be shown that arbitrary unitary operations can be performed on the preceding qubit. For that purpose, we can use a universal set of one-qubit gates composed of the rotation gate and the phase gate which is defined by

$$\hat{U}_{\text{PHASE}}\begin{pmatrix}|0+,0\rangle\\|0-,0\rangle\end{pmatrix} = \begin{pmatrix}1 & 0\\0 & e^{i\varphi}\end{pmatrix}\begin{pmatrix}|0+,0\rangle\\|0-,0\rangle\end{pmatrix}.$$

The basic transformation on a two-qubit system is the controlled-not (CNOT) gate which permutes the state of the second qubit only if the first qubit is in state 1

$$\hat{U}_{\text{CNOT}}\begin{pmatrix}|00\rangle\\|01\rangle\\|10\rangle\\|11\rangle\end{pmatrix} = \begin{pmatrix}1 & 0 & 0 & 0\\0 & 1 & 0 & 0\\0 & 0 & 0 & 1\\0 & 0 & 1 & 0\end{pmatrix}\begin{pmatrix}|00\rangle\\|01\rangle\\|10\rangle\\|11\rangle\end{pmatrix}.$$

There are different ways of defining a two-qubit system in our example. According to the proposal of Sola *et al.* [22], we can choose excitation-parity or parity-excitation of the ϕ vibrator. This gives, respectively, the following definitions:

$$\begin{pmatrix}|00\rangle\\|01\rangle\\|10\rangle\\|11\rangle\end{pmatrix} = \begin{pmatrix}|0+,0\rangle\\|0-,0\rangle\\|1+,0\rangle\\|1-,0\rangle\end{pmatrix} \text{ or } \begin{pmatrix}|00\rangle\\|01\rangle\\|10\rangle\\|11\rangle\end{pmatrix} = \begin{pmatrix}|0+,0\rangle\\|1+,0\rangle\\|0-,0\rangle\\|1-,0\rangle\end{pmatrix}.$$

We explore also the usual realization of a two-qubit system using states of two ϕ and θ vibrators in the double well

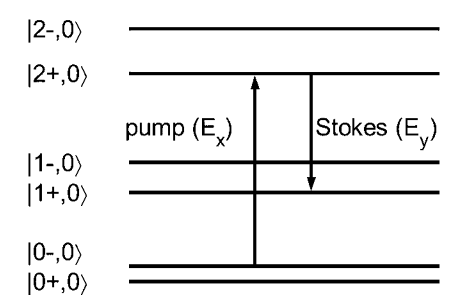
$$\begin{pmatrix}|00\rangle\\|01\rangle\\|10\rangle\\|11\rangle\end{pmatrix} = \begin{pmatrix}|0+,0\rangle\\|0+,1\rangle\\|0-,0\rangle\\|0-,1\rangle\end{pmatrix}.$$

In the next section, we will give examples of control which aim at implementing the Hadamard gate, the phase gate, and the CNOT gate.

A. One-qubit gate

1. Adiabatic process

More complex methods than f-STIRAP strategy have to be used for implementing qubit gates. For one-qubit gates, we follow schemes proposed in [56,57]. We only consider the phase gate. The Hadamard gate can be derived by using a similar strategy. The procedure is composed of two STIRAP processes which are aimed at transferring the population between states $|0-,0\rangle$ and $|1+,0\rangle$ via state $|2+,0\rangle$ which is not populated in the adiabatic limit. Only three pulses can be used because the second one serves as a pump field for the first STIRAP excitation and as a Stokes field for the second STIRAP process. The first part of the scheme can be viewed as follows:



The frequencies are chosen so that the different excitations are resonant, i.e., we have

$$\omega_x = E_{2+,0} - E_{1+,0},$$

$$\omega_y = E_{2+,0} - E_{0-,0},$$

where ω_x and ω_y are respectively the frequencies of the fields along the $\vec{e}_x$ and $\vec{e}_y$ directions. The phase of the first pulse is fixed to φ, the phase of the phase gate, whereas other phases are chosen to be zero. Note that other procedures with different phases can also be considered [56,57]. The eigenvector $|\psi_0\rangle$ of eigenvalue 0 of H_I in the basis $|0-,0\rangle$, $|1+,0\rangle$, and $|2+,0\rangle$ reads as follows during the first STIRAP excitation

$$|\psi_0\rangle = \frac{1}{\sqrt{\Omega_P^2+\Omega_S^2}}(\Omega_S|0-,0\rangle - \Omega_P e^{i\varphi}|1+,0\rangle),$$

and the second STIRAP

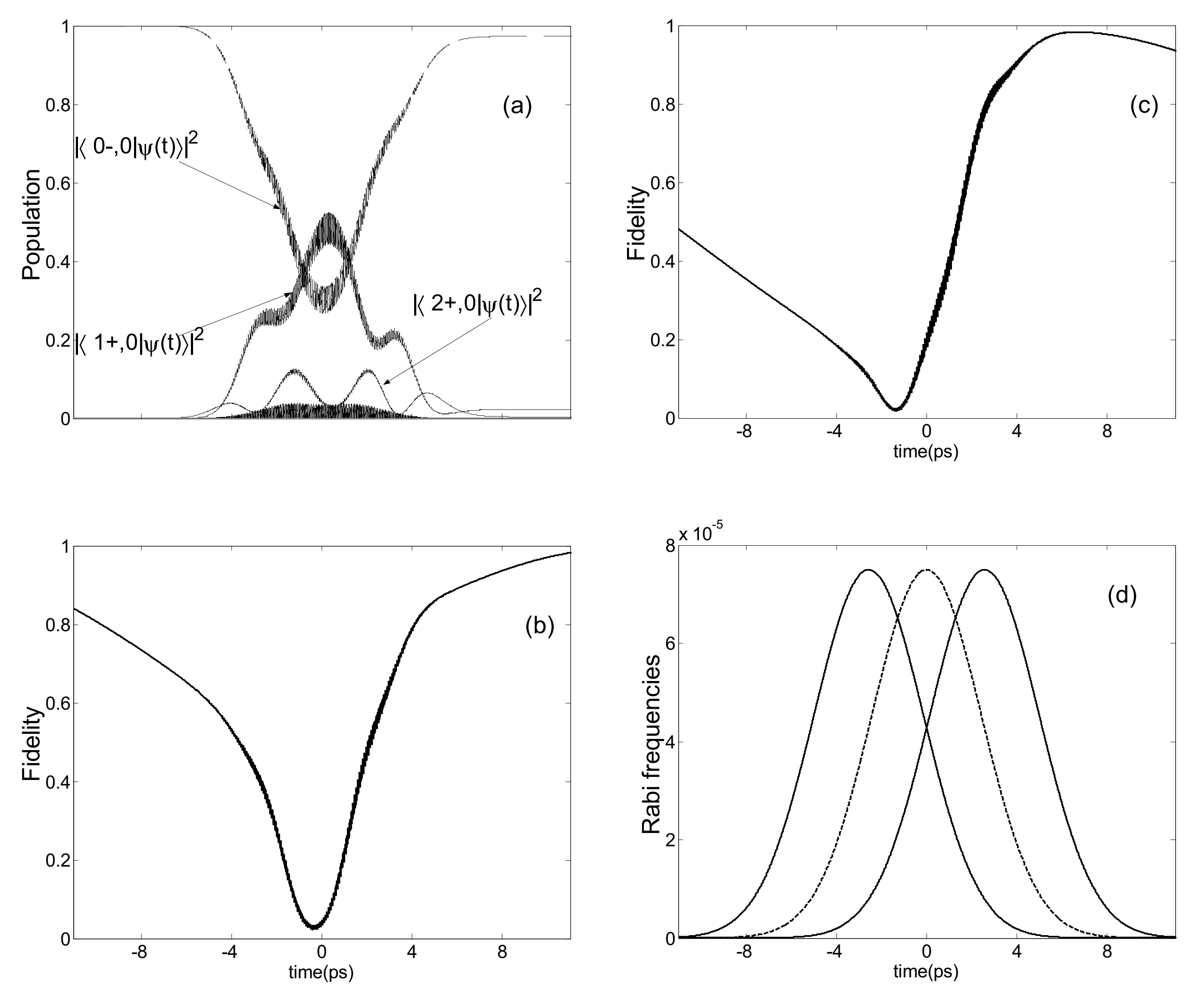


FIG. 11. The phase gate. Panel (a) displays the evolution of populations in the Hamiltonian eigenbasis during the phase gate transformation, the initial state is $|0-,0\rangle$. Panels (b) and (c) represent respectively the evolution of the fidelity for $\varphi=\frac{\pi}{4}$ and $\varphi=\frac{\pi}{2}$. Panel (d) shows the Rabi frequencies of the different pulses. The solid and dashed lines correspond respectively to the field E_x and the field E_y (see text).

$$|\psi_0\rangle = \frac{-e^{i\varphi}}{\sqrt{\Omega_P^2+\Omega_S^2}}(\Omega_S|1+,0\rangle - \Omega_P|0-,0\rangle).$$

In these expressions, the Rabi frequencies are assumed to be real and the dependence on the phase φ has been explicitly written in order to clarify the proof.

It has been more difficult to control and to optimize one qubit gates than processes involved in the double-well scenarios. This point is basically due to the fact that both populations and relative phases have to be controlled in a quantum gate. This difficulty is particularly relevant in this case because the levels of the qubit are not degenerate. The correct unitary transformation is therefore achieved by the adiabatic process only in the interaction representation and not in the bare state basis. The optimization allows to set up the relative phases. Very good results have nevertheless been obtained. Moreover, one of the advantages of adiabatic processes is that the same form of the overall field can be used to realize different quantum gates. This point is illustrated for the phase gate in Fig. 11. Modifying only the phase of the first pulse of the first STIRAP excitation and keeping constant other parameters, two phase gates for $\varphi=\frac{\pi}{4}$ and $\varphi=\frac{\pi}{2}$ have been built by our strategy.

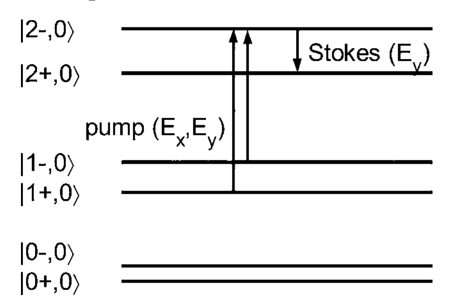
2. Optimal control

OCT confirms its efficiency in order to find fields of smaller duration. We have derived a field for the Hadamard gate on the $|0+,0\rangle$ and $|0-,0\rangle$ states with T=4.5 ps. The field is completely similar to the one used to realize the scheme (9). One obtains exactly the same behavior as shown in Fig. 6. This field is very simple and has been discussed in Sec. IV A. We have also checked that OCT can be used to implement the phase gate.

B. Two-qubit gate

1. Adiabatic process

We only consider the first CNOT gate involving the states $|0+,0\rangle$, $|0-,0\rangle$, $|1+,0\rangle$, and $|1-,0\rangle$. Similar processes can be constructed for other choices of qubits. The control scheme that can be used for the CNOT gate is a strategy similar in its spirit to the preceding process. We make a step further by considering now a superposition of states. The scheme can be represented as follows:



where three different pulses have been considered. The values of the frequencies for the pump pulses and the Stokes field are chosen resonant with the corresponding transition. We consider the subset of levels $|1+,0\rangle$, $|1-,0\rangle$, $|2+,0\rangle$, and $|2-,0\rangle$. In this basis, the total Hamiltonian H_I can be written as

$$\begin{pmatrix} 0 & 0 & 0 & \Omega_{1+} \\ 0 & 0 & 0 & \Omega_{1-} \\ 0 & 0 & 0 & \Omega_S \\ \Omega_{1+} & \Omega_{1-} & \Omega_S & 0 \end{pmatrix},$$

where the Rabi frequencies (with straightforward notations) are assumed to be real. Diagonalizing the matrix CNOT, we determine the corresponding eigenvectors involving the states $|1+,0\rangle$ and $|1-,0\rangle$. These eigenvectors denoted $|h_+\rangle$ and $|h_-\rangle$ of eigenvalues 1 and -1 can be defined as follows:

$$|h_+\rangle = \frac{1}{\sqrt{2}}(|1+,0\rangle + |1-,0\rangle),$$

$$|h_-\rangle = \frac{1}{\sqrt{2}}(|1+,0\rangle - |1-,0\rangle).$$

In the basis $|h_+\rangle$, $|h_-\rangle$, $|2+,0\rangle$, and $|2-,0\rangle$, H_I is given by

$$\begin{pmatrix} 0 & 0 & 0 & \Omega_+ \\ 0 & 0 & 0 & \Omega_- \\ 0 & 0 & 0 & \Omega_S \\ \Omega_+ & \Omega_- & \Omega_S & 0 \end{pmatrix},$$

where a straightforward calculation leads to the following relations:

$$\Omega_+ = \frac{1}{\sqrt{2}}(\Omega_{1+} + \Omega_{1-}),$$

$$\Omega_- = \frac{1}{\sqrt{2}}(\Omega_{1+} - \Omega_{1-}).$$

The idea is then to decouple the eigenvector $|h_+\rangle$ from other states of the basis. For instance, if we choose

$$\Omega_{1+} = \sqrt{2}\Omega_0 \text{ and } \Omega_{1-} = -\sqrt{2}\Omega_0, \quad \text{one obtains for } H_I$$

$$\begin{pmatrix} 0 & 0 & 0 & 0 \\ 0 & 0 & 0 & \Omega_0 \\ 0 & 0 & 0 & \Omega_S \\ 0 & \Omega_0 & \Omega_S & 0 \end{pmatrix}.$$

The last step consists in applying the scheme of the phase gate described above for a phase equal to π. In the adiabatic limit, $|h_+\rangle$ and $|h_-\rangle$ will be respectively transformed into $|h_+\rangle$ and $-|h_-\rangle$ which corresponds to the transformation of the CNOT gate.

Figure 12 shows the results of this strategy. We have obtained a fidelity close to 0.95. The fact that the levels of the two qubits are not degenerate implies a quick loss of the fidelity of the order of 1 ps which seems problematic in view of experimental applications. We emphasize that this behavior can be observed in most of quantum gates constructed from vibrationally excited states. It is a disadvantage of this kind of system in comparison of other schemes such as optical cavity [56,58] where all states are degenerate or almost degenerate.

2. Optimal control

We present only the gate CNOT on the two qubits using fundamental and first excited states of two ϕ and θ vibrators in the double well. We impose the pulse duration $T=4.5$ ps. Figure 13 displays the time evolution of the population when each initial state $|00\rangle=|0+,0\rangle$, $|01\rangle=|0+,1\rangle$, $|10\rangle=|0-,0\rangle$, and $|11\rangle=|0-,1\rangle$ is driven by the optimum field which has been obtained with 21 iterations. Panels (a) and (b) show the inversion of population of the states of the second qubit. Gray lines display intermediate populations of the different eigenstates. Panels (c) and (d) show the population of the first qubit states. The final value is again equal to one at the end of the process even if intermediate depopulation occurs.

The optimal field obtained for this CNOT gate is given in Fig. 14. Only the E_x component is used by the OCT. The maximum of the weak E_y component is of the order of 1.5×10^{-3} V cm^{-1}. The field is again very simple. The Gabor transform [Eq. (21)] shows that a main frequency 1916 cm^{-1} corresponding to the $|0-,0\rangle \rightarrow |0-,1\rangle$ transition acts during the whole process.

VI. CONCLUDING REMARKS

This paper has focused on the application of OCT and adiabatic processes to various situations that can be encountered when a potential energy surface presents a bifurcating region connecting three potential wells (isomerization, tunneling, and implementation of one or two qubits quantum gates). In the present case, the symmetric double well region

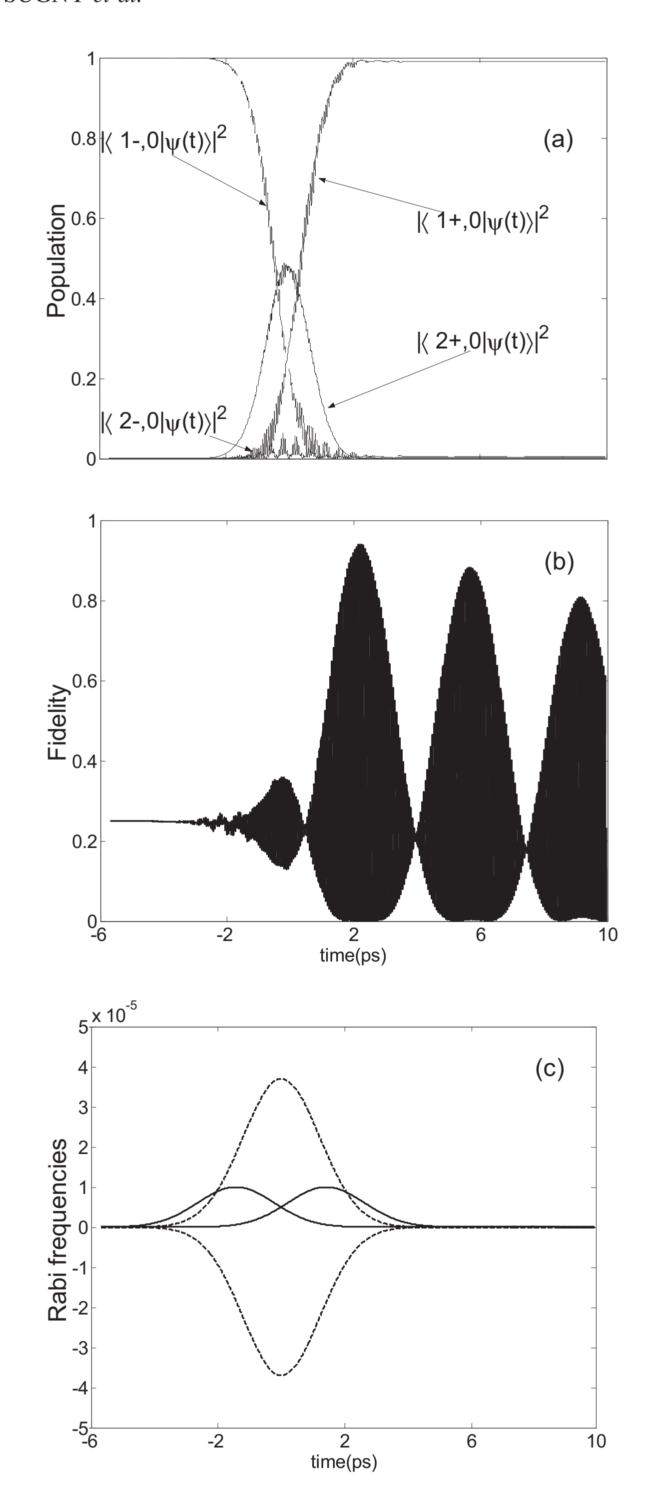


FIG. 12. Same as Fig. 11 but for the CNOT gate involving the states $|0+,0\rangle$, $|0-,0\rangle$, $|1+,0\rangle$, and $|1-,0\rangle$.

is the most favorable to realize control scenarios due to the shape of the dipolar momentum surface. The results are expected to be transposable to other molecules such as H_2POSH presenting the same kind of double well region.

We have also investigated the advantages and limits of the different methods. We recall that the goal of a control is to reach a defined objective, the field solution being subject to some physical constraints: on its duration and its intensity in order to avoid other unwanted chemical processes and on its form and its robustness in view of experimental applications. Some of these constraints are respected by adiabatic processes (simplicity of the form, robustness) and the other by laser pulses determined from OCT (short duration with reasonable intensity). The question which naturally arises is then which strategy is used in a given practical situation. Some problems may seem trivial because they consist basically in a jump between two wells. However, as it is the case for our scheme (20), the structure of the eigenvectors and of the dipolar matrix may generate difficulties and hinder the use of STIRAP. The application of adiabatic processes looks particularly problematic if a small number of levels with small coupling to background states cannot be selected. OCT seems to be the more efficient approach even if, as can be shown in Sec. IV B, there is no guarantee to reach the objective of the control, particularly when the dipole moment is rather flat in a given well. Moreover, if a solution exists there is no more guarantee on the robustness of the optimal field.

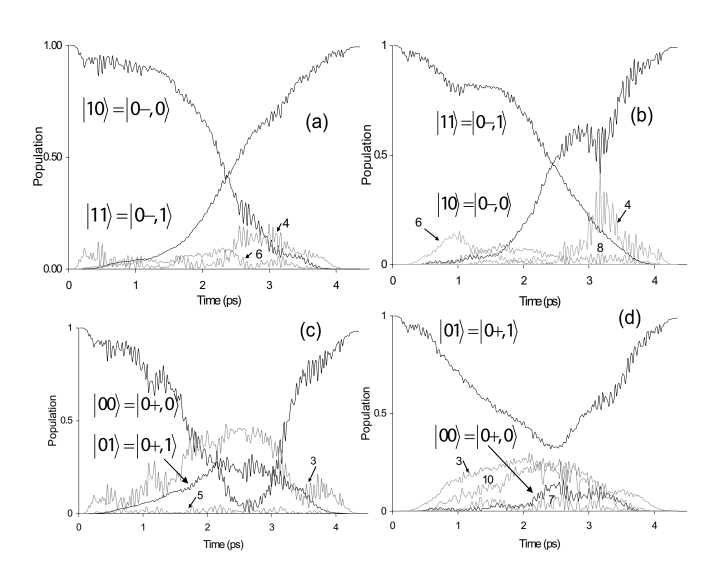


FIG. 13. CNOT gate on the $|0+,0\rangle, |0-,0\rangle, |0+,1\rangle, |0-,1\rangle$ states. Black lines: population of the states of the two-qubit system, gray lines: intermediate transitions towards other eigenstates which are denoted from 3 to 10 and nearly correspond to excitation of the even and odd states of the ϕ vibrator only. The θ vibrator remains in its ground state with no node along θ.

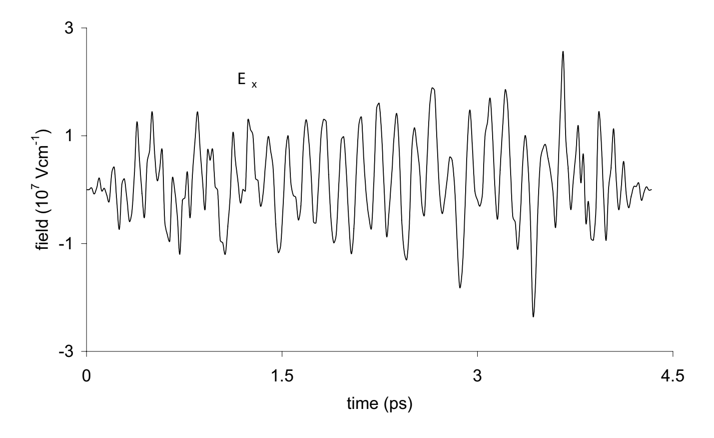


FIG. 14. OCT field for the CNOT gate on the $|0+,0\rangle, |0-,0\rangle, |0+,1\rangle, |0-,1\rangle$ states.

For more simple scenarios of control (double well, qubit gates), several solutions have been obtained, but with different features. In the case of adiabatic processes, one observes that the duration of the overall pulse can be sufficiently reduced (of the order of few picoseconds) by an optimization procedure which also decreases the robustness of the process (Sec. IV A). For quantum gates where both populations and relative phases have to be controlled, we notice that the reduction of this time and the optimization are more difficult. One of the great advantages of adiabatic processes as compared to OCT is the simplicity of the form of the pulse, the price to pay being generally larger duration and intensity. This is not systematically true as can be shown for the Hadamard gate where a very simple optimal field has been derived (Sec. V A) by OCT. We have checked the robustness of this latter field and found it to be very good, whereas this is not the case for optimal pulses with more complex structures. Following this example, it seems possible to establish a link between the simplicity of the optimal field and its robustness. We plan to test this conjecture in other molecules in the near future. Finally, we have focused here on dynamics in reduced dimensionality. It is obvious that the larger the pulse duration is the more dubious this approximation will be. Our next step will be the consideration of coupling with an environment.

ACKNOWLEDGMENTS

We thank Professor M. Persico, Professor H. Jauslin, Dr. S. Guérin, Dr. C. Koch, Dr. D. Lauvergnat, and Dr. F. Remacle for helpful discussions. Dr. G. Dive is research associate of the FNRS of Belgium. The computing facilities of IDRIS (Project numbers 061247 and 2006 0811429) as well the financial support of the FNRS in the University of Liège SGI Nic project are gratefully acknowledged.

APPENDIX

This Appendix gives the analytical expression of the dipole moment that has been used in our calculations. We first define the function μ_{CS} as an approximation of the μ_x in C_S plane (ϕ=0)

$$\mu_{cs}(\theta) = \sum_{k=0}^{4} a_k \cos^k(\theta),$$

where the parameters are given by a_0=0.7, a_1=1.1, a_2=0.5, a_3=−1, a_4=−1.11. The two active coordinates of the dipole moment are then equal to

$$\mu_x(\theta,\phi) = \mu_{cs}(\theta)[f_1(\theta)\cos(\phi) + f_2(\theta)(0.25\cos^2(\phi) + 1.75\cos(\phi) - 1)],$$

$$\mu_y(\theta,\phi) = \mu_{cs}(\theta)[f_3(\theta)\sin(\phi)],$$

where

$$f_1(\theta) = \frac{1}{2}\mathrm{arctg}\left[-3\left(\theta - \frac{\pi}{2}\right)\right] + 0.9,$$

$$f_2(\theta) = \frac{1}{2}\mathrm{arctg}\left[3\left(\theta - \frac{\pi}{2}\right)\right] + 0.9,$$

$$f_3(\theta) = \frac{1}{2}\mathrm{arctg}\left[3\left(\theta - \frac{\pi}{2}\right)\right] + 2.4.$$

[1] M. Dantus and V. V. Lozovoy, Chem. Rev. (Washington, D.C.) **104**, 1813 (2004).

[2] M. Shapiro and P. Brumer, *Principles of Quantum Control of Molecular Processes* (Wiley, New York, 2003).

[3] P. Brumer and M. Shapiro, Annu. Rev. Phys. Chem. **43**, 257 (1992); M. Shapiro and P. Brumer, Rep. Prog. Phys. **66**, 859 (2003).

[4] D. Tannor and S. A. Rice, J. Chem. Phys. **83**, 5013 (1985); D. Tannor, R. Kosloff, and S. A. Rice, J. Chem. Phys. **85**, 5805 (1986).

[5] V. S. Malinovsky, C. Meier, and D. J. Tannor, Chem. Phys. **221**, 67 (1997).

[6] R. S. Judson and H. Rabitz, Phys. Rev. Lett. **68**, 1500 (1992).

[7] W. Zhu, J. Botina, and H. Rabitz, J. Chem. Phys. **108**, 1953 (1998).

[8] W. Zhu and H. Rabitz, J. Chem. Phys. **109**, 385 (1998).

[9] Y. Ohtsuki, G. Turinici, and H. Rabitz, J. Chem. Phys. **120**, 5509 (2004).

[10] U. Gaubatz, P. Rudecki, S. Schiemann, and K. Bergmann, J. Chem. Phys. **92**, 5363 (1990).

[11] N. V. Vitanov, T. Halfmann, B. Shore, and K. Bergmann, Annu. Rev. Phys. Chem. **52**, 763 (2001).

[12] S. Guérin and H. R. Jauslin, Adv. Chem. Phys. **125**, 147 (2003).

[13] N. V. Vitanov, K. A. Suominen, and B. W. Shore, J. Phys. B **32**, 4535 (1999).

[14] K. Hoki, Y. Ohtsuki, and Y. Fujimura, J. Chem. Phys. **114**, 1575 (2001).

[15] M. V. Korolkov, J. Manz, and G. K. Paramonov, J. Chem. Phys. **100**, 10874 (1996).

[16] H. Umeda, M. Takagi, S. Yamada, S. Koseki, and Y. Fujimura, J. Am. Chem. Soc. **124**, 9265 (2002).

[17] N. Došlić, K. Sundermann, L. González, O. Mó, J. Giraud-Girard, and O. Kühn, Phys. Chem. Chem. Phys. **1**, 1249 (1999); O. Kühn, Y. Zhao, F. Shuang, and Y. Yan, J. Chem. Phys. **112**, 6104 (2000); O. Kühn, J. Phys. Chem. A **106**, 7671 (2002).

[18] C. M. Tesch, L. Kurtz, and R. de Vivie-Riedle, Chem. Phys. Lett. **343**, 633 (2001).

[19] C. M. Tesch and R. de Vivie-Riedle, Phys. Rev. Lett. **89**, 157901 (2002).

[20] B. M. R. Korff, U. Troppmann, K. L. Kompa, and R. de Vivie-Riedle, J. Chem. Phys. **123**, 244509 (2005).

[21] D. Babikov, J. Chem. Phys. **121**, 7577 (2004).

[22] U. Troppmann and R. de Vivie-Riedle, J. Chem. Phys. **122**, 154105 (2005).

[23] T. Cheng and A. Brown, J. Chem. Phys. **124**, 034111 (2006).
[24] I. R. Sola, V. S. Malinovsky, J. Santamaria, J. Chem. Phys. **120**, 10955 (2004).
[25] B. Lasorne, G. Dive, D. Lauvergnat, and M. Desouter-Lecomte, J. Chem. Phys. **118**, 5831 (2003).
[26] T. Taketsugu, N. Tajima, and K. Hirao, J. Chem. Phys. **105**, 1933 (1996); T. Taketsugu and Y. Kumeda, *ibid.* **114**, 6973 (2001).
[27] M. V. Basilevsky, Chem. Phys. **24**, 81 (1977); M. V. Basilevsky, Theor. Chim. Acta **72**, 63 (1987).
[28] J. Baker and P. M. W. Gill, J. Comput. Chem. **9**, 465 (1988).
[29] M. Hirsch, W. Quapp, and D. Heidrich, Phys. Chem. Chem. Phys. **1**, 5291 (1999); W. Quapp and V. Melnikov, *ibid.* **3**, 2735 (2001); W. Quapp, M. Hirsch, and D. Heidrich, Theor. Chem. Acc. **112**, 40 (2004).
[30] R. Palmeiro, L. M. Frutos, and O. Castaño, Int. J. Quantum Chem. **86**, 422 (2002).
[31] T. Taketsugu and Y. Kumeda, J. Chem. Phys. **114**, 6973 (2001).
[32] B. Lasorne, G. Dive, and M. Desouter-Lecomte, J. Chem. Phys. **122**, 184304 (2005).
[33] D. Lauvergnat and A. Nauts, J. Chem. Phys. **116**, 8560 (2002).
[34] M. D. Feit, J. A. Fleck, and A. Steiger, J. Comput. Phys. **47**, 412 (1982).
[35] P. Van Leuven and M. Persico, J. Chem. Phys. **124**, 054319 (2006).
[36] F. L. Yip, D. A. Mazziotti, and H. Rabitz, J. Phys. Chem. A **107**, 7264 (2003).
[37] S. Gräfe, C. Meier, and V. Engel, J. Chem. Phys. **122**, 184103 (2005).
[38] M. Sugawara, J. Chem. Phys. **118**, 6784 (2003).
[39] K. Sundermann and R. de Vivie-Riedle, J. Chem. Phys. **110**, 1896 (1999).
[40] J. P. Palao and R. Kosloff, Phys. Rev. Lett. **89**, 188301 (2002).
[41] C. M. Tesch and R. de Vivie-Riedle, J. Chem. Phys. **121**, 12158 (2004).
[42] V. Kurkal and S. A. Rice, Chem. Phys. Lett. **344**, 125 (2001).
[43] I. Vrabel and W. Jakubetz, J. Chem. Phys. **118**, 7366 (2003).
[44] Y. Fujimura, L. González, K. Hoki, J. Manz, and Y. Ohtsuki, Chem. Phys. Lett. **306**, 1 (1999).
[45] M. Amniat-Talab, S. Guérin, N. Sangouard, and H. R. Jauslin, Phys. Rev. A **71**, 023805 (2005).
[46] T. Wang, M. Kostrun, and S. F. Yelin, Phys. Rev. A **70**, 053822 (2004).
[47] N. Sangouard, S. Guérin, M. Amniat-Talab, and H. R. Jauslin, Phys. Rev. Lett. **93**, 223602 (2004).
[48] F. Ticozzi, A. Ferrante, and M. Pavon, IEEE Trans. Autom. Control **49**, 1742 (2004).
[49] C. M. Dion, A. Keller, and O. Atabek, Eur. Phys. J. D **14**, 249 (2001).
[50] D. Sugny, A. Keller, O. Atabek, D. Daems, C. M. Dion, S. Guérin, and H. R. Jauslin, Phys. Rev. A **71**, 063402 (2005).
[51] A. Matos-Abiague and J. Berakdar, Appl. Phys. Lett. **84**, 2346 (2004).
[52] D. Sugny, A. Keller, O. Atabek, D. Daems, S. Guérin, and H. R. Jauslin, Phys. Rev. A **69**, 043407 (2004).
[53] N. Doslic, O. Kühn, J. Manz, and K. Sundermann, J. Phys. Chem. A **102**, 9645 (1998).
[54] M. Sugawara and Y. Fujimura, J. Chem. Phys. **100**, 5646 (1994).
[55] M. A. Nielsen and I. L. Chuang, *Quantum Computation and Quantum Information* (Cambridge University Press, Cambridge, U. K., 2000).
[56] Z. Kis and F. Renzoni, Phys. Rev. A **65**, 032318 (2002).
[57] H. Goto and K. Ichimura, Phys. Rev. A **70**, 012305 (2004).
[58] T. Pellizari, S. A. Gardiner, J. I. Cirac, and P. Zoller, Phys. Rev. Lett. **75**, 3788 (1995).

5.3 Monotonically convergent optimal control theory

Corresponding articles : [8, 13, 18, 20, 22]
This work has been done in collaboration with G. Turinici and J. Salomon of the *CEREMADE, Université Paris Dauphine*, M. Lapert (PhD student in Dijon) and with the group of M. Desouter-Lecomte for the applications to the control of chemical systems.

In this section, we present the principles of monotonically convergent algorithms (MCA) used to solve optimal control problems in quantum mechanics. The first applications of optimal control theory in the control of quantum dynamics began in the late 80's [78, 92]. Steady advances have been achieved in this field until today. One of the major progress was the introduction of MCA and their generalizations to include dissipation and to account for multiple control objectives. These algorithms have been largely used in the chemical-physics literature since the pioneering papers of Tannor et al. [111] and Rabitz et al. [126] based on the work of Krotov. A recent general formulation has been presented in [85]. The proof of convergence has been established in [105, 86] under some general conditions satisfied by control problems in quantum mechanics.

We consider a quantum system whose dynamics is governed by the time-dependent Schrödinger equation written here in atomic units :

$$i\frac{\partial}{\partial t}|\psi(t)\rangle = (H_0 - \mu E(t))|\psi(t)\rangle$$

where H_0 is the field-free Hamiltonian of the dynamics, the operator μ describes the interaction between the quantum system and the laser field and $E(t)$ is the electric field. The initial state of the dynamics is $|\varphi_0\rangle$ and the target state is $|\varphi_f\rangle$. We consider examples where the dimension of the Hilbert space is finite.

We use the optimal control framework to determine the control field [47]. We introduce a cost functional J to be maximized by the field E :

$$J(E) = 2\Re[\langle\psi(t_f)|\varphi_f\rangle] - \alpha\int_0^{t_f} E(t)^2 dt$$

where α is a positive real constant (which can be time-dependent) expressing the relative weights of the two terms of J. The time t_f is the control duration.

One sees that to maximize J, the control field has to maximize the projection onto the final state and minimize the energy of the field. Achieving a better projection comes at the price of an increase of the laser fluence, so the optimal solution finds an equilibrium between the two objectives, i.e. a low laser energy and a final state close to the target one. Note that other cost functionals could be chosen maximizing for instance the mean value of a given observable.

The maximum of J is a critical point of the augmented cost functional

$$\bar{J}(E) = J(E) - 2\Im[\int_0^{t_f} \langle\chi(t)|(i\frac{\partial}{\partial t} - H_0 + \mu E(t))|\psi(t)\rangle]$$

where $|\chi(t)\rangle$ is a Lagrange multiplier called an adjoint state which enforces the dynamics to follow the Schrödinger equation. Setting the variations of $\bar{J}$ with respect to $|\psi(t)\rangle$, $|\chi(t)\rangle$ and $E(t)$ to 0 leads to the following relations satisfied by the critical point :

$$\begin{array}{l} \alpha E(t) + \Im[\langle\chi(t)|\mu|\psi(t)\rangle] = 0 \\ (i\frac{\partial}{\partial t} - H_0 + \mu E(t))|\psi(t)\rangle = 0,\ |\psi(0)\rangle = |\varphi_0\rangle \\ (i\frac{\partial}{\partial t} - H_0 + \mu E(t))|\chi(t)\rangle = 0,\ |\chi(T)\rangle = |\varphi_f\rangle \end{array} .$$

There are different ways to solve numerically these equations such as the gradient methods [47] or the monotonically convergent algorithms (MCA). MCA are efficient strategies which guarantee to improve the cost functional J at each iteration.

MCA can be described as follows. We assume at step $k \geq 1$ of the algorithm that the system is described by a triplet $(|\psi_k(t)\rangle, |\chi_{k-1}(t)\rangle, E_k(t))$ where $|\psi_k(t)\rangle$ is the state of the system, $|\chi_k(t)\rangle$ the adjoint state and $E_k(t)$ the electric field associated to the forward propagation of $|\psi_k(t)\rangle$ and the backward propagation of $|\chi_k(t)\rangle$. We impose the initial condition $|\psi_k(0)\rangle = |\varphi_0\rangle$ and the final one $|\chi_k(t_f)\rangle = |\varphi_f\rangle$. The iteration is initiated by the trial field $E_0(t)$. At step 0 of the algorithm, we propagate forward $|\psi_0\rangle$ and backward $|\chi_0\rangle$ with E_0. We also introduce an intermediate cost functional J_k which is defined by :

$$J_k(E_k) = 2\Re[\langle\psi_k(t_f)|\varphi_f\rangle] - \alpha\int_0^{t_f} E_k(t)^2 dt.$$

The triplet $(|\psi_{k+1}(t)\rangle, |\chi_k(t)\rangle, E_{k+1}(t))$ is determined from the triplet at step k by requiring that $\Delta J = J_{k+1} - J_k \geq 0$. We have :

$$\Delta J = 2\Re[\langle\psi_{k+1}(t_f) - \psi_k(t_f)|\varphi_f\rangle] - \alpha\int_0^{t_f} (E_{k+1}^2 - E_k^2)dt.$$

Using the fact that

$$\langle \psi_{k+1}(t_f) - \psi_k(t_f)|\varphi_f\rangle = \langle \psi_{k+1}(t_f) - \psi_k(t_f)|\chi_k(t_f)\rangle$$
$$= \int_0^{t_f} \langle \psi_{k+1} - \psi_k|\frac{\partial}{\partial t}\chi_k\rangle + \langle \frac{\partial}{\partial t}(\psi_{k+1} - \psi_k)|\chi_k\rangle$$

and the two Schrödinger equations satisfied by $|\psi(t)\rangle$ and $|\chi(t)\rangle$, one deduces that

$$\Delta J = \alpha \int_0^{t_f} dt[(E_k - E_{k+1})(E_k + E_{k+1} + \frac{2}{\alpha}\Im\langle\chi_k|\mu|\psi_{k+1}\rangle)].$$

If we choose now E_{k+1} as a solution of

$$E_{k+1} - E_k = -\lambda(E_{k+1} + E_k + \frac{2}{\alpha}\Im\langle\chi_k|\mu|\psi_{k+1}\rangle)$$

then it is straightforward to see that $\Delta J \geq 0$. The new electric field E_{k+1} is given by

$$E_{k+1}(t) = \frac{1-\lambda}{1+\lambda}E_k(t) + \frac{2\lambda}{1+\lambda}\Im[\langle\chi_k|\mu|\psi_{k+1}\rangle].$$

The structure of the algorithm can be summarized as follows. At step $k+1$ of the algorithm, we propagate backward the adjoint state $|\chi_k(t)\rangle$ with the field E_k, we then propagate forward the state $|\psi_{k+1}\rangle$ computing at the same time the electric field E_{k+1} using the previous equation.

One of the advantages of MCA is their flexibility, in the sense that they can be adapted to non-standard situations. Among others, we can cite the question of the non-linear interaction with the control field [91] and the question of spectral constraints on the field [63]. We have proposed two new formulations of MCA in [8, 13] to solve these open problems.

In [13], for the case of a nonlinear interaction, the monotonic behavior of the algorithm is ensured by a particular choice of the cost which is no more quadratic in the control field but depends on the degree of the nonlinearity. This article is reproduced below. In [8], we have shown how to take into account spectral constraints in MCA. The new formulation is built on the standard framework but at each iteration, the field is taken as a linear combination of the field given by the standard algorithm and its filtered version. The parameter of the linear combination is computed numerically to ensure the monotonic behavior of the algorithm. These two algorithms have been applied to the control of molecular orientation and alignment where such situations appear naturally when the intensity of the electric field is sufficiently large or to determine an optimal solution that could be implemented experimentally by pulse shaping techniques.

In [18, 20, 22], MCA have been used to control intramolecular reactions and to implement quantum gates with or without dissipation. For such complex systems, the algorithm succeeds in constructing an efficient solution but the control field obtained is in general very complicated.

Monotonically convergent optimal control theory of quantum systems under a nonlinear interaction with the control field

M. Lapert,[1] R. Tehini,[1] G. Turinici,[2] and D. Sugny[1,*]

[1]*Institut Carnot de Bourgogne, UMR 5209 CNRS, Université de Bourgogne, 9 Avenue A. Savary, Boîte Postale 47870, F-21078 Dijon Cedex, France*

[2]*CEREMADE, Université Paris Dauphine, Place du Maréchal De Lattre De Tassigny, 75775 Paris Cedex 16, France*

(Received 14 May 2008; published 18 August 2008)

We consider the optimal control of quantum systems interacting nonlinearly with an electromagnetic field. We propose monotonically convergent algorithms to solve the optimal equations. The monotonic behavior of the algorithm is ensured by a nonstandard choice of the cost, which is not quadratic in the field. These algorithms can be constructed for pure- and mixed-state quantum systems. The efficiency of the method is shown numerically for molecular orientation with a nonlinearity of order 3 in the field. Discretizing the amplitude and the phase of the Fourier transform of the optimal field, we show that the optimal solution can be well approximated by pulses that could be implemented experimentally.

DOI: 10.1103/PhysRevA.78.023408 PACS number(s): 32.80.Qk, 37.10.Vz, 78.20.Bh

I. INTRODUCTION

The control of quantum dynamics induced by an intense laser field continues to be a challenge to both experiment and theory [1–3]. In this context, optimal control theory (OCT) is an efficient tool for designing laser pulses able to control quantum processes [4–14]. By construction, the optimal field is the field steering a dynamical system from the initial state to a desired target state and minimizing a cost functional which generally penalizes the energy or the duration of the field. Different methods have been developed to solve the optimal equations [11,15]. Among others, monotonically convergent iterative schemes proposed by Tannor *et al.* [16] and Rabitz *et al.* [4,17,18] have been applied with success to a variety of physical and chemical processes [4,19–22]. These algorithms have the particularity of guaranting the increase of the cost functional at each step of iteration. In this paper, we will consider the Rabitz formulation of iterative algorithms [17]. First introduced to treat pure-state quantum systems, these schemes have been extended and applied to mixed-state quantum systems, dissipative ones [7,8], and non-Markovian dynamics [23]. A majority of works has considered a linear interaction between the quantum system and the electromagnetic field. This linear interaction corresponds, for molecular systems, to the first-order dipolar approximation (permanent dipole moment). Due to the intensity of the field or to the particular structure of the problem, some systems need to go beyond this approximation [24–27]. A typical example is given by the control of molecular orientation and alignment of a linear molecule by nonresonant laser pulses [24,27–29]. When averaging over the rapid oscillations of the field, one observes that the permanent dipole moment plays no role in the control of the dynamics. In this case, molecular alignment and orientation are obtained via the polarizability and the hyperpolarizability terms of the interaction Hamiltonian (see [30] for information on the controllability of these systems). From a methodological point of view, the natural question arises of whether one can apply monotonically convergent algorithms to such systems interacting nonlinearly with the field.

The goal of this work is to answer this question by proposing monotonic algorithms when an arbitrary nonlinearity is considered. A key ingredient to ensure the monotonic convergence of the algorithms is to consider a nonstandard cost functional which instead of penalizing the intensity of the field, i.e., the square of the electric field, penalizes a higher exponent which depends on the order of the nonlinearity. Note that a similar question has been treated in [12]. A family of algorithms different from those proposed in this paper has been developed. In the algorithms of [12], the cost is quadratic in the field and the control is decomposed into n components for a nonlinearity of order n. Thus, for each iteration of the algorithm, $2n$ numerical resolutions of the time-dependent Schrödinger equation are required: n for the wave function and n for the Lagrange multiplier. On the contrary, in this work, we use only one component for the control field but at the price of modifying the cost functional. We construct monotonically convergent algorithms for pure- and mixed-state quantum systems, but they can be generalized straightforwardly to dissipative dynamics. We test the efficiency of these algorithms on the orientation dynamics of a linear molecule with nonlinearity of order 3, corresponding to the hyperpolarizability terms of the molecule [27]. We use as target states the states that maximize the orientation in a finite-dimensional restriction of the Hilbert space. Several works have pointed out the role of these target states, which optimize both the field-free orientation and its duration [31–34]. Promising results have been obtained for both pure- and mixed-state quantum systems corresponding to zero and nonzero temperatures.

Finally, we also analyze the structure of the Fourier transform of optimal control pulses. Our aim is to show that the optimal solutions can be well approximated by pulses that could be implemented experimentally [35–38]. Such pulses, tailored by genetic algorithms, have been successfully applied for experimentally and theoretically controlling different molecular processes [36–41]. In the frequency domain,

*dominique.sugny@u-bourgogne.fr

they are characterized by the fact that both the amplitude and the phase of the Fourier transform (but only for a finite number of frequencies equally distributed over a given frequency interval) are optimized [39–41]. This choice corresponds to the types of pulses that can be implemented by liquid crystal pulse shapers. As an alternative, we use in this paper the results of our monotonic optimization algorithms to construct such pulses. Note that we do not adopt filtering techniques in the iterative algorithm, which have been proposed in several works (see [11] and references therein). The idea consists generally in applying a filter to the control field at each iteration in order to satisfy spectral constraints. This filtering has the drawback that it does not generally yield a monotonic convergence of the algorithm. Instead, we propose to use a simpler solution. Starting from the optimal solution obtained by the monotonic algorithm, we discretize the phase and the amplitude of its Fourier transform into 640 points or less (640 points correspond to the number of pixels usually used in pulse-shaping experiments). From this discretization, we then construct a piecewise constant Fourier transform and a new time-dependent electric field by an inverse Fourier transform [40,41]. We finally compare the optimal result and the one obtained with the discretized field. We show that the difference between the two results is negligible when the structure of the optimal field is sufficiently simple, or equivalently when the number of pixels is sufficiently large.

This paper is organized as follows. We first present the model system in Sec. II A. We determine in Sec. II B the polynomial equation that must be satisfied by the optimal field. We then outline in Sec. II C the principle of monotonically convergent algorithms for nonlinear interaction in both pure- and mixed-state cases. Special attention is paid to the different choices and to the flexibility of the method. Generalizing the proofs of Refs. [17,22], we show the monotonic behavior of the algorithms. Section III is devoted to the application of these strategies to molecular orientation. The results are presented at $T=0$ K (Sec. III B) and $T\neq 0$ K (Sec. III E) for the standard case (i.e., with a linear interaction term) and at $T=0$ K for the averaging case (Sec. III C). We also propose an algorithm well suited to the simultaneous optimization of two laser fields. An example is given by the nonresonant control of molecular orientation by two-color laser pulses [27]. We finally examine in Sec. III D the structure of the Fourier transform of the optimal fields.

II. OPTIMAL CONTROL THEORY

The goal of this section is to propose monotonically convergent algorithms suited to quantum systems interacting nonlinearly with the control field. To simplify the discussion, we consider the case of pure-state quantum systems. Following Ref. [8] and the formalism of superoperators, the proof can be straightforwardly extended to mixed-state quantum systems (see for that purpose Sec. III E). Optimal control theory is invoked in order to maximize the projection onto a target state, but it could be equivalently defined for maximizing the expectation value of a given observable. The proof is a generalization of the standard proof for linear interaction [17] and of the proof given in Ref. [22].

A. The model system

We consider a quantum system interacting with an electromagnetic field whose dynamics is governed by the following time-dependent Schrödinger equation

$$i\frac{\partial}{\partial t}|\psi(t)\rangle = \hat{H}(t)|\psi(t)\rangle, \tag{1}$$

which is written in units such that $\hbar=1$. The Hamiltonian $\hat{H}(t)$ of the system is given by

$$\hat{H}(t) = \hat{H}_0 - \hat{\mu}E(t) - \hat{\alpha}E(t)^2 - \hat{\beta}E(t)^3 \cdots, \tag{2}$$

where $\hat{H}_0$ is the field-free Hamiltonian. The other terms describe the interaction between the system and the laser field $E(t)$. This interaction is written as a polynomial expansion in $E(t)$ whose coefficients are the operators $\hat{\mu},\hat{\alpha},\hat{\beta},\ldots$. For a linear molecule interacting with a linearly polarized laser field, the different operators $\hat{\mu}$, $\hat{\alpha}$, and $\hat{\beta}$ are associated with the permanent dipole moment μ_0, the polarizability components $\alpha_\parallel$ and $\alpha_\perp$, and the hyperpolarizability components $\beta_\parallel$ and $\beta_\perp$ of the molecule [27]. These different molecular constants will be used in the numerical computations of Sec. III.

B. Critical point

Let $|\phi_0\rangle$ and $|\phi_f\rangle$ be the initial and the target states of the control. We denote by t_f the duration of the control. We define the optimal control theory through the following cost functional:

$$J = |\langle\phi_f|\psi(t_f)\rangle|^2 - \int_0^{t_f} \lambda E(t)^{2n} dt, \tag{3}$$

where n is a positive integer. The even exponent of the integrand and the choice $\lambda \geqslant 0$ ensure the negativity of the second term of Eq. (3). n is taken equal to 1 for a linear interaction but we will see that, in order to obtain monotonic algorithms, larger values of n have to be considered when the system interacts nonlinearly with the field. λ is a penalty factor which weights the importance of the laser fluence. Following [42], we will replace in Sec. III this constant by $\lambda/s(t)$, where $s(t)=\sin^2(\pi t/t_f)$, which penalizes more strongly the amplitude of the pulse at the beginning and at the end of the control. This allows us to obtain more realistic optimal solutions.

We introduce the augmented cost functional $\bar{J}$, which is defined through the adjoint state $|\chi(t)\rangle$ as follows:

$$\bar{J} = |\langle\phi_f|\psi(t_f)\rangle|^2 - \int_0^{t_f} \lambda E(t)^{2n} dt - 2\,\mathrm{Im}\left[\langle\psi(t_f)|\phi_f\rangle\int_0^{t_f}\langle\chi(t)|\left(i\frac{\partial}{\partial t} - \hat{H}\right)|\psi(t)\rangle dt\right], \tag{4}$$

where Im denotes the imaginary part. The optimal electric field is the solution of the equation

$$\frac{\delta \bar{J}}{\delta E(t)} = 0, \tag{5}$$

which is a polynomial equation in $E(t)$:

$$2n\lambda E(t)^{2n-1} + 2\,\mathrm{Im}[\langle \psi(t_f)|\phi_f\rangle\langle \chi(t)|\hat{\mu} + 2\hat{\alpha}E(t) + 3\hat{\beta}E(t)^2|\psi(t)\rangle] = 0. \tag{6}$$

The second term of Eq. (6) can be modified by using the fact that

$$\frac{d}{dt}\langle \psi(t)|\chi(t)\rangle = 0. \tag{7}$$

The equation for the optimal field finally reads

$$2n\lambda E(t)^{2n-1} + 2\,\mathrm{Im}[\langle \psi(t)|\chi(t)\rangle\langle \chi(t)|\hat{\mu} + 2\hat{\alpha}E(t) + 3\hat{\beta}E(t)^2|\psi(t)\rangle] = 0. \tag{8}$$

Setting the variations of $\bar{J}$ with respect to $|\psi(t)\rangle$ and $|\chi(t)\rangle$ to 0 ensures that $|\psi(t)\rangle$ and $|\chi(t)\rangle$ satisfy the Schrödinger equation (1). To summarize, an extremum of $\bar{J}$ satisfies the equations

$$\left(i\frac{\partial}{\partial t} - \hat{H}(t)\right)|\psi(t)\rangle = 0,$$

$$|\psi(0)\rangle = |\phi_0\rangle \tag{9}$$

for the state $|\psi(t)\rangle$ and

$$\left(i\frac{\partial}{\partial t} - \hat{H}(t)\right)|\chi(t)\rangle = 0,$$

$$|\chi(t_f)\rangle = |\phi_f\rangle \tag{10}$$

for the adjoint state $|\chi(t)\rangle$, the control field $E(t)$ being the solution of Eq. (8).

C. Monotonically convergent algorithm

We describe different iterative algorithms to solve the optimal equations of Sec. II B. To simplify the presentation of computations, we consider nonlinearity of order 3 and a cost which is quartic in the field ($n=2$).

At step $k \geqslant 1$ of the algorithm, the system is described by the quadruplet $(|\psi_k(t)\rangle, |\chi_{k-1}(t)\rangle, E_k(t), \tilde{E}_{k-1}(t))$ where $|\psi_k(t)\rangle$ is the state of the system, $|\chi_{k-1}(t)\rangle$ the adjoint state, and $E_k(t)$ and $\tilde{E}_{k-1}(t)$ the electric fields associated, respectively, with the forward propagation of $|\psi_k(t)\rangle$ and to the backward propagation of $|\chi_{k-1}(t)\rangle$. $|\psi_k(t)\rangle$ and $|\chi_{k-1}(t)\rangle$ are solutions of the following time-dependent Schrödinger equations:

$$i\frac{\partial}{\partial t}|\psi_k(t)\rangle = \hat{H}(E_k)|\psi_k(t)\rangle \tag{11}$$

and

$$i\frac{\partial}{\partial t}|\chi_{k-1}(t)\rangle = \hat{H}(\tilde{E}_{k-1})|\chi_{k-1}(t)\rangle, \tag{12}$$

where $\hat{H}(E(t)) = \hat{H}_0 - \hat{\mu}E(t) - \hat{\alpha}E(t)^2 - \hat{\beta}E(t)^3$. For $|\psi_k(t)\rangle$, we impose the initial condition $|\psi_k(0)\rangle = |\phi_0\rangle$ and for $|\chi_{k-1}(t)\rangle$ the final condition $|\chi_{k-1}(t_f)\rangle = |\phi_f\rangle$. The iteration is initiated by a trial electric field $E_0(t)$. At step 0 of the algorithm, we propagate forward the state $|\psi_0(t)\rangle$ with the electric field $E_0(t)$. The cost functional J_k at step k is defined by

$$J_k = |\langle \phi_f|\psi_k(t_f)\rangle|^2 - \int_0^{t_f} \lambda E_k^4. \tag{13}$$

The algorithm determines the quadruplet $(|\psi_{k+1}(t)\rangle, |\chi_k(t)\rangle, E_{k+1}(t), \tilde{E}_k(t))$ at step $k+1$ from the one at step k. This is done by requiring that the variation $\Delta J = J_{k+1} - J_k$ of the cost J from step k to step $k+1$ is positive and that the limits (if they exist) of the sequences $(E_k)_{k\in\mathbb{N}}$ and $(\tilde{E}_k)_{k\in\mathbb{N}}$ are solutions of Eq. (8).

For that purpose, we introduce the functions $P_{k+1}(t) = |\langle \chi_k(t)|\psi_{k+1}(t)\rangle|^2$ and $\tilde{P}_{k+1}(t) = |\langle \chi_{k+1}(t)|\psi_{k+1}(t)\rangle|^2$. Differentiating these two functions with respect to time leads to

$$\frac{d}{dt}P_{k+1}(t) = \mu_{k,k+1}(\tilde{E}_k - E_{k+1}) + \alpha_{k,k+1}(\tilde{E}_k^2 - E_{k+1}^2) + \beta_{k,k+1}(\tilde{E}_k^3 - E_{k+1}^3) \tag{14}$$

for P_{k+1} and to

$$\frac{d}{dt}\tilde{P}_{k+1}(t) = \mu_{k+1,k+1}(\tilde{E}_{k+1} - E_{k+1}) + \alpha_{k+1,k+1}(\tilde{E}_{k+1}^2 - E_{k+1}^2) + \beta_{k+1,k+1}(\tilde{E}_{k+1}^3 - E_{k+1}^3) \tag{15}$$

for $\tilde{P}_{k+1}$. In Eqs. (14) and (15), we have introduced the notation

$$A_{k,k'} = 2\,\mathrm{Im}[\langle \psi_{k'}(t)|\chi_k(t)\rangle\langle \chi_k(t)|\hat{A}|\psi_{k'}(t)\rangle] \tag{16}$$

for a given observable $\hat{A}$. The functions P_k and $\tilde{P}_k$ satisfy by definition the following relations:

$$\tilde{P}_{k+1}(t_f) = |\langle \phi_f|\psi_{k+1}(t_f)\rangle|^2 = P_{k+1}(t_f),$$

$$\tilde{P}_{k+1}(0) = |\langle \chi_{k+1}(0)|\phi_0\rangle|^2 = P_{k+2}(0), \tag{17}$$

and a direct integration gives

$$P_k(t_f) = P_k(0) + \int_0^{t_f} \frac{dP_k(t)}{dt}dt. \tag{18}$$

The variation ΔJ is given by

$$\Delta J = J_{k+1} - J_k = |\langle \phi_f|\psi_{k+1}(t_f)\rangle|^2 - |\langle \phi_f|\psi_k(t_f)\rangle|^2 - \int_0^{t_f} \lambda[E_{k+1}(t)^4 - E_k(t)^4]dt. \tag{19}$$

Using the fact that $|\langle \phi_f|\psi_{k+1}(t_f)\rangle|^2 - |\langle \phi_f|\psi_k(t_f)\rangle|^2 = P_{k+1}(t_f) - P_k(t_f)$ and Eqs. (17), one deduces that $\Delta J = P_1 + P_2$ where

$$P_1 = -\int_0^{t_f} \lambda(E_{k+1}^4 - \tilde{E}_k^4) + \int_0^{t_f} [(\tilde{E}_k - E_{k+1})\mu_{k,k+1} + (\tilde{E}_k^2 - E_{k+1}^2)\alpha_{k,k+1} + (\tilde{E}_k^3 - E_{k+1}^3)\beta_{k,k+1}]dt \quad (20)$$

and

$$P_2 = \int_0^{t_f} \lambda(E_k^4 - \tilde{E}_k^4) - \int_0^{t_f} [(\tilde{E}_k - E_k)\mu_{k,k} + (\tilde{E}_k^2 - E_k^2)\alpha_{k,k} + (\tilde{E}_k^3 - E_k^3)\beta_{k,k}]dt. \quad (21)$$

To ensure the monotonic behavior of the algorithm, we choose the fields E_{k+1} and $\tilde{E}_k$ such that the integrals P_1 and P_2 are positive. A sufficient condition is to impose that the two integrands $\mathcal{P}_1$ and $\mathcal{P}_2$ associated with P_1 and P_2 are positive [22]. To be more precise, we first determine $\tilde{E}_k$ from E_k such that P_2 is positive and then we determine E_{k+1} from $\tilde{E}_k$ such that P_1 is positive. $|\psi_{k+1}\rangle$ and $|\chi_k\rangle$ are computed from a forward and a backward propagation with the fields E_{k+1} and $\tilde{E}_k$.

Starting from these conditions, we introduce two algorithms.

Algorithm I. $\mathcal{P}_1$ and $\mathcal{P}_2$ are respectively viewed as functions of E_{k+1} and $\tilde{E}_k$. E_{k+1} and $\tilde{E}_k$ are defined as the control fields which maximize $\mathcal{P}_1$ and $\mathcal{P}_2$. The maxima of these polynomials are positive since $\mathcal{P}_1(\tilde{E}_k)=0$ and $\mathcal{P}_2(E_k)=0$. As already mentioned, we first determine for each time t the maximum of $\mathcal{P}_2$ and then the one of $\mathcal{P}_1$. The integer n of the cost is chosen sufficiently large to ensure that the fields which maximize $\mathcal{P}_1$ and $\mathcal{P}_2$ are finite. This means that we choose n such that the terms $-\lambda E_{k+1}^{2n}$ and $-\lambda \tilde{E}_k^{2n}$ are monomials of higher degree in $\mathcal{P}_1$ and $\mathcal{P}_2$. We then have

$$\lim_{E_{k+1}\to\pm\infty} \mathcal{P}_1(E_{k+1}) = 0,$$

$$\lim_{\tilde{E}_k\to\pm\infty} \mathcal{P}_2(\tilde{E}_k) = 0,$$

which satisfies the requirement. For nonlinearity of order 3, the choice $n=2$ is sufficient. Finally, if we assume that the algorithm converges then we can check that the limits of the sequences $(E_k)_{k\in\mathbb{N}}$ and $(\tilde{E}_k)_{k\in\mathbb{N}}$ are solutions of Eq. (8). For that, we differentiate $\mathcal{P}_1$ and $\mathcal{P}_2$, respectively, with respect to E_{k+1} and $\tilde{E}_k$. We next replace in the derivatives of $\mathcal{P}_1$ and $\mathcal{P}_2$, E_{k+1}, E_k, and $\tilde{E}_k$ by E, $|\psi_{k+1}\rangle$ and $|\psi_k\rangle$ by $|\psi\rangle$, and $|\chi_k\rangle$ by $|\chi\rangle$. It is then straightforward to see that the limit $E(t)$ satisfies the optimal equation (8).

Algorithm II. We first write $\mathcal{P}_1$ and $\mathcal{P}_2$ as follows:

$$\mathcal{P}_1 = (E_{k+1} - \tilde{E}_k)[-\lambda(E_{k+1}^3 + E_{k+1}^2\tilde{E}_k + E_{k+1}\tilde{E}_k^2 + \tilde{E}_k^3) - \mu_{k,k+1} - \alpha_{k,k+1}(E_{k+1} + \tilde{E}_k) - \beta_{k,k+1}(E_{k+1}^2 + \tilde{E}_kE_{k+1} + \tilde{E}_k^2)] \quad (22)$$

and

$$\mathcal{P}_2 = (\tilde{E}_k - E_k)[-\lambda(\tilde{E}_k^3 + \tilde{E}_k^2E_k + E_k^2\tilde{E}_k + E_k^3) - \mu_{k,k} - \alpha_{k,k}(\tilde{E}_k - E_k) - \beta_{k,k}(\tilde{E}_k^2 + E_k\tilde{E}_k + E_k^2)]. \quad (23)$$

We then introduce two positive constants η_1 and η_2 by setting

$$E_{k+1} - \tilde{E}_k = \eta_1[-\lambda(E_{k+1}^3 + E_{k+1}^2\tilde{E}_k + E_{k+1}\tilde{E}_k^2 + \tilde{E}_k^3) - \mu_{k,k+1} - \alpha_{k,k+1}(E_{k+1} + \tilde{E}_k) - \beta_{k,k+1}(E_{k+1}^2 + \tilde{E}_kE_{k+1} + \tilde{E}_k^2)] \quad (24)$$

and

$$\tilde{E}_k - E_k = \eta_2[-\lambda(\tilde{E}_k^3 + \tilde{E}_k^2E_k + E_k^2\tilde{E}_k + E_k^3) - \mu_{k,k} - \alpha_{k,k} \times(\tilde{E}_k + E_k) - \beta_{k,k}(\tilde{E}_k^2 + E_k\tilde{E}_k + E_k^2)]. \quad (25)$$

Equations (24) and (25) are viewed, respectively, as equations in E_{k+1} and $\tilde{E}_k$. E_{k+1} and $\tilde{E}_k$ are defined as one of the solutions of these two equations. By definition of the constants η_1 and η_2, the values of $\mathcal{P}_1$ and $\mathcal{P}_2$ for these fields are positive. The integer n is chosen sufficiently large to ensure that Eqs. (24) and (25) always have real solutions respectively in E_{k+1} and $\tilde{E}_k$. For nonlinearity of order 3, it is sufficient to take $n=2$. When Eqs. (24) and (25) have more than one real solution at time t, we numerically choose the solution that is closest to the one at time $t-dt$ (for the forward propagation) or $t+dt$ (for the backward propagation). The processus is initiated by imposing that $E_k(0)=0$ and $\tilde{E}_k(t_f)=0$. This allows one to obtain smooth optimal fields without discontinuity. As for the algorithm I, we can check that the limits of the sequences $(E_k)_{k\in\mathbb{N}}$ and $(\tilde{E}_k)_{k\in\mathbb{N}}$ satisfy Eq. (8). This can be done by replacing $\tilde{E}_k$ and E_{k+1} by E in Eqs. (24) and (25)

In the two cases, the structure of the algorithms can be summarized as follows. At step $k+1$, we propagate backward in time the adjoint state $|\chi_k\rangle$ with the field $\tilde{E}_k$ determined from P_2. We then compute the forward evolution of $|\psi_{k+1}\rangle$ from $|\phi_0\rangle$. For this second propagation, we use the field E_{k+1} defined from P_1. Note that a simpler solution which gives a slower convergence consists in choosing $\tilde{E}_k=E_k$, i.e., propagating $|\psi_k\rangle$ and $|\chi_k\rangle$ with the same field.

III. CONTROL OF MOLECULAR ORIENTATION

A. Introduction

In this section, we investigate the control of orientation dynamics of a diatomic molecule driven by an electromagnetic field [28,29]. This control is taken as a prototype to test the efficiency of the algorithm. The application of OCT to molecular alignment and orientation is relatively recent [12,22,43]. One of the main results of Ref. [22] is that the optimal oriented state (see below for a definition) is reached by rotational ladder climbing, i.e., by successive rotational excitations. The corresponding optimal pulse is however very long, of the order of 20 rotational periods, which could be problematic for practical applications. We consider

shorter durations in this paper of the order of the rotational period $T_{\rm per}$. We have chosen $t_f = T_{\rm per}$ but other durations can be considered. Note that, for controls much shorter than $T_{\rm per}$, the optimal solution is very close to the kick mechanism largely explored using the sudden-impact model [44]. The CO molecule is taken as an example. The units used are atomic units unless otherwise specified.

The molecule is described in a rigid-rotor approximation interacting with a linearly polarized laser pulse nonresonant with vibronic frequencies. In this case, the Hamiltonian $\hat{H}$ can be written as follows [27,45]:

$$\hat{H} = B\hat{J}^2 - \mu_0 E(t)\cos\theta - \frac{1}{2}[(\alpha_\parallel - \alpha_\perp)\cos^2\theta + \alpha_\perp]E(t)^2 - \frac{1}{6}[(\beta_\parallel - 3\beta_\perp)\cos^3\theta + 3\beta_\perp\cos\theta]E(t)^3, \quad (26)$$

where B and μ_0 are the rotational constant and the permanent dipole moment. $\alpha_\parallel$, $\alpha_\perp$, $\beta_\parallel$, and $\beta_\perp$ are, respectively, the polarizability and the hyperpolarizability components of the molecule. The labels $\parallel$ and $\perp$ indicate the components parallel and perpendicular to the internuclear axis. For the CO molecule, we have chosen the following numerical values: $B = 1.9313\ \mathrm{cm}^{-1}$ and $\mu_0 = 0.044$, $\alpha_\parallel = 15.65$, $\alpha_\perp = 11.73$, $\beta_\parallel = 28.35$, and $\beta_\perp = 6.64$ in atomic units [46,47]. J^2 is the angular momentum operator and θ the angle between the direction of the molecular axis and the polarization vector. A basis of the Hilbert space is given by the spherical harmonics $|j,m\rangle$ with $j \geq 0$ and $-j \leq m \leq j$.

B. Zero rotational temperature

In this section, we consider the limit of zero rotational temperature. We recall that the expectation value $\langle\cos\theta\rangle$ is usually taken as a quantitative measure of orientation [28,29]. Here, we replace this measure by the projection onto a target state $|\phi_f\rangle$. We consider target states recently introduced for the orientation which both maximize the field-free orientation and its duration [31,32]. To construct this target state, we restrict the Hilbert space to a finite-dimensional one defined by a maximum value of j denoted $j_{\rm opt}$. For CO, we have chosen $j_{\rm opt} = 4$ which leads to a maximum of $\langle\cos\theta\rangle$ of the order of 0.9. In this reduced Hilbert space, the operator $\cos\theta$ has a nondegenerate discrete spectrum. The target state $|\phi_f\rangle$ is then defined as the eigenvector of $\cos\theta$ of highest eigenvalue. The initial state is the state $|0,0\rangle$. We also recall that the projection m of the angular momentum j on the field polarization axis is a conserved quantum number due to cylindrical symmetry.

We now apply the monotonically convergent algorithms I and II. The results of the computations are presented in Figs. 1–4. We have used simplified algorithms by assuming that $E_k = \tilde{E}_k$. Figures 1, 3, and 4 correspond, respectively, to the algorithm II for $n=1$, the algorithm II for $n=2$, and the algorithm I for $n=2$. For the algorithm II, we can choose $n=1$ since we have checked that for this value Eqs. (24) and (25) always have a real solution. Note that this latter observation depends on the values of λ and η considered. Numerical values are taken to be $\lambda = 0.05$, $\eta = 1$ for Fig. 1 [λ corresponds to the maximum value of $\lambda(t)$], $\lambda = 6.05 \times 10^4$, $\eta = 1$ for Fig. 3, and $\lambda = 12 \times 10^5$ for Fig. 4. The difference in the values of λ is due to the form of the cost which is either quadratic or quartic in the field. We have checked that the value of η is not relevant even if the value of λ has to be adjusted with respect to that of η. The trial fields are displayed in Figs. 1(a), 3(a), and 4(a). The trial field is a Gaussian pulse of intensity of the order of 1 TW/cm^2. In order to obtain realistic electric fields, the value of λ has been chosen so that the energy of the optimal field is lower than two times the energy of the Gaussian pulse. Note also that for $E \simeq 5 \times 10^{-3}$ a.u.. (which corresponds to the typical amplitude of the optimal field) we have $\mu_0 \simeq \alpha_\perp E$, which shows that the

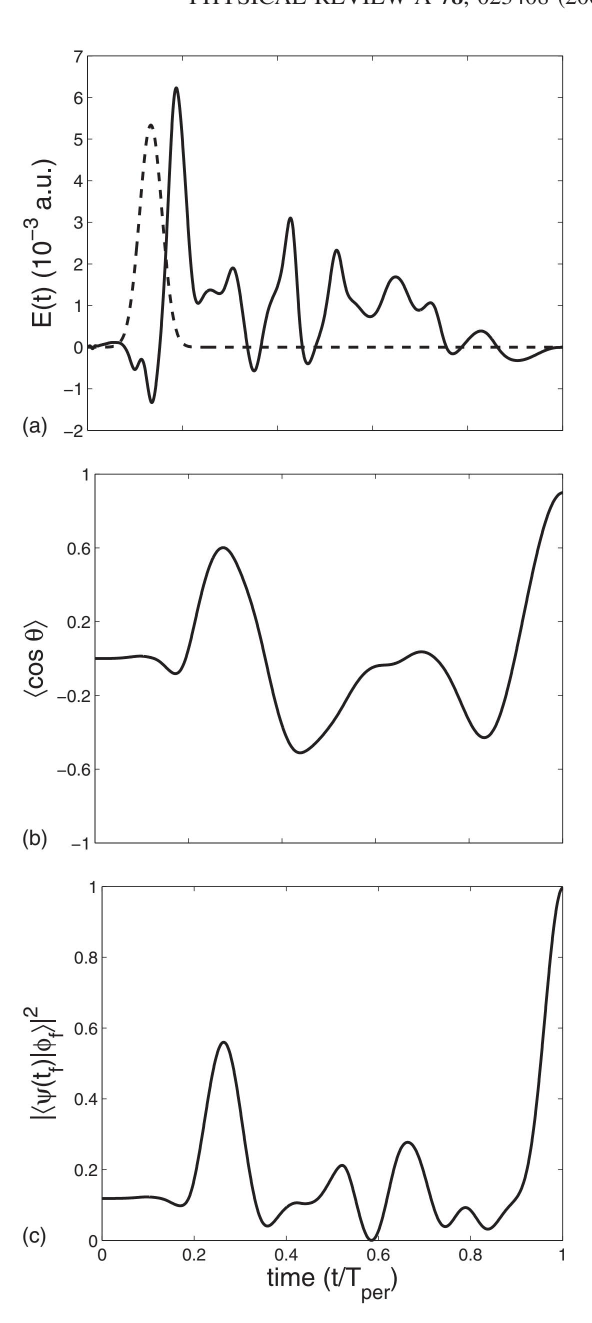


FIG. 1. Plot as a function of the adimensional time $t/T_{\rm per}$ of (a) the optimal field (solid line) and the initial trial field (dashed line), (b) the expectation value $\langle\cos\theta\rangle$, and (c) the projection onto the target state $|\phi_f\rangle$. The abbreviation a.u. corresponds to atomic units.

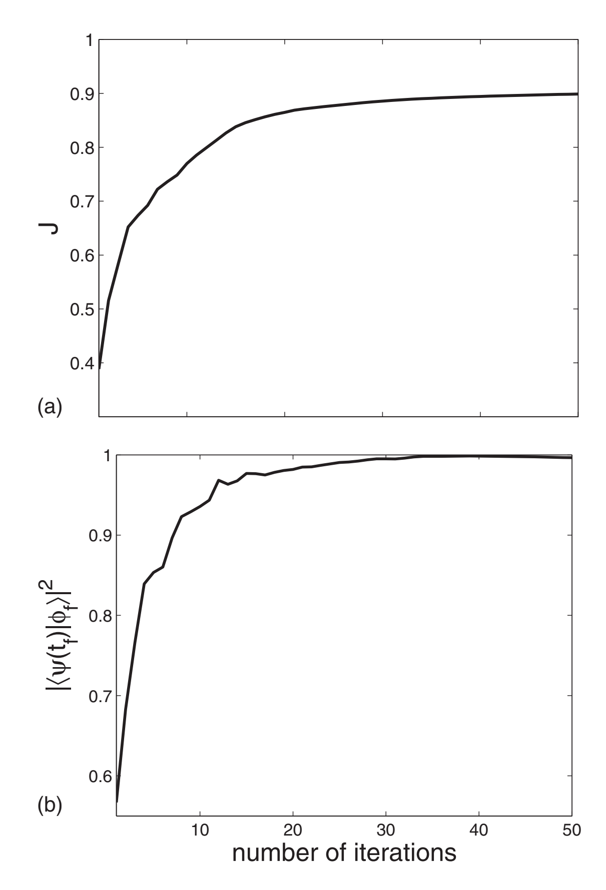


FIG. 2. Plot as a function of the number of iterations of (a) the adimensional cost J defined by Eq. (12) for $n=1$ (a cost quadratic in the field) and (b) the projection onto the target state at time t_f.

polarizability terms are not negligible in the dynamics. In each case, very good results are obtained with a final projection $|\langle\psi(t_f)|\phi_f\rangle|^2$ larger than 0.99 except for the algorithm I where $|\langle\psi(t_f)|\phi_f\rangle|^2$ is of the order of 0.98. Figure 2 illustrates the convergence properties of the algorithm II, which are satisfactory since after 30 iterations we obtain a projection close to 0.98. A similar behavior has been observed in the other cases. A comparison of Figs. 1(a), 3(a), and 4(a) shows that the optimal field for $n=2$ has sharper variations than for $n=1$ for both algorithms. We have also observed that these sharper variations can induce numerical instabilities and high-frequency oscillations in the optimal field. This point is discussed in Sec. III D where we show how to remove the parasite oscillations with a bandpass filter. In practice, it has been found that small values of the exponent n generally produce smoother optimal fields.

C. Nonresonant two-color laser fields

We continue to consider a zero rotational temperature but we assume now that the molecule interacts with a nonresonant two-color laser field [24,27] of the form

$$E(t) = E_1(t)\cos(\omega t) + E_2(t)\cos(2\omega t). \tag{27}$$

After averaging over the rapid oscillations of the field, the Hamiltonian $\hat{H}$ of the system becomes

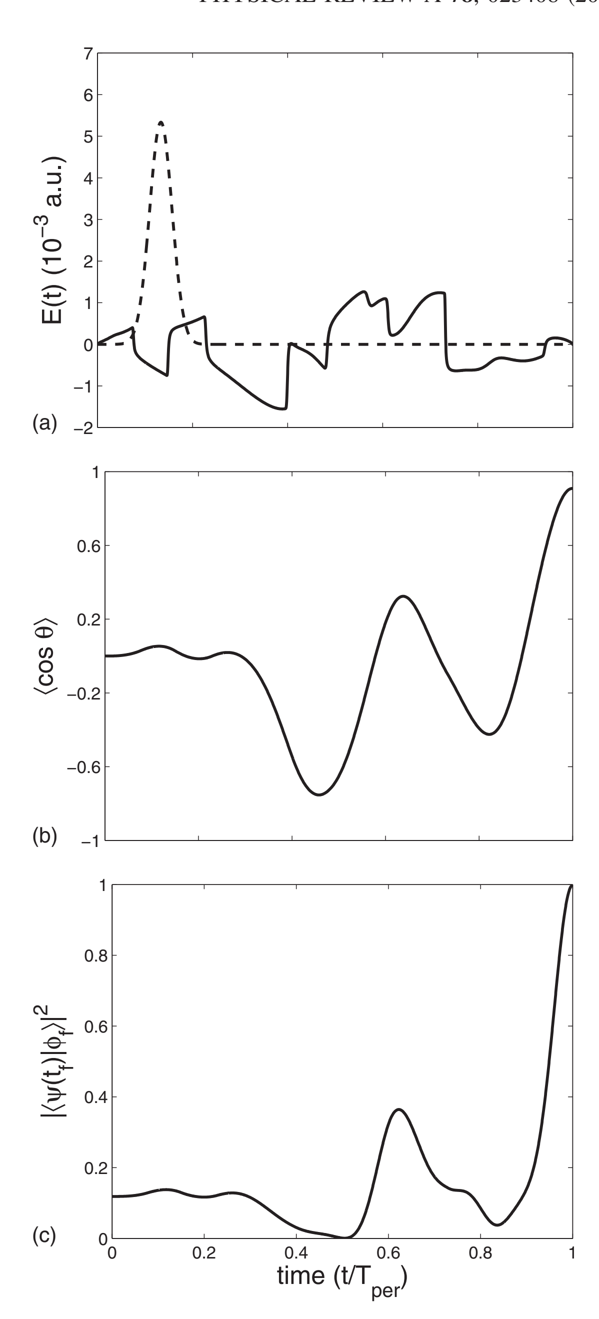


FIG. 3. Same as Fig. 1 but for $n=2$, i.e., a cost quartic in the field.

$$\hat{H} = B\hat{J}^2 - \frac{1}{4}[(\alpha_\parallel - \alpha_\perp)\cos^2\theta + \alpha_\perp][E_1(t)^2 + E_2(t)^2] - \frac{1}{8}[(\beta_\parallel - 3\beta_\perp)\cos^3\theta + 3\beta_\perp\cos\theta]E_1(t)^2E_2(t). \tag{28}$$

The interest of this model is due to the absence of a linear term in the interaction which enhances the difficulty of the control. Two cases can be considered according to the respective values of E_1 and E_2. If $E_1=E_2$, we can use the standard algorithm presented in Sec. II C whereas for $E_1 \neq E_2$ the algorithm has to be slightly generalized. These two

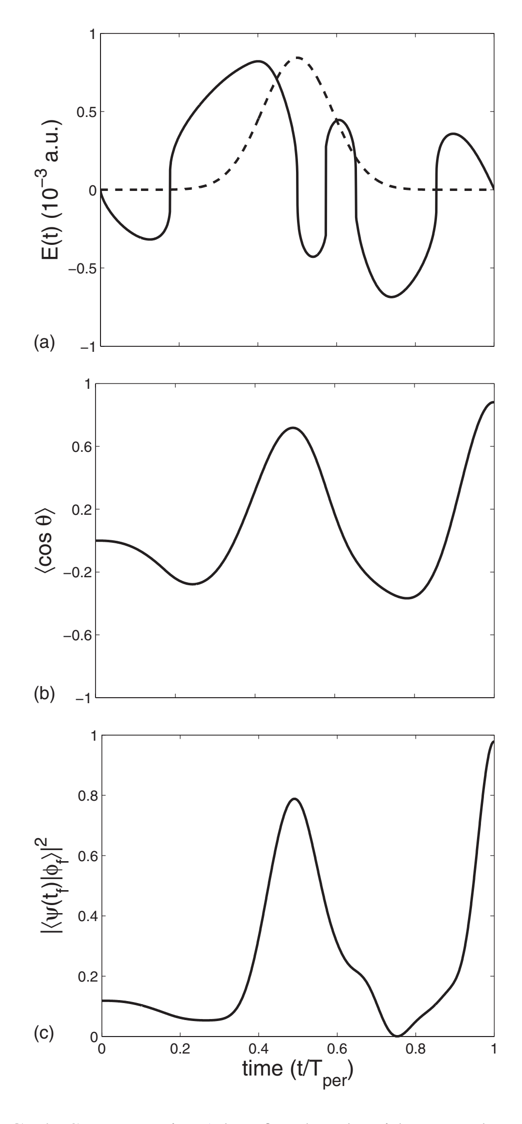


FIG. 4. Same as Fig. 1 but for the algorithm I and $n=2$.

problems are analyzed, respectively, in Secs. III C 1 and III C 2.

1. The case $E_1 \neq E_2$

We first generalized the algorithm of Sec. II C to the case of two control fields. We assume that the cost is quadratic in the field.

We introduce the augmented cost $\bar{J}$ and we determine the critical points with respect to E_1 and E_2. We have

$$\bar{J} = |\langle \phi_f|\psi(t_f)\rangle|^2 - \int_0^{t_f} \lambda[E_1(t)^2 + E_2(t)^2]dt - 2\,\mathrm{Im}\left[\langle \psi(t_f)|\phi_f\rangle \int_0^{t_f} \langle \chi(t)|\left(i\frac{\partial}{\partial t} - \hat{H}\right)|\psi(t)\rangle dt\right], \tag{29}$$

and we compute the variational derivatives $\delta\bar{J}/\delta E_1$ and $\delta\bar{J}/\delta E_2$ which are equal to zero for a critical point. We then obtained the following system of equations:

$$\lambda E_1 + 2\tilde{\alpha}E_1 + 2\tilde{\beta}E_1E_2 = 0,$$

$$\lambda E_2 + 2\tilde{\alpha}E_2 + \tilde{\beta}E_1^2 = 0, \tag{30}$$

which are satisfied by the optimal fields E_1 and E_2. We have used in Eqs. (30) the notations

$$\tilde{\alpha} = 2\,\mathrm{Im}\left\{\langle \psi(t)|\chi(t)\rangle\langle\chi(t)|\frac{1}{4}[(\alpha_\parallel - \alpha_\perp)\cos^2\theta + \alpha_\perp]|\psi(t)\rangle\right\},$$

$$\tilde{\beta} = 2\,\mathrm{Im}\left\{\langle \psi(t)|\chi(t)\rangle\langle\chi(t)|\frac{1}{8}[(\beta_\parallel - 3\beta_\perp)\cos^3\theta + 3\beta_\perp\cos\theta]|\psi(t)\rangle\right\}. \tag{31}$$

We solve the optimal equations by a monotonically convergent algorithm. The proof of monotonicity follows closely the lines of the proof in Sec. II C. We use the same notations, with, for instance, $E_{1,k}$ the field E_1 at iteration k. To simplify the computations, we take equal the fields E_k and $\tilde{E}_k$ for the forward and the backward propagations. We compute $\Delta J = J_{k+1} - J_k$. We obtain the following expressions for the polynomials $\mathcal{P}_1$ and $\mathcal{P}_2$:

$$\mathcal{P}_1 = (E_{1,k+1} - E_{1,k})[(E_{1,k+1} + E_{1,k})\alpha_{k,k+1} + (E_{1,k+1} + E_{1,k})E_{2,k+1}\beta_{k,k+1} - \lambda(E_{1,k+1} + E_{1,k})] \tag{32}$$

and

$$\mathcal{P}_2 = (E_{2,k+1} - E_{2,k})[(E_{2,k+1} + E_{2,k})\alpha_{k,k+1} + E_{1,k}^2\beta_{k,k+1} - \lambda(E_{2,k+1} + E_{2,k})], \tag{33}$$

where

$$\alpha_{k,k+1} = \mathrm{Im}\left\{\langle \psi_{k+1}(t)|\chi_k(t)\rangle\langle\chi_k(t)|\frac{1}{4}[(\alpha_\parallel - \alpha_\perp) + \alpha_\perp]\cos^2\theta|\psi_{k+1}(t)\rangle\right\}$$

$$\beta_{k,k+1} = \mathrm{Im}\left\{\langle \psi_{k+1}(t)|\chi_k(t)\rangle\langle\chi_k(t)|\frac{1}{8}[(\beta_\parallel - 3\beta_\perp)\cos^3\theta + 3\beta_\perp\cos\theta]|\psi_{k+1}(t)\rangle\right\}. \tag{34}$$

$\mathcal{P}_1$ and $\mathcal{P}_2$ are viewed respectively as polynomials in $E_{1,k+1}$ and $E_{2,k+1}$. We first use $\mathcal{P}_2$ to determine the field $E_{2,k+1}$ by the algorithm I or II and then, using this solution, we compute $E_{1,k+1}$ from $\mathcal{P}_1$. We also check that if the algorithm converges then the solutions given by the algorithm correspond to the extremal solutions defined by Eqs. (30). This can be done by replacing $E_{1,k+1}$ and $E_{1,k}$ by E_1 and $E_{2,k+1}$ and $E_{2,k}$ by E_2. The optimal fields are then zeros of the derivatives of $\mathcal{P}_1$ and $\mathcal{P}_2$ with respect to $E_{1,k+1}$ and $E_{2,k+1}$. Figure 5 displays the results we have obtained with the algorithm II for $n=2$ and $\lambda=1$. We have chosen two different trial fields in order to generate two different optimal fields E_1 and E_2. With the same trial field for the fields E_1 and E_2, the algorithm leads to two

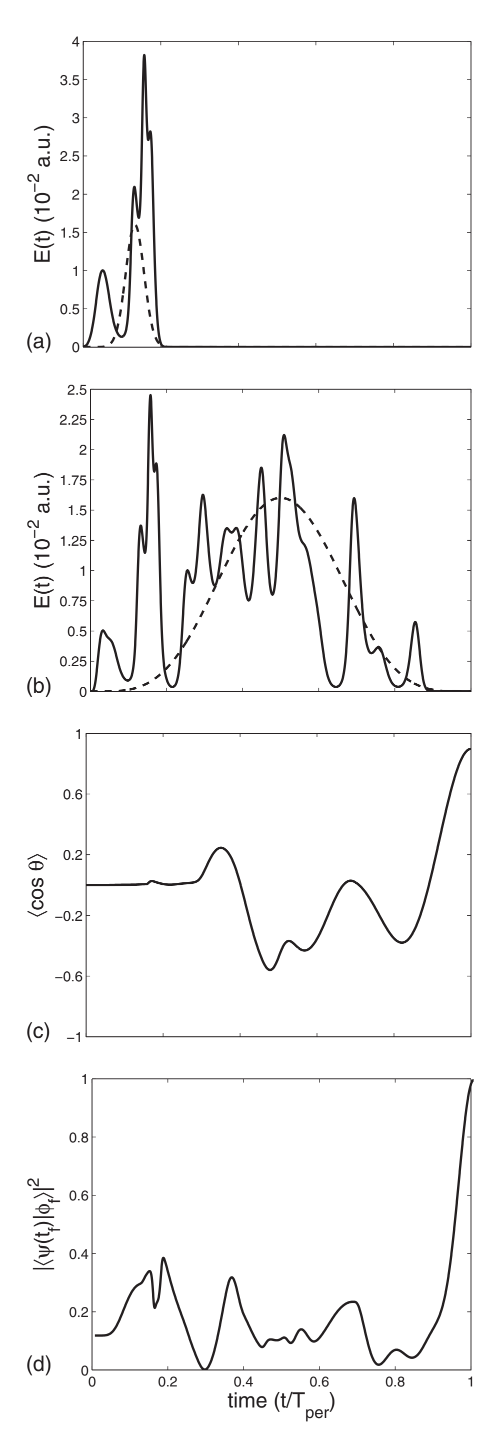


FIG. 5. Same as Fig. 1 but for two-color laser fields with $E_1 \neq E_2$. (a) and (b) correspond, respectively, to the fields E_1 and E_2.

solutions which are very close to each other. Larger values of electric fields have been used due to the absence of linear interaction term in the Hamiltonian.

A remarkable characteristic of the optimal fields is the fact that E_1 vanishes for $t > 0.2T_{\text{per}}$. This means that the dissymmetry producing the orientation (dissymmetry due to the term in $E_1^2E_2$ in the Hamiltonian) acts only during this duration. This provides a nonintuitive method to produce orientation using a long laser field E_2 and a short laser field E_1.

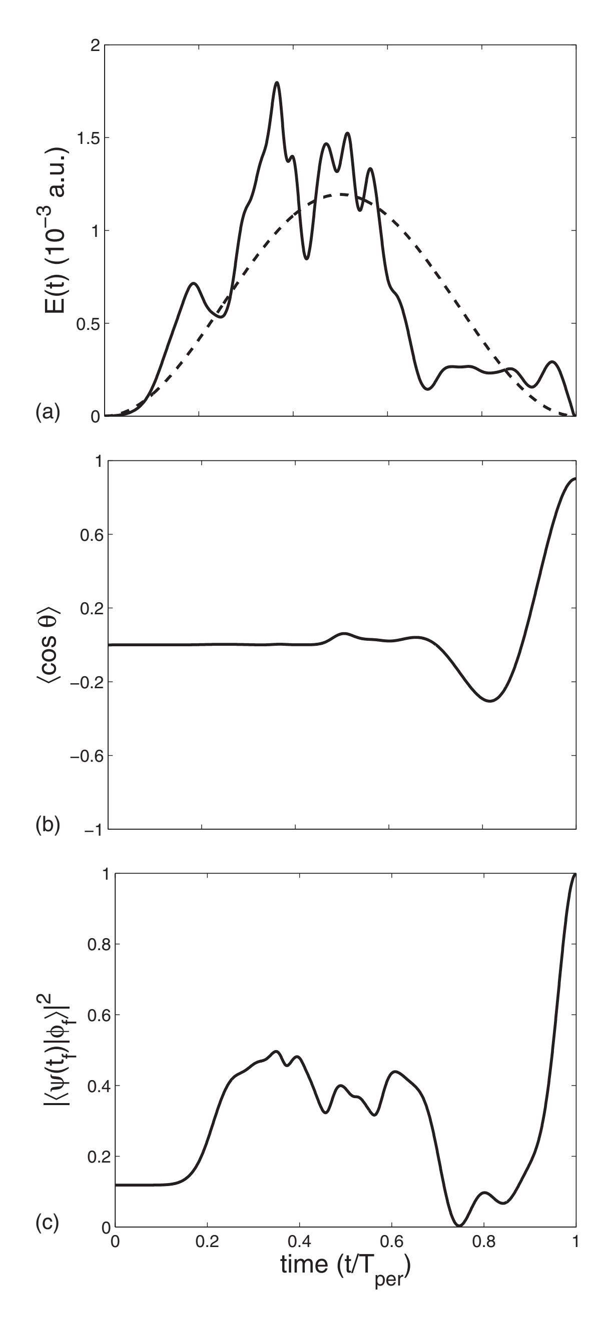


FIG. 6. Same as Fig. 1 but for the averaging case with $E_1 = E_2$.

2. The case $E_1 = E_2$

We use the monotonic algorithm II proposed in Sec. II. Figure 6 illustrates the different results. They have been obtained for $n=2$ and $\lambda=5$. The trial field is a Gaussian pulse whose duration corresponds to the rotational period. From the equations of the algorithm, it is straightforward to see that the algorithm cannot generate an optimal field different from zero at time t if the trial field is zero at that time. This is simply due to the absence of linear interaction term in the Hamiltonian. The algorithm only modifies the envelope of the trial field, whose choice is therefore crucial.

D. Analysis of the Fourier spectrum

We analyze in this section the Fourier transforms of the optimal solutions. Our goal is to show that optimal solutions

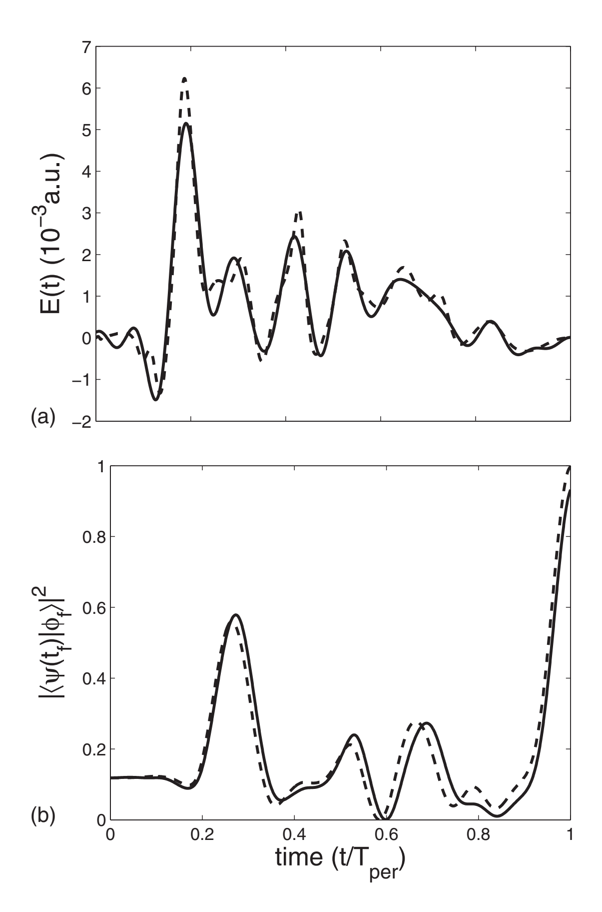


FIG. 7. Plot as a function of time t/T_{per} of (a) the optimal (dashed line) and the approximate fields (solid line) and (b) the projection onto the target state $|\phi_f\rangle$.

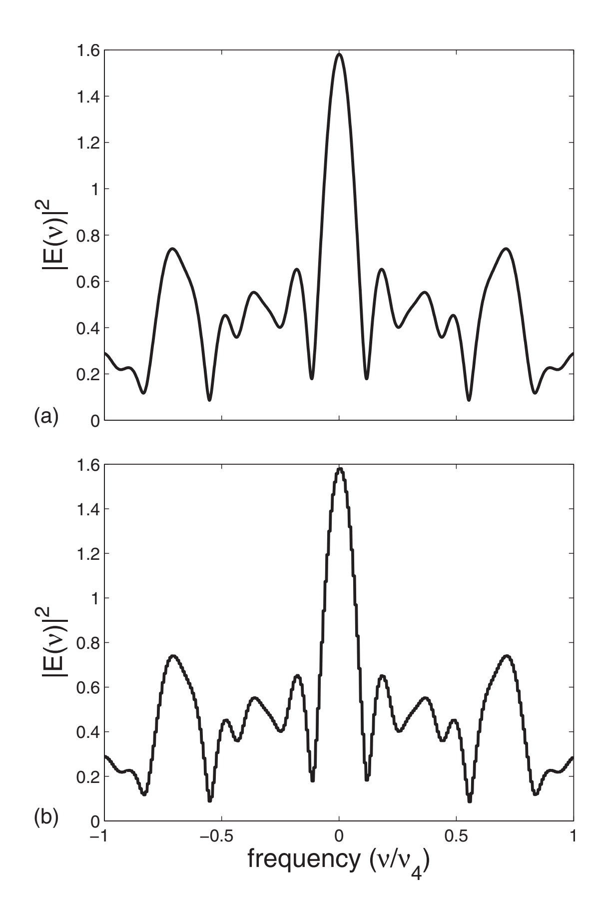


FIG. 8. Plot as a function of the frequency ν of the squared modulus of the Fourier transform of the optimal field (a) and of its piecewise constant approximation (b). The Fourier transform has been discretized over the interval $[-\nu_4,\nu_4]$.

determined in Sec. II A can be well approximated by solutions that could be implemented experimentally. We consider experiments coupled with genetic algorithms optimizing the phase and the amplitude of the Fourier transform of a finite number of frequency components. The discretization is done over a frequency interval chosen with respect to the quantum transition frequencies involved in the control (see below). Note that we do not take into account, in this paper, technology constraints for the choice of this frequency interval. Standard pulse shapers usually work with optical frequencies of the order of 800 nm. With such a technology, only the nonresonant laser fields of Sec. III C could be experimentally implemented.

Following [40,41], we assume that the solution obtained by genetic algorithms is a piecewise constant function in frequency both in amplitude and in phase. We have chosen 640 frequencies or less to discretize the optimal field. By an inverse Fourier transform, we then determine a new time-dependent electric field. Figure 7 presents the results obtained with the optimal pulse of Fig. 1. Using only 128 frequencies, we show that the final projection obtained by the optimal pulse and its approximation are very close to each other. For 256 frequencies, the difference is negligible and cannot be distinguished at the resolution of the plots. Figures 8 and 9 give information on the Fourier transform of the optimal pulse. One introduces the rotational frequencies ν_{j+1} given by

$$\nu_{j+1}=E_{j+1}-E_j=2B(j+1), \qquad (35)$$

where E_j is the energy of the state $|j,0\rangle$. The target state being associated to $j_{\mathrm{opt}}=4$, only five rotational states from $j=0$ to 4 have to be populated by the control field. It is thus natural to discretize the Fourier transform over the interval $[-\nu_4,\nu_4]$. Higher frequencies do not contribute to reach the

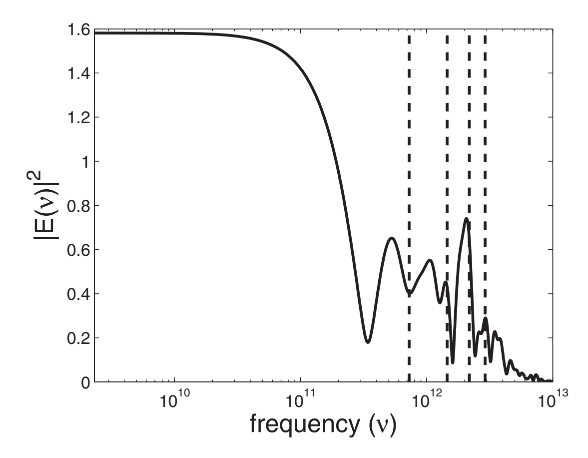


FIG. 9. Same as Fig. 8(a) but as a function of the frequency ν. Vertical lines indicate the positions of the frequencies ν_1, ν_2, ν_3, and ν_4.

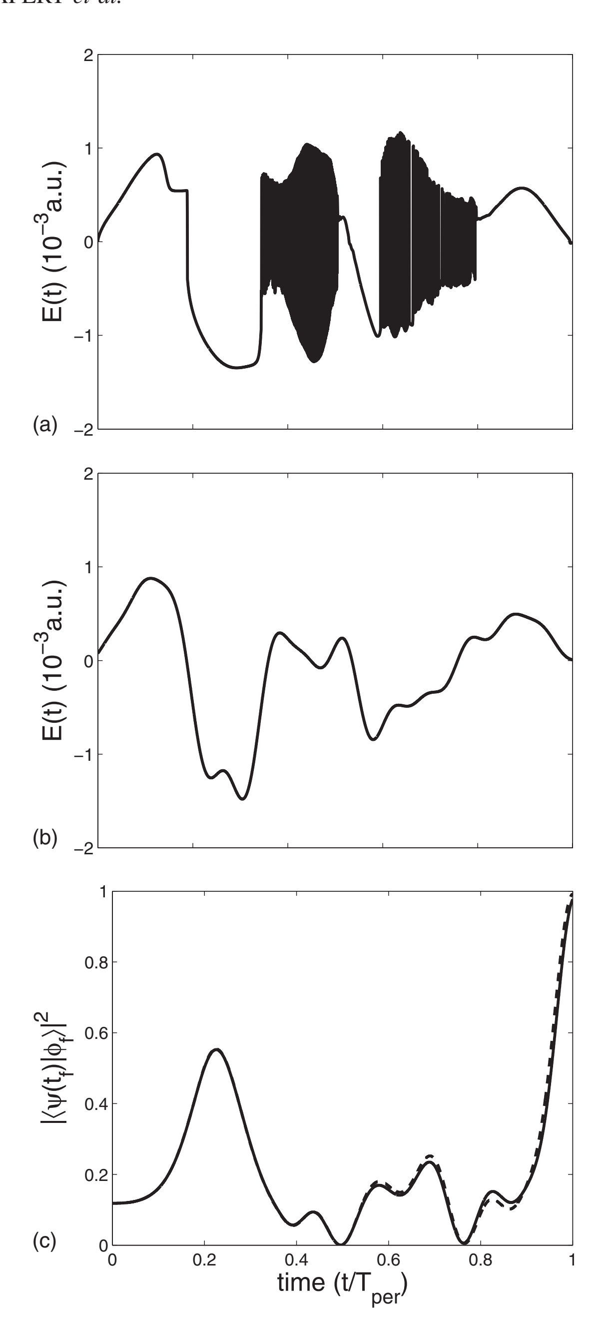


FIG. 10. Plot as a function of time t/T_{per} of (a) the optimal (solid line) and (b) the approximate fields (dashed line), and (c) the projection onto the target state $|\phi_f\rangle$.

target state. A similar behavior has been observed for the other optimal solutions. Another example is given by Fig. 10. The corresponding optimal solution obtained by the algorithm I presents rapid unwanted oscillations. To obtain a smooth solution displayed in Fig. 10(b), we filter this optimal pulse in the frequency domain. The bandwidth of the filter is chosen to cut off frequencies higher than ν_4, which produce rapid oscillations. As in the first case, we also observe that the discretization does not significantly modify the final result.

E. Finite rotational temperature

We investigate the temperature effects on the optimal solutions. The system is described by a density matrix ρ whose dynamics is governed by the von Neumann equation. The initial density operator $\rho(0)$ is the equilibrium density operator at temperature T which can be written

$$\rho(0) = \frac{1}{Z}\sum_{j=0}^{+\infty}\sum_{m=-j}^{j} e^{-Bj(j+1)/(k_BT)}|j,m\rangle\langle j,m|, \tag{36}$$

where k_B is the Boltzmann constant and Z the partition function. The objective of the control is to maximize the projection of $\rho(t_f)$ onto a target state ρ_{opt}. We consider here the target state introduced in Ref. [33] which is unitarily equivalent to the initial mixed state $\rho(t_i)$ and optimizes both the orientation and its duration. We refer the reader to Ref. [33] for the complete construction of ρ_{opt} and for proofs of its attainability by unitary controls. Note that the definition of ρ_{opt} depends on the polarization used. We consider here the optimum for a linear polarization. ρ_{opt} can be defined as follows. The first step consists in reducing the dimension of the Hilbert space to a finite one $\mathcal{H}^{(j_{\mathrm{opt}})}$ where j_{opt} is the highest j for which the corresponding rotational levels are significantly populated. The dimension of this space depends on the temperature and on the intensity of the field used. For CO and $T=1$, 5, and 10 K, we have chosen $j_{\mathrm{opt}}=4$. We denote by $\mathcal{H}_m^{(j_{\mathrm{opt}})}$ the subspace of $\mathcal{H}^{(j_{\mathrm{opt}})}$ associated with a given value of m. The target state $\rho_{\mathrm{opt}}^{(j_{\mathrm{opt}})}$ of the control, which therefore depends on the choice of j_{opt}, is given by

$$\rho_{\mathrm{opt}}^{(j_{\mathrm{opt}})} = \sum_{m=-j_{\mathrm{opt}}}^{m=j_{\mathrm{opt}}}\sum_{k=1}^{j_{\mathrm{opt}}-|m|+1} \omega_k^{(m)}|\chi_k^{(m)}\rangle\langle\chi_k^{(m)}|, \tag{37}$$

where the $\omega_k^{(m)}$'s are the eigenvalues of $\rho(t_i)$ restricted to $\mathcal{H}_m^{(j_{\mathrm{opt}})}$ and ordered. The vectors $|\chi_k^{(m)}\rangle$ are the eigenvectors of the restriction of the operator $\cos\theta$ to $\mathcal{H}_m^{(j_{\mathrm{opt}})}$. The vectors $|\chi_k^{(m)}\rangle$ are also ordered according to the values of the corresponding eigenvalues.

We have used the algorithm II with $n=2$ to determine the optimal solutions. We denote by $\chi(t)$ the adjoint density matrix state. In superoperator notations, the structure of the algorithm is very similar to the one for pure states. The cost functional J is given by

$$J = |\langle\langle\rho_{\mathrm{opt}}|\rho(t_f)\rangle\rangle|^2 - \int_0^{t_f}\lambda E(t)^4 dt \tag{38}$$

and the augmented cost functional $\bar{J}$ reads

$$\bar{J} = |\langle\langle\rho_{\mathrm{opt}}|\rho(t_f)\rangle\rangle|^2 - 2\,\mathrm{Im}\left[\langle\langle\rho(t_f)|\rho_{\mathrm{opt}}\rangle\rangle\int_0^{t_f}\langle\langle\chi(t)|\left(i\frac{\partial}{\partial t}-\hat{H}\right)\times|\rho(t)\rangle\rangle dt\right] - \int_0^{t_f}\lambda E(t)^4 dt, \tag{39}$$

where $\langle\langle\chi|\rho\rangle\rangle=\mathrm{Tr}(\chi^\dagger\rho)$ and $\langle\langle\chi|M|\rho\rangle\rangle=\mathrm{Tr}[\chi^\dagger(M,\rho)]$ for a given observable M. $\rho(t)$ and $\chi(t)$, which satisfy the von Neumann equation, are propagated forward and backward with initial condition $\rho(0)=\rho_0$ and final condition $\chi(t_f)=\rho_{\mathrm{opt}}$. Numerical parameters are respectively taken to be $\lambda=6\times10^4$, 65×10^2, and 90 for $T=1$, 5, and 10 K. η is equal to 1 in all the cases. The values of λ are chosen so that the total energy of the field stays approximatively constant when

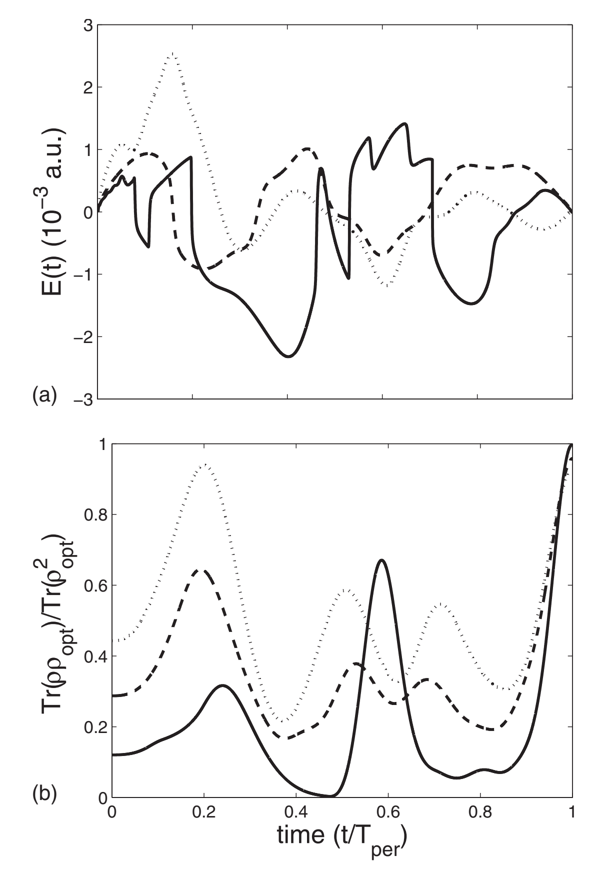


FIG. 11. Plot as a function of the adimensional time t/T_{per} of (a) the optimal electric field and (b) the projection onto the target state ρ_{opt}. Solid, dashed, and dotted-dashed lines correspond, respectively, to $T=1$, 5, and 10 K.

the temperature is increased. The trial field is the same for the three cases considered.

Figure 11 presents the results obtained for three different temperatures. We observe that the structures of the optimal fields and of the projection onto the target state as a function of time are very different. As expected, we note a decrease of the final projection with increasing temperature. This computation allows us to show the robustness with respect to the temperature of the optimal fields. For $T=10$ K, we still obtain an efficient field since the final projection is of the order of 0.9. We also point out sharp variations of the optimal fields due to the use of a cost that is quartic in the control field. These variations do not affect the temporal evolution of the projection.

IV. SUMMARY

We have presented a family of monotonically convergent algorithms for the computation of the optimal control of a quantum system interacting nonlinearly with a laser field. One key for the convergence of these algorithms is to consider costs that are not quadratic in the field. In comparison with the algorithms of Ref. [12], this allows us to consider only one wave function and one adjoint state per iteration of the algorithm, whatever the nonlinearity used. This is thus less demanding from a numerical point of view, especially when the degree of the nonlinearity is important. As a prospect, an open question in this field is the applicability of the present method to more complicated systems involving, for instance, non-Markovian dynamics or a time-dependent target state [48]. Special attention has to be paid to the convergence properties and to the stability of the method, especially when the cost is quartic in the control field.

ACKNOWLEDGMENTS

We thank E. Hertz for many helpful discussions. We acknowledge support from the Agence Nationale de la Recherche (ANR CoMoc, C-QUID). G.T. acknowledges support from INRIA Rocquencourt (MicMac project) and a PICS CNRS-NSF program on quantum control.

[1] W. Warren, H. Rabitz, and M. Dahleb, Science **259**, 1581 (1993).
[2] H. Rabitz, R. de Vivie-Riedle, M. Motzkus, and K. Kompa, Science **288**, 824 (2000).
[3] M. A. Nielsen and I. L. Chuang, *Quantum Computation and Quantum Information* (Cambridge University Press, Cambridge, U.K., 2000).
[4] W. Zhu and H. Rabitz, J. Chem. Phys. **109**, 385 (1998).
[5] Y. Maday and G. Turinici, J. Chem. Phys. **118**, 8191 (2003).
[6] S. G. Schirmer, M. D. Girardeau, and J. V. Leahy, Phys. Rev. A **61**, 012101 (1999).
[7] Y. Ohtsuki, W. Zhu, and H. Rabitz, J. Chem. Phys. **110**, 9825 (1999).
[8] Y. Ohtsuki, G. Turinici, and H. Rabitz, J. Chem. Phys. **120**, 5509 (2004).
[9] B. Bonnard and D. Sugny (unpublished).
[10] D. Sugny, C. Kontz, and H. R. Jauslin, Phys. Rev. A **76**, 023419 (2007).
[11] J. Werschnik and E. K. U. Gross, J. Phys. B **40**, R175 (2007).
[12] Y. Ohtsuki and K. Nakagami, Phys. Rev. A **77**, 033414 (2008).
[13] H. Jirari and W. Potz, Phys. Rev. A **72**, 013409 (2005).
[14] M. Wenin and W. Potz, Phys. Rev. A **74**, 022319 (2006).
[15] A. E. Bryson and Y. Ho, *Applied Optimal Control* (Hemisphere Publishing, Washington, 1975).
[16] R. Kosloff, S. Rice, P. Gaspard, S. Tersigni, and D. Tannor, Chem. Phys. **139**, 201 (1989).
[17] W. Zhu, J. Botina, and H. Rabitz, J. Chem. Phys. **108**, 1953 (1998).
[18] W. Zhu and H. Rabitz, J. Chem. Phys. **110**, 7142 (1999).
[19] M. Ndong, L. Bomble, D. Sugny, Y. Justum, and M. Desouter-Lecomte, Phys. Rev. A **76**, 043424 (2007).
[20] D. Sugny, C. Kontz, M. Ndong, Y. Justum, G. Dive, and M. Desouter-Lecomte, Phys. Rev. A **74**, 043419 (2006).
[21] D. Sugny, M. Ndong, D. Lauvergnat, Y. Justum, and M. Desouter-Lecomte, J. Photochem. Photobiol., A **190**, 359 (2007).

[22] J. Salomon, C. M. Dion, and G. Turinici, J. Chem. Phys. **123**, 144310 (2005).
[23] Y. Ohtsuki, Y. Teranishi, P. Saalfrank, G. Turinici, and H. Rabitz, Phys. Rev. A **75**, 033407 (2007).
[24] B. Friedrich and D. Herschbach, Phys. Rev. Lett. **74**, 4623 (1995).
[25] B. J. Sussman, M. Y. Ivanov, and A. Stolow, Phys. Rev. A **71**, 051401(R) (2005).
[26] J. G. Underwood, M. Spanner, M. Y. Ivanov, J. Mottershead, B. J. Sussman, and A. Stolow, Phys. Rev. Lett. **90**, 223001 (2003).
[27] R. Tehini and D. Sugny, Phys. Rev. A **77**, 023407 (2008).
[28] H. Stapelfeldt and T. Seideman, Rev. Mod. Phys. **75**, 543 (2003).
[29] T. Seideman and E. Hamilton, Adv. At., Mol., Opt. Phys. **52**, 289 (2006).
[30] G. Turinici, in *Control of Coupled Partial Differential Equations*, International Series on Numerical Mathematics Vol. 155 (Birkhäuser, Basel, 2007), pp. 293–309.
[31] D. Sugny, A. Keller, O. Atabek, D. Daems, C. M. Dion, S. Guérin, and H. R. Jauslin, Phys. Rev. A **69**, 033402 (2004).
[32] D. Sugny, A. Keller, O. Atabek, D. Daems, C. M. Dion, S. Guérin, and H. R. Jauslin, Phys. Rev. A **71**, 063402 (2005).
[33] D. Sugny, A. Keller, O. Atabek, D. Daems, C. M. Dion, S. Guérin, and H. R. Jauslin, Phys. Rev. A **72**, 032704 (2005).
[34] D. Sugny, C. Kontz, and H. R. Jauslin, Phys. Rev. A **74**, 053411 (2006).
[35] R. S. Judson and H. Rabitz, Phys. Rev. Lett. **68**, 1500 (1992).
[36] A. Assion, T. Baumer, M. Bergt, T. Brixner, B. Kiefer, V. Seyfried, M. Strehle, and G. Gerber, Science **282**, 919 (1998).
[37] R. J. Levis, G. M. Menkir, and H. Rabitz, Science **292**, 709 (2001).
[38] C. Daniel, J. Full, L. Gonzàlez, C. Lupulescu, J. Manz, A. Merli, S. Vadja, and L. Woste, Science **299**, 536 (2003).
[39] O. M. Shir, V. Beltrani, T. Back, H. Rabitz, and M. Vrakking, J. Phys. B **41**, 074021 (2008).
[40] E. Hertz, A. Rouzée, S. Guérin, B. Lavorel, and O. Faucher, Phys. Rev. A **75**, 031403(R) (2007).
[41] A. Rouzée, E. Hertz, B. Lavorel, and O. Faucher, J. Phys. B **41**, 074002 (2008).
[42] K. Sundermann and R. de Vivie-Riedle, J. Chem. Phys. **110**, 1896 (1999).
[43] A. Pelzer, S. Ramakrishna, and T. Seideman, J. Chem. Phys. **126**, 034503 (2007).
[44] D. Sugny, A. Keller, O. Atabek, D. Daems, S. Guérin, and H. R. Jauslin, Phys. Rev. A **69**, 043407 (2004).
[45] T. Kanai and H. Sakai, J. Chem. Phys. **115**, 5492 (2001).
[46] H. Sekino and R. J. Bartlett, J. Chem. Phys. **98**, 3022 (1993).
[47] G. Maroulis, J. Phys. Chem. **100**, 13466 (1996).
[48] I. Serban, J. Werschnik, and E. K. U. Gross, Phys. Rev. A **71**, 053810 (2005).

5.4 Geometric optimal control theory for simple quantum systems

Corresponding articles : [2, 3, 5, 6, 10, 11, 12, 14, 19]
This work has been done in collaboration with B. Bonnard of the *Institut de Mathématiques de Bourgogne* and with some other collaborators such as M. Chyba of the *University of Hawaï* or H. R. Jauslin.

This section is devoted to another aspect of optimal control theory in quantum mechanics. A first purely numerical application was developed with the monotonic convergent algorithms. These algorithms are efficient approaches to solve the optimal equations. Another more geometric point of view, called geometric optimal control theory, consists in using the optimal equations in their Hamiltonian version (i.e. the one associated to the Pontryagin Maximum Principle, see below) and to use geometric tools to select the extremal and the optimal solutions. It is this aspect that we are going to describe in this section.

Let us begin by a brief description of geometric optimal control theory and its application in quantum mechanics. Optimal control theory can be viewed as a generalization of the classical calculus of variations for problems with dynamical constraints. Optimal control was born with the Pontryagin Maximum Principle (PMP) in the late 1950's [97]. Its development was originally inspired by problems of space dynamics, but it is now a key tool to study a large spectrum of applications such as robotics, economics, and quantum mechanics. Solving an optimal control problem means finding a particular control law, the optimal control, such that the corresponding trajectory satisfies given boundary conditions and minimizes a cost criterion. The cost functionals of physical interests are the energy of the field and the control duration. The strategy for solving an optimal control problem consists in finding extremal trajectories which are solutions of a generalized Hamiltonian system subject to the maximization condition of the PMP. In a second step, one selects among the extremals the ones which effectively minimize the cost criterion [36, 3]. Although its implementation looks straightforward, the practical use of the PMP is far from being trivial and each control problem has to be analyzed with geometric and numerical methods. The article [2] for non specialist readers gives an introduction to

geometric optimal control and its applications in quantum mechanics.

Whereas conservative finite-dimensional quantum systems were already studied in geometric optimal control theory [46, 76], the dissipative case is currently at the initial stage. In [19, 12, 11, 10, 5, 3], we solved the time-optimal control of two-level dissipative quantum systems whose dynamics is governed by the Lindblad equation. The dissipation effects are described by three parameters Γ, γ_{12} and γ_{21} where Γ is the dephasing rate and γ_{12} and γ_{21} the relaxation rates respectively from level 2 to level 1 and from level 1 to level 2. They satisfy the following inequalities $2\Gamma \geq \gamma_+ \geq |\gamma_-|$ with $\gamma_+ = \gamma_{12} + \gamma_{21}$ and $\gamma_- = \gamma_{12} - \gamma_{21}$. In [19], assuming the control field real, we solve different control problems on the plane $\mathbb{R}^2$. In [12] and [11], we give the complete solution for all the dissipative quantum systems. The integrable case for $\gamma_- = 0$ is treated in [12]. Integrable means here that the Hamiltonian constructed from the PMP is integrable. The generic case is studied in [11] which is reproduced in this manuscript. A complete overview of these two cases with a different presentation is given in [10]. In [14], we also show how to combine geometric optimal control techniques and von Neumann measurements for a three-level quantum system.

In the different papers, the following strategy has been followed. The time-optimal control problems are modeled by affine control systems in $\mathbb{R}^n$ where $n = N^2 - 1$ for a N-level quantum system :

$$\frac{dq}{dt} = F_0(q) + \sum_{i=1}^{m} u_i F_i(q),\ q \in \mathbb{R}^n,$$

where F_i, $i = 0, \cdots, m$ are smooth vector fields, $u = (u_1, \cdots, u_m)$ is the control satisfying the constraint $|u| \leq 1$. In the control of dissipative quantum systems, F_0 represents the interaction of the quantum system with the environment and the F_i, $i = 1, \cdots, m$ correspond to the interaction with the control fields.

From the PMP, the optimal trajectories are the projections on $\mathbb{R}^n$ of extremal trajectories solutions of a generalized Hamiltonian system on $T^*\mathbb{R}^n$. The generalized Hamiltonian function which depends on the control fields satisfies the maximization condition. In the case of the time-minimal control problems, under some general conditions, one can find explicitly the control fields as functions on $T^*\mathbb{R}^n$. The problem then reduces to the study of a

Hamiltonian system given by

$$H(p,q) = H_0(p,q) + (\sum_{i=1}^{m} H_i^2(p,q))^{1/2},$$

where $H_i(p,q) = \langle p, F_i(q)\rangle$ for $i = 0, \cdots, m$, $p \in T^*\mathbb{R}^n$ is the adjoint vector and $u_i = H_i/(\sum_{i=1}^m H_i^2(p,q))^{1/2}$. Finding the optimal trajectory means finding the initial value $p(0)$ such that the extremal trajectory satisfies the boundary conditions. One then selects among all the solutions, the one which minimizes the time. In other words, by using this Hamiltonian we have replaced the optimization of an infinite number of parameters by a finite one.

Some specific problems have to be considered to complete the analysis. The first point is the singularity analysis. One must determine the behavior of extremal curves near the switching surface of $T^*\mathbb{R}^n$ characterized by $H_i = 0$, $i = 1, \cdots, m$. For single control problems where the control is of the form $u_1 = \text{sign } H_1$, the singularity analysis leads to complicated behaviors. The optimal solution can be the concatenation of bang (with $|u_1| = 1$) and singular arcs where $|u_1| \leq 1$. We also consider the second order optimality conditions to determine the local optimality of the extremal trajectories. These conditions are related to a generalization of the concept of conjugate points in the classical calculus of variations. From a numerical point of view, we use the existing COTCOT code for determining the position of conjugate points [48].

The optimal control problem is solved in practice by using a shooting algorithm to determine the initial value of the adjoint vector. Here, since the dissipative quantum system naturally depends on parameters which describe the interaction with the environment, one can use a smooth continuation method to initialize the shooting algorithm [37]. We show in [12] that for a particular value of the dissipative parameters ($\gamma_+ = \Gamma$ and $\gamma_- = 0$), the time-optimal control problem of two-level dissipative quantum systems can be reduced to a Riemannian problem on a two-sphere of revolution, the Grushin model. Local (conjugate locus) and global (cut locus) optimality results are known for this model. The cut and the conjugate loci are respectively the set of points where the extremal trajectories cease to be globally and locally optimal. The Grushin model is used as a starting point for the geometrical analysis of the control problem and for the continuation method [5]. In [5], we also show the relation between the conjugate points and the failure of

the continuation approach.

We reproduce here the article [11].

Time-Minimal Control of Dissipative Two-level Quantum Systems: the Generic Case

Bernard Bonnard, Monique Chyba and Dominique Sugny

***Abstract*—The objective of this article is to complete preliminary results from [5], [19] concerning the time-minimal control of dissipative two-level quantum systems whose dynamics is governed by the Lindblad equation. The extremal system is described by a 3D-Hamiltonian depending upon three parameters. We combine geometric techniques with numerical simulations to deduce the optimal solutions.**

***Index Terms*—Time optimal control, conjugate and cut loci, quantum control**

I. INTRODUCTION

IN this article, we consider the time-minimal control analysis of two-level *dissipative* quantum systems whose dynamics is governed by the *Lindblad equation*. More generally, according to [12], [15], the dynamics of a finite-dimensional quantum system in contact with a dissipative environment is described by the evolution of the *density matrix* ρ which is a positive semidefinite Hermitian operator having $\mathrm{tr}(\rho) = 1$ and $\mathrm{tr}(\rho^2) \leq 1$ [1], [12], [15]. The evolution of ρ is given by

$$i\frac{\partial \rho}{\partial t} = [H_0 + H_1, \rho] + i\mathcal{L}(\rho), \quad (1)$$

where H_0 is the field-free Hamiltonian of the system, H_1 represents the interaction with the control field and $\mathcal{L}$ the dissipative part of the equation; $[A, B]$ is the commutator of the operators A and B defined by $[A, B] = AB - BA$. Equation (1) is written in units such that $\hbar = 1$. In the eigenbasis of H_0, the components of the density matrix satisfy the following equations:

$$\begin{aligned} \dot{\rho}_{nn} &= -i[H_0 + H_1, \rho]_{nn} - \textstyle\sum_{k\neq n} \gamma_{kn}\rho_{nn} + \sum_{k\neq n} \gamma_{nk}\rho_{kk} \\ \dot{\rho}_{kn} &= -i[H_0 + H_1, \rho]_{kn} - \Gamma_{kn}\rho_{kn}, \;\; k \neq n \end{aligned}$$

where $1 \leq k \leq N$ and $1 \leq n \leq N$ for a N-level quantum system. The parameters γ_{kn} describe the population relaxation from state k to state n whereas Γ_{kn} is the dephasing rate of the transition from state k to state n. Note that not every positive parameter γ_{kn} or Γ_{kn} is acceptable from a physical point of view due to the properties of the density matrix.

The analysis is motivated by physical reasons. We consider a fundamental model in quantum control extending the control of quantum systems in the conservative case [7], [14] and describing a variety of physical systems. An example is given by the control of molecular alignment by laser fields in dissipative media where dissipation effects are due to molecular collisions. For a diatomic molecule driven by a linearly polarized laser field, molecular alignment means an increased probability distribution along the polarization axis. In this context, it has been proposed theoretically [16] and confirmed experimentally that such systems are governed by the Lindblad equation [21]. For molecular alignment, the dimension of the Hilbert space is infinite but can be truncated to a finite one if the intensity of the laser field is sufficiently weak. In standard experiments on molecular alignment, about twenty modes have generally to be taken into account.

In this article, we consider as a first step the control of two-level quantum systems controlled by laser fields. This three dimensional system allows us to conduct a thorough geometric analysis. It provides a test-bed case to run numerical computations based on the *Cotcot-code* [3] (including *shooting methods* and *second order optimality conditions*) and continuation methods on the set of parameters. Also this case describes the dynamics of a spin $1/2$ particle in a magnetic field [10]. Hence, particularizing to $N = 2$ in equation (1) and assuming that H_1 is of the form

$$H_1 = -\mu_x E_x - \mu_y E_y,$$

where the operators μ_x and μ_y are proportional to the Pauli matrices σ_x and σ_y in the eigenbasis of H_0. The electric field is the superposition of two linearly polarized fields E_x and E_y and we assume that these two fields are in resonance with the Bohr frequency $E_2 - E_1$. For a spin $1/2$ particle, we can consider the same Hamiltonian where H_0 corresponds to a constant magnetic field along the z-axis and the dynamics is controlled by two magnetic fields B_x and B_y polarized respectively along the x- and y- axis.

In the *Rotating Wave Approximation* which consists in an averaging procedure over the rapid oscillations of the field [13], the time evolution of $\rho(t)$ satisfies the following form of the Lindblad equation $i\frac{\partial}{\partial t}\rho = M\rho$ where ρ is written as a vector $(\rho_{11}, \rho_{12}, \rho_{21}, \rho_{22})$ and

$$M = \begin{pmatrix} -i\gamma_{12} & -E^* & E & i\gamma_{21} \\ -E & -\omega - i\Gamma & 0 & E \\ E^* & 0 & \omega - i\Gamma & -E^* \\ i\gamma_{12} & E^* & -E & -i\gamma_{21} \end{pmatrix}. \quad (2)$$

The field E is equal to $E = ue^{i\omega t}/2$ where u is *the complex Rabi frequency* of the laser field (the real and imaginary parts of u are the amplitudes of the real fields E_x and E_y up to a multiplicative constant). The frequency ω is the difference of

B. Bonnard is with the Institut de Mathématiques de Bourgogne, UMR CNRS 5584, 9 Avenue Alain Savary, BP 47 870 F-21078 DIJON Cedex FRANCE (bernard.bonnard@u-bourgogne.fr).

M. Chyba is with the University of Hawaii, Department of Mathematics, Honolulu, HI 96822, USA (mchyba@math.hawaii.edu).

D. Sugny is with the Institut Carnot de Bourgogne, UMR 5209 CNRS-Université de Bourgogne, 9 Av. A. Savary, BP 47 870, F-21078 DIJON Cedex, FRANCE (dominique.sugny@u-bourgogne.fr).

energy between the ground and excited states of the system. In the interaction representation, M becomes

$$\tilde{M} = \begin{pmatrix} -i\gamma_{12} & -u^*/2 & u/2 & i\gamma_{21} \\ -u/2 & -i\Gamma & 0 & u/2 \\ u^*/2 & 0 & -i\Gamma & -u^*/2 \\ i\gamma_{12} & u^*/2 & -u/2 & -i\gamma_{21} \end{pmatrix}. \quad (3)$$

The interaction representation means that we have transformed the mixed-state ρ with the unitary transformation $U = \text{diag}(1, e^{i\omega t}, e^{-i\omega t}, 1)$. The new matrix $\tilde{M}$ is then given by $\tilde{M} = U^{-1}MU - iU^{-1}dU/dt$. Since $\text{Tr}[\rho] = 1$ and $\rho = \rho\dagger$, the $N \times N$ coefficients representing the density matrix can be replaced by $N^2 - 1$ real parameters. For a two-level quantum system, the density matrix ρ can be represented by the vector $q = (x, y, z)$ where $x = 2\Re[\rho_{12}]$, $y = 2\Im[\rho_{12}]$ and $z = \rho_{22} - \rho_{11}$ and q belongs to the *Bloch ball* $|q| \leq 1$. The Lindblad equation takes the form:

$$\begin{cases} \dot{x} = -\Gamma x + u_2 z \\ \dot{y} = -\Gamma y - u_1 z \\ \dot{z} = (\gamma_{12} - \gamma_{21}) - (\gamma_{12} + \gamma_{21})z + u_1 y - u_2 x \end{cases}. \quad (4)$$

$\Lambda = (\Gamma, \gamma_+, \gamma_-)$ is the set of parameters such that $\gamma_+ = \gamma_{12} + \gamma_{21}$ and $\gamma_- = \gamma_{12} - \gamma_{21}$. Since the Bloch ball $|q| \leq 1$ is invariant, it follows from the Lindblad equation [18] that $2\Gamma \geq \gamma_+ \geq |\gamma_-|$. The distance to the origin of the ball represents the purity of the system. A point of the Bloch sphere corresponds to a pure state. The control is $u = u_1 + iu_2$ where u_1 and u_2 are two real functions. We can write the control field $u = |u|e^{i\phi}$ where $|u| \leq C$ and up to a rescaling of the time and dissipative parameters we can assume that $|u| \leq 1$. It is a neat geometric representation, in which the state of the system is identified to a point of the unit ball, the drift term represents the dissipation and the components of the laser fields correspond to rotations along the x and y axes. Also this leads to a representation of the system using spherical coordinates: ρ denotes the distance to the origin, θ is the angle of revolution around the $z-$axis and ϕ is the angle along the meridian.

If we consider the optimal control problems, the costs important for applications are the time minimal transfer or the energy minimization and we shall concentrate on the first problem (both problems share similar geometric properties and can be handled using the same techniques but in the time-minimal case the control constraints can be taken into account directly and the geometric analysis is more striking). Hence, we have to analyze a time-minimal control problem for a *bilinear system* of the form:

$$\dot{q} = F_0(q) + \sum_{i=1}^{2} u_i F_i(q), \; |u| \leq 1,$$

where the drift term F_0 depends upon three parameters. This is a very difficult problem whose analysis requires advanced mathematical tools from geometric control theory and numerical simulations. Numerous geometric optimal control results exist in the conservative case e.g. [7], [14], but only partial ones for this problem: a pioneering work [19] assuming u real and a second one [5] for u complex but restricted to $\gamma_- = 0$. Using spherical coordinates, outside the switching surface Σ : $p_\phi = p_\theta \cot\phi = 0$, the extremal curves are smooth solutions of the Hamiltonian differential equation defined by:

$$H_r = [\gamma_- \cos\phi - \rho(\gamma_+ \cos^2\phi + \Gamma \sin^2\phi)]p_\rho + p_\phi[-\frac{\gamma_- \sin\phi}{\rho} + \frac{\sin(2\phi)}{2}(\gamma_+ - \Gamma)] + \sqrt{p_\phi^2 + p_\theta^2 \cot^2\phi}.$$

In the case $\gamma_- = 0$, the extremal system is integrable and we have obtained in [5] a complete geometric analysis based on a geometric continuation method on the set of dissipative parameters starting from the case $\Gamma = \gamma_+$, where the analysis is reduced to a Riemannian problem on a two-sphere of revolution for the metric $g = d\phi^2 + \tan^2\phi d\theta^2$. The general case where $\gamma_- \neq 0$ cannot be deduced from the integrable case, although some geometric properties persist: two types of asymptotic behaviors for the extremal trajectories connected to the existence or not of *conjugate points*, which will conduct our computations. Indeed our analysis will show bifurcations phenomena for the accessibility set which distinguishes the integrable case from the generic case. The aim of this article is to complete the integrable case and to make a complete study for every generic parameter in Λ, combining mathematical reasoning and *intensive* numerical simulations using shooting techniques and including computations of *conjugate points* to test optimality. Based on the Cotcot code [3], they can be used in practice to compute the true optimal control, once the physical parameters are identified.

The organization of this article is the following. In section II, we complete the classification of the time-minimal synthesis of [19] corresponding to the case where u is real but introducing more general tools to handle the problem. It corresponds to a time-minimal control problem of a two-dimensional bilinear system in the single-input case. The optimal synthesis for a fixed initial point can be constructed by gluing together local optimal syntheses. We can also make estimates of switching points by lifting the system on a semi-direct product Lie group. *This classification is physically relevant to analyze the 3D-case because, using the symmetry of revolution of the problem, it gives the time-minimal synthesis for initial points* $q_0 = (0, 0, \pm 1)$. This geometric property is explained in section III. Moreover, using spherical coordinates the system can be viewed as a system on a *two-sphere of revolution* coupled with the evolution of the distance to the origin, which represents the *purity* of the system. According to the maximum principle, smooth extremals are solutions of the Hamiltonian vector field $\vec{H}_r$ where $H_r = H_0 + (H_1^2 + H_2^2)^{1/2}$, $H_i = \langle p, F_i(q) \rangle$, and the control components are given by $u_i = H_i/(H_1^2 + H_2^2)^{1/2}$, $i = 1, 2$. Non smooth extremals can be constructed by connecting smooth subarcs of the switching surface Σ: $H_1 = H_2 = 0$. In general this problem is technically very difficult to analyze and the existence of the switching surface can lead to complicated behaviors for the extremal trajectories. A contribution of this article in section III is to classify the possible connections in our problem. We proved that every non smooth extremal is either a solution of the 2D-single input system, assuming u real, or occurs when meeting the equatorial plane of the Bloch ball. In the second case, the switching can be handled numerically using an integrator with an adaptative step. In the same section, we

combine analytical and numerical analysis to determine the extremals and to compute conjugate points. This completes the analysis from [5] in the integrable case. The physical interpretation is presented as a conclusion.

II. THE 2D-CASE

Following [19], a first step in the analysis is to consider the following reduced system. Assuming u real, the x-coordinate is not controllable and we can consider the planar single-input system:

$$\begin{array}{l} \dot{y} = -\Gamma y - u_1 z \\ \dot{z} = \gamma_- - \gamma_+ z + u_1 y, |u_1| \leq 1 \end{array} . \quad (5)$$

The parameters satisfy the following inequalities:

$$2\Gamma \geq \gamma_+ \geq | \gamma_- | .$$

The goal is to obtain the time-optimal synthesis when the initial state $q(0) = (y(0), z(0))$ is a pure state on the $z-$axis, that is $q(0) = (0, \pm 1)$. Using a discrete symmetry group associated to reflections with respect to the two axes, one can assume that the initial point is $(0, 1)$ and moreover we can restrict our analysis to the domain $y \geq 0$. This is connected to the symmetry of revolution of the whole system around the $z-$axis.

We proceed as follows.

A. The feedback classification

Due to the complexity of the study, a first step in our analysis is to consider the feedback classification problem. The system is written in a more compact form as follows:

$$\dot{q} = F(q) + uG(q)$$

where F and G are affine vector fields. To make the feedback classification, we relax the control bound $|u| \leq 1$. According to [4], the geometric invariants are related to the sets:

- The singular set: $S = \{q, \det(G, [F, G]) = 0\}$ where are located the singular trajectories.
- The collinear set: $C = \{q, \det(F, G) = 0\}$ corresponding to the set of points where F and G are collinear.

A singular control u_s is given by the relation:

$$\langle p[[G, F], F]\rangle + u_s \langle p, [[G, F], G]\rangle = 0.$$

Moreover a singular trajectory can be small time minimal or small time maximal. In the $2D-$case, this status is tested by Lie brackets configurations as follows, see [4]. We introduce:

$$D = \det(G, [G, F], G), D'' = \det(G, F).$$

The trajectory is time-minimal if $DD'' > 0$ and time-maximal if $DD'' < 0$.

A straightforward computation gives in our case:

Lemma 1.

- *The set S is given by: $y[2(\Gamma - \gamma_+)z + \gamma_-] = 0$ and if $\gamma_+ \neq \Gamma$, the singular set is defined by the two lines $y = 0$ and $z = \gamma_-/[2(\gamma_+ - \Gamma)]$.*

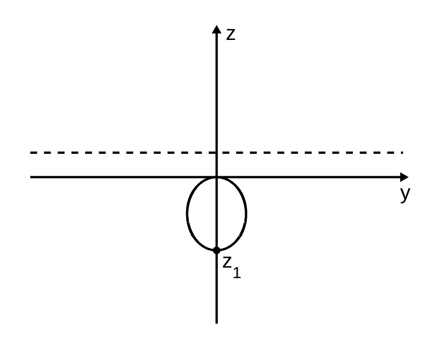


Fig. 1. Diagram of the sets S and C in solid lines for $\gamma_- = -0.2$, $\gamma_+ = 0.4$ and $\Gamma = 1$. The equation of the horizontal dashed line is $z = \gamma_-/2(\gamma_+ - \Gamma)$.

- *The set C is defined by: $\gamma_+ z^2 + \Gamma y^2 - \gamma_- z = 0$. It is a closed curve containing $(0, 0)$ and $(z_1, 0)$, with $z_1 = \gamma_-/\gamma_+$ (the equilibrium state of the free motion) which shrinks into $(0, 0)$ when $\gamma_- = 0$.*
- *If $\gamma_- \neq 0$, the intersection of C and S is empty except in the case where $\gamma_+ = 2\Gamma$.*

We represent on Fig. 1 the sets S and C for a situation with $\gamma_- < 0$ and $\gamma_+ - \Gamma < 0$.

Lemma 2.

- *For the singular direction $y = 0$, we get:*

$$DD'' = 2z^2(\gamma_+ - \Gamma)\gamma_+(z - \frac{\gamma_-}{2(\gamma_+ - \Gamma)})(z - \frac{\gamma_-}{\gamma_+}).$$

Near the origin, the sign is always positive if $\gamma_- \neq 0$. If $\gamma_- = 0$, the sign is given by $(\gamma_+ - \Gamma)$.
- *For the singular direction $z = \gamma_-/[2(\gamma_+ - \Gamma)]$, we have:*

$$DD'' = \frac{y^2}{2(\gamma_+ - \Gamma)}[\gamma_-^2(\gamma_+ - 2\Gamma) - 4\Gamma y^2(\gamma_+ - \Gamma)^2].$$

Hence, near the origin one gets that $DD'' > 0$ if $\gamma_+ - \Gamma < 0$ and $DD'' < 0$ if $\gamma_+ - \Gamma > 0$.

One further step in the classification is to compute a normal form for the action of the feedback group. We have:

Proposition 1. *The system is feedback equivalent to:*

$$\begin{array}{l} \dot{x} = \frac{\gamma_-^2}{4(\gamma_+ - \Gamma)} - 2\Gamma x + (\Gamma - \gamma_+)z^2 \\ \dot{z} = \frac{\gamma_-(\gamma_+ - 2\Gamma)}{2(\gamma_+ - \Gamma)} - \gamma_+ z + u_1 \end{array} .$$

Proof: Using polar coordinates:

$$y = \rho\cos\phi, \; z = \rho\sin\phi,$$

one gets:

$$\begin{array}{l} \dot{\rho} = \gamma_- \sin\phi + \rho[-\Gamma + (\Gamma - \gamma_+)\sin^2\phi] \\ \dot{\phi} = \frac{\gamma_- \cos\phi}{\rho} + (\Gamma - \gamma_+)\frac{\sin(2\phi)}{2} + u_1 \end{array} .$$

If we use the coordinates $x = \rho^2/2$ and z, the system becomes:

$$\begin{array}{l} \dot{x} = -2\Gamma x + \gamma_- z + z^2(\Gamma - \gamma_+) \\ \dot{z} = \gamma_- - \gamma_+ z + u_1\sqrt{2x - z^2} \end{array} .$$

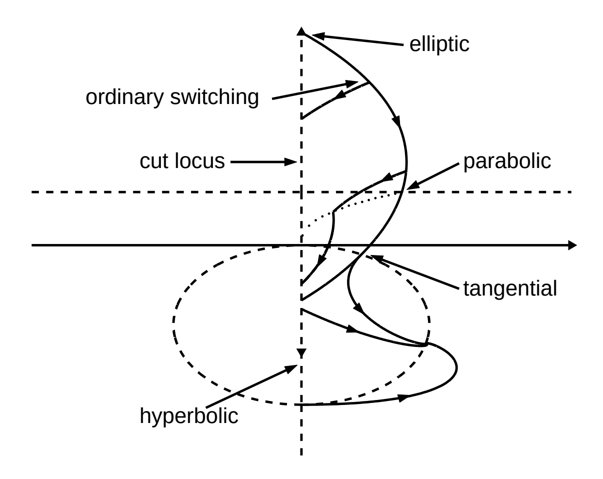


Fig. 2. Cut and switching loci for the case $\gamma_- < 0$. The sets C and S are represented in dashed lines, the switching locus in dotted lines.

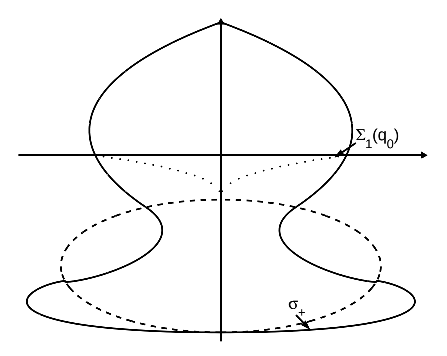


Fig. 3. Fish-shape of the accessibility set.

Making a feedback transformation of the form $u_1 \to \beta u_1$ where β is a function of x and z, we can consider the system:

$$\begin{aligned} \dot{x} &= -2\Gamma x + \gamma_- z + z^2(\Gamma - \gamma_+) \\ \dot{z} &= \gamma_- - \gamma_+ z + u_1 \end{aligned} .$$

If we set $z = Z + z_0$ where $z_0 = \gamma_-/[2(\gamma_+ - \Gamma)]$, we obtain the system in the form of the proposition. ■

In this simplified model, where the control is rescaled by the positive function β, we keep most of the information about the initial system. In particular, all the feedback invariants in the plane minus the z-axis are preserved: the collinear set corresponds to $\dot{x} = 0$ and the singular set is identified to $z = 0$ (and the optimality status is clear in the normal form).

For the simplified model, the adjoint system takes the form:

$$\begin{aligned} \dot{p}_x &= 2\Gamma p_x \\ \dot{p}_z &= -2zp_x(\Gamma - \gamma_+) + p_z\gamma_- \end{aligned} ,$$

and can be easily integrated to compute the time-minimal synthesis with $| u_1 | \leq 1$.

B. The time-minimal syntheses

We use [4] as general reference on time-minimal synthesis, see also [9]. The initial condition is fixed to $q_0 = (0, 1)$ and we consider the problem of constructing the time-minimal synthesis from this initial point. This amounts to computing two objects:

- The switching locus $\Sigma(q_0)$ of optimal trajectories which is deduced from the switching locus of extremal trajectories.
- The cut locus $C(q_0)$ which is formed by the set of points where a minimizer ceases to be optimal.

In order to achieve this task, we must glue together local time minimal syntheses which are classified. To be more precise, take the case (d) of [19], the gluing being indicated on Fig. 2 on which we have represented the local extremal classifications of [4] which are crucial to deduce the optimal syntheses. In this case, the cut locus is a segment of the $z-$axis starting at the initial point $(0, 1)$ which is a consequence of the so-called elliptic situation. The switching locus is the union of an optimal singular trajectory, corresponding to a so-called hyperbolic point and a curve $\Sigma_1(q_0)$ whose existence is related to a so-called parabolic situation. Note also the importance of the tangential point where the arcs σ_+ and σ_- corresponding to $u = +1$ and $u = -1$ are tangent leading to the fish-shaped accessibility set $A^+(q_0)$ represented on Fig. 3. This set is not closed since the arcs $\sigma_\pm$ starting from $(0, z_1)$ are not in $A^+(q_0)$. We next give the list of local syntheses we need to construct the global synthesis.

List of local syntheses:

We use the notation $\sigma_1\sigma_2$ for an arc σ_1 followed by an arc σ_2. The first two cases are standard situations.

- **Ordinary switching points**: The local synthesis is given by $\sigma_-\sigma_+$ or $\sigma_+\sigma_-$. The two cases are distinguished using for instance the clock form $\omega = pdq$ with $\langle p, G\rangle = 0$ and $\langle p, F\rangle = 1$ which is also useful to get more global results [4].
- **The fold case**: This case is due to the existence of singular directions located on S. In this case the singular control is given by the relation:

$$\langle p, [[G, F], F]\rangle + u_s\langle p, [[G, F], G]\rangle = 0.$$

In order to be admissible, it must satisfy the constraint $|u_s| \leq 1$. Assume it is not saturating, i.e., $|u_s| \neq 1$ we have three cases:

1) **Hyperbolic case**: The singular arc is admissible and time minimal. The optimal synthesis is of the form $\sigma_\pm\sigma_s\sigma_\pm$ where σ_s is a singular arc.
2) **Elliptic case**: The singular arc is admissible but is small time maximal. An optimal arc is bang-bang with at most one switching. Not every extremal trajectory is optimal and we have the existence of a cut locus.
3) **Parabolic point**: It corresponds to the existence of a singular arc for which $|u_s| > 1$. Every extremal curve is bang-bang with at most two switchings. In our case, the initial point is fixed and the switching locus starts with the intersection of σ_- with the singular line (see Fig. 4).

In our problem, two more complicated cases occur.

- **Saturating case**:
  A small time minimal singular trajectory is such that the singular control is saturating at a point M. A consequence is the appearance of a switching curve at M (see Fig. 5).

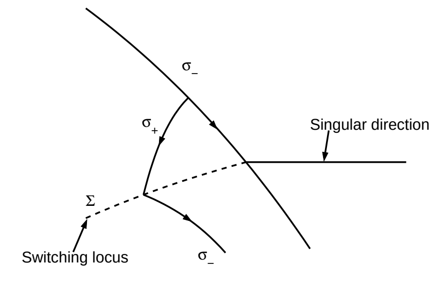


Fig. 4. Parabolic case.

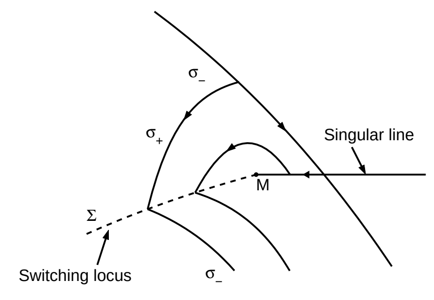


Fig. 5. Saturating case

- **A $C \cap S \neq \emptyset$ case**:
  A *time minimal* singular trajectory meets the set C and becomes *time maximal*. (see Fig. 6)

C. The switching function

The switching function Φ is defined as $\Phi(t) = p(t)G(q(t))$ and switching occurs when $\Phi(t) = 0$. The dynamics of p is given by the adjoint equation:

$$\dot{p} = -p(\frac{\partial F}{\partial q} + u\frac{\partial G}{\partial q}),\ u = \pm 1.$$

The corresponding dynamics is linear and p can be either oscillating if the eigenvalues are complex or non oscillating if they are real.

An equivalent but more geometric test is the use of the standard Θ-function introduced in [9] and defined as follows. Let v be the tangent vector solution of the variational equation:

$$\dot{v} = (\frac{\partial F}{\partial q} + u\frac{\partial G}{\partial q})v,\ u = \pm 1,$$

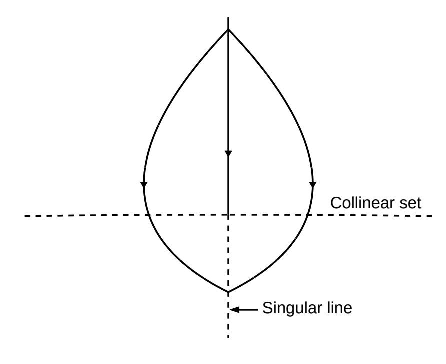


Fig. 6. A $C \cap S \neq \emptyset$ case

whose dynamics is similar to the one of the adjoint vector. Let $0,\ t$ be two consecutive switching times on an arc σ_+ or σ_-. By definition, we have:

$$p(0)G(q(0)) = p(t)G(q(t)) = 0.$$

We denote by $v(\cdot)$ the solution of the variational equation such that $v(t) = G(q(t))$ and where this equation is integrated backwards from time t to time 0. By construction $p(0)v(0) = 0$ and we deduce that at time 0, $p(0)$ is orthogonal to $G(q(0))$ and to $v(0)$. Therefore, $v(0)$ and $G(q(0))$ are collinear; $\Theta(t)$ is defined as the angle between $G(q(0))$ and $v(0)$ measured counterclockwise. One deduces that switching occurs when $\Theta(t) = 0\ [\pi]$. In the analytic case, $\Theta(t)$ can be computed using Lie brackets. Indeed, for $u = \varepsilon$, $\varepsilon = \pm 1$, we have by definition

$$v(0) = e^{-t\mathrm{ad}(F+\varepsilon G)}G(q(t)),$$

and in the analytic case, the ad-formulae [4] gives :

$$v(0) = \sum_{n \geq 0} \frac{(-t)^n}{n!}\mathrm{ad}^n(F + \varepsilon G)G(q(t)).$$

In [19], the Θ function is computed using numerical simulations. Here, to make the computation explicit, we take advantage of the fact that we can lift our bilinear system into an invariant system onto the semi-direct product Lie group $GL(2,\mathbb{R}) \times_S \mathbb{R}^2$ identified to the set of matrices of $GL(3,\mathbb{R})$:

$$\begin{pmatrix} 1 & 0 \\ g & v \end{pmatrix},\ g \in GL(2,\mathbb{R}),\ v \in \mathbb{R}^2,$$

acting on the subspace of vectors in $\mathbb{R}^3$: $\begin{pmatrix} 1 \\ q \end{pmatrix}$.

Lie brackets computations are defined as follows. We set:

$$F(q) = Aq + a,\ G(q) = Bq,$$

and F, G are identified to (A, a), $(B, 0)$ in the Lie algebra $\underline{gl}(2,\mathbb{R}) \times \mathbb{R}^2$. The Lie brackets computations on the semi-direct product Lie algebra are defined by:

$$[(A', a'), (B', b')] = ([A', B'], A'b' - B'a').$$

We now compute $\exp[-t\mathrm{ad}(F + \varepsilon G)]$. The first step consists in determining $\exp[-t\mathrm{ad}(A+\varepsilon B)]$ which amounts to compute $\mathrm{ad}(A + \varepsilon B)$. We write $\underline{gl}(2,\mathbb{R}) = c \oplus \underline{sl}(2,\mathbb{R})$ where c is the center

$$\mathbb{R}\begin{pmatrix} 1 & 0 \\ 0 & 1 \end{pmatrix}.$$

We choose the following basis of $\underline{sl}(2,\mathbb{R})$:

$$B = \begin{pmatrix} 0 & -1 \\ 1 & 0 \end{pmatrix},\ C = \begin{pmatrix} 0 & 1 \\ 1 & 0 \end{pmatrix} \text{ and } D = \begin{pmatrix} 1 & 0 \\ 0 & -1 \end{pmatrix}.$$

The matrix A is decomposed into:

$$A = \begin{pmatrix} -\Gamma & 0 \\ 0 & -\gamma_+ \end{pmatrix} = \begin{pmatrix} \lambda & 0 \\ 0 & \lambda \end{pmatrix} + \begin{pmatrix} s & 0 \\ 0 & -s \end{pmatrix}$$

and hence $\lambda = -(\Gamma + \gamma_+)/2$ and $s = (\gamma_+ - \Gamma)/2$. In the basis ($B$, C, D), $\mathrm{ad}(A + \varepsilon B)$ is represented by the matrix:

$$\begin{pmatrix} 0 & -2s & 0 \\ -2s & 0 & 2\varepsilon \\ 0 & -2\varepsilon & 0 \end{pmatrix}.$$

The characteristic polynomial is $P(\lambda) = -\lambda(\lambda^2+4(\varepsilon^2-s^2))$ and the eigenvalues are $\lambda = 0$ and $\lambda_i = \pm 2\sqrt{s^2-\varepsilon^2}$, $i = 1, 2$; λ_1 and λ_2 are distinct and real if $|\gamma_+ - \Gamma| > 2$ and we note $\lambda_1 = 2\sqrt{s^2-\varepsilon^2}$, $\lambda_2 = -\lambda_1$; λ_1 and λ_2 are distinct and imaginary if $|\gamma_+ - \Gamma| < 2$ and we note $\lambda_1 = 2i\sqrt{\varepsilon^2-s^2}$, $\lambda_2 = -\lambda_1$. To compute $e^{-t\text{ad}(A+\varepsilon B)}$, we must distinct two cases.

Real case: In the basis B, C, D, the eigenvectors corresponding to $\{0, \lambda_1, \lambda_2\}$ are respectively: $v_0 = (\varepsilon, 0, s)$, $v_1 = (2s, -\lambda_1, 2\varepsilon)$ and $v_2 = (2s, -\lambda_2, 2\varepsilon)$. Therefore, in this eigenvector basis, $\exp[-t\text{ad}(A+\varepsilon B)]$ is the diagonal matrix: $\text{diag}(1, e^{-\lambda_1 t}, e^{-\lambda_2 t})$. To compute $\exp[-t\text{ad}(A+\varepsilon B)]B$, we use the decomposition $B = \alpha v_0 + \beta v_1 + \beta v_2$, with:

$$\alpha = \frac{\varepsilon}{\varepsilon^2 - s^2},\ \beta = \frac{s}{4(s^2-\varepsilon^2)}.$$

Hence one gets:

$$e^{-t\text{ad}(A+\varepsilon B)}B = \alpha v_0 + \beta e^{-\lambda_1 t}v_1 + \beta e^{-\lambda_2 t}v_2.$$

To test the collinearity at q_0, we compute

$$\det(B(q_0), e^{-t\text{ad}(A+\varepsilon B)}B(q_0)) = 0$$

where the determinant is equal to

$$(z_0^2 - y_0^2)(\alpha s + 2\varepsilon(\beta e^{-\lambda_1 t} + \beta e^{-\lambda_2 t})) + 2y_0 z_0(\lambda_1 \beta e^{-\lambda_1 t} + \lambda_2 \beta e^{-\lambda_2 t}),$$

which simplifies into

$$(z_0^2 - y_0^2)[\alpha s + 4\varepsilon\beta\cosh(\lambda_1 t)] - 4y_0 z_0 \beta\lambda_1 \sinh(\lambda_1 t).$$

Imaginary case: In this case, we note $\lambda_1 = i\varphi$ the eigenvalue associated to the eigenvector $(2s, -i\varphi, 2\varepsilon)$. We consider the real part $v_1 = (2s, 0, 2\varepsilon)$ and the imaginary part $v_2 = (0, -\varphi, 0)$. In the basis $v_0 = (\varepsilon, 0, s)$, v_1, v_2, $\text{ad}(A+\varepsilon B)$ takes the normal form:

$$\text{diag}(0, \begin{pmatrix} 0 & \varphi \\ -\varphi & 0 \end{pmatrix}).$$

Hence, we have in this basis:

$$e^{-t\text{ad}(A+\varepsilon B)} = \text{diag}(1, \begin{pmatrix} \cos(\varphi t) & -\sin(\varphi t) \\ \sin(\varphi t) & \cos(\varphi t) \end{pmatrix}).$$

We decompose B in the same basis: $B = \alpha v_0 + \beta v_1 + \gamma v_2$, where

$$\alpha = \frac{\varepsilon}{\varepsilon^2 - s^2},\ \beta = \frac{s}{4(s^2-\varepsilon^2)},\ \gamma = 0.$$

Hence, we get:

$$e^{-t\text{ad}(A+\varepsilon B)}B = \alpha v_0 + \beta[\cos(\varphi t)v_1 + \sin(\varphi t)v_2].$$

Computing we obtain:

$$\det(Bq_0, e^{-t\text{ad}(A+\varepsilon B)}B(q_0)) = (z_0^2 - y_0^2)(\alpha s + 4\varepsilon\beta\cos(\varphi t)) + 4\beta\varphi\sin(\varphi t)y_0 z_0.$$

We proved:

Proposition 2. *Assume $\gamma_- = 0$ and that a switching occurs at times 0, t along an arc σ_ε initiating from (y_0, z_0) . Then*

1) *if $|\gamma_+ - \Gamma| > 2$, we must have:*

$$(z_0^2 - y_0^2)(\alpha s + 4\varepsilon\beta\cosh(\lambda_1 t)) - 4y_0 z_0\beta\lambda_1\sinh(\lambda_1 t) = 0$$

where $\lambda_1 = 2\sqrt{s^2-\varepsilon^2}$, $\alpha = \frac{\varepsilon}{\varepsilon^2-s^2}$, $\beta = \frac{s}{4(s^2-\varepsilon^2)}$. In particular if $(y_0, z_0) = (0, 1)$ there is no switching for $t > 0$.

2) *if $|\gamma_+ - \Gamma| < 2$, we must have:*

$$(z_0^2 - y_0^2)(\alpha s + 4\varepsilon\beta\cos(\varphi t)) + 4\beta\varphi\sin(\varphi t)y_0 z_0 = 0$$

where $\varphi = 2\sqrt{\varepsilon^2 - s^2}$, $\alpha = \frac{\varepsilon}{\varepsilon^2-s^2}$, $\beta = \frac{s}{4(s^2-\varepsilon^2)}$. In particular if $(y_0, z_0) = (0, 1)$ switching occurs periodically with a period $2\pi/\varphi$.

Case $\gamma_- \neq 0$: The computations are more complex but this case is similar. The vector field $F + \varepsilon G$ is an affine vector field and to simplify the computations it is transformed into the linear vector field $A + \varepsilon B$ making the following translation in the $\mathbb{R}^2$ space: $Y = y + \tilde{y}$, $Z = z + \tilde{z}$ with $\tilde{y} = \varepsilon\gamma_-/(\Gamma\gamma_+ + \varepsilon^2)$ and $\tilde{z} = -\Gamma\gamma_-/(\Gamma\gamma_+ + \varepsilon^2)$. G is transformed into the affine vector $Bq + w$ where w is the vector (w_1, w_2) with $w_1 = -\Gamma\gamma_-/(\Gamma\gamma_+ + \varepsilon^2)$ and $w_2 = -\varepsilon\gamma_-/(\Gamma\gamma_+ + \varepsilon^2)$. The vector field $\text{ad}(F + \varepsilon G)$ acts on the vector space $\underline{gl}(2, \mathbb{R}) \oplus \mathbb{R}^2$ and the action on the space $\underline{gl}(2, \mathbb{R})$ has been previously computed. According to the definition of the Lie bracket, the action on the $\mathbb{R}^2$ space is simply the action of the linear operator $A + \varepsilon B$. The characteristic polynomial is $P = \lambda^2 + (\Gamma + \gamma_+)\lambda + (\Gamma\gamma_+ + \varepsilon^2)$. We must distinguish two cases:

Real case: If $|\Gamma - \gamma_+| > 2$, we have two real eigenvalues

$$\sigma_1 = \frac{-(\Gamma+\gamma_+) + 2\sqrt{s^2-\varepsilon^2}}{2}$$
$$\sigma_2 = \frac{-(\Gamma+\gamma_+) - 2\sqrt{s^2-\varepsilon^2}}{2}$$

with corresponding eigenvectors f_1 and f_2. Writing the vector w as $\delta_1 f_1 + \delta_2 f_2$, one gets using the previous computations

$$e^{-t\text{ad}(F+\varepsilon G)}G = \alpha v_0 + \beta e^{-\lambda_1 t}v_1 + \gamma e^{-\lambda_2 t}v_2 + \delta_1 e^{-\sigma_1 t}f_1 + \delta_2 e^{-\sigma_2 t}f_2.$$

Complex case: If $|\Gamma - \gamma_+| < 2$, we have two complex eigenvalues $-(\Gamma + \gamma_+) \pm 2i\sqrt{\varepsilon^2 - s^2}/2$. The computation for the exponential of the operator is similar using a real Jordan normal form .

Generalization: This technique can be generalized to the time-minimal control problem when the control is complex, replacing the control domain $|u| \leq 1$ by $|u_1|, |u_2| \leq 1$.

D. Classification of the optimal syntheses

We describe the different time-optimal syntheses in the single-input case. Without loss of generality, we restrict the study to the initial point $q_0 = (0, 1)$. The classification is done with respect to the relative positions of the feedback invariants C and S and to the optimal status of the singular extremals which are time minimal or time maximal according to the values of Γ, γ_+ and γ_-.

For $\gamma_- = 0$, the set C is restricted to the origin and we have two cases according to the sign of $\Gamma - \gamma_+$. Note that the form of the extremals σ_+ and σ_- starting from q_0 depends on the sign of $|\Gamma - \gamma_+| - 2$. Two cases for $\Gamma > \gamma_+$ are presented in [19]. We complete this study with the optimal synthesis for $\Gamma < \gamma_+$ and $|\Gamma - \gamma_+| < 2$ displayed in Fig. 7a.

For $\gamma_- \neq 0$, we distinguish four cases according to the signs of γ_- and $\Gamma - \gamma_+$. One case ($\Gamma > \gamma_+$ and $\gamma_- < 0$)

is treated in [19]. We consider here three types of optimal synthesis represented in Fig. 7b, 7c and 7d. Note that in a same class of synthesis the reachable set from the initial point q_0 depends on the dissipative parameters which can modify the structure of the synthesis. The last case $\gamma_- > 0$ and $\gamma_+ > \Gamma$ can be deduced from the case $\gamma_- > 0$ and $\gamma_+ < \Gamma$ since the horizontal singular line plays no role in both cases. The synthesis of Fig. 7d is very similar to the one of Fig. 2 except the fact that a part of the horizontal singular line is admissible. The switching locus has been computed numerically using the switching function Φ.

The role of the parameter γ_- is clearly illustrated in Figs. 7a and 7c. The case $\gamma_- = 0$ is a degenerate case where the set C shrinks into a point. The variation of γ_- induces a *bifurcation* of the control system leading to new structures of the optimal synthesis. For $\gamma_- \neq 0$, the set C is a non trivial closed curve. The optimal status of the vertical singular line changes when this line crosses the set C in Fig. 7c.

III. The bi-input case

A. Geometric analysis

The system is written in short in Cartesian coordinates as follows:

$$\dot{q} = F_0(q) + u_1 F_1(q) + u_2 F_2(q),\ \ |u| \le 1.$$

Introducing the Hamiltonians $H_i = \langle p, F_i \rangle,\ \ i = 0, 1, 2$, the pseudo-Hamiltonian associated to the time-optimal control problem is:

$$H = H_0 + \sum_{i=1}^{2} u_i H_i + p_0,$$

where $p_0 \le 0$. The time-optimal control is given outside the switching surface Σ: $H_1 = H_2 = 0$, by $u_i = H_i / \sqrt{H_1^2 + H_2^2}$, $i = 1, 2$, with the corresponding true Hamiltonian:

$$H_r = H_0 + \sqrt{H_1^2 + H_2^2},$$

whose solutions (outside Σ) are smooth and are called *extremals of order 0*. More general non smooth extremals can be obtained by connecting such arcs through Σ.

To conduct the geometric analysis and to highlight the symmetry of revolution, the system is written using the spherical coordinates:

$$x = \rho \sin\phi \cos\theta,\ \ y = \rho \sin\phi \sin\theta,\ \ z = \rho \cos\phi$$

and a feedback transformation:

$$v_1 = u_1 \cos\theta + u_2 \sin\theta,\ \ v_2 = -u_1 \sin\theta + u_2 \cos\theta.$$

We obtain the system:

$$\dot{\rho} = \gamma_- \cos\phi - \rho(\gamma_+ \cos^2\phi + \Gamma \sin^2\phi) \qquad (6a)$$

$$\dot{\phi} = -\frac{\gamma_- \sin\phi}{\rho} + \frac{\sin(2\phi)}{2}(\gamma_+ - \Gamma) + v_2 \qquad (6b)$$

$$\dot{\theta} = -\cot\phi\, v_1. \qquad (6c)$$

Hence, one deduces that the true Hamiltonian is:

$$H_r = [\gamma_- \cos\phi - \rho(\gamma_+ \cos^2\phi + \Gamma \sin^2\phi)]p_\rho + p_\phi[-\frac{\gamma_- \sin\phi}{\rho} + \frac{\sin(2\phi)}{2}(\gamma_+ - \Gamma)] + \sqrt{p_\phi^2 + p_\theta^2 \cot^2\phi}.$$

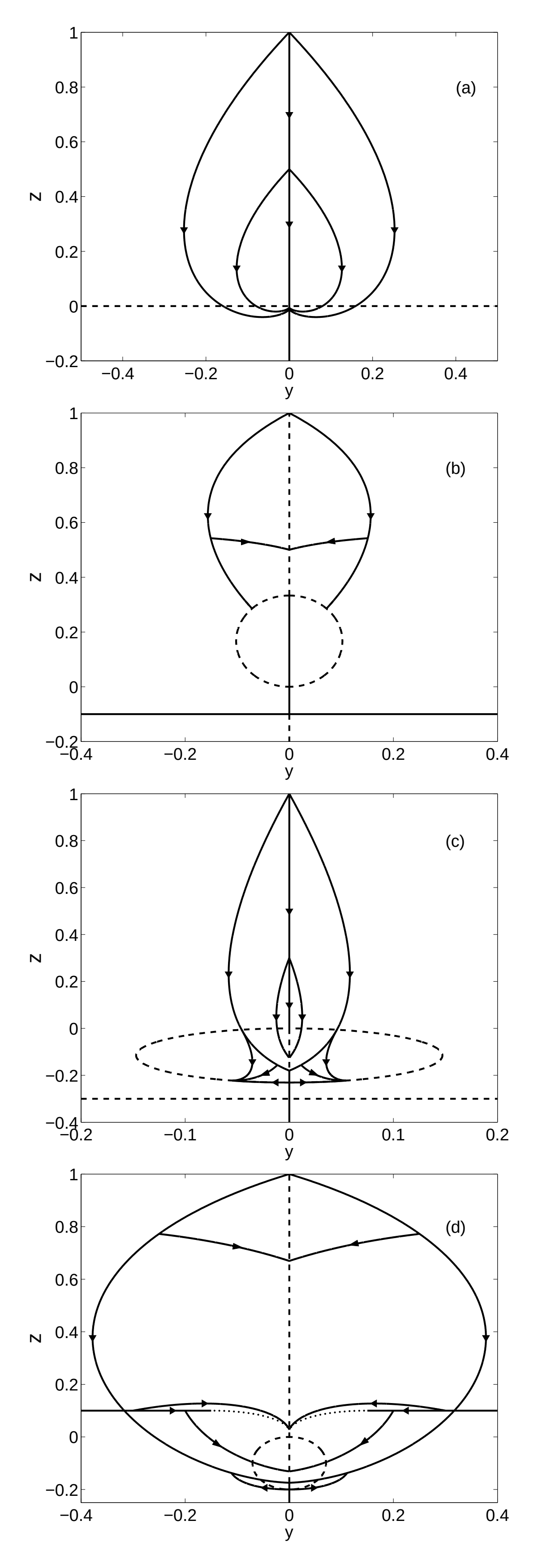


Fig. 7. Optimal syntheses for (a) ($\Gamma = 1.1$, $\gamma_+ = 1.6$, $\gamma_- = 0$), (b) ($\Gamma = 4$, $\gamma_+ = 1.5$, $\gamma_- = 0.5$), (c) ($\Gamma = 4$, $\gamma_+ = 6.5$, $\gamma_- = -1.5$) and (d) ($\Gamma = 1$, $\gamma_+ = 0.5$, $\gamma_- = -0.1$). Solid and dashed vertical and horizontal lines correspond respectively to fast and slow singular lines. The set C is represented in dashed lines. The switching locus is plotted in dotted line. In (d), only the admissible singular horizontal line is represented in solid line.

From this, we deduce the following lemma:

Lemma 3.
(i)- The angle θ is a cyclic variable and p_θ is a first integral (symmetry of revolution).
(ii)- For $\gamma_- = 0$, using the coordinate $r = \ln\rho$, the Hamiltonian takes the form:

$$H_r = -(\gamma_+ \cos^2\phi + \Gamma\sin^2\phi)p_r + \sin(2\phi)(\gamma_+ - \Gamma)p_\phi + \sqrt{p_\phi^2 + p_\theta^2\cot^2\phi}. \tag{7}$$

Hence, r is an additional cyclic variable and p_r is a first integral. The system is thus Liouville integrable.

As a consequence, we can deduce two properties. First of all, the z-axis is an axis of revolution and the state $q_0 = (0,0,1)$ is a pole. This means that by making a rotation around (Oz) of the extremal synthesis for the 2D-system, we generate the extremal synthesis for the 3D-system.

More generally, we have for $\gamma_- = 0$ a system on the *two-sphere of revolution* described by Eqs. (6b) and (6c) coupled with the one dimensional system (6a) describing the evolution of the physical variable ρ corresponding to the purity of the system. Moreover, the system is invariant for the transformation $\phi \mapsto \pi - \phi$ which is associated to a reflexional symmetry with respect to the equator for the system (6) restricted to the two-sphere of revolution. This property is crucial in the analysis of the integrable case.

If $\gamma_- \neq 0$ then the situation is more intricate. The extremal solutions of order 0 satisfy the equations which are singular for $\rho = 0$:

$$\begin{aligned} \dot\rho &= \gamma_-\cos\phi - \rho(\gamma_+\cos^2\phi + \Gamma\sin^2\phi) \\ \dot\phi &= -\frac{\gamma_-\sin\phi}{\rho} + \frac{\sin(2\phi)}{2}(\gamma_+ - \Gamma) + \frac{p_\phi}{Q} \\ \dot\theta &= \frac{p_\theta\cot^2\phi}{Q}, \end{aligned} \tag{8}$$

and

$$\begin{aligned} \dot p_\rho &= (\gamma_+\cos^2\phi + \Gamma\sin^2\phi)p_\rho - \frac{\gamma_-\sin\phi}{\rho^2}p_\phi \\ \dot p_\phi &= [\gamma_-\sin\phi + \rho(\Gamma - \gamma_+)\sin(2\phi)]p_\rho - \\ &\quad [-\frac{1}{\rho}\cos\phi\gamma_- + (\gamma_+ - \Gamma)\cos(2\phi)]p_\phi + \frac{p_\theta^2\cos\phi}{Q\sin^3\phi} \\ \dot p_\theta &= 0, \end{aligned}$$

where $Q = \sqrt{p_\theta^2\cot^2\phi + p_\phi^2}$.

B. Regularity analysis

The smooth extremal solutions of $\vec{H}_r$ are not the only extremals because more complicated behaviors are due to the existence of the switching surface Σ: $H_1 = H_2 = 0$. Hence, in order to get singularity results, we must analyze the possible connections of two smooth extremals crossing Σ to generate a piecewise smooth extremal. This can also generate complex singularities of the Fuller type, where the switching times accumulate. In our problem, the situation is less complex because of the symmetry of revolution. The aim of this section is to make the singularity analysis of the extremals near Σ.

The structure of optimal trajectories is described by the following proposition.

Proposition 3. *Every optimal trajectory is:*

- *Either an extremal trajectory with $p_\theta = 0$ contained in a meridian plane and time-optimal solution of the 2D-system, where $u = (u_1, 0)$.*
- *Or subarcs solutions of $\vec{H}_r$, where $p_\theta \neq 0$ with possible connections in the equator plane for which $\phi = \pi/2$.*

Proof: The first assertion is clear. If $p_\theta = 0$ then the extremals are such that $\dot\theta = 0$ and up to a rotation around the z-axis, they correspond to solutions of the 2D-system. The switching surface Σ is defined by: $p_\theta\cot\phi = p_\phi = 0$. We cannot connect an extremal with $p_\theta \neq 0$ to an extremal where $p_\theta = 0$ since at the connection the adjoint vector has to be continuous. Hence, the only remaining possibility is to connect subarcs of $\vec{H}_r$ with $p_\theta \neq 0$ at a point of Σ leading to the conditions $p_\phi = 0$ and $\phi = \pi/2$. ■

Further work is necessary to analyze the behaviors of such extremals near Σ.

Normal form: A first step in the analysis is to construct a normal form. Taking the system in spherical coordinates and setting $\psi = \pi/2 - \phi$, the approximation is:

$$\begin{aligned} \dot\rho &= \gamma_-\psi - \rho[\Gamma + (\gamma_+ - \Gamma)\psi^2] \\ \dot\psi &= \frac{\gamma_-}{\rho}(1 - \psi^2/2) - \psi(\gamma_+ - \Gamma) - v_2 \\ \dot\theta &= -\psi v_1, \end{aligned}$$

with the corresponding Hamiltonian:

$$\begin{aligned} H_r &= p_\rho[\gamma_-\psi - \rho(\Gamma + (\gamma_+ - \Gamma)\psi^2)] + \\ &\quad p_\psi[\frac{\gamma_-}{\rho}(1 - \psi^2/2) - \psi(\gamma_+ - \Gamma)] + \sqrt{p_\psi^2 + p_\theta^2\psi^2}. \end{aligned}$$

Proposition 4. *Near $\psi = 0$, $p_\psi = 0$, we have two distinct cases for the optimal trajectories:*

- *If $\gamma_- = 0$, for the 2D-system, the line $\psi = 0$ is a singular trajectory with admissible zero control if $\gamma_+ - \Gamma \neq 0$. It is time maximal if $(\gamma_+ - \Gamma) > 0$ and time minimal if $(\gamma_+ - \Gamma) < 0$. Hence, for this system, we get only extremal trajectories through Σ in the case $(\gamma_+ - \Gamma) < 0$, where ψ is of order t and p_ψ of order t^2. They are the only non-smooth optimal trajectories passing through Σ.*
- *If $\gamma_- \neq 0$, for the 2D-system, the set $\psi = p_\psi = 0$ becomes a set of ordinary switching points where ψ and p_ψ are of order t. Moreover, connections for extremals of $\vec{H}_r$ are eventually possible, depending upon the set of parameters and initial conditions.*

Proof: For the normal form, the adjoint system is:

$$\begin{aligned} \dot p_\rho &= p_\rho(\Gamma + (\gamma_+ - \Gamma)\psi^2) + \frac{p_\psi}{\rho^2}\gamma_-(1 - \frac{\psi^2}{2}) \\ \dot p_\psi &= -p_\rho(\gamma_- - 2\psi\rho(\gamma_+ - \Gamma)) + p_\psi(\frac{\gamma_-\psi}{\rho} + (\gamma_+ - \Gamma)) \\ &\quad + v_1 p_\theta. \end{aligned}$$

In order to make the evaluation of smooth arcs reaching or departing from Σ, the technique is simple: a solution of the form $\psi(t) = at + o(t)$, $p_\psi(t) = bt + o(t)$ is plugged in the

equations to determine the coefficients. From the equations, we observe that the contacts with Σ differ in the case $\gamma_- = 0$ from the case $\gamma_- \neq 0$ that we discuss separately.

First of all, we consider the case $\gamma_- = 0$; $p_\theta = 0$, $\psi = 0$ is an admissible singular direction (with zero control) which can be slow if $(\gamma_+ - \Gamma) > 0$ or fast if $(\gamma_+ - \Gamma) < 0$. In the first case, there is no admissible extremal through Σ while it is possible if $\gamma_+ - \Gamma < 0$. If we compute the different orders, we have that ψ is of order t, p_ψ is of order t^2 while p_ρ has to be non zero if $p_\theta = 0$. If we consider extremals with $p_\theta \neq 0$, we can conclude with the orders alone. Indeed the Hamiltonian is $H_r = \varepsilon$, $\varepsilon = 0, 1$ and in both cases, we have:

$$-p_\rho \rho(\gamma_+ - \Gamma)\psi^2 - p_\psi \psi(\gamma_+ - \Gamma) + \sqrt{p_\psi^2 + p_\theta^2 \psi^2} = 0.$$

The conclusion using orders is then straightforward. For instance, if ψ and p_ψ are of order one, this gives $p_\psi = p_\theta \psi = 0$ which is impossible. The other cases are similar.

In the case $\gamma_- \neq 0$, the analysis is more intricate and we must analyze the equations. We introduce the Hamiltonians:

$$H_1 = -p_\theta \psi, \ H_2 = p_\psi.$$

Differentiating H_1 and H_2 with respect to t, one gets:

$$\dot{H}_1 = \{H_1, H_0\} + v_2\{H_1, H_2\}$$
$$\dot{H}_2 = \{H_2, H_0\} + v_1\{H_2, H_1\}$$

and at a point of Σ, we obtain the relations:

$$\dot{H}_1 = -p_\theta(\gamma_- - v_2), \ \dot{H}_2 = \gamma_- p_\rho - v_1 p_\theta.$$

In order to analyze the singularity, we use a polar blowing up:

$$H_1 = r\cos\alpha, \ H_2 = r\sin\alpha,$$

and we get:

$$\begin{array}{l} \dot{r} = \gamma_-[-\frac{p_\theta \cos\alpha}{\rho} + p_\rho \sin\alpha] \\ \dot{\alpha} = \frac{1}{r}[\gamma_- p_\rho \cos\alpha + \frac{p_\theta \gamma_- \sin\alpha}{\rho} - p_\theta] \end{array}.$$

Hence, the extremals crossing Σ are given by solving $\dot{\alpha} = 0$, while the sign of $\dot{r}$ is given by the first equation above.

Depending upon the parameters and the initial conditions on (p_ρ, ρ), the equation $\dot{\alpha} = 0$ can have at most two distinct solutions on $[0, 2\pi]$, while in the case $p_\theta = 0$, we get an ordinary switching point for the single-input system. The assertion 4 is proved. ∎

C. Geometric analysis and numerical solution

We first analyze the integrable case $\gamma_- = 0$. We only present a summary of the result of [5] in order to be generalized to the case $\gamma_- \neq 0$.

1) The case $\gamma_- = 0$: The system (7) is associated to a system on the two-sphere of revolution of the form:

$$\dot{q} = G_0(q) + \sum_{i=1}^{2} u_i G_i(q).$$

It defines a Zermelo navigation problem [2] on the two-sphere of revolution where the drift term G_0 represents the current:

$$G_0 = \frac{\sin(2\phi)}{2}(\gamma_+ - \Gamma)\frac{\partial}{\partial\phi}, \tag{9}$$

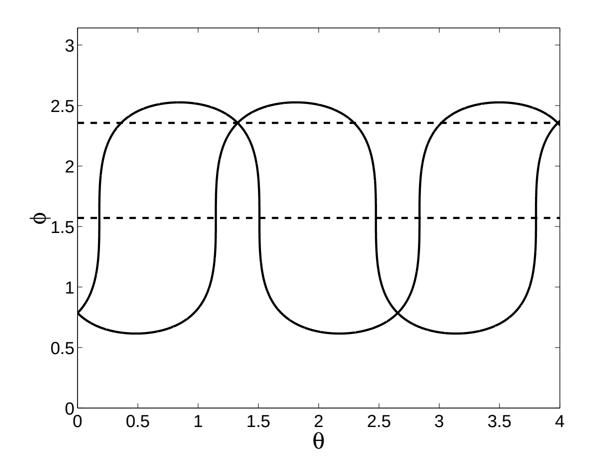


Fig. 8. Extremal trajectories for $\Gamma = 2.5$, $\gamma_+ = 2$ and $\gamma_- = 0$. Other parameters are taken to be $p_\phi(0) = -1$ and 2.33, $\phi(0) = \pi/4$, $p_\rho = 1$ and $p_\theta = 2$. Dashed lines represent the equator and the antipodal parallel located at $\phi = 3\pi/4$.

and $G_1 = \frac{\partial}{\partial\phi}$, $G_2 = -\cot\phi\frac{\partial}{\partial\theta}$ form a frame for the metric $g = d\phi^2 + \tan^2\phi d\theta^2$ which is singular at the equator $\phi = \pi/2$. The drift can be compensated by a feedback with $|u| < 1$ if $|\gamma_+ - \Gamma| < 2$. This leads to the following discussion.

Case $|\gamma_+ - \Gamma| < 2$: In this case, the system reduced to the two-sphere defines a Finsler geometry for which the extremals are a deformation of the extremals of $g = d\phi^2 + \tan^2\phi d\theta^2$ [2]. The main problem properties are described in the next proposition.

Proposition 5. *If for a fixed (p_r, p_θ), the level set of $H_r = \varepsilon$ ($\varepsilon = 0, 1$) is compact without singular point and has a central symmetry with respect to $(\phi = \pi/2, p_\phi = 0)$ then it contains a periodic trajectory (ϕ, p_ϕ) of period T and if $p_\phi^\pm(0)$ are distinct, we have two distinct extremal curves $q^+(t)$, $q^-(t)$ starting from the same point and intersecting with the same length $T/2$ at a point such that $\phi(T/2) = \pi - \phi(0)$ (see Fig. 8).*

Case $|\gamma_+ - \Gamma| > 2$: We have two types of extremals characterized by their projection on the two-sphere: those occurring in a band near the equator and described by proposition 5 and those crossing a band near $\phi = \pi/4$ and with asymptotic properties of proposition 6:

Proposition 6. *If $|\Gamma - \gamma_+| \geq 2$ then we have extremal trajectories such that $\dot{\phi} \to 0$, $|p_\phi| \to +\infty$ when $t \to +\infty$ while $\dot{\theta} \to 0$.*

Both behaviors are represented on Fig. 9.

2) The case $\gamma_- \neq 0$: We present numerical results about the behavior of extremal solutions of order 0 and conjugate point analysis.

Extremal trajectories:
We begin by analyzing the structure of extremal trajectories. The description is based on a direct integration of the system (8). We observe two different asymptotic behaviors corresponding to the stationary points of the dynamics which

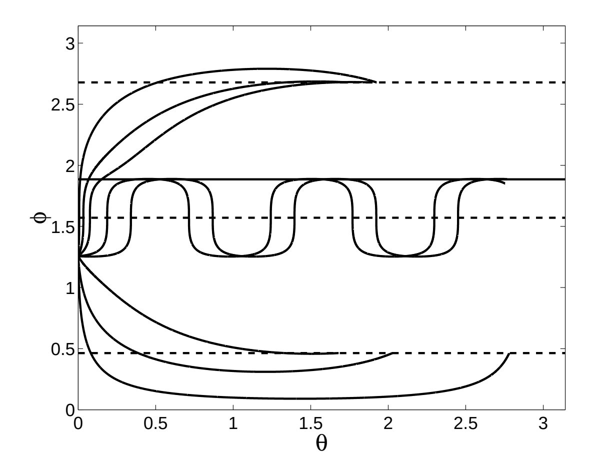


Fig. 9. Extremal trajectories for $\Gamma = 4.5$, $\gamma_+ = 2$ and $\gamma_- = 0$. Dashed lines represent the equator and the locus of the fixed points of the dynamics. The solid line corresponds to the antipodal parallel. Numerical values of the parameters are taken to be $\phi(0) = 2\pi/5$, $p_\theta = 8$ and $p_\rho(0) = 0.25$. The different initial values of p_ϕ are -50, -10, 0, 2.637, 3, 5, 10 and 50.

are described by the following results.

Proposition 7. *In the case denoted (a) where $|p_\phi(t)| \to +\infty$ when $t \to +\infty$, the asymptotic stationary points $(\rho_f, \phi_f, \theta_f)$ of the dynamics are given by $\rho_f = |\gamma_-|\sqrt{1+\Gamma^2}/(1+\gamma_+\Gamma)$ and $\phi_f = \arctan(1/\Gamma)$ if $\gamma_- > 0$ or $\phi_f = \pi - \arctan(1/\Gamma)$ if $\gamma_- < 0$.*

Proof: We assume that $|p_\phi(t)| \to +\infty$ as $t \to +\infty$ and that $\cot(\phi)$ remains finite in this limit. One deduces from the system (8) that (ρ_f, ϕ_f) satisfy the following equations:

$$\begin{array}{l} \gamma_- \cos\phi_f = \rho_f(\gamma_+ \cos^2\phi_f + \Gamma \sin^2\phi_f) \\ \frac{\gamma_- \sin\phi_f}{\rho_f} = (\gamma_+ - \Gamma)\cos\phi_f \sin\phi_f + \varepsilon \end{array},$$

where $\varepsilon = \pm 1$ according to the sign of p_ϕ. The quotient of the two equations leads to

$$(\gamma_+ - \Gamma)\cos\phi_f \sin\phi_f + \varepsilon = \tan\phi_f(\gamma_+ \cos^2\phi_f + \Gamma \sin^2\phi_f)$$

which simplifies into

$$\tan\phi_f = \frac{\varepsilon}{\Gamma}.$$

Using the fact that $\phi_f \in]0,\pi[$ and $\gamma_- \cos\phi_f \geq 0$, one arrives to $\phi_f = \arctan(1/\Gamma)$ if $\gamma_- > 0$ and $\phi_f = \pi - \arctan(1/\Gamma)$ if $\gamma_- < 0$. From the equation

$$\gamma_- \cos\phi_f = \rho_f(\gamma_+ \cos^2\phi_f + \Gamma \sin^2\phi_f),$$

one finally obtains that

$$\rho_f = \frac{\gamma_- \sqrt{1+\Gamma^2}}{1+\gamma_+\Gamma}.$$

■

Proposition 8. *In the case denoted (b) where $\lim_{t\to+\infty}\phi(t) = 0$ or π, the asymptotic limit of the dynamics is characterized by $\rho_f = |\gamma_-|/\gamma_+$ and $\phi_f = 0$ if $\gamma_- > 0$ or $\phi_f = \pi$ if $\gamma_- < 0$.*

Proof: Using the relation

$$\gamma_- \cos\phi_f = \rho_f(\gamma_+ \cos^2\phi_f + \Gamma \sin^2\phi_f),$$

one deduces that $\gamma_- \cos\phi_f \geq 0$ and that $\rho_f = |\gamma_-|/\gamma_+$ if $\phi_f = 0$ or π. ■

We have numerically checked that if $|\Gamma - \gamma_+| > 2$ then only the case (a) is encountered whereas if $|\Gamma - \gamma_+| < 2$, the extremals are described by the case (b). One particularity of the case (a) is the fact that the limit of the dynamics only depends on Γ and on the sign of γ_- and not on $\phi(0)$ or γ_+. The structure of the extremals is also simple in case (b) since the limit of ϕ is 0 or π independently of the values of Γ, γ_+ or γ_-. The different behaviors of the extremals are illustrated in Fig. 10 for the case $|\Gamma - \gamma_+| > 2$ and in Fig. 12 for the case $|\Gamma - \gamma_+| < 2$. The corresponding optimal control fields v_1 and v_2 are represented in Fig. 11 for the case (a) and in Fig 13 for the case (b). In Fig. 11, note that the control v_1 tends to 0 whereas v_2 is close to -1 for t sufficiently large. This is due to the fact that $|p_\phi| \to +\infty$ when $t \to +\infty$ and can be easily checked from the definition of v_1 and v_2. We observe a similar behavior for the case (b) in Fig. 13. The control field v_2 acquires here a bang-bang structure which is related to the unbounded and oscillatory behavior of $p_\phi(t)$ (see Fig. 13). In this case, numerical simulations show that $|p_\phi|$ dominates $\cot\phi$ at infinity.

Conjugate points:
The Cotcot code is used to evaluate the conjugate points. This occurs only in case (b) and the numerical simulations give that the first conjugate points appear before an uniform number of oscillations of the ϕ variable. This phenomenon is represented on Fig. 14. Cutting the trajectory at the first conjugate point avoids such a behavior. Note that due to the symmetry of revolution, the global optimality is lost for $\theta \leq \pi$.

IV. Physical conclusions

We give some qualitative conclusions on the time-optimal control of two-level dissipative systems. The discussion concerns the role of dissipation which can be beneficial or not for the dynamics and the robustness with respect to dissipative parameters of the optimal control.

The dissipation effect is well summarized by Fig. 2. In this case $\Gamma > \gamma_+$ and one sees that as long as the purity of the state decreases (for $0 \leq z \leq 1$), it is advantageous to use a control field, the dissipation being undesirable. On the contrary, when the purity starts increasing (for $-\gamma_-/\gamma_+ \leq z \leq 0$) then the dissipation alone becomes more efficient and its role positive. The quickest way to accelerate the purification of the state consists in letting the dissipation act. This constitutes a non-intuitive physical conclusion which, however, crucially depends on the respective values of Γ and γ_+. For instance, if $\gamma_+ > \Gamma$ then all the preceding conclusions are modified. This result can also be interpreted in the control of a spin $1/2$ particle by magnetic fields. Equation (5) describes the evolution of the spin system in the basis of the z component of the spin, the magnetic field being only along the $y-$ axis. The north and the south poles of the Bloch sphere correspond to the two positions of the spin along the $z-$axis. A control problem is to change in minimum time the orientation of

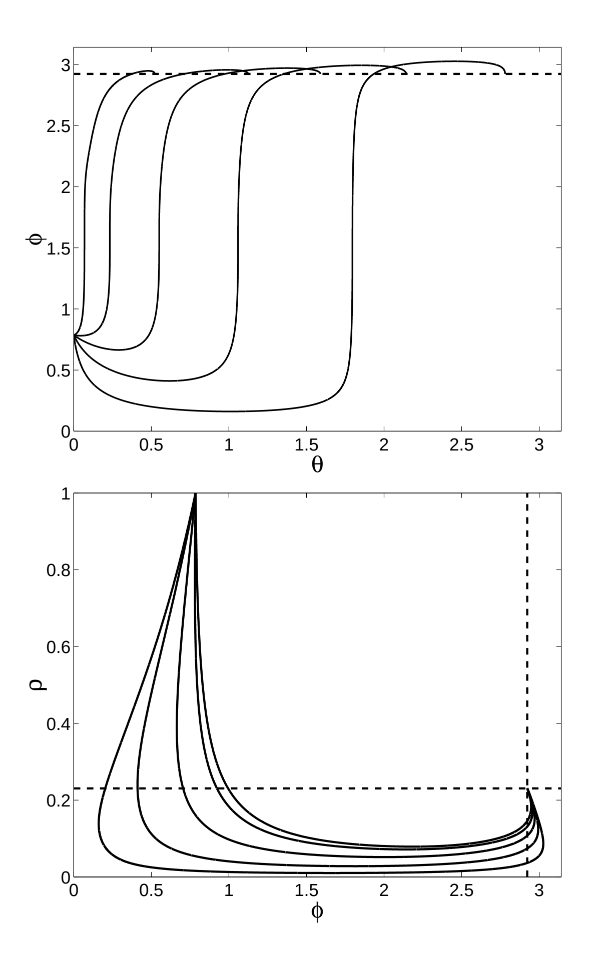


Fig. 10. Extremal trajectories for $\Gamma = 4.5$, $\gamma_+ = 2$ and $\gamma_- = -0.5$. The equations of the dashed lines are $\phi = \pi - \arctan(1/\Gamma)$ and $\rho = |\gamma_-|\sqrt{1+\Gamma^2}/(1+\gamma_+\Gamma)$ (see the text). Numerical values of the parameters are taken to be $\phi(0) = \pi/4$, $p_\theta = 2$, $p_\rho(0) = 0.1$ and $\rho(0) = 1$. $p_\phi(0)$ is successively equal to -10, -2.5, 0, 2.5 and 10 for the different extremals.

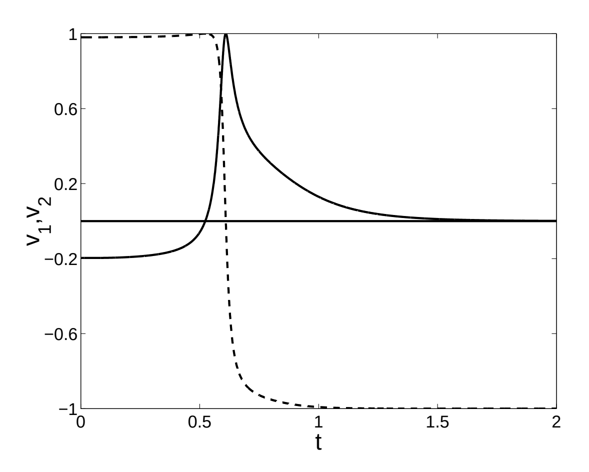


Fig. 11. Plot of the optimal control fields v_1 (solid line) and v_2 (dashed line) as a function of time t for the extremal trajectory of Fig. 10 with $p_\phi(0) = 5$. The equation of the horizontal solid line is $v = 0$.

the spin system i.e. to pass from the north pole to the south pole. In the conservative case, the solution is a bang control equal to ± 1 [7]. In the dissipative case, we assume that $\gamma_-/\gamma_+ = -1$ in order to ensure that the south pole belongs to the closure of the accessible set of the north pole. The choice

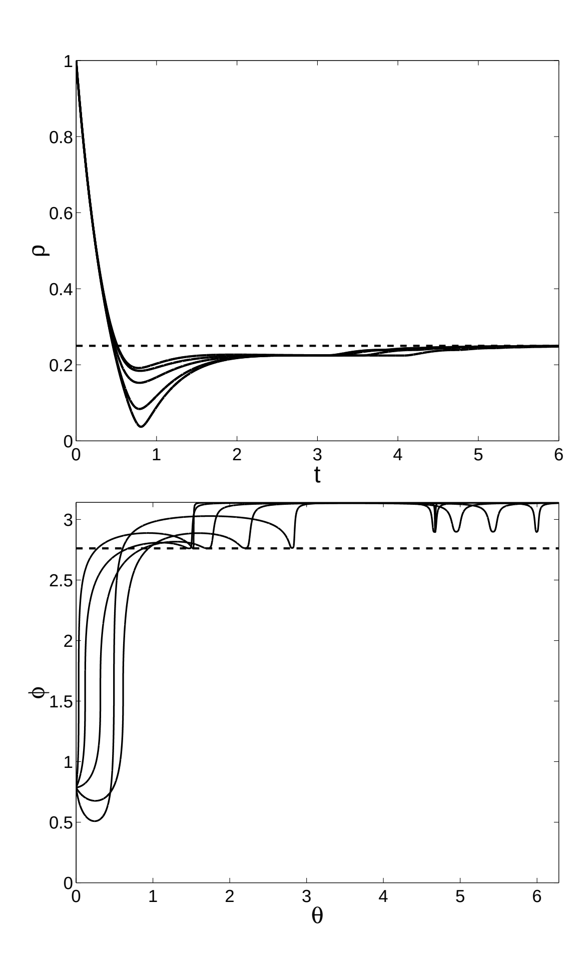


Fig. 12. Same as Fig. 10 but for $\Gamma = 2.5$. The equation of the dashed line is $\rho = |\gamma_-|/\gamma_+$.

$\gamma_-/\gamma_+ = -1$ corresponds to $\gamma_{12} = 0$ and $\gamma_{21} = 1$. Such dissipative parameters are obtained when dissipation effects are due to spontaneous emission. In this case, the answer to the optimal control problem is given by Fig. 7d. The solution is a combination of a bang arc and a singular arc along the $z-$axis with a control field equal to 0. The south pole is reached asymptotically in infinite time. Other optimal syntheses of Fig. 7 can be interpreted along the same lines.

The robustness of the optimal control with respect to dissipative parameters is illustrated by the double-input control. We give different examples. If $\gamma_- = 0$ then the integrability of the Hamiltonian and the geometrical properties of the extremals are preserved when $|\Gamma - \gamma_+| < 2$. If $\gamma_- \neq 0$ then the asymptotic behavior of the extremals slightly depends on the parameters Γ, γ_+ and γ_- (see Propositions 7 and 8). Fig. 11 and 13 show that the extremal control fields have also asymptotic behaviors independent of the dissipation. In case (a), the control fields tend to a constant whereas a bang-bang structure appears in case (b). This conclusion could be interesting for practical applications where robustness with respect to physical parameters and simple control fields are needed. In addition, due to the simple structure of the time-optimal synthesis, shooting techniques will be particularly efficient to determine the control fields especially in case (a).

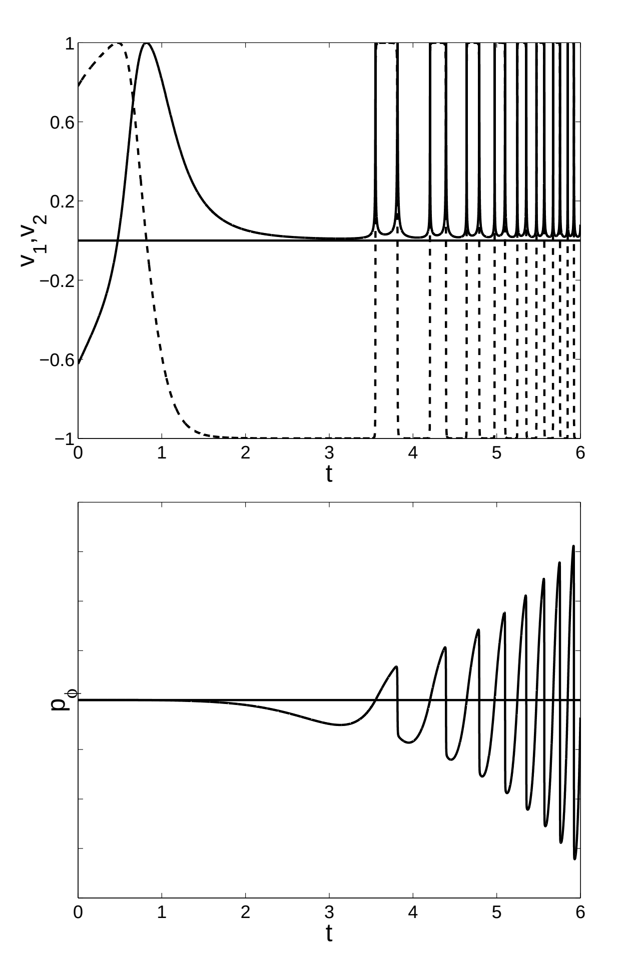


Fig. 13. (top) Same as Fig. 11 but for the extremal of Fig. 12 with $p_\phi(0) = 2.5$. (bottom) Evolution of p_ϕ for the same extremal as a function of t.

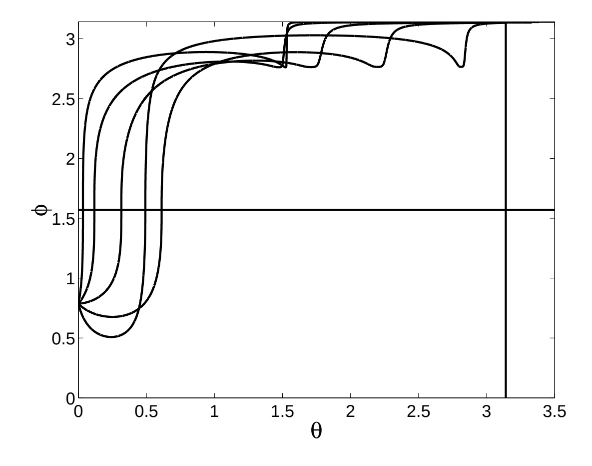


Fig. 14. Plot of the extremals of Fig. 12 up to the first conjugate point. The coordinates θ of the conjugate points are respectively 3.149, 3.116, 3.332, 3.386 and 3.535 for $p_\phi(0)$ equal to -10, -2.5, 0, 2.5 and 10. The equations of the horizontal and vertical solid lines are respectively $\phi = \pi/2$ and $\theta = \pi$.

REFERENCES

[1] C. ALTAFINI, *Controllability properties for finite dimensional quantum Markovian master equations*, J. Math. Phys. **44**, 2357 (2002).

[2] D. BAO, C. ROBLES AND Z. SHEN, *Zermelo navigation on Riemannian manifolds*, J. Differential Geom. **66**, no. 3, 377-435 (2004).

[3] B. BONNARD, J.-B. CAILLAU AND E. TRÉLAT, *Second-order optimality conditions in the smooth case and applications in optimal control*, ESAIM : COCV **13**, no. 2, 207-236 (2007)

[4] B. BONNARD AND M. CHYBA, *Singular trajectories and their role in control theory*, Math. and Applications 40, Springer-Verlag, Berlin (2003)

[5] B. BONNARD AND D. SUGNY, *Time-minimal control of dissipative two-level quantum systems: The integrable case*, to be published in SIAM J. Control Optim (2009).

[6] B. BONNARD AND E. TRÉLAT, *Une approche géométrique du contrôle optimal de l'arc atmosphérique de la navette spatiale*, ESAIM : COCV **7**, 179-222 (2002).

[7] U. BOSCAIN, G. CHARLOT, J.-P. GAUTHIER, S. GUÉRIN AND H .R. JAUSLIN, *Optimal control in laser-induced population transfer for two- and three-level quantum systems*, J. Math. Phys. **43**, no. 5, 2107 (2002).

[8] U. BOSCAIN AND Y. CHITOUR, *On the minimum time problem for driftless left-invariant control systems on $SO(3)$*, Comm. Pure Appl. Anal., **1**, no. 3, 128 (2002).

[9] U. BOSCAIN AND B. PICCOLI, *Optimal syntheses for control systems on 2-D manifolds*, Springer-Verlag, Berlin (2003).

[10] U. BOSCAIN AND P. MASON, *Time minimal trajectories for a spin 1/2 particule in a magnetic field.*, J. Math. Phys., **47**, 062101 (2006).

[11] C. CARATHÉODORY, *Calculus of variations and partial differential equations of first order*, Chelsea Publishing Company, New-York (1982).

[12] V. GORINI, A. KOSSAKOWSKI AND E. C. G. SUDARSHAN, *Completely positive dynamical semigroups of N-level systems*, J. Math. Phys., **17**, 821 (1976).

[13] S. GUÉRIN AND H. R. JAUSLIN, *Control of quantum dynamics by laser pulses: Adiabatic Floquet theory*, Adv. Chem. Phys., **125**, 147 (2003).

[14] N. KHANEJA, R. BROCKETT AND S. J. GLASER, *Time optimal control in spin systems*, Phys. Rev. A, **63**, 032308 (2001).

[15] G. LINDBLAD, *On the generators of quantum dynamical semi-groups*, Comm. Math. Phys., **48**, 119 (1976).

[16] S. RAMAKRISHNA AND T. SEIDEMAN, *Intense laser alignment in dissipative media as a route to solvent dynamics*, Phys. Rev. Lett., **95**, 113001 (2005).

[17] H. SCHÄTTLER, *The local structure of time-optimal trajectories in dimension three under generic conditions*, SIAM J. Control Optim., **26**, no. 5, 1145-1162, (1987).

[18] S. G. SCHIRMER AND A. I. SOLOMON, *Constraints on relaxation rates for N-level quantum systems*, Phys. Rev. A, **70**, 022107 (2004).

[19] D. SUGNY, C. KONTZ AND H. R. JAUSLIN, *Time-optimal control of a two-level dissipative quantum system*, Phys. Rev. A, **76**, 023419 (2007).

[20] H. J. SUSSMANN, *Regular synthesis for time-optimal control of single-input real analytic system in the plane: the general real analytic case*, SIAM J. Control Optim., **26**, no. 4, 899-918, (1988).

[21] T. VIELLARD, F. CHAUSSARD, D. SUGNY, B. LAVOREL AND O. FAUCHER, *Field-free molecular alignment of CO_2 mixtures in presence of collisional relaxation*, J. Raman Spec., **39**, 694 (2008).

PLACE PHOTO HERE

Bernard Bonnard Bernard Bonnard was born in Metz (France) on October 7, 1952. He received the Ph.D. degrees of Mathematics from the University of Metz, in 1978, and the Thèse d'Etat from the University of Grenoble in 1983. From 1979 to 1991 he was a researcher in control engineering at the CNRS and he got a Professor of Mathematics position at University of Burgundy in 1991. His present research interest are in the areas of optimal control, non linear systems, space mechanics and applications.

PLACE
PHOTO
HERE

Monique Chyba Monique Chyba was born in Geneva (Switzerland) on October 31, 1969. She received the Ph.D. degrees of Mathematics from the University of Geneva, in 1997. In August 2002, she joined the department of Mathematics at the University of Hawaii - Manoa, where she is currently an associate professor. Geometric control theory is her main area of research with an emphasis on the implementation of the theoretical tools to concrete applications.

PLACE
PHOTO
HERE

Dominique Sugny Dominique Sugny was born in Grenoble (France) on July 9, 1974. He received the Ph.D. degrees of Theoretical Physics from the University of Grenoble, in 2002. In September 2003, he joined the department of Physics at the University of Burgundy - France, where he is currently an associate professor. His main areas of research are the study of dynamical systems and the application of geometric control theory to the control of quantum systems.

Chapitre 6

Conclusion

Ce mémoire décrit mes activités de recherche à l'Institut Carnot de Bourgogne depuis ma soutenance de thèse en 2002. Il résume, après une brève description de mon parcours scientifique et de mes activités d'enseignement et administratives, mes différents résultats de recherche. Ces travaux ont été orientés vers l'étude et la caractérisation des systèmes dynamiques et vers le contrôle des systèmes quantiques.

Sur la base de ces différents résultats, mes projets de recherche s'orientent vers plusieurs axes. Mes projets pour la structure des systèmes dynamiques sont regroupés sous la forme du projet SyDIS (Singularités de systèmes dynamiques intégrables et leurs manifestations en physique classique et quantique, et en optique non-linaire) mis en place avec D. A. Sadovskií de l'Université de Dunkerque. Ce projet regroupe une quinzaine de chercheurs mathématiciens et physiciens. Dans le cadre du contrôle quantique, mon premier objectif sera de travailler sur des applications en RMN avec l'équipe de S. Glaser à Munich et sur le contrôle de l'orientation et de l'alignement moléculaire avec l'équipe de O. Faucher et B. Lavorel. Mon second axe sera le développement des méthodes mathématiques pour le contrôle quantique, que ce soit pour le contrôle géométrique ou pour les algorithmes monotones.

Singularités des systèmes intégrables

1- Systèmes intégrables et géométrie complexe, applications à des systèmes physiques

Mes objectifs dans cette thématique sont liés au projet SIDyS. Nous voudrions continuer à développer les applications de la géométrie complexe et de ses outils (théorie de Picard-Lefschetz, connexion de Gauss-Manin, intégrales abéliennes) à l'étude de la topologie des systèmes Hamiltoniens intégrables. La compréhension exacte du lien entre ses deux théories n'est pas complétement clarifiée. Notre premier travail sur le sujet illustre un lien possible entre ces deux domaines [17]. Nous travaillons actuellement avec K. Efstathiou sur la question de la bidromie. L'idée est de généraliser notre approche complexe à des systèmes Hamiltoniens possédant une bidromie non-triviale [104]. Un article est en préparation sur le sujet. Un projet à plus long terme serait d'obtenir une classification des différents types de monodromie possibles dans les systèmes Hamiltoniens. Nous nous baserons sur la théorie des catastrophes [39] et la théorie des singularités [40] pour débuter cette classification. Un exemple est donné par le phénomène de bidromie dont la structure Hamiltonienne sous-jacente peut être associée à la catastrophe *swallow-tail* ou queue d'aronde.

Mon autre projet dans ce domaine concerne les applications à des systèmes physiques. Le premier champ d'étude est la physique moléculaire. Nous étudions actuellement le spectre vibrationelle de la molécule HOCl. Le diagramme de bifurcation de cette molécule a une structure très particulière [71] qui fait apparître une sorte de bidromie fractionnaire couplant monodromie fractionnaire et bidromie. Un article est en préparation sur le sujet. L'autre axe de recherche est basé sur les questions de monodromie dynamique. Le but est de trouver des systèmes atomiques ou moléculaires possédant ce type de propriété topologique [53]. Les systèmes controlés de manière adiabatique par champs laser semblent être une solution possible. Le contrôle permet de modifier dans ces systèmes les valeurs de l'énergie et du moment et ainsi de tourner autour de la singularité de manière dynamique.

2- Dynamique des systèmes non-linéaires contrapropagatifs

Un autre axe majeur que je voudrais développer dans le futur est l'étude des systèmes à nombre infini de degrés de liberté dont la dynamique est

décrite par des équations aux dérivés partielles non linéaires comme l'équation de Schrödinger non linéaire. L'idée générale est d'utiliser des techniques géométriques connues pour obtenir des informations sur les solutions des équations aux dérivées partielles et notamment leurs solutions stationnaires. Un premier exemple sur la propagation contrapropagative d'ondes non linéaires a été en parti résolu [9]. Il reste du travail dans ce domaine pour comprendre toutes les implications de ce résultat. Suite aux résultats obtenus dans la thèse de S. Lagrange, nous travaillons actuellement avec A. Picozzi sur les fibres optiques non-linéaires pour généraliser le phénomène d'attraction de polarisation connu pour les polarisations circulaires à tous les types de polarisations. L'attraction de polarisation est un échange de polarisation entre la pompe et le signal le long de la fibre. Cette propriété peut être expliquée par la géométrie du tore singulier. Nous voudrions également analyser le cas où le système Hamiltonien stationnaire n'est plus intégrable mais proche d'un système intǵrable. On peut alors se demander si le phénomène d'attraction persistera dans ce cas et si de nouvelles structures comme des points fixes hyperboliques joueront un rôle particulier. A plus long terme, nous voudrions généraliser cette étude aux solitons vectoriels et montrer la relation entre tores singuliers et solitons dans ce type de systèmes.

Contrôle quantique

1- Contrôle de l'orientation et de l'alignement moléculaire

Un premier objectif sur lequel nous travaillons depuis quelques mois déjà concerne la délocalisation planaire de molécules en l'absence de champs. La question est de savoir s'il est possible de confiner en permanence un des axes de la molécule dans un plan. Notre réponse est positive. Nous avons déterminé, en collaboration avec S. Guérin et M. Lapert, les états cibles correspondant et nous avons construit différentes stratégies pour atteindre cet état. Des expériences sur cette délocalisation menées par E. Hertz sont en cours dans le laboratoire. Un article est en préparation sur le sujet.

A plus long terme, mes projets s'orientent vers les questions d'orientation et d'alignement 3D pour les molécules polyatomiques non-linéaires. Comment généraliser les états cibles dans ce cas et quelles sont les stratégies de contrôle permettant de les atteindre seront les questions auxquelles nous aurons à répondre.

2- Contrôle en Résonance Magnétique Nucléaire

Je compte dans les années à venir particulièrement m'impliquer dans les questions de contrôle en RMN en phase liquide. Le contrôle de la dynamique des spins semble être un exemple très bien adapté pour appliquer les techniques du contrôle optimal géométrique. Les avantages d'un point de vue théorique sont nombreux. La petite dimension de ces systèmes permet une analyse géométrique. Expérimentalement, des champs complexes avec des variations temporelles rapides (comme par exemple les champs de type bang-bang où la valeur du contrôle passe brusquement de +1 à -1 ou de -1 à +1) peuvent être implémentés avec une grande précision. Le dernier avantage repose sur la simplicité des modèles et le très bon accord théorie-expérience même lorsque les effets de la dissipation sont pris en compte. Nous envisageons d'étudier différents types de contrôles à la fois sur un spin 1/2 en interaction avec un environnement ou sur un ensemble de spins couplés. Les champs théoriques pourront être testés expérimentalement dans l'équipe de S. Glaser à Munich. Le premier exemple que nous analysons actuellement est le contrôle d'un spin 1/2 lorsque les effets de dissipation et de mesure (radiation damping) sont tous deux pris en comptes. L'objectif du contrôle est de passer de l'état d'équilibre du système à une aimantation nulle. Nous avons montré que suivant l'intensité maximum du champ magnétique autorisée, les stratégies de contrôle sont différentes et utilisent en particulier des trajectoires singulières. Un article est en préparation sur le sujet. Une question plus difficile en RMN que nous voudrions aborder serait de déterminer des champs de contrôle robustes vis à vis du désaccord de fréquence (chaque spin ayant un environnement chimique différent peut avoir des fréquences de transition différentes) et des inhomogénéités du champ (chaque spin en solution ne voit pas exactement le même champ).

3- Contrôle optimal géométrique

Mon principal projet est de continuer mon travail avec B. Bonnard et son groupe sur le contrôle quantique. Nous envisageons dans un premier temps d'étendre nos résultats sur les systèmes à deux niveaux dissipatifs à des systèmes possédant trois niveaux ou plus. Etant donnée la dimension de ces systèmes, l'analyse sera avant tout numérique à partir de méthodes de tir pour déterminer le vecteur adjoint initial ou de méthodes de continuation. L'idée des algorithmes de continuation est de déterminer de proche en

proche ce vecteur adjoint en modifiant un des paramètres du problème de contrôle. Pour ces exemples, l'analyse géométrique permettra tout de même de déterminer les coordonnées les mieux adaptées à l'étude et de faciliter ainsi l'utilisation des algorithmes numériques. Nous travaillerons également sur ce projet avec M. Chyba et son équipe d'Hawaï. Des applications à des systèmes physiques sont également envisagées.

Nous projettons également pour étudier des systèmes quantiques de plus grandes dimensions de développer nos techniques numériques. Nous voudrions ansi coupler les méthodes directes (optimisation globale d'une discrétisation du champ et de l'état) aux méthodes indirectes (détermination du vecteur adjoint initial) et les algorithmes monotones aux méthodes indirectes. Le but de ce couplage est d'augmenter le domaine de convergence des méthodes indirectes qui est en général assez petit. En d'autres mots, ce couplage devrait permettre de trouver une bonne approximation du vecteur adjoint initial utilisé par les algorithmes de tir. Toutes ces méthodes sont à ma connaissance complètement nouvelles en contrôle quantique et demanderont beaucoup d'investissements.

4- Algorithmes monotones

Nous envisageons également de continuer à développer les algorithmes monotones pour pouvoir les appliquer à tous les types de problèmes de contrôle en mécanique quantique. Une première étape sur laquelle nous travaillons actuellement avec Julien Salomon de l'Université Paris Dauphine est de généraliser ces algorithmes pour un critère de coût type temps minimal. Jusqu'à présent, ces algorithmes ne pouvaient s'appliquer qu'à des problèmes à temps fixé où l'énergie du champ est minimisée. Cette nouvelle formulation est testée sur un système de spins 1/2 en interaction, qui est un exemple typique que l'on peut rencontrer en Résonance Magnétique Nucléaire. Nous cherchons dans ce système à implémenter des portes quantiques à deux et trois qubits (CNOT et Toffoli) et des algorithmes plus complets comme celui d'un additioneur. Un article est en préparation sur le sujet. Un de nos autres projets est d'introduire les conditions du second d'ordre dans les algorithmes monotones. Ces conditions permettent d'obtenir des résultats d'optimalité locaux et sont bien connues en théorie du contrôle optimal. A ma connaissance, les algorithmes monotones utilisés actuellement en chimie-physique ne construisent que des champs extrémaux. Mes autres

projets, plus numériques, ont pour but de continuer à appliquer les algorithmes monotones à différentes situations physiques que ce soit en RMN ou en physique moléculaire, pour par exemple le contrôle de l'orientation et de l'alignement. Nos techniques seront dans ces cas appliquées à des situations expérimentales réalistes et confrontées aux résultats expérimentaux.

Bibliographie

[1] D. Sugny, P. Mardesic, M. Pelletier and H. R. Jauslin,*La monodromie : Du tour du monde en 80 jours à la physique quantique*, UB Science, Editions de l'Université de Bourgogne, 2009.

[2] B. Bonnard and D. Sugny, *Contrôle optimal des systèmes quantiques*, UB Science, Editions de l'Université de Bourgogne, 2009.

[3] B. Bonnard and D. Sugny, *Optimal control theory with applications in space and quantum mechanics*, submitted to AIMS Series on Applied Maths.

[4] S. Lagrange, D. Sugny, A. Picozzi and H. R. Jauslin, *Singular tori as attractors of nonlinear counterpropagating wave systems*, submitted to Phys. Rev. E.

[5] B. Bonnard, N. Shcherbakova and D. Sugny, *The smooth continuation method in optimal control with application to quantum systems*, submitted to ESAIM : COCV.

[6] U. Boscain, T. Chambrion, P. Mason, M. Sigalotti and D. Sugny, *Controllability of the rotation of a quantum planar molecule*, submitted to IEEE, cdc 2009.

[7] D. Sugny, L. Bomble, T. Ribeyre, O. Dulieu and M. Desouter-Lecomte, *Rovibrational quantum computing by optimized STIRAP techniques and optimal control theory*, submitted to Phys. Rev. A.

[8] M. Lapert, R. Tehini, G. Turinici and D. Sugny, *Monotonically convergent optimal control theory of quantum systems with spectral constraints*, Phys. Rev. A. 79, 063411 (2009).

[9] D. Sugny, A. Picozzi, S. Lagrange and H. R. Jauslin, *On the role of singular tori in the spatio-temporal dynamics of nonlinear wave systems*, to appear in Physical Review Letters.

[10] B. Bonnard and D. Sugny, *Geometric optimal control in two-level dissipative quantum systems*, to appear in Control and Cybernetics.

[11] B. Bonnard, M. Chyba and D. Sugny, *Time-minimal control of dissipative two-level quantum systems : The generic case*, to appear in I.E.E.E, transactions on automatic and control.

[12] B. Bonnard and D. Sugny, *Time-minimal control of dissipative two-level quantum systems : The integrable case*, SIAM, Journal on control and optimization 48, 1289 (2009).

[13] M. Lapert, R. Tehini, G. Turinici and D. Sugny, *Monotonically convergent optimal control theory of quantum systems under a nonlinear interaction with the control field*, Phys. Rev. A 78, 023408 (2008).

[14] D. Sugny and C. Kontz, *Optimal control of a three-level quantum system by laser fields plus von Neumann measurements*, Phys. Rev. A 77, 063420 (2008).

[15] R. Tehini and D. Sugny, *Field-free molecular orientation by non-resonant and quasi-resonant two-color laser pulses*, Phys. Rev. A 77, 023407 (2008).

[16] T. Viellard, F. Chaussard, D. Sugny, B. Lavorel and O. Faucher, *Field-free molecular alignment of CO2 mixtures in presence of collisional relaxation*, J. Raman. Spec. 39, 694 (2008).

[17] D. Sugny, P. Mardesic, M. Pelletier, A. Jebrane and H.R. Jauslin, *Fractional hamiltonian monodromy from a Gauss-Manin monodromy*, J. Math. Phys. 49, 042701 (2008).

[18] M. Ndong, L. Bomble, D. Sugny, Y. Justum and M. Desouter-Lecomte, *Not gate in a cis-trans photoisomerization model*, Phys. Rev. A 76, 043424 (2007).

[19] D. Sugny, C. Kontz and H. R. Jauslin, *Time-optimal control of a two-level dissipative quantum system*, Phys. Rev. A 76, 023419 (2007).

[20] D. Sugny, M. Ndong, D. Lauvergnat, Y. Justum and M. Desouter-Lecomte, *Laser control in open molecular systems : STIRAP and Optimal control*, J. Photochem. Photob. 190, 259 (2007).

[21] D. Sugny, C. Kontz and H. R. Jauslin, *Target states and control of molecular alignment in a dissipative medium*, Phys. Rev. A 74, 053411 (2006).

[22] D. Sugny, C. Kontz, M. Ndong, Y. Justum, G.Dive and M. Desouter-Lecomte, *Laser control in a bifurcating region*, Phys. Rev. A 74, 043419 (2006).

[23] D. Sugny, A. Keller, O. Atabek, D. Daems, C. M. Dion, S. Guérin and H. R. Jauslin, *Control of mixed-state quantum systems by a train of short pulses*, Phys. Rev. A 72, 032704 (2005).

[24] D. Daems, S. Guérin, D. Sugny and H. R. Jauslin, *Efficient and long-lived field-free orientation of molecules by a single hybrid short pulse*, Phys. Rev. Lett. 94, 153003 (2005).

[25] D. Sugny, A. Keller, O. Atabek, D. Daems, C. M. Dion, S. Guérin and H. R. Jauslin, *Laser control for the optimal evolution of pure quantum states*, Phys. Rev. A 71, 063402 (2005).

[26] G. Michalski, R. Jost, D. Sugny, M. Joyeux and M. Thiemens, *Dissociation energies of six NO2 isotopologues by laser induced fluorescence spectroscopy and zero point energy of some triatomic molecules*, J. Chem. Phys. 121, 7153 (2004).

[27] D. Sugny, A. Keller, O. Atabek, D. Daems, S. Guérin and H. R. Jauslin, *Time-dependent unitary perturbation theory for intense laser driven molecular orientation*, Phys. Rev. A 69, 043407 (2004).

[28] D. Sugny, A. Keller, O. Atabek, D. Daems, C. M. Dion, S. Guérin and H. R. Jauslin, *Reaching optimally oriented molecular states by laser kicks*, Phys. Rev. A 69, 033402 (2004).

[29] M. Joyeux and D. Sugny, *Canonical perturbation theory for highly excited dynamics*, Can. J. Phys. 80, 1459 (2002).

[30] M. Joyeux, D. Sugny and M. Lombardi, *A local diabatic representation of non-born-oppenheimer dynamics*, Chem. Phys. Lett. 352, 99 (2002).

[31] D. Sugny and M. Joyeux, *A new canonical perturbation procedure for studying nonadiabatic dynamics*, Chem. Phys. Lett. 337, 319 (2001)

[32] M. Joyeux, D. Sugny, M. Lombardi, R. Jost, R. Schinke, S. Skokov and J. Bowman, *Vibrational dynamics up to the dissociation threshold : A case study of two-dimensional HOCl*, J. Chem. Phys. 113, 9610 (2000).

[33] D. Sugny, M. Joyeux and E. Sibert, *Investigation of the vibrational dynamics of the HCN/CNH isomers through high order canonical perturbation theory*, J. Chem. Phys. 113, 7165 (2000).

[34] M. Joyeux, D. Sugny, V. Tyng, M.E. Kellman, H. Ishikawa, R.W. Field, C. Beck and R. Schinke, *Semiclassical study of the isomerization states of HCP*, J. Chem. Phys. 112, 4162 (2000).

[35] D. Sugny and M. Joyeux, *On the application of canonical perturbation theory to floppy molecules*, J. Chem. Phys. 112, 31 (2000).

[36] A. A. Agrachev and Y. L. Sachkov, *Control theory from the geometric viewpoint*, Springer-Verlag, Berlin, 2004.

[37] E. L. Allgower and K. Georg, *Introduction to numerical continuation methods*, Classics in Applied Math, 45, SIAM Philadelphia, 2003.

[38] Vl. I. Arnol'd, *Mathematical methods of classical mechanics*, Graduate texts in mathematics, Springer-Verlag, New-York, 1989.

[39] Vl. I. Arnol'd, *Catastrophe theory*, Springer-Verlag, Berlin, 1992.

[40] Vl. I. Arnol'd, S. M. Gusein-Zade and A. N. Varchenko, *Singularities of differentiable maps. Vol. II. Monodromy and asymptotics of integrals*, volume 83 of Monographs in Mathematics. Birkhäuser Boston Mass, 1988.

[41] A. Assion, T. Baumert, M. Bergt, T. Brixner, B. Kiefer, V. Seyfried, M. Strehle and G. Gerber, *Control of chemical reactions by feedback-optimized phase-shaped femtosecond laser pulses*, Science 282, 919 (1998).

[42] I. S. Averbukh and R. Arvieu, *Angular focusing, squeezing and rainbow formation in a strongly driven quantum rotor*, Phys. Rev. Lett. 87, 163601 (2001).

[43] A. Ben Haj-Yedder, A. Auger, C. M. Dion, E. Cancès, A. Keller, C. Le Bris and O. Atabek, *Numerical optimization of laser fields to control molecular orientation*, Phys. Rev. A 66, 063401 (2002).

[44] L. Bomble, D. Lauvergnat, F. Remacle and M. Desouter-Lecomte, *Vibrational computing : Simulation of a full adder by optimal control*, J. Chem. Phys. 128, 064110 (2008).

[45] B. Bonnard and M. Chyba, *Singular trajectories and their role in control theory*, Mathematics and Applications, 40, Springer-Verlag, Berlin, 2003.

[46] U. Boscain, G. Charlot, J.-P. Gauthier, S. Guérin and H. R. Jauslin, *Optimal control in laser induced population transfer for two and three-level quantum systems*, J. Math. Phys. 43, 2107 (2002).

[47] A. E. Bryson and Y.-C. Ho, *Applied optimal control*, Taylor and Francis, 1975.

[48] Cotcot : http ://apo.enseeiht.fr/cotcot.

[49] R. H. Cushman and L. Bates, *Global aspects of classical integrable systems*, Birkhäuser, Basel, 1997.

[50] R. H. Cushman, H. R. Dullin, A. Giacobbe, D. D. Holm, M. Joyeux, P. Lynch, D. A. Sadovskií and B. I. Zhilinskií, *CO_2 molecule as a quantum realization of the 1 :1 :2 resonant swing-spring with monodromy*, Phys. Rev. Lett. 93, 024302 (2004).

[51] R. H. Cushman and D. A. Sadovskií, *Monodromy in the hydrogen atom in crossed fields*, Physica D 142, 166 (2000).

[52] D. Daems, S. Guérin, E. Hertz, H. R. Jauslin, B. Lavorel and O. Faucher, *Field-free two-direction alignment alternation of linear molecules by elliptic laser pulses*, Phys. Rev. Lett. 95, 063005 (2005).

[53] G. Dhont, J. B. Delos, D. A. Sadovskií and B. I. Zhilinskií, *Dynamical manifestation of Hamiltonian monodromy*, Europhys. Lett. 83, 24003 (2008).

[54] C. M. Dion, A. B. Haj-Yedded, E. Cancès, C. Le Bris, A. Keller and O. Atabek, *Optimal laser control of orientation : the kicked molecule*, Phys. Rev. A 65, 063408 (2002).

[55] J. J. Duistermaat, *On global action-angle coordinates*, Comm. Pure Appl. Math. 33, 687 (1980).

[56] H. R. Dullin and H. Waalkens, *Nonuniqueness of the phase shift in central scattering due to monodromy*, Phys. Rev. Lett. 101, 070405 (2008).

[57] K. Efstathiou, R. H. Cushman and D. A. Sadovskií, *Fractional monodromy of the 1 :-2 resonance*, Adv. Math. 209, 241 (2007).

[58] B. Friedrich and D. Herschbach, *Alignment and trapping of molecules in intense laser fields*, Phys. Rev. Lett. 74, 4623 (1995).

[59] A. L. Gaeta, R. W. Boyd, J. R. Ackerhalt and P. W. Milonni, *Instabilities and chaos in the polarizations of counterpropagating light fields*, Phys. Rev. Lett. 58, 2432 (1987).

[60] D. J. Gauthier, M. S. Malcuit and R. W. Boyd, *Polarization bistability in counterpropagating laser beams*, Phys. Rev. Lett. 64, 1721 (1990).

[61] O. Ghafur, A. Rouzée, A. Gijsbertsen, W. Kiu Siu, S. Stolte and M. J. J. Vrakking, *Impulsive orientation and alignment of quantum-state-selected NO molecules*, Nature physics 5, 289 (2009).

[62] A. Giacobbe, R. H. Cushman, D. A. Sadovskií and B. I. Zhilinskií, *Monodromy of the quantum 1 :1 :2 resonant swing spring*, J. Math. Phys. 45, 5076 (2004).

[63] C. Gollub, M. Kowalewski and R. de Vivie-Riedle, *Monotonic convergent optimal control theory with strict limitations on the spectrum of optimized laser fields*, Phys. Rev. Lett. 101, 073002 (2008).

[64] H. Goto and K. Ichimura, *Multiqubit controlled unitary gate by adiabatic passage with an optical cavity*, Phys. Rev. A 70, 012305 (2004).

[65] S. Guérin, L. P. Yatsenko, H. R. Jauslin, O. Faucher, B. Lavorel, *Orientation of polar molecules by laser induced adiabatic passage*, Phys. Rev. Lett. 88, 233601 (2002).

[66] S. Guérin and H. R. Jauslin, *Control of quantum systems by adiabatic passage techniques*, Adv. Chem. Phys. 125, 147 (2003).

[67] M. F. Hamilton and D. T. Blackstock, *Nonlinear acoustics*, Academic press, 1998.

[68] E. Hamilton, T. Seideman, T. Ejdrup, M. D. Poulsen, C. Z. Bisgaard, S. S. Viftrup and H. Stapelfeldt, *Alignment of symmetric top molecules by short laser pulses*, Phys. Rev. A 72, 043402 (2005).

[69] E. Hertz, A. Rouzée, S. Guérin, B. Lavorel and O. Faucher, *Optimization of fild-free molecular alignment by phase-shaped laser pulses*, Phys. Rev. A 75, 031403(R) (2007).

[70] E. Infeld and G. Rowlandsn, *Nonlinear waves, solitons and chaos*, Cambridge University press, Cambridge 1992.

[71] R. Jost, M. Joyeux, S. Skokov and J. Bowman *Vibrational analysis of HOCl up to 98% of the dissociation energy with a Fermi resonance Hamiltonian*, J. Chem. Phys. 111, 6807 (1999).

[72] M. Joyeux, *Study of vibrational energy localization and redistribution in hydrogen peroxide H_2O_2 at low energy*, J. Chem. Phys. 122, 074303 (2005).

[73] M. Joyeux, R. Jost and M. Lombardi, *An effective model for the $X^2A_1-A^2B_2$ conical intersection in NO_2*, J. Chem. Phys. 119, 5923 (2003).

[74] R. S. Judson and H. Rabitz, *Teaching lasers to control molecules*, Phys. Rev. Lett. 68, 1500 (1992).

[75] T. Kanai and H. Sakai, *Numerical simulations of molecular orientation using strong, nonresonant, two-color laser fields*, J. Chem. Phys. 115, 5492 (2001).

[76] N. Khaneja, R. Brocket and S. Glaser, *Time-optimal control in spin systems*, Phys. Rev. A 63, 032308 (2001).

[77] Z. Kis and F. Renzoni, *Qubit rotation by stimulated Raman adiabatic passage*, Phys. Rev. A 65, 032318 (2002).

[78] R. Kosloff, S. A. Rice, P. Gaspard, S. Tersigni and D. J. Tannor, *Wavepacket dancing : Achieving chemical selectiviy by shaping light pulses*, Chem. Phys. 139, 201 (1989).

[79] V. Kurkal and S. A. Rice, *Sequential STIRAP-based control of the HCN-CNH isomerization*, Chem. Phys. Lett. 344, 125 (2001).

[80] J. J. Larsen, K. Hald, N. Bjerre, H. Stapelfeldt and T. Seideman, *Three-dimensional alignment of molecules using elliptically polarized laser fields*, Phys. Rev. Lett. 85, 2470 (2000).

[81] K. F. Lee, D. M. Villeneuve, P. B. Corkum, A. Stolow and J. G. Underwood, *Field-free three dimensional alignment of polyatomic molecules*, Phys. Rev. Lett. 97, 173001 (2006).

[82] M. Leibscher, I. S. Averbukh and H. Rabitz, *Molecular alignment by trains of short laser pulses*, Phys. Rev. Lett. 90, 213001 (2003).

[83] M. Leibscher, I. S. Averbukh, P. Rozmej and R. Arvieu, *Semiclassical catastrophes and cumulative angular squeezing of a kicked quantum rotor*, Phys. Rev. A 69, 032102 (2004).

[84] R. J. Levis, G. M. Menkir and H. Rabitz, *Selective bond dissociation and rearrangement with optimality tailored, strong-field laser pulses*, Science 292, 709 (2001).

[85] Y. Maday and G. Turinici, *New formulations of monotonically convergent quantum control algorithms*, J. Chem. Phys. 118, 8191 (2003).

[86] Y. Maday, J. Salomon and G. Turinici, *Monotonic time-discretized schemes in quantum control*, Numer. Math. 103, 323 (2006).

[87] N. N. Nekhoroshev, D. A. Sadovskií and B. I. Zhilinskií, *Fractional monodromy of resonant classical and quantum oscillators*, Comp. Rend. Acad. Sci., Série I Math. 335(11), 985 (2002).

[88] N. N. Nekhoroshev, D. A. Sadovskií and B. I. Zhilinskií, *Fractional Hamiltonian monodromy*, Ann. H. Poincaré 7(6), 1099 (2006).

[89] N. N. Nekhoroshev, *Fractional monodromy in the case of arbitrary resonances*, Sbornik Math. 198, 383 (2007).

[90] M. Ndong, D. Lauvergnat, X. Chapuisat and M. Desouter-Lecomte, *Optimal control simulation of the Deutsch-Jozsa algorithm in a two-dimensional double well coupled to an environment*, J. Chem. Phys. 126, 244505 (2007).

[91] Y. Ohtsuki and K. Nakagami, *Monotonically convergent algorithms for solving quantum optimal control problems of a dynamical system nonlinearly interacting with a control*, Phys. Rev. A 77, 033414 (2008).

[92] A. P. Peirce, M. A. Dahleh and H. Rabitz, *Optimal control of quantum mechanical systems : Existence, numerical approximation and applications*, Phys. Rev. A 37, 4950 (1988).

[93] E. Péronne, M. D. Poulsen, C. Z. Bisgaard, H. Stapelfeldt and T. Seideman, *Nonadiabatic alignment of asymmetric top molecules : Field-free alignment of Iodobenzene*, Phys. Rev. Lett. 91, 043003 (2003).

[94] S. Pitois, A. Picozzi, H. R. Jauslin and M. Haelterman, *Polarization and modal attractors in conservative counterpropagating four-wave interaction*, Europhys. Lett. 70, 88 (2005).

[95] S. Pitois, J. Fatome and G. Millot, *Polarization attraction using counterpropagating waves in optical fiber at telecommunication wavelengths*, Opt. Express 16, 6643 (2008).

[96] S. Pitois, G. Millot and S. Wabnitz, *Polarization domain wall solitons with counterpropagating laser beams*, Phys. Rev. Lett. 81, 1409 (1998).

[97] L. S. Pontryagin et al., *The mathematical theory of optimal processes*, Pergamon Press, Oxford, 1964.

[98] S. Ramakrishna and T. Seideman, *Intense laser alignment in dissipative media as a route to solvent dynamics*, Phys. Rev. Lett. 95, 113001 (2005).

[99] S. Ramakrishna and T. Seideman, *Coherence spectroscopy in dissipative media : A Liouville space pathway approach*, J. Chem. Phys. 122, 084502 (2005).

[100] H. Rabitz, R. de Vivie-Riedle, M. Motzkus and K. Kompa, *Wither the future of controlling quantum phenomena ?*, Science 288, 824 (2000).

[101] S. Rice and M. Zhao, *Optimal control of molecular dynamics*, Wiley, New York (2000).

[102] A. Rouzée, E. Hertz, B. Lavorel and O. Faucher, *Towards the adaptative optimization of field-free molecular alignment*, J. Phys. B 41, 074002 (2008).

[103] D. A. Sadovskií and B. I. Zhilinskií, *Monodromy, diabolic points and angular momentum coupling*, Physics Letters A 256, 235 (1999).

[104] D. A. Sadovskií and B. I. Zhilinskií, *Hamiltonian systems with detuned 1 :1 :2 resonance : Manifestation of bidromy*, Annals of physics 322, 164 (2007).

[105] J. Salomon, *Contrôle en chimie quantique : conception et analyse de schémas d'optimisation*, PhD thesis (2007).

[106] J. Salomon, C. M. Dion and G. Turinici, *Optimal molecular alignment and orientation through rotational ladder climbing*, J. Chem. Phys. 123, 144310 (2005).

[107] T. Seideman and E. Hamilton, *Nonadiabatic alignment by intense pulses. Concepts, theory and directions*, Adv. At. Mol. Opt. Phys. 52, 289 (2006).

[108] M. Shapiro and P. Brumer, *Principles of quantum control of molecular processes*, Wiley, New York (2003).

[109] H. Stapelfeldt and T. Seideman, *Aligning molecules with strong laser pulses*, Rev. Mod. Phys. 75, 543 (2003).

[110] D. J. Tannor, *Introduction to quantum mechanics : A time-dependent perspective*, University science books, Sausalito, California (2007).

[111] D. Tannor, V. Kazakov and V. Orlov, *Control of photochemical branching : Novel procedures for finding optimal pulses and global upper bounds*, in Time dependent quantum molecular dynamics, edited by J. Broeckhove, L. Lathouwers, 347 (1992).

[112] C. M. Tesch and R. de Vivier-Riedle, *Vibrational molecular computing : Basis set independence and theoretical realization of the Deutsch-Jozsa algorithm*, J. Chem. Phys. 121, 12158 (2004).

[113] M. Trippenbach, Y. B. Band and P. S. Julienne, *Theory of four-wave mixing of matter waves from a bose-einstein condensate*, Phys. Rev. A 62, 023608 (2000).

[114] J. G. Underwood, B. J. Sussman and A. Stolow, *Field-free three dimensional molecular axis alignment*, Phys. Rev. Lett. 94, 143002 (2005).

[115] B. L. Van de Waerden, *Optical Solitons : From fibers to photonic crystals*, Academic Press, 2003.

[116] J. Vala, Z. Amitay, B. Zhang, S. R. Leone and R. Kosloff, *Experimental implementation of the Deutsch-Jozsa algorithm for three-qubit functions using pure coherent molecular superpositions*, Phys. Rev. A 66, 062316 (2002).

[117] N. V. Vitanov, T. Halfmann, B. Shore and K. Bergmann, *Laser-induced population transfer by adiabatic passage techniques*, Annu. Rev. Phys. Chem. 52, 763 (2001).

[118] I. Vrabel and W. Jakubetz, *Counterintuitive multiphoton pulse sequences in molecular isomerization : Selectivity and robustness of competing multiphoton stimulated Raman adiabatic passage processes*, J. Chem. Phys. 118, 7366 (2003).

[119] M. J. J. Vrakking and S. Stolte, *Coherent control of molecular orientation*, Chem. Phys. Lett. 271, 209 (1997).

[120] S. Vu Gnoc, *Quantum monodromy in integrable systems*, Commun. Math. Phys. 203, 465 (1999).

[121] D. Weidinger and M. Gruebele, *Quantum computing with energy-multiplexed molecular vibrations*, Mol. Phys. 10, 1999 (2007).

[122] J. Weiland and H. Wilhelmsson, *Coherent nonlinear interaction of waves in plasmas*, Pergamon, Oxford, 1977.

[123] J. Werschnik and E. K. U. Gross, *Quantum optimal control theory*, J. Phys. B, 40, R175 (2007).

[124] B. I. Zhilinskií, *Symmetry, invariants and topology in molecular models*, Physics Reports 341, 85 (2001).

[125] B. I. Zhilinskií, *Interpretation of quantum Hamiltonian monodromy in terms of lattice defects*, Acta Applicandae Mathematicae 87, 281 (2005).

[126] W. Zhu and H. Rabitz, *A rapid monotonically convergent iteration algorithm for quantum optimal control over the expectation value of a positive definite operator*, J. Chem. Phys. 109, 385 (1998).

Chapitre 7

Annexe : Liste des travaux

7.1 Liste des travaux

7.1.1 Ouvrage

Optimal control theory with applications in space and quantum mechanics
B. Bonnard and D. Sugny
submitted to AIMS Series on Applied Maths

7.1.2 Articles publiés

[28]- **On the role of singular tori in the spatio-temporal dynamics of nonlinear wave systems**
D. Sugny, A. Picozzi, S. Lagrange and H. R. Jauslin
to be published in Physical Review Letters

[27]- **Monotonically convergent optimal control theory of quantum systems with spectral constraints**
M. Lapert, R. Tehini, G. Turinici and D. Sugny
Phys. Rev. A 79, 063411 (2009).

[26]- **Geometric optimal control in two-level dissipative quantum systems**
B. Bonnard and D. Sugny
to be published in *Control and Cybernetics*

[25]- **Time-minimal control of dissipative two-level quantum systems : The generic case**
B. Bonnard, M. Chyba and D. Sugny
to be published in *I.E.E.E, transactions on automatic and control*

[24]- **Time-minimal control of dissipative two-level quantum systems : The integrable case**
B. Bonnard and D. Sugny
SIAM, Journal on control and optimization 48, 1289 (2009).

[23]- **Monotonically convergent optimal control theory of quantum systems under a nonlinear interaction with the control field**
M. Lapert, R. Tehini, G. Turinici and D. Sugny
Phys. Rev. A 78, 023408 (2008)

[22]- **Optimal control of a three-level quantum system by laser fields plus von Neumann measurements**
D. Sugny and C. Kontz
Phys. Rev. A 77, 063420 (2008)

[21]- **Field-free molecular orientation by non-resonant and quasi-resonant two-color laser pulses**
R. Tehini and D. Sugny
Phys. Rev. A 77, 023407 (2008)

[20]- **Field-free molecular alignment of CO2 mixtures in presence of collisional relaxation**
T. Viellard, F. Chaussard, D. Sugny, B. Lavorel and O. Faucher
J. Raman. Spec. 39, 694 (2008)

[19]- **Fractional hamiltonian monodromy from a Gauss-Manin monodromy**
D. Sugny, P. Mardesic, M. Pelletier, A. Jebrane and H.R. Jauslin
J. Math. Phys. 49, 042701 (2008)

[18]- **Not gate in a cis-trans photoisomerization model**

M. Ndong, L. Bomble, D. Sugny, Y. Justum and M. Desouter-Lecomte
Phys. Rev. A 76, 043424 (2007)

[17]- **Time-optimal control of a two-level dissipative quantum system**
D. Sugny, C. Kontz and H. R. Jauslin
Phys. Rev. A 76, 023419 (2007)

[16]- **Laser control in open molecular systems : STIRAP and Optimal control**
D. Sugny, M. Ndong, D. Lauvergnat, Y. Justum and M. Desouter-Lecomte
J. Photochem. Photob. 190, 259 (2007)

[15]- **Target states and control of molecular alignment in a dissipative medium**
D. Sugny, C. Kontz and H. R. Jauslin
Phys. Rev. A 74, 053411 (2006)

[14]- **Laser control in a bifurcating region**
D. Sugny, C. Kontz, M. Ndong, Y. Justum, G.Dive and M. Desouter-Lecomte
Phys. Rev. A 74, 043419 (2006)

[13]- **Control of mixed-state quantum systems by a train of short pulses**
D. Sugny, A. Keller, O. Atabek, D. Daems, C. M. Dion, S. Guérin and H. R. Jauslin
Phys. Rev. A 72, 032704 (2005)

[12]- **Efficient and long-lived field-free orientation of molecules by a single hybrid short pulse**
D. Daems, S. Guérin, D. Sugny and H. R. Jauslin
Phys. Rev. Lett. 94, 153003 (2005)

[11]- **Laser control for the optimal evolution of pure quantum states**
D. Sugny, A. Keller, O. Atabek, D. Daems, C. M. Dion, S. Guérin and H. R. Jauslin

Phys. Rev. A 71, 063402 (2005)

[10]- **Dissociation energies of six NO2 isotopologues by laser induced fluorescence spectroscopy and zero point energy of some triatomic molecules**
G. Michalski, R. Jost, D. Sugny, M. Joyeux and M. Thiemens
J. Chem. Phys. 121, 7153 (2004)

[9]- **Time-dependent unitary perturbation theory for intense laser driven molecular orientation**
D. Sugny, A. Keller, O. Atabek, D. Daems, S. Guérin and H. R. Jauslin
Phys. Rev. A 69, 043407 (2004)

[8]- **Reaching optimally oriented molecular states by laser kicks**
D. Sugny, A. Keller, O. Atabek, D. Daems, C. M. Dion, S. Guérin and H. R. Jauslin
Phys. Rev. A 69, 033402 (2004)

[7]- **Canonical perturbation theory for highly excited dynamics**
M. Joyeux and D. Sugny
Can. J. Phys. 80, 1459 (2002)

[6]- **A local diabatic representation of non-born-oppenheimer dynamics**
M. Joyeux, D. Sugny and M. Lombardi
Chem. Phys. Lett. 352, 99-105 (2002)

[5]- **A new canonical perturbation procedure for studying nonadiabatic dynamics**
D. Sugny and M. Joyeux
Chem. Phys. Lett. 337, 319-326 (2001)

[4]- **Vibrational dynamics up to the dissociation threshold : A case study of two-dimensional HOCl**
M. Joyeux, D. Sugny, M. Lombardi, R. Jost, R. Schinke, S. Skokov and J. Bowman

J. Chem. Phys. 113, 9610-9620 (2000)

[3]- **Investigation of the vibrational dynamics of the HCN/CNH isomers through high order canonical perturbation theory**
D. Sugny, M. Joyeux and E. Sibert
J. Chem. Phys. 113, 7165-7177 (2000)

[2]- **Semiclassical study of the isomerization states of HCP**
M. Joyeux, D. Sugny, V. Tyng, M.E. Kellman, H. Ishikawa, R.W. Field, C. Beck and R. Schinke
J. Chem. Phys. 112, 4162-4172 (2000)

[1]- **On the application of canonical perturbation theory to floppy molecules**
D. Sugny and M. Joyeux
J. Chem. Phys 112, 31-39 (2000)

7.1.3 Articles soumis

[33]- **Singular tori as attractors of nonlinear counterpropagating wave systems**
S. Lagrange, D. Sugny, A. Picozzi and H. R. Jauslin
submitted to Phys. Rev. E

[32]- **Fractional monodromy in the vibrational spectrum of HOCl**
D. Sugny, M. Joyeux and H. R. Jauslin
submitted to Phys. Rev. A

[31]- **The smooth continuation method in optimal control with application to quantum systems**
B. Bonnard, N. Shcherbakova and D. Sugny
submitted to ESAIM : COCV

[30]- **Controllability of the rotation of a quantum planar molecule**
U. Boscain, T. Chambrion, P. Mason, M. Sigalotti and D. Sugny
submitted to IEEE, cdc 2009

[29]- **Rovibrational quantum computing by optimized STIRAP techniques and optimal control theory**
D. Sugny, L. Bomble, T. Ribeyre, O. Dulieu and M. Desouter-Lecomte
submitted to Phys. Rev. A

7.1.4 Articles de vulgarisation

Contrôle optimal des systèmes quantiques
B. Bonnard and D. Sugny
UB Science, Editions universitaires de Bourgogne, 2009.

La monodromie : du tour du monde en 80 jours à la physique quantique
D. Sugny, P. Mardesic, M. Pelletier and H. R. Jauslin
UB Science, Editions universitaires de Bourgogne, 2009.

Manipulation du monde quantique par LASER
S. Guérin, D. Sugny, O. Faucher, B. Lavorel and H. R. Jauslin
La physique : du laboratoire au quotidien
Editions universitaires de Bourgogne, 2006.

7.1.5 Proceedings

Dynamics of mixed classical-quantum systems, geometric quantization and coherent states
H. R. Jauslin and D. Sugny
to appear in *World Singapore* (2009)

Control of molecular orientation and alignment by laser kicks
D. Sugny
J. Phys. IV 135 (2006)

7.2 Conférences invitées

D. Sugny
Physcon, Catana (Italia), September 2009

Time-optimal control of a spin 1/2 particle with relaxation and damping effects

P. Mardesic, D. Sugny, M. Pelletier and H. R. Jauslin
Monodromy and geometric phases in classical and quantum mechanics, Leiden (Netherlands), June 2009
Hamiltonian monodromy from a Gauss-Manin monodromy

D. Sugny, P. Mardesic, M. Pelletier and H. R. Jauslin
Singularités des champs de vecteurs du plan, bifurcations et applications, CIRM, Marseille (France), May 2009
Hamiltonian monodromy from a Gauss-Manin monodromy

D. Sugny
Concepts and methods in quantum control : theory and experience, Santa Barbara (USA), May 2009
Time-optimal control of two-level dissipative quantum systems

B. Bonnard and D. Sugny
Pontryagin Conference on Optimal Control Theory, Moscow (Russia), June 2008
Optimal control of two-level dissipative quantum systems

D. Sugny
2ième journées semi-classiques (Institut Fourier), Grenoble (France), February 2004
Control of molecular orientation by laser kicks

M. Joyeux and D. Sugny
Telluride workshop on Spectroscopy and dynamics in the time and frequency domains, Telluride, Colorado (USA), August 2000
Highly excited vibrational dynamics

M. Joyeux and D. Sugny
CECAM workshop on Spectroscopy and Computational Challenges in Vibrationally Highly Excited Polyatomic Molecules, Lyon (France), July 2000

Quantum vibrational chaos : how subtle a concept is it ?

M. Joyeux and D. Sugny
68ème congrès de l'Association Canadienne-Franaise pour l'Avancement des Sciences (ACFAS) Montreal (Canada), May 2000
La mécanique classique au secours de la compréhension des spectres quantiques

7.3 Communications orales et posters

M. Lapert and D. Sugny
CoCoChem 2009, London (United Kingdom), April 2009
Monotonically convergent algorithm for the control of molecular dynamics under non-linear interaction with the control field

Th. Viellard, F. Chaussard, D. Sugny, B. Lavorel and O. Faucher
Ecamp X, Conference on atoms, molecules and photons Igls (Austria), May 2008
High density molecular gases in strong ultrashort laser fields : Alignment and collisional relaxation

M. Desouter-Lecomte, D. Sugny, D. Lauvergnat, L. Bomble and M. Ndong
Ecamp IX, Conference on atoms, molecules and photons Crete (Greece), May 2007
Laser control of photoinduced processes : logical gates

D. Sugny, M. Desouter-Lecomte, Y. Justum, L. Bomble and M. Ndong
Ecamp IX, Conference on atoms, molecules and photons Crete (Greece), May 2007
Laser control of photoinduced processes : alignment and reactivity

S. Guérin, D. Sugny and H. Jauslin
Ecamp IX, Conference on atoms, molecules and photons Crete (Greece), May 2007
Efficient orientation of molecules

Th. Viellard, F. Chaussard, D. Sugny, B. Lavorel and O. Faucher
Ecamp IX, Conference on atoms, molecules and photons Saint-Petersboug (Russia), May 2007
Field-free molecular alignment in presence of collisional relaxations

D. Sugny, C. Kontz
Pamo 2006, Physique atomique et moléculaire Dijon (France), July 2006
Contrôle de l'orientation et de l'alignement moléculaire par un train d'impulsions soudaines

D. Sugny, M. Dessouter-Lecomte, Y. Justum, C. Kontz and M. Ndong
CCP6 Workshop on Coherent Control of Molecules Birmingham (England), July 2006
Laser control of photoinduced dynamics : Molecular alignment and reactivity

D. Sugny, M. Dessouter-Lecomte, Y. Justum, C. Kontz and M. Ndong
CCP6 Workshop on Coherent Control of Molecules Birmingham (England), July 2006
Laser control of photoinduced dynamics : Quantum gates

S. Guérin, D. Sugny, H. R. Jauslin
Workshop, Orsay (France), March 2005
Contrôle de processus quantiques par impulsions laser intenses : transfert sélectif de population, alignement moléculaire et information quantique

D. Sugny
Coloq 9, Colloque sur les lasers et l'optique quantique, Dijon (France), September 2005
Contrôle de l'orientation et de l'alignement moléculaire par un train d'impulsions soudaines

H. Jauslin, S. Guérin, O. Sapin and D. Sugny
2ièmes journées semi-classiques, Grenoble (France), February 2004
KAM techniques and resonances

D.Sugny, M. Joyeux, A. Keller and O. Atabek
Specmo 2004 Dunkerque (France), June 2004
Application de la théorie des perturbations canoniques à la dynamique moléculaire

D. Sugny
Journée des théoriciens d'Orsay, Orsay (France), June 2003
Application de la théorie des perturbations canoniques à la dynamique moléculaire

D. Sugny
18th Colloquium on High Resolution Molecular Spectroscopy, Dijon (France), September 2003
On the application of canonical perturbation theory to molecular dynamics

D. Sugny and M. Joyeux
6èmes Journées Francophones des Jeunes Physico-Chimistes, Marseille (France), July 2002
Hamiltoniens effectifs et Dynamique vibrationnelle

D. Sugny and M. Joyeux
17th colloquium on High Resolution Molecular Spectroscopy Nijmegen (the Netherlands), September 2001
New canonical perturbation procedures for studying nonadiabatic dynamics and chemical reactions

M. Joyeux and D. Sugny
3ème réunion des Physico-Chimistes Théoriciens Rhône-Alpes Lyon (France), March 2001
Théorie des perturbations canoniques, réactions chimiques et dynamique non-Born-Oppenheimer

D. Sugny and M. Joyeux
Colloque de la Division de Physique Atomique, Moléculaire et Optique de la SFP, Lyon (France), July 2000
Hamiltoniens effectifs et dynamique vibrationnelle

M. Joyeux and D. Sugny

Workshop on Molecular Dynamics : Quantum, Classical and Semi-classical, Grenoble (France), April 2000
Effective Hamiltonians and highly excited vibrational dynamics

M. Joyeux, D. Sugny and R. Jost
16th Colloquium on High Resolution Molecular Spectroscopy Dijon (France), September 1999
The highly excited vibrational dynamics of HCP, DCP and HOCl

D. Sugny and M. Joyeux
16th Colloquium on High Resolution Molecular Spectroscopy, Dijon (France), September 1999
A hindered-rotor model Hamiltonian for HCN/CNH

M. Joyeux, D. Sugny, C. Beck and R. Schinke
217th national meeting of the American Chemical Society, Anaheim (California), March 1999
Isomerization in HCP : from full quantum mechanical calculations to a semiclassical analysis

7.4 Séminaires

Laboratoire de Spectrométrie Physique de l'Université Joseph Fourier de Grenoble (France)
Octobre 2002

Laboratoire de Physique de l'Université de Bourgogne, Dijon (France)
Novembre 2002 et mai 2003

Laboratoire de Photophysique Moléculaire de l'Université Paris-Sud Orsay (France)
Avril 2003

Institut de Mathématiques de l'Université de Bourgogne, Dijon (France)
Septembre 2005 et janvier 2006

Institut Utinam, Besançon (France)
Avril 2008

Department Chemie, Technische Universität München, München (Germany)
Janvier 2009